KINEMATIC AND TEMPORAL EVOLUTION OF THE SOUTHERN APPALACHIAN FORELAND FOLD-THRUST BELT: CONSTRAINTS FROM STRUCTURAL, MAGNETIC AND RADIOMETRIC ANALYSES

by

James Stephen Hnat

A dissertation submitted in partial fulfillment
of the requirements for the degree of
Doctor of Philosophy
(Geology)
in The University of Michigan
2009

Doctoral Committee:

Professor Ben A. van der Pluijm, Co-Chair
Professor Rob Van der Voo, Co-Chair
Professor Roman Hryciw
Associate Professor Todd Ehlers
Assistant Professor Nathan Niemi

To Amanda, with love and thanks

ACKNOWLEDGEMENTS

Many people provided me with support and friendship during my time here as a graduate student. Firstly, I must thank Ben van der Pluijm for allowing me the opportunity to work with him, for his constant encouragement and for the insightful discussions we have had pertaining to geology, great television shows and life in general. I am deeply grateful to Rob Van der Voo, whose patience, support and education over the years has helped me develop into a scientist and for serving as a role model. I genuinely appreciate the significant effort of patiently reviewing this dissertation by my other committee members Roman Hryciw, Todd Ehlers and Nathan Niemi.

This dissertation would not have been remotely possible without the many geologists I worked with who have local geologic knowledge and who graciously helped me during my fieldwork. Pete Lemiszki, from the Tennessee Geological Survey, generously provided me with assistance for all phases of my research in Tennessee. The help of Ed Osborne (Alabama Geological Survey), Jon Goodwin and Bob Mumm (Illinois Geological Survey) and Ray Daniel and Ryan Pinkston (Kentucky Geological Survey) is also appreciated. I am thankful for the many discussions with the modern titans of Appalachian geology, Bill Thomas and Bob Hatcher, both of whom provided help with many aspects of this dissertation.

Josep Parés is thanked for assistance in the paleomagnetic lab, along with the great conversations and friendship. Ar-Ar dating would not have been possible without Chris Hall. I am thankful to the many graduate students and postdocs from the PaSTeL group over the years. Eric Tohver, John Solum, Jeff Rahl, Phil McCausland, Belén Oliva-Urcia, Philip Ong, Maodu Yan, Sam Haines, Sara Tourscher, Sasha Abrajevitch, Daming Wang, Matt Domeier, Anja Schleicher and Charlie Verdel all deserve mentioning as each provided me with both guidance and friendship. I also appreciate the friendship of my fellow graduate students, Franek Hasiuk, Matt Manon, Sarah Rilling, Matt Densmore and Darius Dixon, who all gave me a reason to look forward to Thursdays.

I owe thanks to two of my previous educators, my 8th grade earth science teacher, Emory Keith, and my undergraduate advisor, Paul Ryberg, both of whom inspired me to pursue a career in the earth sciences.

My family's love and support over the years was essential to my development as a scientist. My grandfather, perhaps unwittingly, planted the seeds for my love of science and discovery at an early age. I will always appreciate the effort my parents made during my high school years to drive their nerdy kid to and from various science team practices. Finally, I am eternally grateful to my wife, whose love, support and encouragement has provided me with the strength to trudge through this whole process.

TABLE OF CONTENTS

LIST OF FIGURES

LIST OF TABLES

LIST OF APPENDICES

ABSTRACT

KINEMATIC AND TEMPORAL EVOLUTION OF THE SOUTHERN APPALACHIAN FORELAND FOLD-THRUST BELT: CONSTRAINTS FROM STRUCTURAL, MAGNETIC AND RADIOMETRIC ANALYSES

by

James Stephen Hnat

Co-Chairs: Ben A. van der Pluijm and Rob Van der Voo

Formed during the Alleghanian orogeny, the southern Appalachian foreland fold-thrust belt displays curvature at the scale of an individual structure to the entire thrust belt. Using an integrated approach, this study shows that secondary rotations are not required to accommodate curvature, which contrasts with observation in curved belts elsewhere.

In the Tennessee salient, the southern Appalachian fold-thrust belt displays a significant degree of curvature (~55°). Early, layer-parallel paleostress orientations recorded in calcite twins show a systematically fanned distribution that correlates with the overall strike distribution for limestone sites within both the fold-thrust belt and the "undeformed" foreland, indicating primary curvature of the salient. Moreover, the degree of fanning matches the geometry of the hinterland Blue Ridge front instead of the most forward section of the belt, implying that indentation by

the Blue Ridge allochthon produced both the curvature of the Tennessee salient and the radial paleostress pattern. Paleomagnetic data from three lithologic units complement this scenario, as remagnetized directions show no correlation with orogenic strike. The synfolding remagnetization indicates that by the Middle to Late Pennsylvanian, approximately 50% of the folding in the fold-thrust belt was completed and suggests that deformation progressed from the hinterland toward the foreland. Direct constraints on the timing of deformation within the belt are provided by radiometric dating of illitic fault gouge. Illite $^{40}Ar/^{39}Ar$ ages from fault gouges show that the entire frontal thrust wedge was active simultaneously at approximately 278 Ma, such that the southern Appalachian foreland fold-thrust belt acted as a critically-stressed Coulomb wedge during the waning stages of Alleghanian deformation in the Early Permian. Shale ages from the extended foreland reflect local diagenetic conditions, rather than a far-field fluid-flow event associated with Alleghanian deformation.

This study shows that the kinematic and temporal evolution of curved fold-thrust belts can be understood by integrating multiple approaches. Paleomagnetic and structural data give insight into the regional processes driving deformation, with direct fault dating giving temporal constraints. The research also shows that diagenetic grade has a significant effect on the interpretation of $^{40}Ar/^{39}Ar$ ages, which is significant for future studies of sedimentary basins and fault gouge.

CHAPTER I

INTRODUCTION

Over the past two centuries, the Appalachians (Figure 1.1) have been the focus of an immense amount of geological research and resulting controversy. Along with its European continuation, the Caledonidian and Variscan orogens, the Appalachians would appear to be the most-studied orogen. Major geologic concepts, such as geosynclines (Hall, 1883), thin-skinned thrusting (Rich, 1934) and the plate tectonic Wilson cycle (Wilson, 1966) trace their roots to studies of Appalachian geology. Despite such a long legacy, many geological questions remain regarding Appalachian deformation and regional tectonics. It is the aim of this dissertation to provide new insight into a key aspect of Appalachian geology, namely the evolution of the southern Appalachian foreland fold-thrust belt in both a kinematic and temporal framework. Moreover, the kinematic and temporal relationships in the Appalachians presented here give new context for the framework of fold-thrust belts in general.

OROGENIC CURVATURE

The evolution of foreland fold-thrust belts has long been an active area of research for geologists, especially given their propensity for hydrocarbon

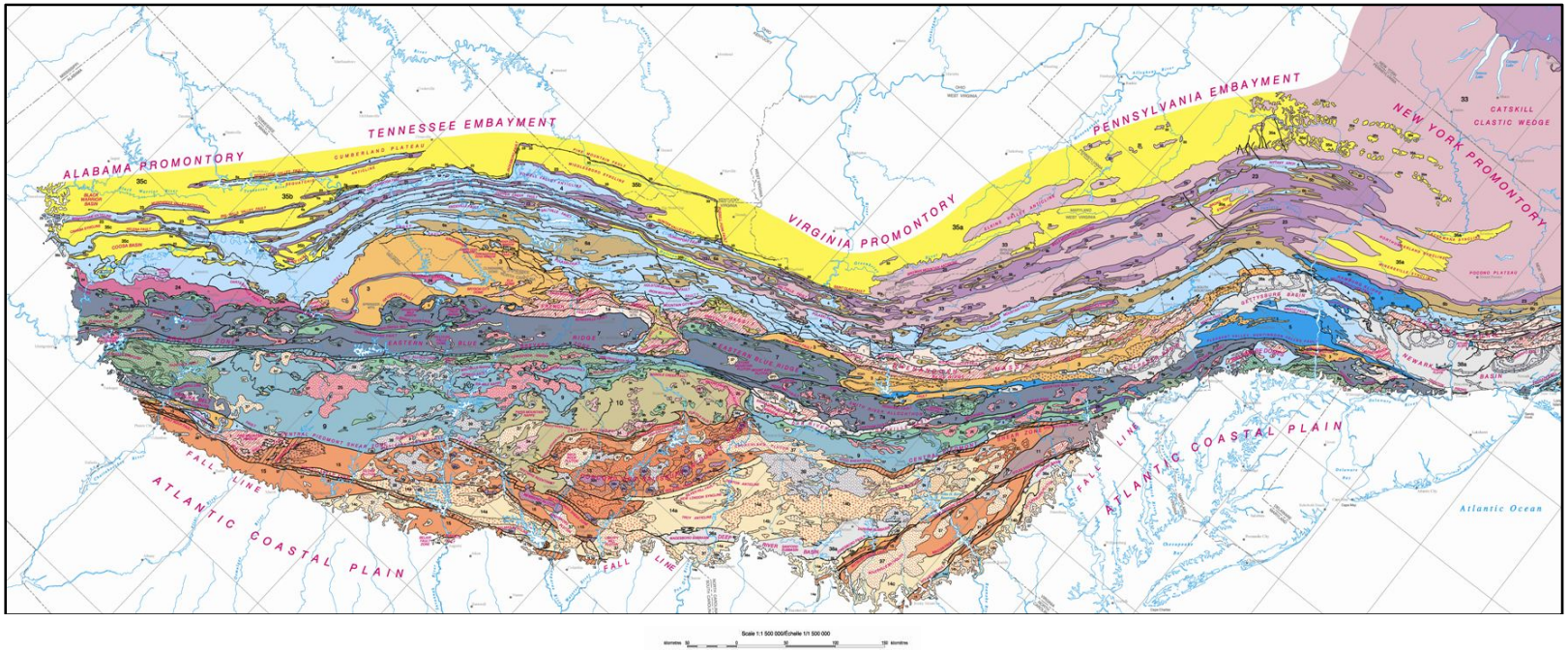

Figure 1.1 Lithotectonic map of the US Appalachians, showing the main tectonic units and subdivision in this part of the Appalachian-Caledonian-Variscan Chain (Hibbard et al., 2006).

accumulation (Boyer and Elliot, 1982; Davis et al., 1983; McClay, 1992; McClay, 2004). Understanding the three-dimensional processes that formed these belts is therefore an essential ingredient for any kinematic or mechanical model of their evolution. A feature common to most fold-thrust belts worldwide is some degree of curvature, defined by orogenic strike that systematically varies along the trace of the belt (Carey, 1955; Lowrie and Hirt, 1986; Weil and Sussman, 2004), as seen in the Appenine, Jura and Wyoming-Idaho fold-thrust belts, among others. Assessing which mechanism or mechanisms are responsible for the formation of arcuate belts requires information about the kinematic history, and, in particular, determining the magnitude of vertical-axis rotations. Curvature in fold-thrust belts has been attributed to features that include foreland obstacles, hinterland indenters, sedimentary basin morphology and changes along strike in mechanical properties and stratigraphic thickness (Macedo and Marshak, 1999; Marshak, 2004; Weil and Sussman, 2004). Rotations are indeed often associated with such features and are attributed to gradients in displacement along strike. However, whether individual structures or an entire thrust wedge necessitate rotations when displacement gradients are present is often not constrained.. Because of poorly defined kinematic and temporal histories, ambiguity regarding the main mechanism(s) driving curvature in arcuate fold-thrust belts worldwide remains. These considerations provided the primary source of motivation for Chapters II, III and IV of this dissertation.

Orogenic curvature and rotations are commonly examined using paleomagnetism (e.g., Eldredge et al., 1985; Lowrie and Hirt, 1986; McCaig and

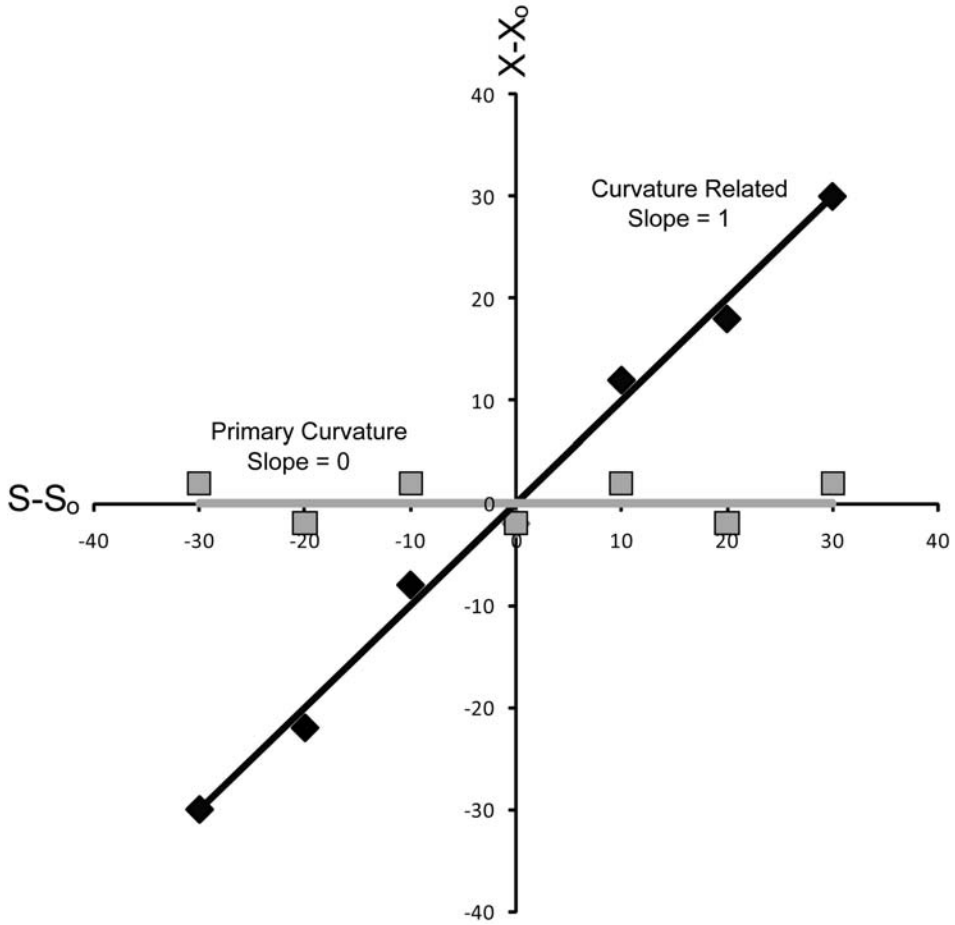

Figure 1.2: Plot of directional data (X) vs. strike (S) normalized to a reference direction (X_o) and strike (S_o). Black squares and trendline indicate the data is related to curvature formation. If data are paleomagnetic, they signify secondary curvature. Gray squares and trendline indicate primary curvature.

McClelland, 1992; Allerton et al., 1993; Bayona et al., 2003; Weil and Sussman, 2004), although other techniques, such as anisotropy of magnetic susceptibility (AMS), calcite twinning and other features, have been used (e.g., Nickelsen, 1979; Craddock et al., 1988; Gray and Mitra, 1993; Apotria, 1995; Kollmeier et al., 2000; Cifelli et al., 2004; Somma, 2006; Ong et al., 2007). Comparing directional data from areas with varying orogenic strike is often employed to evaluate curvature (Figure 1.2; Eldredge et al., 1985; Weil and Sussman, 2004). Correlation of such directional data with orogenic strike implies that they record some aspect of curvature formation. For example, if paleomagnetic data are otherwise unrelated to deformation, then the correlation suggests that the curvature is secondary (bent from an originally straighter geometry). If data are related to deformation, such as layer-parallel stress directions derived from calcite twinning analysis, then measurments from outside the belt must also be included to provide a reference. A lack of correlation between directional data and strike indicates primary curvature, where the belt formed in its original curved shape. A combination of these two end-member conditions would reflect partial secondary curvature.

A series of salients (convex toward the foreland) and recesses (concave toward the foreland) characterizes the trace of the fold-thrust belt in the Appalachians (Figure 1.1). The kinematic history of these curved segments has been investigated by numerous workers, using a variety of approaches (Miller and Kent, 1986; Kent, 1988; Stamatakos and Hirt, 1994; Spraggins and Dunne, 2002; Wise, 2004; Cederquist et al., 2006; Ong et al., 2007). The Pennsylvania salient, in

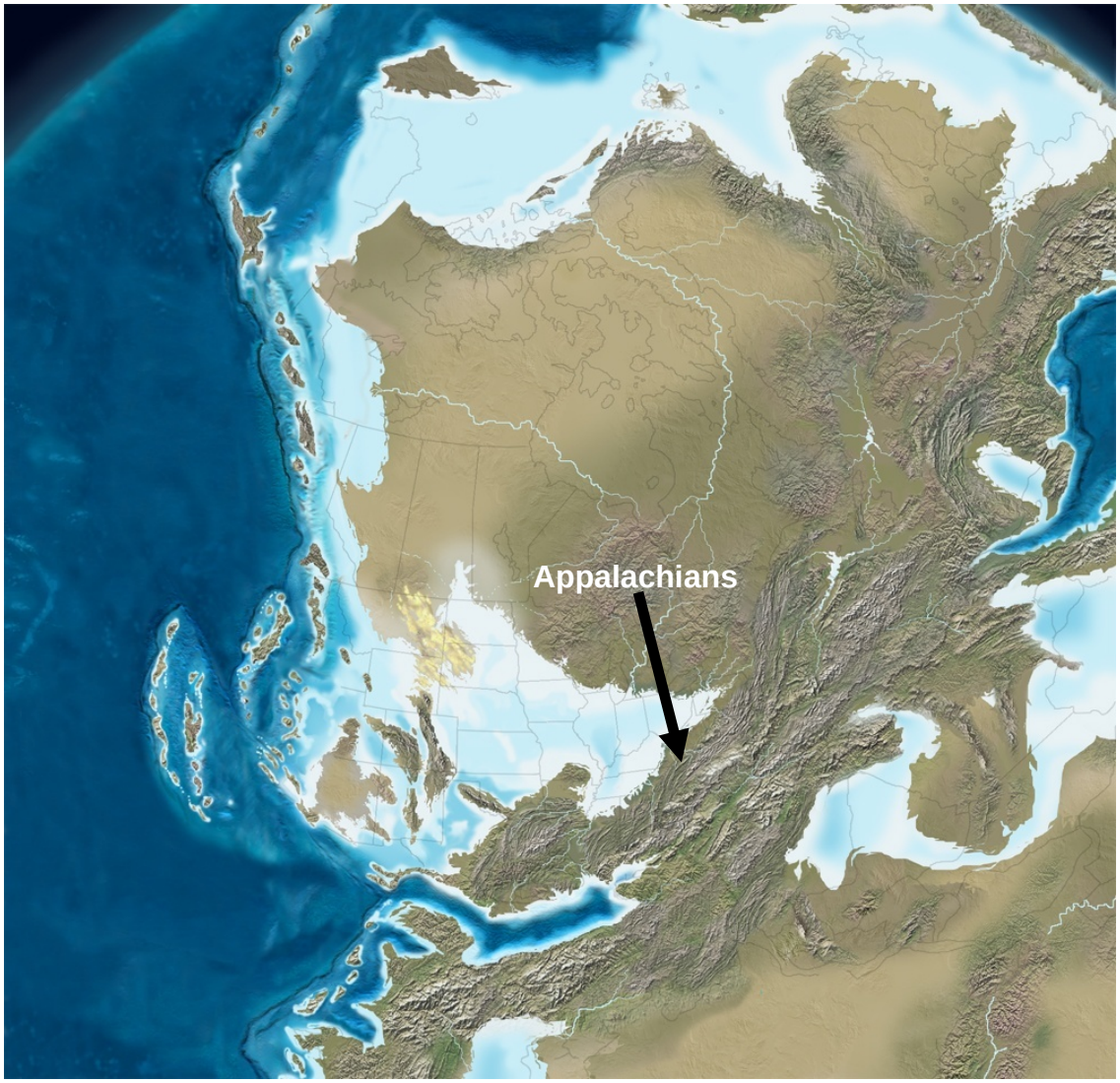

Figure 1.3: Paleogeographic map of North America during Late Pennsylvanian time (~300 Ma) showing the Laurentia-Gondwana collision at the pinnacle of the Alleghanian orogeny (Blakey, http://jan.ucc.nau.edu/~rcb7/nam.html).

particular, has received a great deal of attention on curvature formation. Paleomagnetic data have shown that primary magnetizations display rotation between the limbs of the salient (Miller and Kent, 1986; Kent, 1988; Stamatakos and Hirt, 1994), whereas rock units remagnetized during deformation display no such rotation (Stamatakos and Hirt, 1994; Cederquist et al., 2006). Data from calcite twinning analysis indicate that the ~55° of curvature in the Pennsylvania salient is secondary in nature (Ong et al., 2007). However, it is unclear as to whether all Appalachian curvature is secondary in origin, or if secondary rotation is limited to the Pennsylvania salient. This prompted the hypothesis that all curvature in the Appalachians is secondary (one of the many hypotheses tested in this dissertation) and is addressed in Chapters III and IV.

AGE OF DEFORMATION

Along with kinematic questions in the southern Appalachian fold-thrust belt presented in the previous section, the age of deformation for this belt is also ambiguous. Although a number of orogenic events have been identified along eastern North America, it is widely accepted that deformation in the thrust belt is dominated by the final collision of Gondwana with Laurentia (Figure 1.3), known as the late Paleozoic Alleghanian orogeny in North America (Woodward, 1957; Rodgers, 1970; Secor et al., 1986; Hatcher et al., 1989). Radiometric evidence suggests that the Alleghanian orogeny occurred during Pennsylvanian-Permian times (Dallmeyer et al., 1986; Secor et al., 1986; Hadizadeh et al., 1991; Steltenpohl et al., 1992; Goldberg and Dallmeyer, 1997). However, directages of the foreland

expression of this mountain-building event are largely absent. Stratigraphic evidence for the age of deformation is limited to deformed Lower Permian rocks of the Dunkard Group (299-271 Ma) in the central Appalachians of West Virginia (Hatcher et al., 1989; Becker et al., 2006). Paleomagnetic data from the central Appalachians preserve Permian, synfolding remagnetizations, further indicating that deformation occurred during the Permian (Stamatakos et al., 1996).

In the southern Appalachian fold-thrust belt, the age of deformation is constrained by the youngest deformed units, which consist of clastic rocks of Pennsylvanian age (318-299 Ma). Synfolding paleomagnetic results are present in the thrust belt, although the inferred age of magnetization ranges between Mississippian (Symons and Stratakos, 2002; Pannalal et al., 2003) and Pennsylvanian (Bachtadse et al, 1987), giving a broad range for the age of deformation. Within the more internal parts of the southern Appalachians, radiometric ages from metamorphic shear zones suggest a Permian age of deformation (Hatcher et al., 1988; Hadizadeh et al., 1991; Goldberg and Dallmeyer, 1997). Constraining the timing of deformation in the Appalachian fold-thrust belt through paleomagnetism and direct fault dating provided the motivation for the research presented in Chapters III and V, respectively. These data test the hypothesis of a Permian age for deformation in the southern Appalachian fold-thrust belt.

OUTLINE OF DISSERTATION

The overarching theme of this dissertation is the evolution of the southern Appalachian fold-thrust belt, giving insight into the kinematic and temporal development of the belt. Chapters are arranged by scale and the primary method applied.

Chapter II, published as Hnat, van der Pluijm, Van der Voo and Thomas (2008) in *Journal of Structural Geology*, is a study of the displacement history of the Jones Valley thrust in the Alabama section of the southern Appalachian fold-thrust belt. Palinspastic reconstructions of Thomas and Bayona (2005) reveal a significant displacement gradient along the trace of the thrust before being obscured by Cretaceous coastal plain sediments. Paleomagnetism and anisotropy of magnetic susceptibility (AMS) on redbeds of the Silurian Red Mountain Formation, as well as calcite twinning analysis of Ordovician limestones, were used to test whether this displacement gradient is attributable to rotation. Prefolding remanence directions and AMS fabrics are subparallel between the hanging wall and footwall of the thrust, suggesting no relative rotation has occurred on the Jones Valley thrust. Instead, differential displacement via self-similar thrusting is interpreted to have occurred.

Chapter III, submitted as Hnat, van der Pluijm and Van der Voo to *Tectonophysics*, represents a broadening in scope from Chapter II. Here, paleomagnetic data from three lithologic units in the Tennessee salient are presented to constrain the timing of deformation as well as to assess the nature of curvature in the salient. Remanence directions from limestones of the Middle-to-Upper Ordovician Chickamauga Group and redbeds of both the Middle Cambrian

Rome Formation and the Silurian Red Mountain Formation reveal a Pennsylvanian remagnetization. The syntilting nature of the Chickamauga Group directions suggests that deformation in the Tennessee salient was about half completed by the Late Pennsylvanian. Furthermore, the data fail to reveal any deviation in paleomagnetic declinations, suggesting that no rotation had occurred between the limbs of the Tennessee salient. Therefore, the Tennessee salient developed either as a curved structure from its initiation or secondary rotation, if any, had occurred prior to remagnetization.

Chapter IV, to be submitted to *Lithosphere*, applies calcite twinning analysis to assess curvature development in the Tennessee salient. Layer-parallel paleostress orientations collected from limestones within the thrust belt are compared with those from the "undeformed" foreland. Both datasets reveal a systematically fanned distribution of paleostress directions, implying that curvature of the Tennessee salient formed as a primary feature. Moreover, the degree of fanning exceeds the frontal curvature of the belt, but matches the shape of the more curved Blue Ridge front of the hinterland. This observation suggests that the advancing Blue Ridge block imparted a radial stress field on foreland rocks prior to producing the present day curvature of the Tennessee salient, a model that is further supported by sandbox geometric modeling.

Chapter V sets the stage for direct dating of deformation in the Southern Appalachians. It focuses on the effect of diagenetic grade on the interpretation of ages of neocrystallized illite in both fault rocks from the Appalachian fold-thrust belt and shales from the neighboring midcontinent. $^{40}Ar/^{39}Ar$ dating of encapsulated

clay aliquots produces two ages per sample: a total gas age, which incorporates the recoiled ^{39}Ar fraction produced during neutron irradiation, and a retention age, which omits the recoiled fraction. Determining which age is meaningful for Illite Age Analysis (comparing the radiometric age to the percent of detrital $2M_1$ illite) is dependent on whether radiogenic argon (^{40}Ar) was lost to nature during radiogenic decay. Previous studies (Dong et al., 1995; 2000; Hall et al., 2000) have shown that diagenetic grade, and more specifically crystallite thickness, may influence this behavior, but was not further explored until this study. Based on the results from this study, it is proposed that crystallites thicker than 10 nm require the retention age model be used, because of ^{40}Ar loss from potassium bearing defects. Smaller crystallites have little or no defects, requiring the total gas age model that was used in previous gouge dating studies (van der Pluijm et al., 2001; Solum and van der Pluijm, 2006; Haines and van der Pluijm, 2008). Total gas ages are used for one of the faults and all three shale samples, since they have crystallites <10 nm in their fine fractions. Thick crystallites characterize the illite from the other fault rocks, requiring the retention age model be used. The shale ages are varied and may represent local diagenetic events, whereas the ages of fault gouges indicate that the latest major period of fault motion occurred during the Early Permian (~278 Ma) within an internally deforming thrust wedge.

Chapter VI summarizes the outcomes of the dissertation research, integrating the results from the various studies into an overall spatio-temporal context. Three appendices are included in this dissertation. Appendix A presents a paleomagnetic study of the Portage Lake volcanics (~1.1 Ga) from the Upper

Peninsula of Michigan. Published as Hnat, van der Pluijm and Van der Voo (2006) in *Tectonophysics*, primary magnetizations display no correlation with strike along the arcuate Mid-Continent Rift, indicating primary curvature. Appendix B is a procedure manual for calcite twinning analysis that builds on previous versions that were included in the Master's theses of John Harris, John Kollmeier and Philip Ong. Appendix C is also a procedure manual, describing the preparation of samples for illite dating by way of the $^{40}Ar/^{39}Ar$ technique. This manual includes descriptions of sample collection, preparation and vacuum encapsulation.

REFERENCES

Allerton, S., Lonergan, L., Platt, J.P., Platzman, E.S. and McClelland, E., 1993. Palaeomagnetic rotations in the eastern Betic Cordillera, southern Spain. Earth and Planetary Science Letters 119, 225-241.

Apotria, T.G., 1995. Thrust sheet rotation and out-of-plane strains associated with oblique ramps: An example from the Wyoming salient, U.S.A. Journal of Structural Geology 17, 647-662.

Bachtadse, V., Van der Voo, R., Hayes, F.M. and Kesler, S.A., 1987. Late Paleozoic remagnetization of mineralized and unmineralized Ordovician carbonates from east Tennessee: evidence for a post-ore chemical event. Journal of Geophysical Research B: Solid Earth 92, 14165-14176.

Bayona, G., Thomas, W.A. and Van der Voo, R., 2003. Kinematics of thrust sheets within transverse zones: a structural and paleomagnetic investigation in the Appalachian thrust belt of Georgia and Alabama. Journal of Structural Geology 25, 1193-1212.

Becker, T.P., Thomas, W.A. and Gehrels, G.E., 2006. Linking late Paleozoic sedimentary provenance in the Appalachian Basin to the history of Alleghanian deformation. American Journal of Science 306, 777-798.

Blakey, R., Paleogeography and Geologic Evolution of North America. http://jan.ucc.nau.edu/~rcb7/nam.html. (accessed January 27, 2009)

Boyer, S. and Elliot, D., 1982. Thrust systems. American Association of Petroleum Geologists Bulletin 66, 1196-1230.

Carey, S.W., 1955. The orocline concept in geotectonics. Proceedings of the Royal Society of Tasmania 89, 255-289.

Cifelli, F., Rossetti, F., Mattei, M., Hirt, A.M., Funiciello, R. and Tortorici, L., 2004. An AMS, structural and paleomagnetic study of Quaternary deformation in eastern Sicily. Journal of Structural Geology 26, 29-46.

Craddock, J.P., Kopania, A.A. and Wiltschko, D.V., 1988. Interaction between the northern Idaho-Wyoming thrust belt and bounding basement blocks, central western Wyoming. Geological Society of America Memoir 171, 333-351.

Dallmeyer, R.D., Wright, J.E., Secor Jr, D.T. and Snoke, A.W., 1986. Character of the Alleghanian Orogeny in the Southern Appalachians; Part II, Geochronological constraints on the tectonothermal evolution of the eastern Piedmont in South Carolina. Geological Society of America Bulletin 97, 1329-1344.

Davis, D., Suppe, J. and Dahlen, F.A., 1983. Mechanics of fold-and-thrust belts and accretionary wedges. Journal of Geophysical Research 88, 1153-1172.

Dong, H., Hall, C.M., Peacor, D.R. and Halliday, A.N., 1995. Mechanisms of argon retention in clays revealed by laser ^{40}Ar-^{39}Ar dating. Science 267, 355-359.

Dong, H., Hall, C.M., Peacor, D.R., Halliday, A.N. and Pevear, D.R., 2000. Thermal $^{40}Ar/^{39}Ar$ separation of diagenetic from detrital illitic clays in Gulf Coast shales. Earth and Planetary Science Letters 175, 309-325.

Cederquist, D.P., Van der Voo, R., van der Pluijm, B.A., 2006. Syn-folding remagnetization of Cambro-Ordovician carbonates from the Pennsylvania Salient post-dates oroclinal rotation. Tectonophysics 422, 41-54.

Eldredge, S.V., Bachtadse, V. and Van der Voo, R., 1985. Paleomagnetism and the orocline hypothesis. Tectonophysics 119,153-179.

Goldberg, S.A. and Dallmeyer, R.D., 1997. Chronology of Paleozoic metamorphism and deformation in the Blue Ridge thrust complex, North Carolina and Tennessee. American Journal of Science 297, 488-526.

Gray, M.B. and Mitra, G., 1993. Migration of deformation fronts during progressive deformation: evidence from detailed structural studies in the Pennsylvania Anthracite region, U.S.A. Journal of Structural Geology 15, 435-449.

Hadizadeh, J., Babaie, H.A. and Babaie, A., 1991. Development of interlaced mylonites, cataclasites and breccias; examples from the Towaliga Fault, south central Appalachians. Journal of Structural Geology 13, 63-70.

Haines, S.H. and van der Pluijm, B.A., 2008. Clay quantification and Ar-Ar dating of synthetic and natural gouge: Application to the Miocene Sierra Mazatán detachment fault, Sonora, Mexico. Journal of Structural Geology 30, 525-538.

Hall, J., 1883. Contributions to the geological history of the American continent. American Association for the Advancement of Science, Proceedings 31, 29-69.

Hall, C.M., Kesler, S.E., Simon, G. and Fortuna, J., 2000. Overlapping Cretaceous and Eocene alteration, Twin Creeks Carlin-type deposit, Nevada. Economic Geology 95, 1739-1752.

Hatcher Jr, R.D., Hooper, R.J., McConnell, K.I., Hevin, T. and Costello, J.O., Geometric and time relationships between thrusts in the crystalline Southern Appalachians. In: Mitra, G. and Wojtal, S.F., Editors, 1988. *Geometries and mechanism of thrusting, with special reference to the Appalachians.* Geological Society of America Special Paper 222, 185-196.

Hatcher Jr, R.D., Thomas, W.A., Geiser, P.A., Snoke, A.W., Mosher, S. and Wiltschko, D.V., Alleghanian orogen. In: Hatcher Jr, R.D., Thomas, W.A. and Viele, G.E., Editors, 1989. *The Appalachian-Ouachita Orogen in the United States, The Geology of North America Volume F-2.* Geological Society of America, Boulder, Colorado, 233-318.

Hibbard, J.P., van Staal, C.R., Rankin, D.W., and Williams, H., 2006. Lithotectonic map of the Appalachian Orogen, Canada-United States of America; Geological Survey of Canada, Map 2096A, scale 1:1500000.

Kent, D.V., 1988. Further paleomagnetic evidence for oroclinal rotation in the central folded Appalachians from the Bloomsburg and the Mauch Chunk Formations. Tectonics 7, 749-759.

Kollmeier, J.M., van der Pluijm, B.A. and Van der Voo, R., 2000. Analysis of Variscan dynamics; early bending of the Cantabria-Asturias Arc, northern Spain. Earth and Planetary Science Letters 181, 203-216.

Lowrie, W. and Hirt, A.M. Paleomagnetism in arcuate mountain belts. In: Wezel, Forese-Carlo, Editor, 1986. *The Origin of Arcs*. Elsevier, Amsterdam, Netherlands, 141-157.

Macedo, J. and Marshak, S., 1999. Controls on the geometry of fold-thrust belt salients. Geological Society of America Bulletin 111, 1808-1822.

Marshak, S., Salients, recesses, arcs, oroclines, and syntaxes; a review of ideas concerning the formation of map-view curves in fold-thrust belts. In: McClay, K.R., Editor, 2004. *Thrust tectonics and hydrocarbon systems*. American Association of Petroleum Geologists Memoir 82, 131-156.

McCaig, A.M. and McClelland, E., 1992. Paleaeomagnetic techniques applied to thrust belts. In: McClay, K.R., Editor, *Thrust Tectonics*. Chapman and Hall, New York, New York, 209-216.

McClay, K.R., Editor, 1992. *Thrust tectonics.* Chapman-Hall, London, England, 447p.

McClay, K.R., Editor, 2004. *Thrust tectonics and hydrocarbon systems.* American Association of Petroleum Geologists Memoir 82, 667p.

Miller, J.D. and Kent, D.V., 1986. Paleomagnetism of the Upper Devonian Catskill Formation from the southern limb of the Pennsylvania Salient; possible evidence of oroclinal rotation. Geophysical Research Letters 13, 1173-1176.

Nickelsen, R.P., 1979. Sequence of structural stages of the Alleghany orogeny, Bear Valley strip mine, Shamokin, PA. American Journal of Science 279, 225-271.

Ong, P.F., van der Pluijm, B.A. and Van der Voo, R., 2007. Early rotation in the Pennsylvania Salient (US Appalachians): Evidence from calcite-twinning analysis of Paleozoic carbonates. Geological Society of America Bulletin 119, 796-804.

Pannalal, S.J., Symons, D.T.A. and Misra, K.C., 2003. Sweetwater Ba-F-Zn district, eastern Tennesseel a paleomagnetic age for dolomitisation from fluid flow. Journal of Geochemical Exploration 78-79, 235-241.

Rich, J.L., 1934. Mechanics of low-angle overthrust faulting as illustrated by Cumberland thrust bloc, Virginia, Kentucky and Tennessee. American Association of Petroleum Geologists Bulletin 18, 1584-1596.

Rodgers, J., 1970. *The tectonics of the Appalachians*. Wiley Interscience, New York, New York, 271p.

Secor Jr, D.T., Snoke, A.W. and Dallmeyer, R.D., 1986. Character of the Alleghanian Orogeny in the Southern Appalachians; Part III, Regional tectonic relations. Geological Society of America Bulletin 97, 1345-1353.

Solum, J.G. and van der Pluijm, B.A., Reconstructing the Snake River-Hoback Canyon section of the Wyoming thrust belt through direct dating of clay-rich fault rocks. Sears, J.W., Harms, T.A. and Evenchick, C.A., Editors, 2007. *Whence the mountains? Inquiries into the evolution of orogenic systems; a volume in honor of Raymond A. Price.* Geological Society of America Special Paper 433, 183-196.

Somma, R., 2006. The south-western side of the Calabrian Arc (Peloritani Mountains): Geological, structural and AMS evidence for passive clockwise rotations. Journal of Geodynamics 41, 422-439.

Spraggins, S.A. and Dunne, W.M., 2002. Deformation history of the Roanoke Recess, Appalachian, USA. Journal of Structural Geology 24, 411-433.

Stamatakos, J. and Hirt, A.M., 1994. Paleomagnetic considerations of the development of the Pennsylvania Salient in the Central Appalachians. Tectonophysics 231, 237-255.

Stamatakos, J., Hirt, A.M. and Lowrie, W., 1996. The age and timing of folding in the Central Appalachians from paleomagnetic results. Geological Society of America Bulletin 108, 815-829.

Steltenpohl, M.G. and Kunk, M.J., 1993. $^{40}Ar/^{39}Ar$ thermochronology and

Alleghanian development of the southernmost Appalachian Piedmont, Alabama and southwest Georgia. Geological Society of America Bulletin 105, 819-833.

Steltenpohl, M.G., Goldberg, S.A., Hanley, T.B. and Kunk, M.J., 1992. Alleghanian development of the Goat Rock fault zone, southernmost Appalachians; temporal compatibility with the master decollement. Geology 20, 845-848.

Symons, D.T.A. and Stratakos, K.K., 2002. Paleomagnetic dating of Alleghenian orogenesis and mineralization in the Mascot-Jefferson City zinc district of East Tennessee, USA. Tectonophysics 348, 51-72.

Thomas, W.A. and Bayona, G., 2005. The Appalachian thrust belt in Alabama and Georgia: Thrust-belt structure, basement structure, and palinspastic reconstruction. Geological Survey of Alabama Monograph 16, 48pp.

van der Pluijm, B.A., Hall, C.M., Vrolijk, P.J., Pevear, D.R. and Covey, M.C., 2001. The dating of shallow faults in the Earth's crust. Nature 412, 172-175.

Weil, A.B. and Sussman, A.J., Classification of curved orogens based on the timing relationships between structural development and vertical-axis rotations, In: Weil, A.B. and Sussman, A.J., Editors, 2004. *Orogenic curvature; Integrating paleomagnetic and structural analyses.* Geological Society of America Special Paper 383*, 1-17.*

Wilson, J.T., 1966. Did the Atlantic close and then re-open? Nature 211, 676-681.

Wise, D.U., 2004. Pennsylvania salient of the Appalachians: a two-azimuth transport model based on new compilations of Piedmont data. Geology 32, 777-780.

Woodward, H.P., 1957. Chronology of Appalachian folding. American Association of Petroleum Geologists 41, 2312-2327.

CHAPTER II

DIFFERENTIAL DISPLACEMENT AND ROTATION IN THRUST FRONTS: A MAGNETIC, CALCITE TWINNING AND PALINSPASTIC STUDY OF THE JONES VALLEY THRUST, ALABAMA, US APPALACHIANS

ABSTRACT

To test whether a displacement gradient along a curved fault structure requires rotation, we studied the northeast-striking, northwest-verging, large-displacement Jones Valley thrust fault of the Appalachian thrust belt in Alabama. Paleomagnetism, anisotropy of magnetic susceptibility (AMS) and calcite twinning analysis, complemented by balanced cross-sections, were used to evaluate the presence and magnitude of any rotation. Remanence directions from the Silurian Red Mountain Formation reveal a prefolding magnetization acquired in the Pennsylvanian, whereas magnetic analysis shows a strong, bedding-parallel compaction fabric with a tectonic lineation. Paleomagnetic directions and magnetic lineations reveal no relative rotation between the hanging wall and footwall of the thrust fault. Rather than rotation, therefore, we interpret the Jones Valley thrust sheet as a structure that developed in a self-similar fashion, with lateral growth of the fault surface occurring coincident with growth into the foreland.

INTRODUCTION

Rotations have been recognized as common features in most foreland thrust belts (McCaig and McClelland, 1992; Allerton, 1998; Macedo and Marshak, 1999; Marshak, 2004; Weil and Sussman, 2004; Sussman et al., 2004). On the scale of individual thrust sheets, thrust displacement gradients along strike of a structure are often cited as the cause of that rotation (Bates, 1989; Allerton et al., 1993; Allerton, 1998; Bayona et al., 2003; Pueyo et al., 2004; Sussman et al., 2004; Soto et al., 2006; Oliva-Urcia and Pueyo, 2007), but this hypothesis has remained a topic of debate. Identifying rotations in thrust sheets is also important for understanding the three-dimensional development of thrust belts and has implications for evolution on the orogenic scale (i.e., oroclinal bending; Marshak, 2004; Weil and Sussman, 2004; Sussman et al., 2004). Along rotated thrust sheets, traditional methods of restoring balanced cross-sections underestimate the amount of true displacement, because plane strain conditions do not apply. Whether rotations predicted from variations in displacement along strike, as seen in a series of strike perpendicular balanced cross-sections, necessitate significant vertical-axis rotations has been tested only in a few cases. This provided the motivation for our integrated study of the Jones Valley thrust fault in the southern US Appalachians.

Rotations have been recognized in many thrust belts, especially through paleomagnetism (e.g., McCaig and McClelland, 1992; Bayona et al., 2003; Sussman et al., 2004; Satolli et al., 2005), which has a resolution of about 10^{o}, depending on the quality of the data (Weil and Sussman, 2004). Many of these investigations, however, focused on regional kinematics in areas where significant variation in

strike of bedding, faults and fold axial surfaces is observed (Schwartz and Van der Voo, 1984; Weil et al., 2000; 2001; Speranza et al., 2003). Less common are studies that explore the role of rotations in the evolution of an individual thrust sheet, which often do not display a large variation in strike orientation between the hanging wall and footwall. In the Subbetic Zone of southern Spain, Allerton (1994) showed that 68° of rotation on an individual structure was accommodated by a change in thrust displacement of 8.5 km over 3.7 km along strike. While this example is perhaps extreme, the evolution of the Santo Domingo anticline, an 80 km long structure in the External Sierras of the Southern Pyrenees (Pueyo et al., 2002; 2004; Oliva-Urcia and Pueyo, 2007), may be a more common case. In that area, the thrust displacement gradient from a series of four balanced cross-sections predicts a clockwise rotation that is matched by the ~25° rotation seen in paleomagnetic analysis.

Relative rotations can be identified via other methods other than paleomagnetism. Magnetic lineations determined from anisotropy of magnetic susceptibility (AMS) can also be used for identification of vertical-axis rotations (Somma, 2006; Cifelli et al., 2004). Additionally, a method not using magnetic properties for recognizing rotations involves paleostress orientations from analysis of calcite twins (e.g., Craddock et al., 1988; Kollmeier et al., 2000; Ong et al., 2007). Changes in the orientations of other pre-thrusting features such as cleavage, fractures and paleocurrent data can also be used (Nickelsen, 1979; Gray and Mitra, 1993; Apotria, 1995).

The Jones Valley thrust sheet in central Alabama (Figure 2.1) offers an excellent opportunity to study the role, if any, of rotation in the formation of a curved fault structure. On the basis of restoration of balanced cross-sections described in this paper, the Jones Valley thrust fault with the associated detachment fold from which it emerged, progressively increases in displacement along strike over ~80 km, where it is appears to decrease in displacement and is obscured by a cover of younger sediments to the southwest. A minimum rotation of 15° and upwards of 23° would be required to accommodate this displacement change. We considered this possibility by testing the hypothesis that the displacement gradient is the result of the self-similar evolution of the detachment fold and thrust rather than an artifact of rotation.

STRUCTURAL SETTING

Appalachian foreland thrust belt

The study area lies within the Appalachian foreland thrust belt in Alabama (Figure 2.1a) and is characterized by late Paleozoic (Alleghanian) deformation in the form of large scale, northeast-striking, generally northwest-verging thrust faults and associated folds (Rodgers, 1970; Hatcher et al., 1989; Thomas and Bayona, 2005). To the northwest, the belt is bounded by the Black Warrior foreland basin, consisting of late Paleozoic undeformed strata, and to the southeast, by the metamorphic thrust sheets of the Talladega slate belt and the Piedmont (Thomas and Bearce, 1986; Tull, 1998).

Figure 2.1: (A) Map of Alleghanian thrust belt in Alabama and associated features (Redrawn from Thomas and Bayona, 2002). (B) Geologic map of study area based on Szabo et al. (1988). Lines labeled 13 – 18 represent cross-section lines of Figure 2.2. OV – Opossum Valley thrust fault; JV – Jones Valley thrust; Paleomagnetic (circles) from both this study and Hodych et al (1985) and calcite twinning (triangles) sites are also shown.

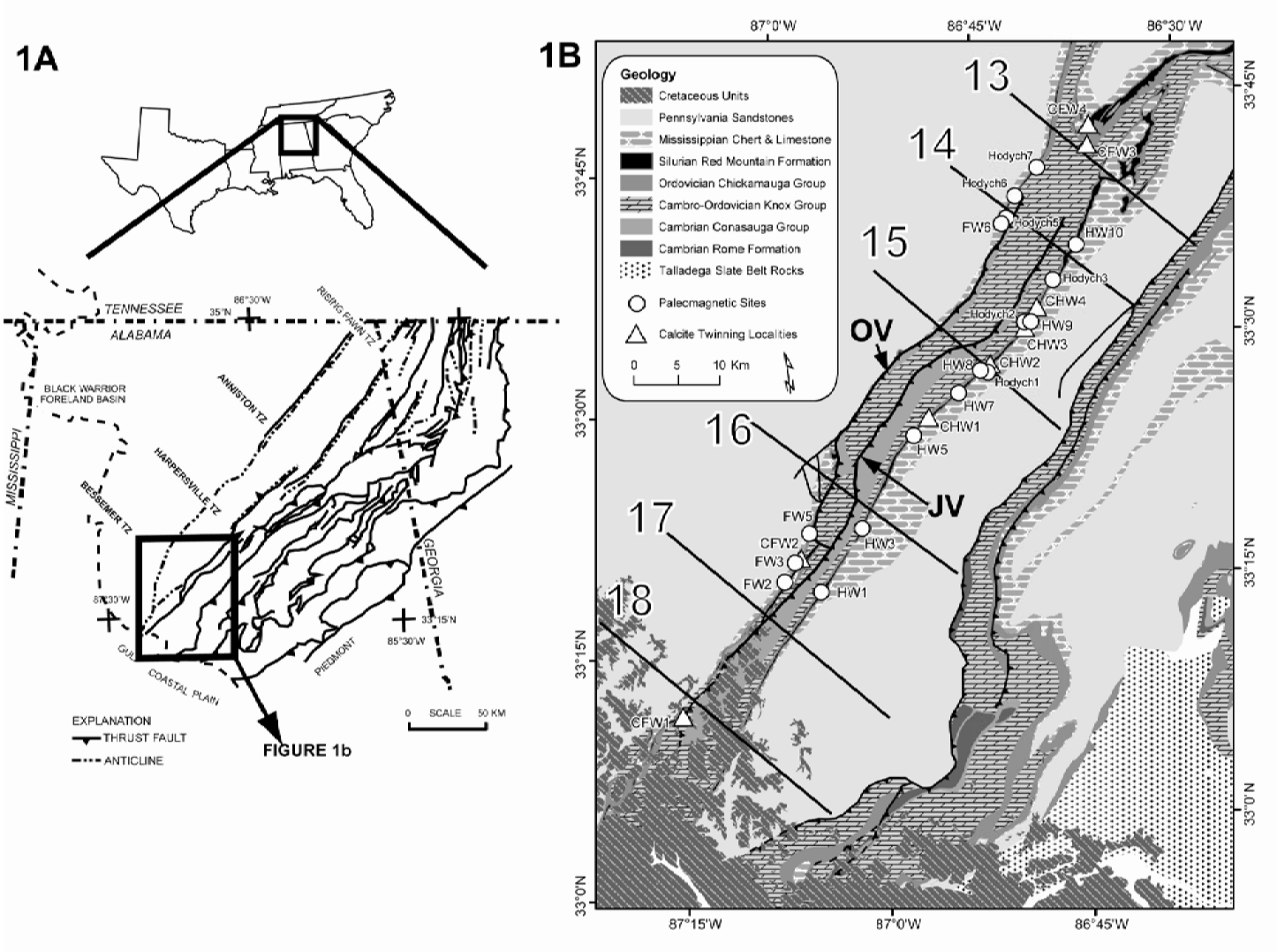
1A
TENNESSEE
ALABAMA
86°30'W
35°N
BLACK WARRIOR FORELAND BASIN
MISSISSIPPI
ANNISTON TZ
RIDING FAWN TZ
HARPERSVILLE TZ
BESSEMER TZ
GEORGIA
87°30'W
33°15'N
85°30'W
PIEDMONT
COASTAL PLAIN
0 SCALE 50 KM
EXPLANATION
THRUST FAULT
ANTICLINE
FIGURE 1b
1B
87°0'W
86°45'W
86°30' W
33°45'N
33°30'N
33°15'N
33°0'N
87°15'W
Geology
Cretaceous Units
Pennsylvania Sandstones
Mississippian Chert & Limestone
Silurian Red Mountain Formation
Ordovician Chickamauga Group
Cambro-Ordovician Knox Group
Cambrian Conasauga Group
Cambrian Rome Formation
Talladega Slate Belt Rocks
Palecmagnetic Sites
Calcite Twinning Localities
0 5 10 Km
13
14
15
16
17
18
OV
JV
CFW4
CFW3
Hodych7
Hodych6
Hodych5
FW6
HW10
Hodych3
CHW4
Hodych2
HW9
CHW3
HW8
CHW2
Hodych1
HW7
CHW1
HW5
FW5
HW3
CFW2
FW3
FW2
HW1
CFW1

Jones Valley thrust fault

The large-displacement Jones Valley thrust fault and the associated Birmingham anticlinorium (Figures 2.1b & 2.2) are in the southernmost exposed part of the Appalachian thrust belt. The Jones Valley thrust is a northeast-striking, northwest-verging thrust fault (Szabo et al., 1988) acting as the roof of a ductile duplex (defined as mushwad; Thomas, 2001; Thomas and Bayona, 2005), which consists of tectonically thickened Cambrian shales in the core of the Birmingham anticlinorium. The location of the Jones Valley thrust ramp is dictated by a down-to-the-southwest basement normal fault beneath the allochthon. Ahead of the Jones Valley thrust, within the anticlinorium, the Opossum Valley thrust fault (Figures 2.1b and 2.2a), a footwall splay, parallels the Jones Valley thrust; however, at the Bessemer transverse zone, the Opossum Valley thrust sheet ends abruptly at a lateral ramp. The footwall of the Jones Valley/Opossum Valley thrust system within the forelimb of the Birmingham anticlinorium is continuous and steeply dipping to overturned to the northwest, whereas the hanging wall is gently dipping to the southeast and forms the trailing limb of the anticlinorium. The asymmetry of the anticlinorium and presence of the Palmerdale/Bessemer ductile duplex defines the Birmingham anticlinorium as a complex detachment fold offset by the Jones Valley/Opossum Valley thrust system (Thomas, 2001; Thomas and Bayona, 2005). Little difference exists between the strike of bedding in the footwall and hanging wall along the length of the fault except for a minor variation at the position of the Bessemer transverse zone. Bayona et al. (2003) interpreted rotations, using changes in local strike orientations at lateral ramps, as well as thrust displacement

gradients in transverse zones to the northeast of the study area. However, similar to the work of Allerton (1994), the lack of significant variation in map-view strike orientation between hanging wall and footwall of the Jones Valley thrust gives no information as to the presence or amount of rotation.

In the northeast, the Jones Valley thrust sheet emerges from a small anticline in the crest of the Birmingham anticlinorium. The appearance of the Jones Valley thrust fault in the northeast is along the alignment of the cross-strike links in the Harpersville transverse zone. Along strike to the southwest, the Jones Valley thrust fault crosses the Bessemer transverse zone, where a lateral ramp accommodates displacement at the end of the leading Opossum Valley thrust fault. Farther to the southwest, other than the small displacement Blue Creek fault and a very minor backthrust, the Jones Valley thrust fault is the only structure accommodating shortening within the anticlinorium. At the southwest end of the study area, the Jones Valley thrust fault and associated Birmingham anticlinorium are covered by Cretaceous coastal plain sediments.

Displacement along the Jones Valley thrust fault

A series of previously published cross-sections in the Appalachian thrust belt of Alabama allow comparison of displacement magnitudes along strike for the Jones Valley thrust fault (Figure 2.2; Table 2.1)(Thomas and Bayona, 2005). The cross-sections were constructed perpendicular to thrust belt strike and based on seismic profiles, outcrop data and wells. Palinspastic restoration was completed using a

Figure 2.2: Cross-section lines (modified from Thomas and Bayona, 2005) used to determine displacement variation. The Jones Valley thrust sheet terminates between cross-sections 13 and 14 and increases in displacement to the southwest in cross-sections 17 and 18.

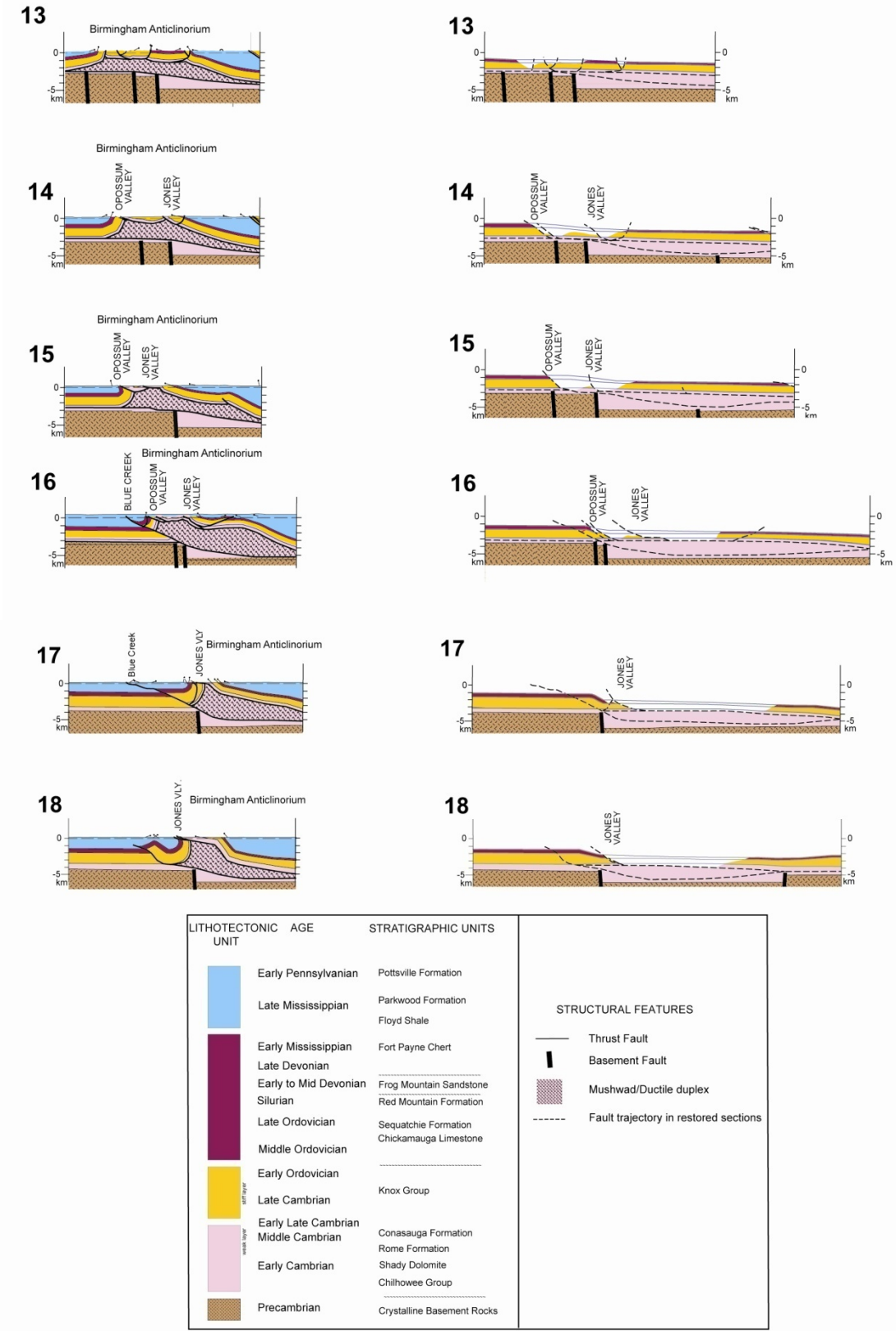
13
Birmingham Anticlinorium
0
-5
km
13
0
0
-5
km
-5
km
Birmingham Anticlinorium
14
OPOSSUM VALLEY
JONES VALLEY
0
-5
km
14
OPOSSUM VALLEY
JONES VALLEY
0
0
-5
km
-5
km
Birmingham Anticlinorium
15
OPOSSUM VALLEY
JONES VALLEY
0
-5
km
15
OPOSSUM VALLEY
JONES VALLEY
0
0
-5
km
-5
km
Birmingham Anticlinorium
16
BLUE CREEK
OPOSSUM VALLEY
JONES VALLEY
0
-5
km
16
OPOSSUM VALLEY
JONES VALLEY
0
0
-5
km
-5
km
17
Blue Creek
JONES VLY
Birmingham Anticlinorium
0
-5
km
17
JONES VALLEY
0
0
-5
km
-5
km
18
JONES VLY.
Birmingham Anticlinorium
0
-5
km
18
JONES VALLEY
0
0
-5
km
-5
km
LITHOTECTONIC UNIT
AGE
STRATIGRAPHIC UNITS
Early Pennsylvanian
Pottsville Formation
Late Mississippian
Parkwood Formation
Floyd Shale
Early Mississippian
Fort Payne Chert
Late Devonian
Early to Mid Devonian
Frog Mountain Sandstone
Silurian
Red Mountain Formation
Late Ordovician
Sequatchie Formation
Chickamauga Limestone
Middle Ordovician
Early Ordovician
Knox Group
Late Cambrian
Early Late Cambrian
Middle Cambrian
Conasauga Formation
Rome Formation
Early Cambrian
Shady Dolomite
Chilhowee Group
Precambrian
Crystalline Basement Rocks
STRUCTURAL FEATURES
Thrust Fault
Basement Fault
Mushwad/Ductile duplex
Fault trajectory in restored sections

combination of bed-length and area-balancing techniques (e.g. Dahlstrom, 1969; Marshak and Mitra, 1988).

While displacement estimates in the southern Appalachians are not as well constrained as those in other, younger thrust belts (e.g., Pyrenees, Wyoming-Idaho, Taiwan belts) due to the lack of preserved hanging wall cutoffs, the series of cross-sections (Figure 2.2; Thomas and Bayona, 2005) provides estimates of minimum displacement on the Jones Valley thrust fault. A comparison of the palinspastically restored cross-sections of the Jones Valley thrust sheet shows a displacement increase of greater than 20 km from the northeast termination (cross-sections 13 and 14) to the southwest (cross-sections 17 and 18). Thrust displacement on is near zero at the northeast termination (cross-sections 13 and 14), where regional shortening is largely accommodated by folding in the Birmingham anticlinorium. Displacement increases to more than 20 km farther southwest (cross-sections 17) and appears to decrease slightly farther to the southwest (cross-sections 18). A minimum vertical-axis rotation of approximately 15° could produce this strike-parallel displacement gradient. This estimate is a minimum:

1) Rotation would entail out-of-plane motion of the thrust sheet, thereby underestimating displacement values from the strike-perpendicular cross-sections
2) Hangingwall cutoffs are not preserved and displacement estimates are at a minimum in the southwestern section (cross-section 17). However, estimates are not a minimum in the northeastern section (cross-sections 13 and 14) where much of the shortening is taken up in the folding of the

Birmingham anticlinorium. This situation would, therefore allow a greater angle of rotation

3) Thermal data from vitrinite reflectance of Pennsylvanian coals suggest a high temperature anomaly in the eroded footwall of the Jones Valley thrust sheet (Winston, 1990; O'Hara et al., 2006). Assuming that the thermal anomaly results from a greater cover due to additional tectonic burial by the Jones Valley thrust sheet, greater displacement and hence rotation magnitude would be expected.

While the lower limit of the postulated rotation is near the resolution limit for paleomagnetism (~10°), the high quality of the paleomagnetic data from this study allows for the determination of role of vertical-axis rotations in the evolution of the Jones Valley thrust sheet.

Assuming negligible internal shortening, which is typical of foreland thrust sheets of the southern Appalachians (House and Gray, 1982; Hatcher et al, 1989), one interpretation of the displacement geometry of the thrust sheet involves a vertical-axis rotation of 15°-23° of the Jones Valley thrust sheet toward the foreland, whereas an alternative scenario simply involves differential translation on the thrust (Figure 2.3). The rotation model has a fixed hinge point and treats the thrust sheet as a rigid body. Conversely, the differential translation model requires that there is no fixed hinge and that the thrust grew laterally while displacing toward the foreland. This self-similar style growth (Elliott, 1976; Fischer and Woodward, 1992) would require internal deformation of the thrust sheet in the form of minor

Cross-section	Distance from Tip (km)	Displacement(km)
14	4.8	2.0
15	20.9	5.0
16	42.4	14.0
17	59.9	21.0
18	73.2	16.0

Table 2.1: Table presenting displacement data derived from cross-sections and length from tip data derived from the map. Displacements are minima, as hanging wall cutoffs are not preserved in the Appalachians.

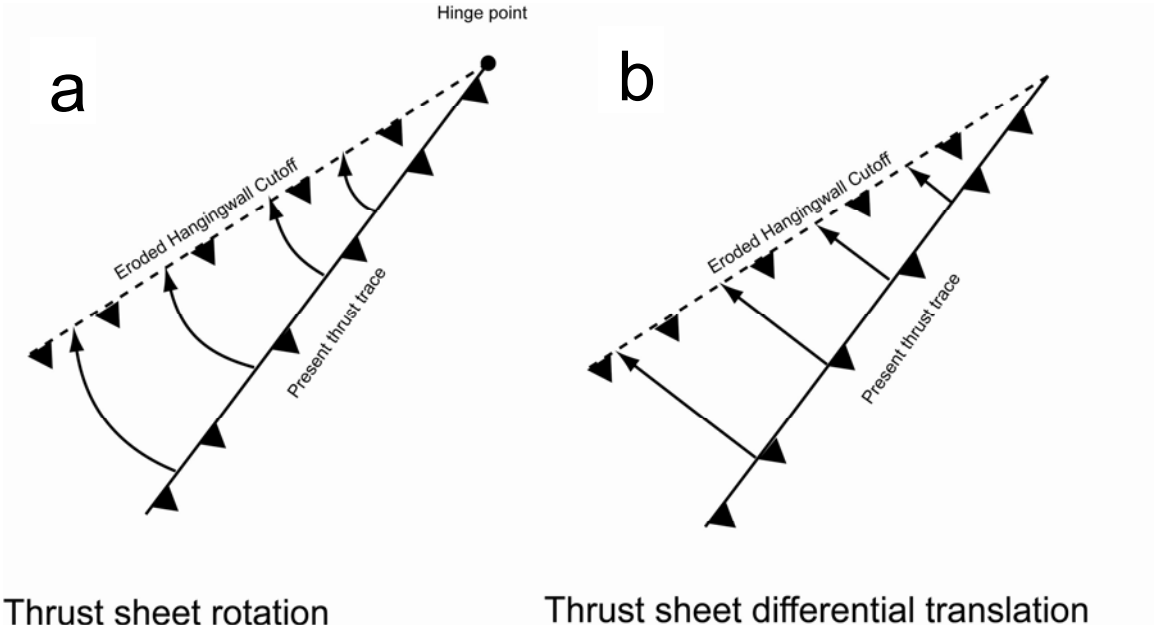

Figure 2.3: Schematic illustration showing two scenarios for the development of a thrust sheet with the same displacement gradient. In (a), the thrust sheet rotates to its final position. In (b), the thrust sheet displaces differentially along strike.

shear strain, with implications for the continuity of the thrust sheet (Wilkerson, 1992).

The relatively straight frontal ramp of the Jones Valley thrust fault, the large displacement gradient from northeast to southwest and the presence of suitable rock types allows for a relatively simple test of the role of vertical-axis rotation for the evolution of the Jones Valley thrust sheet. To investigate both the occurrence and amount of rotation, we employ paleomagnetic and anisotropy of magnetic susceptibility (AMS) analysis of the Silurian Red Mountain Formation, as well as calcite twinning of the underlying Chickamauga Group limestones.

UNIT DESCRIPTION

The stratigraphy of the study area is the regionally characteristic succession in most of the southern Appalachians (e.g. Butts, 1926; Chowns and McKinney, 1980; Thomas, 1977). Lower to Middle Cambrian sediments (Chilhowee Group, Shady Dolomite, Rome Formation and Conasauga Formation) associated with Iapetan rifting overlie faulted Precambrian basement and represent the regional basal detachment level (Thomas, 1991). Mudstones and limestones of the Middle Cambrian Conasauga Formation form the oldest exposed rocks and represent the major ductile unit involved in duplex development. The Cambro-Ordovician Knox Group dolomites and limestones form the regional stiff layer contained in thrust sheets (Thomas and Bayona, 2005).

Unconformably overlying the Knox Group are limestones of the Middle to Upper Ordovician Chickamauga Group. The Chickamauga Group consists of a range

of limestone units, including calcareous mudstones, peloidal grainstones and fossiliferous grainstones (Rindsberg and Osborne, 2001; Rindsberg et al., 2003). For calcite twinning analysis, emphasis was placed on sampling the coarser grainstones.

The Red Mountain Formation is a heterogeneous clastic unit that comprises the entire package of Silurian stratigraphy within the thrust belt in Alabama (Chowns and McKinney, 1980). It unconformably overlies the Chickamauga Group limestones. Biostratigraphic studies indicate that the unit ranges from Early Silurian (Llandoverian) age (Berry and Boucot, 1970) to Late Silurian (Pridolian) age (Berdan et al., 1986) with various internal disconformities (Rindsberg et al., 2003). The lithology of the Red Mountain Formation includes massive and laminated reddish hematitic sandstones, oolitic ironstones, interbedded shales and gray sandstone, lesser pebble conglomerate beds and some minor limestone lenses. Sampling of the Red Mountain Formation focused on the hematitic sandstones and ironstones best suited for paleomagnetic analysis. In the study region, the Red Mountain Formation is unconformably overlain by the Devonian Chattanooga Shale, Mississippian Maury Shale or the Mississippian Fort Payne Chert, although thin units of the Devonian (Frog Mountain Formation) are present in some locations. The youngest units involved in the deformation are Pennsylvanian clastic deposits.

PALEOMAGNETISM AND MAGNETIC SUSCEPTIBILITY

Methods

Samples were collected from eleven sites in the Red Mountain Formation along the strike of the Jones Valley thrust sheet. Sampling focused on red

sandstones and ironstones that had been successfully analyzed in past studies of the formation (Perroud and Van der Voo, 1984; Hodych et al., 1985). Four sites are located on the northwest-dipping to overturned footwall and seven sites on the southeast-dipping hanging wall (Figure 2.1b). Site selection was controlled by both limited outcrop availability in this area due to the high degree of weathering, and position along strike with respect to the Jones Valley thrust fault. Between seven and twelve 2.5 cm diameter samples were collected at each site using a portable gasoline powered drill, so 106 total samples were collected. Bedding attitude and core orientations were measured using a magnetic compass. Prior to analysis, the samples were cut into 2.5 x 2.2 cm cylindrical specimens at the University of Michigan's Paleomagnetic Laboratory for paleomagnetic and anisotropy of magnetic susceptibility (AMS) work.

All 2.5 x 2.2 cm specimens of the Red Mountain Formation were first measured for anisotropy of magnetic susceptibility (AMS). Specimens were measured in the fifteen-position method of Jelinek (1978) on a Geofyzika Brno Kappabridge KLY-2.03 susceptibility-bridge at a frequency of 920 Hz (coil sensitivity is approximately 5×10^{-7} SI). Analysis was performed using linear perturbation analysis producing a statistical bootstrap of the data using the 'bootams' program of Tauxe (1998). Bootstrap eigenvectors are plotted and displayed as a smear of points on a stereonet (e.g., Pares and van der Pluijm, 2002a). To infer relative contributions of ferromagnetic (generally magnetite and hematite) and paramagnetic (commonly phyllosilicate) grains to the susceptibility, bulk susceptibility was measured both at room temperature (~290K) and at the

temperature of liquid nitrogen (77K). Bulk susceptibility of ferromagnetic grains does not change at low temperature while that of paramagnetic grains increases ~3.8 times at 77K according to the Curie-Weiss law (Richter and van der Pluijm, 1994; Pares and van der Pluijm, 2002b).

Thermal demagnetization was carried out on all samples within a magnetically shielded, low-field room using an Analytical Service Co. (ASC) thermal demagnetizer. Samples were measured in a three-axis, cryogenic 2G Enterprises Model 755 Superconducting magnetometer after each heating step, with stepwise demagnetization ranging from 100°C and 680°C. Demagnetization was discontinued when the sample intensity approached zero percent of the natural remanent magnetization (NRM) or became erratic because of spurious magnetizations acquired during the cooling process.

Principal component analysis (Kirschvink, 1980) of linear vectors selected from orthogonal projection demagnetization plots (Zijderveld, 1967) was used to calculate the characteristic remanent magnetization (ChRM) with the SuperIAPD software package (Torsvik et al., 1999). Individual sample ChRM directions were used to determine site means using Fisher's (1953) method. The age of magnetization relative to deformation was tested using a fold-test on the site mean directions (McElhinny, 1964).

Paleomagnetic results

Intensities of the NRM for the Red Mountain Formation vary between 10 and 220 mA/m. Stepwise thermal demagnetization typically reveals univectorial decay

Figure 2.4: Representative thermal demagnetization plots of the Red Mountain Formation in geographic coordinates and associated intensity plots. Intensity plots show normalized intensity versus temperature in degrees Celsius. In the demagnetization plots, closed (open) symbols represent vector endpoints plotted in the horizontal (vertical) plane. Temperature steps are in degrees Celsius. A) Representative footwall sample showing the southeast and up direction. B and C) Representative hanging wall samples showing southeast and down direction. Sharp decreases in intensity occur near 640°C in most samples. Ticks represent 50 mA/m.

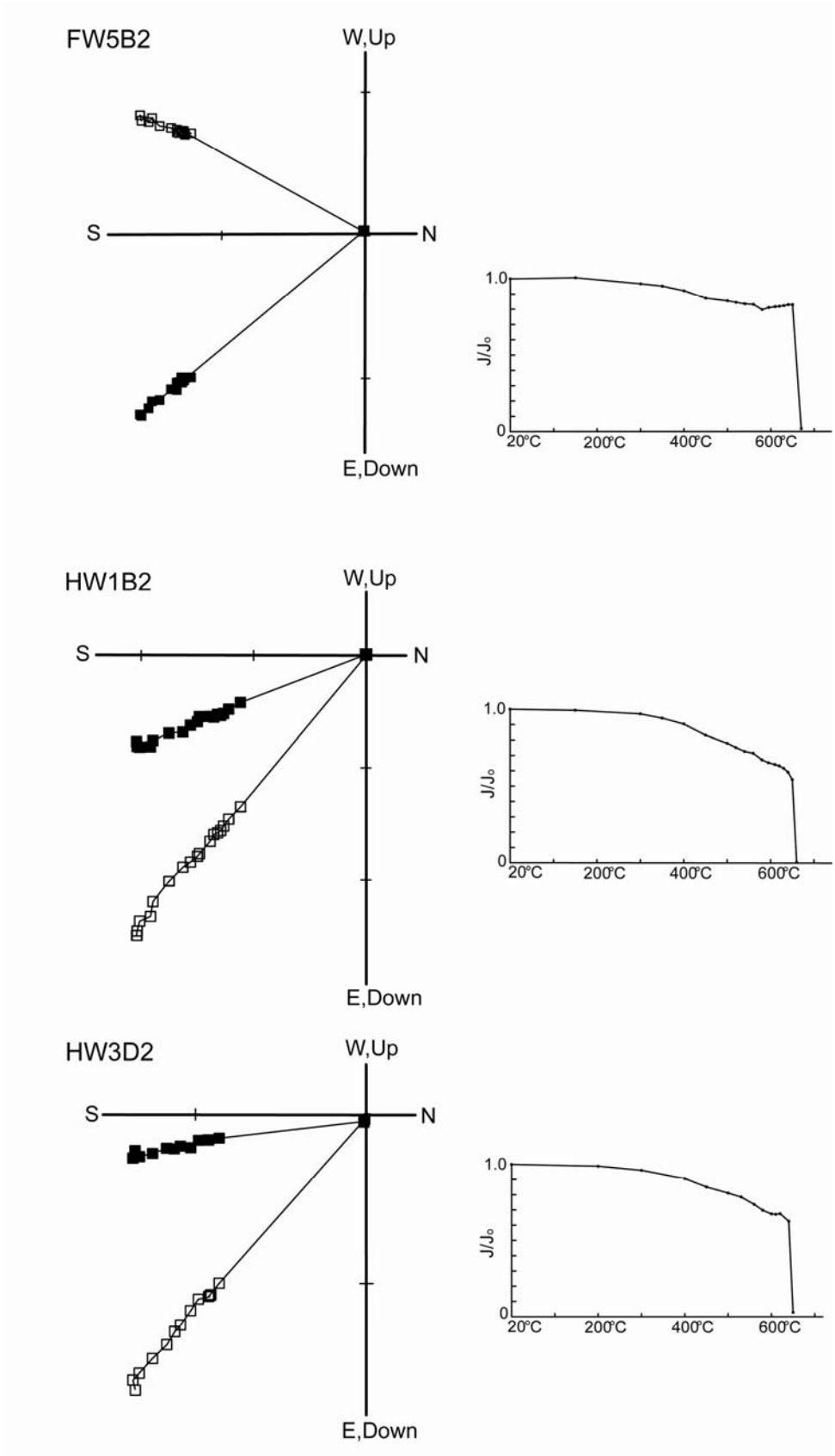
FW5B2
W,Up
S
N
E,Down
1.0
J/Jo
0
20°C
200°C
400°C
600°C
HW1B2
W,Up
S
N
E,Down
1.0
J/Jo
0
20°C
200°C
400°C
600°C
HW3D2
W,Up
S
N
E,Down
1.0
J/Jo
0
20°C
200°C
400°C
600°C

Table 2.2: Paleomagnetic results from the Red Mountain Formation. Mean directions are calculated from site means (Fisher, 1953); N/N_o, number of samples (sites) accepted/studied; Dec, declination; Inc, inclination; $\alpha 95$, radius of confidence circle in degrees; *k*, precision parameter (Fisher, 1953). Means calculated with and without sites from Hodych et al (1985). Site FW2 dip is 110°, indicating overturned bedding.

	Latitude	Longitude	Strike	Dip	N/No	Dec Insitu	Inc Insitu	Dec Tilt	Inc Tilt	α95	k
Footwall											
FW2	33.304°N	87.076°W	218°	110°	7/7	222.2°	-61.8°	157.3°	15.6°	14.9°	17.27
FW3	33.323°N	87.057°W	238°	40°	8/9	149.9°	-20.2°	149.9°	19.8°	5.3°	110.31
FW5	33.352°N	87.037°W	193°	58°	10/10	137.6°	-25.7°	136.9°	23.5°	7.2°	45.53
FW6	33.646°N	86.743°W	190°	75°	7/9	149.9°	-42.6°	142.5°	24.1°	6.3°	92.69
Mean	-	-	-	-	**4/4**	-	-	**146.8°**	**20.9°**	**10.5°**	**77.88**
Hodych5	33.645°N	86.743°W	185°	73°	8	145.5°	-33.5°	138.3°	20.2°	4.5°	153
Hodych6	33.657°N	86.738°W	207°	52°	9	149.6°	-18.9°	151.3°	25.4°	9.4°	31
Hodych7	33.678°N	86.717°W	214°	41°	8	153.6°	-15.8°	154.4°	20.1°	6.3°	77
Mean with Hodych sites	-	-	-	-	**7/7**	-	-	**147.3°**	**21.4°**	**6.1°**	**97.96**
Hangingwall											
HW1	33.290°N	87.032°W	35°	38°	12/12	169.5°	57.4°	149.7°	25.3°	5.2°	70.04
HW3	33.349°N	86.970°W	32°	34°	9/9	163.6°	44.6°	151.8°	18.3°	7.6°	46.69
HW5	33.437°N	86.890°W	42°	20°	11/12	154.2°	25.0°	152.0°	6.6°	6.1°	57.23
HW7	33.474°N	86.826°W	35°	20°	9/9	146.5°	36.6°	143.0°	17.7°	4.4°	140.66
HW8	33.496°N	86.789°W	62°	18°	9/9	157.0°	38.4°	156.2°	20.5°	5.7°	81.15
HW9	33.536°N	86.725°W	58°	15°	11/11	155.2°	29.9°	154.5°	15.0°	5.0°	83.53
HW10	33.610°N	86.654°W	47°	12°	9/9	161.7°	27.0°	159.8°	16.0°	5.7°	83.24
Mean	-	-	-	-	**7/7**	-	-	**152.4**	**17.1°**	**5.7°**	**112.5**
Hodych1a	33.495°N	86.788°W	57°	20°	5	150.9°	40.3°	150.2°	20.3°	2.5°	929
Hodych1c	33.495°N	86.788°W	54°	21°	3	150°	37.1°	149°	16.2°	3.4°	1284
Hodych1d	33.495°N	86.788°W	54°	21°	11	152°	37.9°	150.6°	17.1°	3.7°	156
Hodych1e	33.495°N	86.788°W	54°	21°	3	146°	37.1°	145.7°	16.1°	6.2°	396
Hodych1f	33.495°N	86.788°W	45°	20°	3	155.1°	37.5°	151.7°	18.5°	9.5°	171
Hodych2	33.537°N	86.723°W	34°	13°	6	158°	24°	155.6°	13.1°	9°	57
Hodych3	33.560°N	86.707°W	40°	16°	4	152.5°	37.1°	149.2°	22.1°	10.1°	84
Mean with Hodych sites	-	-	-	-	**14/14**	-	-	**151.4°**	**17.4°**	**3.0°**	**181.98**
Overall mean	-	-	-	-	**11/11**	-	-	**150.4°**	**18.5°**	**4.8°**	**92.29**
Overall mean with Hodych sites	-	-	-	-	**21/21**	-	-	**150.2°**	**19.0°**	**3.5°**	**107.74**

of a single magnetic component (Figure 2.4). Heating steps began at 100°C intervals up to 400°C and then were decreased progressively during heating until 10°C intervals were used above 620°C. In general, specimen intensity tends to remain stable up to a range from 640°C to 680°C, where intensity drops suddenly to <20% of the NRM. This high laboratory unblocking temperature (T_{lab}) indicates that hematite is the carrier of the magnetization, as expected.

In situ, site mean directions for the seven hanging wall sites reveal an intermediate down and southeast direction in all sites (Figures 2.4 and 2.5) while in situ footwall site mean directions display intermediate up and southeast directions except for site FW2, which has a steeply up and southwest direction. After tilt correction, the site means cluster in a southeast down direction of D = 150.4°, I = 18.5°, α95 = 4.8° and *k* = 92.29 (Table 2.2). This direction for the Red Mountain Formation agrees with those of two previous studies by Perroud and Van der Voo (1984) and Hodych et al. (1985).

Relative timing of magnetization

To obtain the timing of acquisition of the magnetization, a fold test was carried out on all site means. Progressive unfolding of the site mean directions indicates that the magnetization was acquired prior to tectonic tilt; the precision parameter *k* increases from 3.8 at 0% unfolding to 92.3 at 100% unfolding (Figure 2.5). Because the footwall sites lie on the steeply dipping forelimb and the hanging wall sites are in the gently dipping trailing limb of the Birmingham anticlinorium, a 100% positive fold test implies that the magnetization was acquired prior to

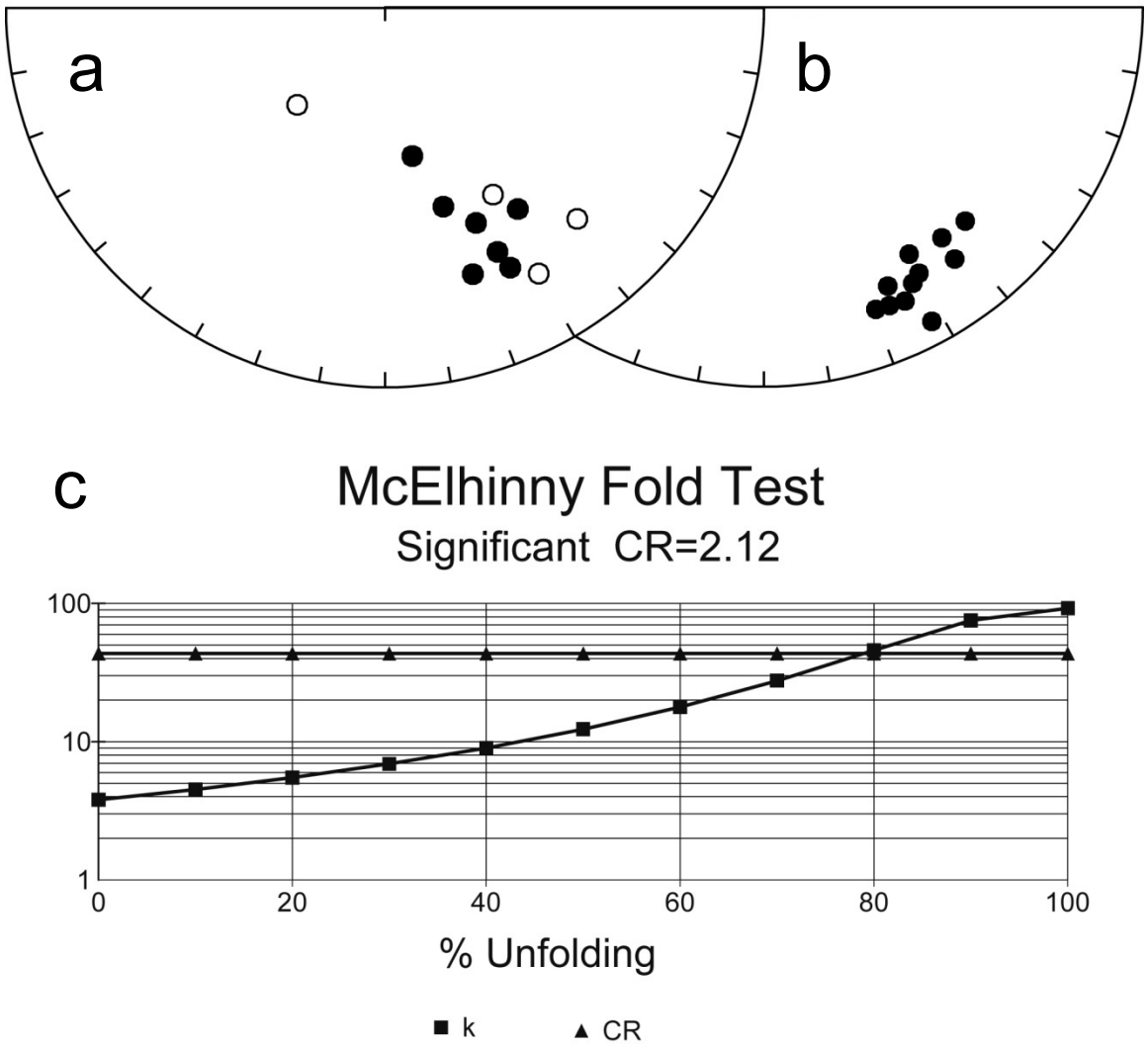

Figure 2.5: (a and b) Equal area projections of site means in geographic (a) and tilt-corrected (b) coordinates. Solid (open) circles represent down (up) directions. (v) Incremental fold test of site means plotting *k* on logarithmic scale versus percent unfolding. Squares represent *k* values and triangles represent the critical ratio (CR) at which *k* values become significant at the 95% confidence level for the number of data entries (McElhinny, 1964).

formation of the anticlinorium. Therefore, because the Jones Valley thrust fault and its frontal imbricate, the Opossum Valley thrust fault, are intimately related to the formation of the Birmingham anticlinorium, the magnetization was acquired prior to motion on the Jones Valley thrust fault.

Although the magnetization is clearly pre-deformation (Figure 2.5), a conglomerate test by Perroud and Van der Voo (1984) showed a well clustered ($k \approx 170$), non-random distribution of directions from pebbles from a conglomerate layer, with a tectonically corrected mean direction similar to the other sites. This implies a post-depositional, remagnetized direction for the Red Mountain Formation. Comparison of our calculated paleopole position (38°N 130°E) with the Laurentian apparent polar wander path (APWP: Van der Voo, 1993) indicates that the Red Mountain Formation acquired a remanence by chemical remagnetization during the Pennsylvanian, which is in agreement with the conclusions of previous workers (Perroud and Van der Voo, 1984; Hodych et al., 1985).

AMS Results

Anisotropy of Magnetic Susceptibility (AMS) of the Red Mountain Formation reveals a compaction foliation in most sites, as indicated by perpendicular orientation of the minimum susceptibility axes (K_{min}) to the bedding plane (Figure 2.6); most AMS ellipsoids display a triaxial shape. This foliation is typically strong and dominates most samples, as indicated by the Flinn diagram (Figure 2.7a). However, in the footwall, site FW2 shows a spread of K_{min} from horizontal to vertical, creating a swath in the bootstrap eigenvector plot (Figure 2.6). Also, site FW5 displays a K_{min} that is bedding-parallel and orthogonal to the trace

Figure 2.6: Lower hemisphere, equal area projections showing AMS tensor properties for each site. Left stereoplot for each site shows calculated sample eigenvectors, with squares representing K_{max}, triangles representing K_{int} and circles representing K_{min}. The right projection is the bootstrapped eigenvectors derived from the data on the left showing a smear of points that better illustrates the tectonic lineation. All projections are in tilt-corrected coordinates

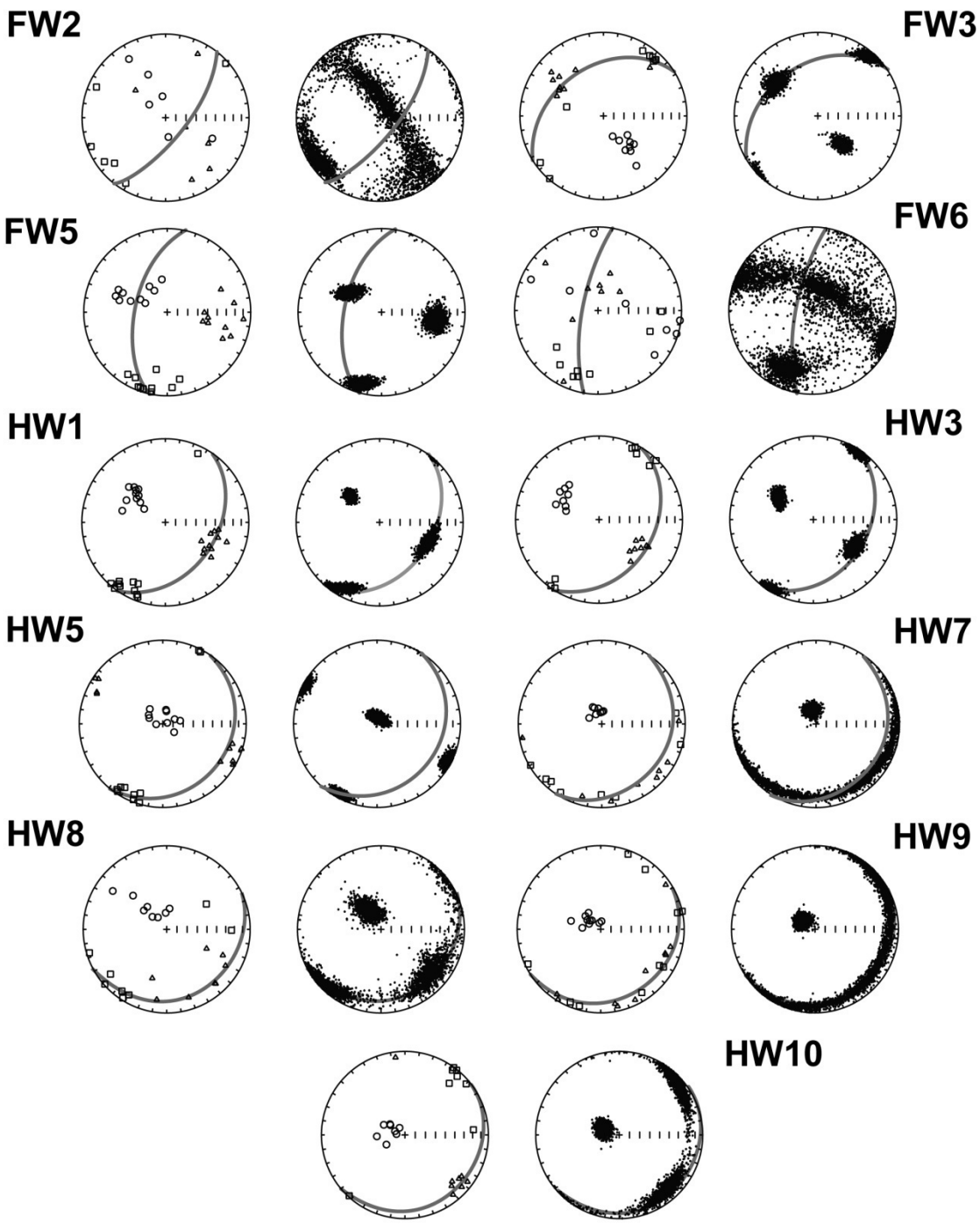
FW2
FW3
FW5
FW6
HW1
HW3
HW5
HW7
HW8
HW9
HW10

	Strike	Dip	N	$\tau 1$	$\tau 1$ T/P	$\tau 2$	$\tau 2$ T/P	$\tau 3$	$\tau 3$ T/P	χ m	L	F	P	T
Footwall														
FW2	218°	110°	7	0.33629	48.4°/15.5°	0.33240	244.1°/74.0°	0.33131	139.5°/4.1°	144.42	1.014	1.005	1.020	0.471
FW3	238°	40°	9	0.33839	222.6°/5.8°	0.33415	312.8°/1.5°	0.32746	57.0°/84.0°	508.46	1.014	1.021	1.035	0.104
FW5	193°	58°	10	0.33725	203.1°/11.7°	0.33363	61.6°/75.1°	0.32912	295.0°/9.0°	252.14	1.012	1.016	1.027	0.140
FW6	190°	75°	9	0.33522	202.0°/22.9°	0.33318	42.7°/65.7°	0.33160	295.3°/7.7°	350.93	1.009	1.008	1.016	0.160
Hangingwall														
HW1	35°	38°	12	0.33590	209.8°/9.1°	0.33432	112.7°/37.7°	0.32978	311.2°/50.8°	371.06	1.005	1.015	1.019	0.445
HW3	32°	34°	9	0.33658	34.5°/3.1°	0.33390	127.1°/40.1°	0.32951	300.8°/49.8°	664.96	1.009	1.014	1.023	0.241
HW5	42°	20°	12	0.33761	206.6°/5.3°	0.33363	116.3°/3.3°	0.32876	354.0°/83.8°	498.02	1.012	1.015	1.027	0.063
HW7	35°	20°	9	0.33857	238.6°/0.7°	0.33805	328.7°/6.7°	0.32338	142.5°/83.2°	802.81	1.004	1.048	1.052	0.807
HW8	62°	18°	9	0.33509	42.4°/1.1°	0.33394	132.5°/4.6°	0.33097	299.1°/85.3°	359.03	1.004	1.017	1.020	0.547
HW9	58°	15°	11	0.33806	40.6°/2.2°	0.33769	131.2°/14.0°	0.32426	301.9°/75.8°	683.64	1.003	1.040	1.044	0.796
HW10	47°	12°	9	0.33567	45.5°/6.7°	0.33423	137.2°/13.9°	0.33010	290.3°/74.5°	223.70	1.005	1.013	1.018	0.421

Table 2.3: Anisotropy of Magnetic Susceptibility (AMS) results from the Red Mountain Formation. N, number of specimens; τ_n, eigenvalues; τ_n T/P, Trend and plunge of eigenvectors in situ; χ_m, mean bulk susceptibility; $L = \bar{\tau}_1/\tau_2$; $F = \bar{\tau}_2/\tau_3$; $P = \tau_1/\tau_3$; $T = 2*(((\log(\tau_2/\tau_3))/(\log(\tau_1/\tau_3)))$

of the Jones Valley thrust fault. This effect occurs during layer-parallel shortening (LPS) that may be expected on the footwall/leading limb of a fault-related fold (Saint-Bezar et al., 2002).

At many sites, the maximum susceptibility axes (K_{max}) are oriented in a dominantly NE-SW orientation that is approximately parallel to the trace of the Jones Valley thrust fault. This intersection lineation is well defined in all footwall sites. On the hanging wall, it is well developed to the southwest at HW1, HW3 and HW5, as well as HW8. The tectonic lineation is less apparent in HW7, HW9 and HW10, where the AMS ellipsoid represents a purely compaction fabric. While all site means from the hanging wall lie in the oblate realm of the Flinn diagram (Figure 2.7a), some footwall site means lie in the prolate domain of the plot, once again indicating greater amounts of LPS in the footwall.

Comparison of the bulk susceptibility at low temperature (~77K) and at room temperature (~290K) reveals a ratio of 1.1 (Figure 2.7b). The lack of variation between low temperature and room temperature bulk susceptibilities indicates that the susceptibility is dominated by ferromagnetic grains. As previously mentioned, the high T_{lab} and sharp drop in intensity during thermal demagnetization signify hematite as the dominant ferromagnetic component. Therefore, the susceptibility is inferred to be dominantly carried by hematite.

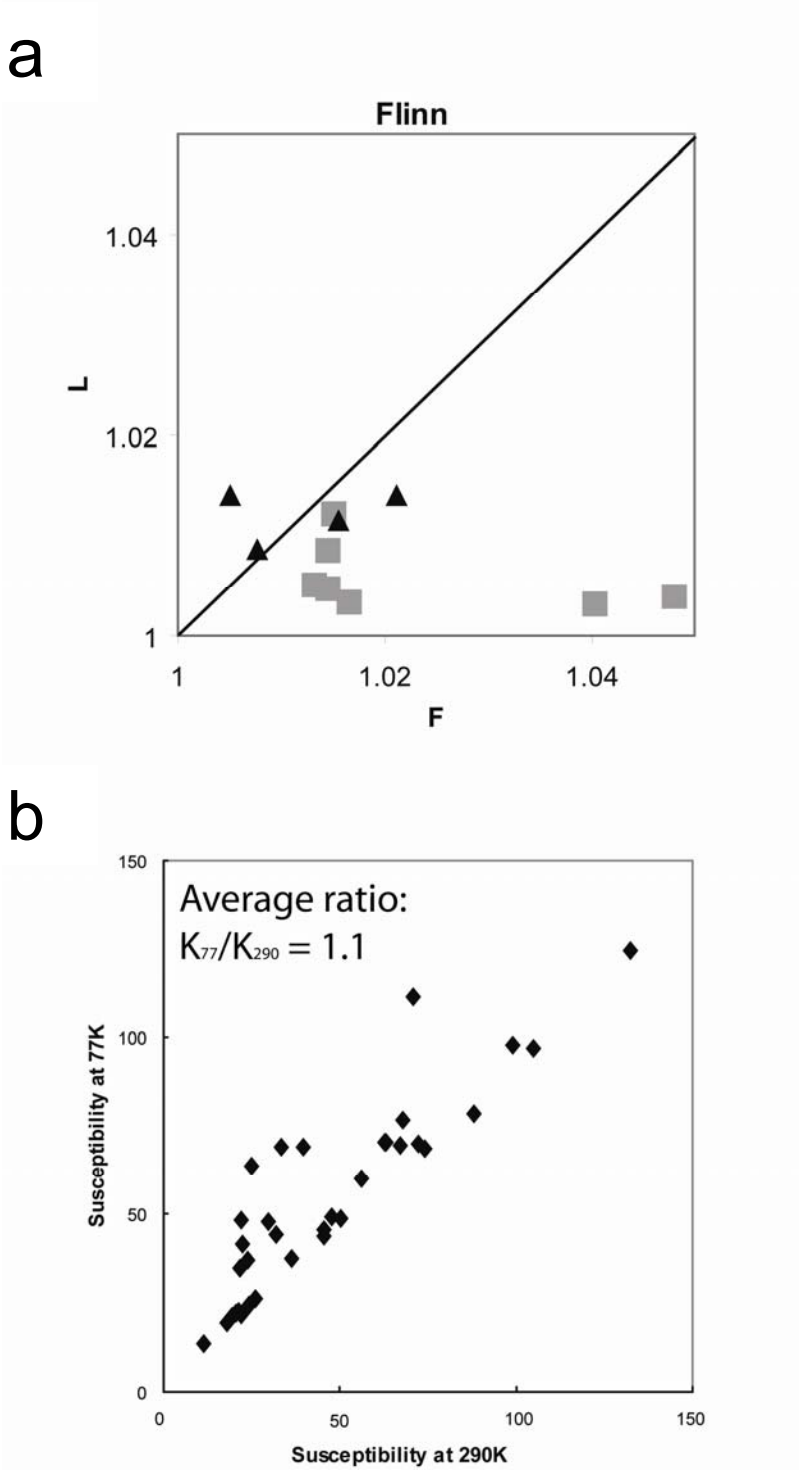

Figure 2.7: (a) Flinn diagram plotting L (K_{int}/K_{max}) and F (K_{int}/K_{min}). Squares (triangles) represent hanging wall (footwall) site means. (b) Bulk susceptibility given in SI units measured at both room temperature (290K) and liquid nitrogen temperature (77K). Average ratio between the two measurements is 1.1.

CALCITE TWINNING

Methods

Both oriented hand samples and standard paleomagnetic cores of fossiliferous limestones of the Middle to Upper Ordovician Chickamauga Group were collected from two sites on the steep to overturned footwall (Sites CFW1-2), two sites to the northeast of the termination of the Jones Valley thrust fault (Sites CFW3-4), and four sites from the hanging wall (Sites CHW1-4) of the Jones Valley thrust sheet for paleostress/strain analysis using calcite twin analysis (Figure 2.1b). Since the formation of calcite twins is a strain hardening process (Teufel, 1980), twinning patterns commonly preserve bedding-parallel shortening, recording the earliest deformation (e.g. Groshong, 1972; 1974; Engelder, 1979; Spang and Groshong, 1981), and therefore act as a passive marker to record rotation (Craddock et al, 1988., Kollmeier et al., 2000, Ong et al., 2007). Because of the limited number of suitable samples that could be analyzed, limestone samples were cut into three mutually perpendicular thin sections to maximize data acquisition and were measured on a Zeiss Universal Stage (U-Stage) microscope. Only straight, continuous twinsets were measured to ensure the most accurate results. The measurements generally followed the procedure in Evans and Groshong (1994). After rotating thin sections into a common coordinate system, compression axes were calculated for each twinset using the method of Turner (1953) and mean paleostress orientations were determined using dynamic analysis of the compression axes (Spang, 1972). Strain tensor determinations using Groshong's (1972; 1974) method were calculated to separate positive and negative expected

	Latitude	Longitude	Strike	Dip	N	Std Error	% Strain	% NEV	N NEV	e1	e1 T/P	e2	e2 T/P	e3	e3 T/p	σ1 T/P	σ2 T/P	σ3 T/P
Footwall																		
CFW1	33.18°N	87.23°W	274°	101° N	60	0.117	1.582	1.7	1	-1.778	195.4°/12.4°	0.525	39.8°/76.4°	1.253	286.6°/5.4°	204.1°/12.2°	73.3°/71.8°	297.0°/13.4°
CFW2	33.33°N	87.05°W	212°	76° W	82	0.137	1.385	0.0	0	-1.533	98.1°/17.8°	0.372	1.6°/19.6°	1.161	227.2°/63.1°	100.0°/14.3°	349.7°/53.7°	199.4°/32.5°
CFW3	33.71°N	86.62°W	193°	4°W	92	0.052	0.615	2.2	2	-0.702	291.8°/1.3°	0.26	21.8°/2.0°	0.442	169.8°/87.6°	292.0°/2.7°	22.4°/8.1°	183.4°/81.5°
CFW4	33.73°N	86.62°W	290°	3°N	134	0.131	1.526	0.0	0	-1.496	96.4°/11.3°	-0.058	278.1°/78.7°	1.554	186.5°/0.3°	96.6°/14.2°	252.3°/74.5°	5.1°/6.1°
Hangingwall																		
CHW1	33.45°N	86.87°W	58°	25° SE	87	0.095	0.987	1.1	1	-0.989	310.7°/12.1°	0.004	218.5°/10.2°	0.985	89.6°/74.1°	307.5°/13.0°	38.0°/2.0°	136.6°/76.8°
CHW2	33.50°N	86.79°W	55°	19° SE	83	0.043	0.828	2.4	2	-0.874	307.0°/5.5°	0.102	216.4°/6.0°	0.772	78.8°/81.8°	309.3°/3.0°	39.5°/4.8°	186.8°/84.3°
CHW3	33.53°N	86.73°W	60°	24° SE	105	0.034	0.595	1.9	2	-0.640	319.0°/6.1°	0.103	228.8°/1.6°	0.536	123.7°/83.7°	309.8°/5.9°	41.2°/12.9°	195.9°/75.8°
CHW4	33.55°N	86.71°W	41°	12° SE	84	0.037	0.404	6.0	5	-0.354	171.7°/7.8°	-0.086	81.3°/2.7°	0.44	332.4°/81.7°	180.6°/6.4°	270.7°/0.4°	4.2°/83.6°

Table 2.4: Calcite twinning results from the Ordovician Chickamauga limestones. N, number of twinsets; Std Error, nominal error; % Strain, total strain; % NEV, percent negative expected values; N NEV, number of negative expected values; e_n, maximum (e_1), medium (e_2) and minimum (e_3) strains; e_n T/P, orientation of strain axes; σ_n T/P, orientation of stress axes.

values in order to "clean" the data and identify multiple deformations (Teufel, 1980; Groshong et al., 1984). All twinning calculations were performed using the GSG/Strain99 program of Evans and Groshong (1994).

Results

Calcite twinning analysis reveals compression directions that are mostly within the bedding plane and tension directions that are approximately orthogonal to the bedding plane at all sites, indicating a prefolding, layer-parallel fabric in all sites (Table 2.4). Calculated strain-axis orientations are similar to the Turner stress axes, ($\sigma1 \approx e1$, $\sigma2 \approx e2$, $\sigma3 \approx e3$). However, the layer-parallel $\sigma1$ orientations show significant variation between sites (Table 2.4). Due to the limited number of sample sites and the fact that sample sites could not be selected due to exposure to be paired across the thrust for calcite twinning analysis, a systematic correlation between footwall and hanging wall results could not be determined (Table 2.4). Therefore, our hypothesis testing is primarily based on the paleomagnetic and magnetic susceptibility data.

DISCUSSION

Our combined results from the analyses of samples in the hanging wall and the footwall of the Jones Valley thrust sheet are used to determine the presence and amount, if any, of rotation on the thrust front. To augment our paleomagnetic data, we include prior results from Hodych et al. (1985), who sampled the northeastern portion of the Birmingham anticlinorium (northeast of site HW8; Figure 2.1b).

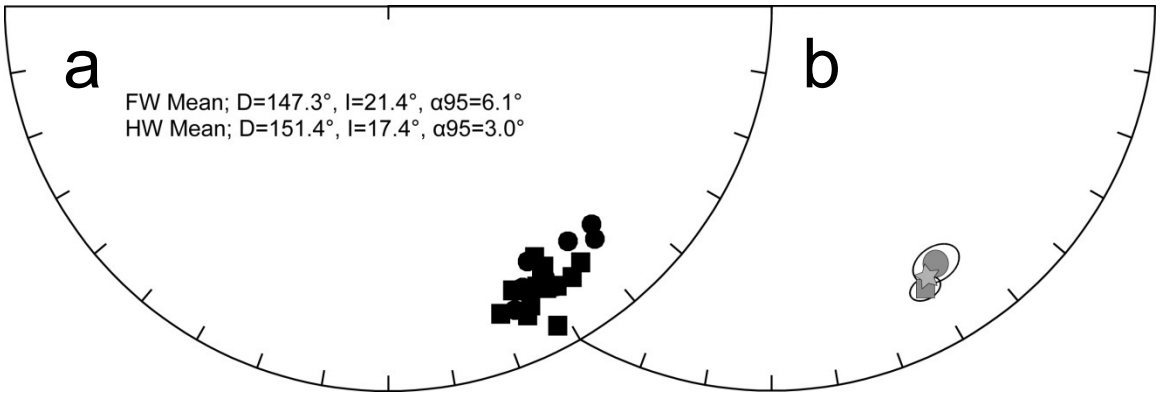

Figure 2.8: (a) Lower hemisphere, equal area projections showing tilt corrected site means including data from Hodych et al (1985). Squares (circles) represent hanging wall (footwall) sites. (b) Comparison of footwall (circle) and hanging wall (square) mean directions and associated α95's. Star represents mean direction of Perroud and Van der Voo (1984).

Included from Hodych et al. (1985) are three results from the footwall and seven results from the hanging wall, although five of these hanging wall sites are near site HW8. When comparing the tilt corrected directions (Figure 2.8), no discernable difference in declination is seen between hanging wall rocks and footwall rocks. A comparison of the mean directions for the footwall (D = 147.3°, I = 21.4°, α95 = 6.1°, k =97.96) and hanging wall (D = 151.4°, I = 17.4°, α95 = 3.0°, k =181.98) also shows that lack of declination difference (Figure 2.8). Perroud and Van der Voo (1984) obtained results from the entire thrust belt in Alabama and therefore offer an independent average direction for the Red Mountain Formation. Comparison of our directions with their result (D = 150.0°, I = 20.0°, α95 = 3.5°, k = 64) also shows no statistical difference (Figure 2.8). Thus, paleomagnetism of the Red Mountain Formation reveals no significant vertical-axis rotation of the hanging wall of the Jones Valley thrust sheet.

Layer-parallel magnetic fabrics provide a similar result for a test of vertical-axis rotations of the Jones Valley thrust sheet. The mean trend for the K_{max} for the footwall is approximately 37° and for the hanging wall 40°, both of which are approximately parallel to the thrust trace. The generally thrust-parallel trend of K_{max} and the lack of deviation between the footwall and hanging wall layer-parallel magnetic lineations support the conclusion that no relative rotation occurred after acquisition of the fabric. Strain and AMS ellipsoids are inherently difficult to compare for a variety of reasons (see Borradaile and Henry, 1997; Pares and van der Pluijm, 2002a; Evans et al., 2003). However, in the footwall, the greater intensity of the tectonic lineation is indicative of larger strains (Figure 2.7a). In the

hanging wall, many sites are dominated by a compaction fabric, but tectonic lineations appear to be better developed to the southwest, where we predict more strain within the thrust sheet on the basis of cross-section restoration.

Rotation of the Jones Valley thrust fault is not supported by paleomagnetism or magnetic fabrics. Rotation, therefore, cannot explain the displacement gradient despite the geometrically measured 15°-23° apparent rotation of the thrust sheet. Therefore, instead of a rotating thrust sheet with a fixed hinge, we propose that the thrust developed by self-similar growth, with displacement perpendicular to the strike of the ramp and lateral growth of the fault coincident with increased displacement into the foreland (Figure 2.9). The proposed scenario envisions growth of the thrust sheet with straight, parallel displacement vectors into the foreland, while the surface expression of the fault grows laterally in both directions. Our favored model assumes that some deformation must be accommodated within the thrust sheet to maintain continuity without tear faults, which may be accomplished by cataclastic flow within the thrust sheet (Wilkerson, 1992; Ismat and Mitra, 2005).

Our model also has implications for the thrust belt structure beneath the coastal plain cover. Displacement on the Jones Valley thrust sheet should continue to decrease southwest of cross-section 18. Therefore, to the southwest, we might expect a footwall splay to appear in a similar position as the Opossum Valley thrust fault in the northeast. This prediction would allow for further transfer of displacement from the Jones Valley thrust fault. New work to the southwest

Figure 2.9: Three steps in the development of a self-similar thrusting model. Transport toward the foreland occurs within the detachment fold, followed by progressive breaking of the fold and lateral growth of the thrust surface. The bulk of the transported fold has been eroded away in the Jones Valley thrust sheet.

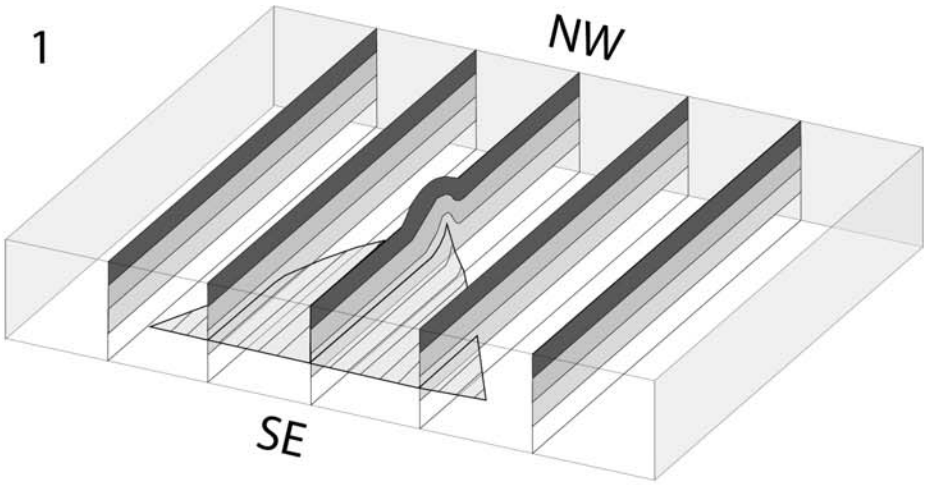
1
NW
SE

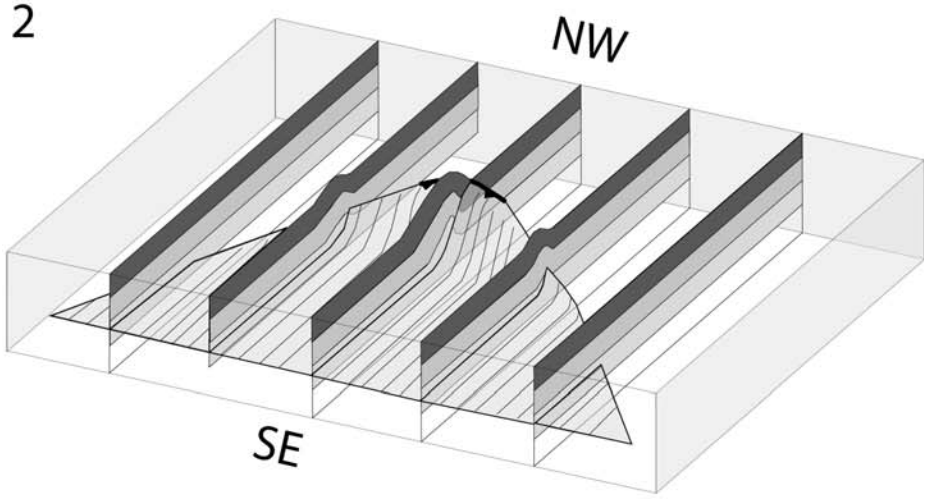
2
NW
SE

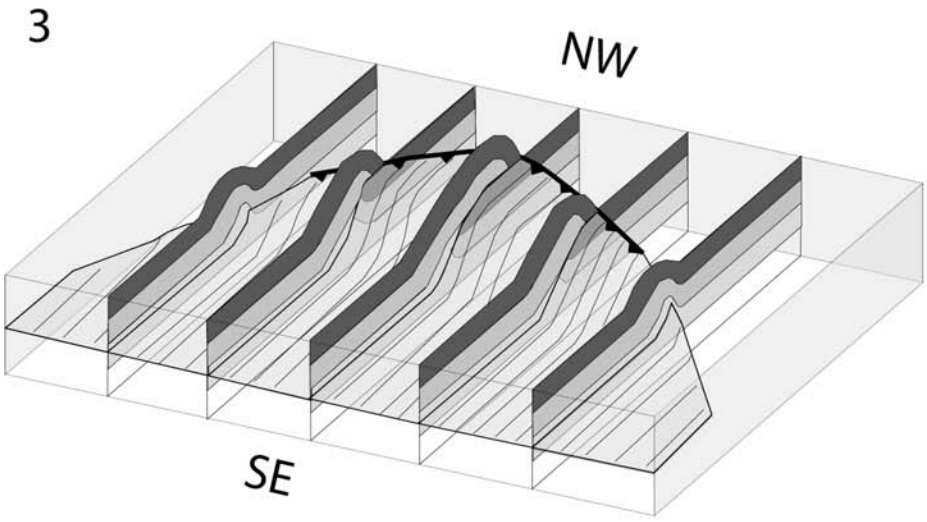
3
NW
SE

beneath the Coastal Plain cover would be useful to fully understand this relationship.

Several studies have documented displacement-length relationships on faults and determined a power-law relationship, $D_{max}=cL_{max}^{n}$, where D_{max} is the maximum displacement, L_{max} is the maximum fault length and c and n are constants (e.g., Davis et al., 2005). The half-length/displacement relationships of thrust faults from Davis et al. (2005) and Hatcher (2004) were compiled and converted into apparent rotation vs. displacement to evaluate whether the Jones Valley thrust fault has a similar relationship between calculated rotation and half-length (Figure 2.10). The range of apparent rotation angles (15°-23°) for the Jones Valley thrust fault is consistent with other thrust faults. Therefore, the proposed displacement gradient is comparable to other non-rotated thrust sheets.

CONCLUSION

Paleomagnetism of the Red Mountain Formation reveals a prefolding magnetization, likely acquired in the Pennsylvanian, prior to motion on the Jones Valley thrust fault. The displacement gradient on the Jones Valley thrust fault produced 15°-23° of curvature. However, paleomagnetic directions and magnetic fabric K_{max} orientations reveal no discernable difference between the hanging wall and the footwall of the Jones Valley thrust sheet. Thus, vertical-axis rotation of the hanging wall does not explain the observed displacement gradient. Instead, using a self-similar model of thrusting, we argue that the Jones Valley thrust sheet grew

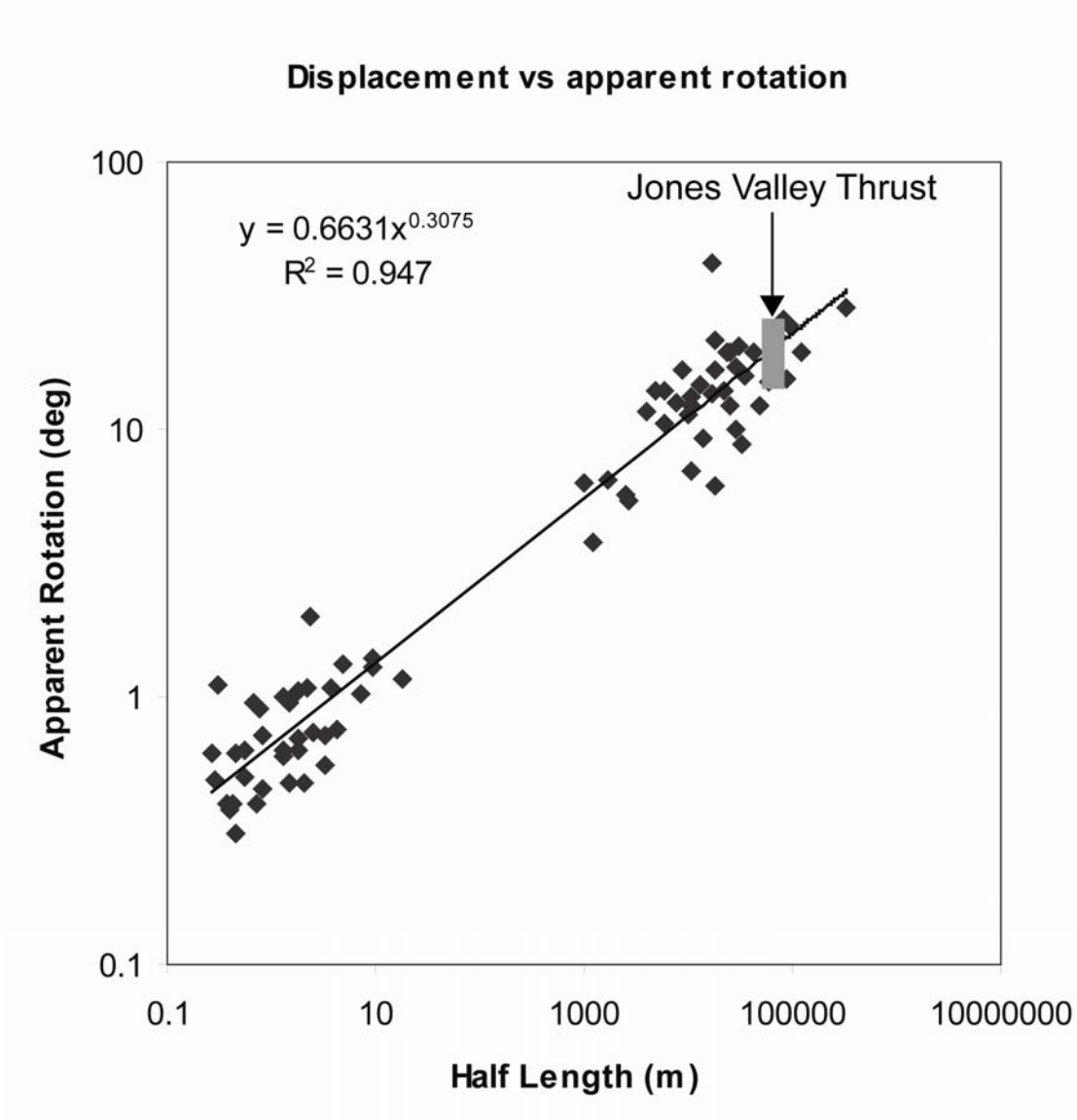

Figure 2.10: Plot of the relationship between fault half-length and the apparent rotation. The range of apparent rotations angles for the Jones Valley thrust lies within the scale of many thrusts. Data taken from Davis et al (2005) and Hatcher (2004).

laterally as it progressed into the foreland and created a displacement gradient without significant rotation. Accommodating strain is proposed to have accumulated within the thrust sheet as it developed via cataclastic flow. This work shows that displacement gradients do not need to be associated with vertical-axis rotations. Also, caution is advised when interpreting rotations in foreland thrust belts based purely on kinematic modeling without independent data, such as paleomagnetism or other passive structural markers.

ACKNOWLEDGEMENTS

Appalachian research at the University of Michigan was supported by grants from the American Chemical Society-Petroleum Research Fund (most recently 45893-AC8), by the Scott Turner Fund and student grants from the Geological Society of America. We thank Franek Hasiuk and Ed Osborne for field support, Josep Parés for laboratory support and Rick Allmendinger for his Stereonet program. The authors would also like to thank journal reviewers David Wiltschko and Emilio Pueyo for thorough and thoughtful reviews that significantly improved the manuscript.

REFERENCES

Allerton, S., 1994. Vertical-axis rotation associated with folding and thrusting; an example from the eastern Subbetic Zone of southern Spain. Geology 22, 1039-1042.

Allerton, S., 1998. Geometry and kinematics of vertical axis rotations in fold and thrust belts. Tectonophysics 299, 15-30.

Allerton, S., Lonergan, L., Platt, J.P., Platzman, E.S. and McClelland, E., 1993. Palaeomagnetic rotations in the eastern Betic Cordillera, southern Spain. Earth and Planetary Science Letters 119, 225-241.

Apotria, T.G., 1995. Thrust sheet rotation and out-of-plane strains associated with oblique ramps: An example from the Wyoming salient, U.S.A. Journal of Structural Geology 17, 647-662.

Bates, M.P., 1989. Palaeomagnetic evidence for rotations and deformation in the Nogueras Zone, Central Southern Pyrenees, Spain. Journal of the Geological Society of London 146, 459-476.

Bayona, G., Thomas, W.A. and Van der Voo, R., 2003. Kinematics of thrust sheets within transverse zones: a structural and paleomagnetic investigation in the Appalachian thrust belt of Georgia and Alabama. Journal of Structural Geology 25, 1193-1212.

Berdan, J.M., Boucot, A.J. and Ferrill, B.A., 1986. The first fossiliferous Pridolian beds from the Southern Appalachians in northern Alabama, and the age of the uppermost Red Mountain Formation. Journal of Paleontology 60, 180-185.

Berry, W.B.N, Boucot, A.J., Editors, 1970. *Correlation of the North American Silurian rocks*. Geological Society of America Special Paper 102, 289pp.

Borradaile, G., Henry, B., 1997. Tectonic applications of magnetic susceptibility and its anisotropy. Earth-Science Reviews 42, 49-93.

Butts, C., 1926. The Paleozoic rocks *in* Geology of Alabama: Alabama Geological Survey Special Report 14, 41-230.

Chowns, T.M. and McKinney, F.K., Depositional facies in Middle-Upper Ordovician and Silurian rocks of Alabama and Georgia. In: Frey, Robert W, Editor, 1980. *Excursions in Southeastern geology; Volume II, Geological Society of America Annual Meeting Field Trip Guide, Atlanta, Georgia*. American Geological Institute: Falls Church, Virginia, 323-348.

Cifelli, F., Rossetti, F., Mattei, M., Hirt, A.M., Funiciello, R. and Tortorici, L., 2004. An

AMS, structural and paleomagnetic study of Quaternary deformation in eastern Sicily. Journal of Structural Geology 26, 29-46.

Craddock, J.P., Kopania, A.A. and Wiltschko, D.V., 1988. Interaction between the northern Idaho-Wyoming thrust belt and bounding basement blocks, central western Wyoming. Geological Society of America Memoir 171, 333-351.

Dahlstrom, C.D.A., 1969. Balanced cross sections. Canadian Journal of Earth Sciences 6, 743-757.

Davis, K., Burbank, D.W., Fisher, D., Wallace, S. and Nobes, D., 2005. Thrust-fault growth and segment linkage in the active Ostler fault zone, New Zealand. Journal of Structural Geology 27, 1528-1546.

Elliott, D., 1976. The energy balance and deformation mechanisms of thrust sheets. Philosophical Transactions of the Royal Society of London A 283, 289-312.

Engelder, T., 1979. The nature of deformation within the outer limits of the central Appalachian foreland fold and thrust belt in New York State. Tectonophysics 55, 289-310.

Evans, M.A. and Groshong, R.H., 1994. A computer program for the calcite strain-gauge technique. Journal of Structural Geology 16, 277-282.

Evans, M.A., Lewchuk, M.T. and Elmore, R.D., 2003. Strain partitioning of deformation mechanisms in limestones; examining the relationship of strain and anisotropy of magnetic susceptibility (AMS). Journal of Structural Geology 25, 1525-1549.

Fischer, M.P. and Woodward, N.B., The geometric evolution of foreland thrust systems. In: McClay, K. R., Editor, 1992. *Thrust Tectonics*. Chapman & Hall, London, United Kingdom.

Fisher, R.A., 1953. Dispersion on a sphere. Proceedings of the Royal Society of London A **217,** 295–305.

Gray, M.B. and Mitra, G., 1993. Migration of deformation fronts during progressive deformation: evidence from detailed structural studies in the Pennsylvania Anthracite region, U.S.A. Journal of Structural Geology 15, 435-449.

Groshong, R.H., 1972. Strain calculated from twinning in calcite. Geological Society of America Bulletin 83, 2025-2038.

Groshong, R.H., 1974. Experimental test of least-squares strain gage calculation using twinned calcite. Geological Society of America 85, 1855-1864.

Groshong, R.H., Teufel, L.W. and Gasteiger, C., 1984. Precision and accuracy of the calcite strain-gauge technique. Geological Society of America 95, 357-363.

Hatcher Jr, R.D., Properties of thrusts and upper bounds for the size of thrust sheets. In: McClay, K.R., Editor, 2004. *Thrust tectonics and hydrocarbon systems*. American Association of Petroleum Geologists Memoir 82, 18-29.

Hatcher Jr, R.D., Thomas, W.A., Geiser, P.A., Snoke, A.W., Mosher, S. and Wiltschko, D.V., Alleghanian orogen. In: Hatcher Jr, R.D., Thomas, W.A. and Viele, G.E., Editors, 1989. *The Appalachian-Ouachita Orogen in the United States, The Geology of North America Volume F-2.* Geological Society of America, Boulder, Colorado, 233-318.

Hodych, J.P., Paetzold, R.R. and Buchan, K.L., 1985. Chemical remanent magnetization due to deep-burial diagenesis in oolitic hematite-bearing ironstones of Alabama. Physics of the Earth and Planetary Interiors 37, 261-284.

House, W.M. and Gray, D.R., 1982. Cataclasites along the Saltville thrust, USA and their implications for thrust sheet emplacement. Journal of Structural Geology 4, 257-269.

Ismat, Z. and Mitra, G., 2005. Fold-thrust belt evolution expressed in an internal thrust sheet, Sevier Orogen; the role of cataclastic flow. Geological Society of America Bulletin 117, 764-782.

Jelinek, V., 1978. Statistical processing of anisotropy of magnetic susceptibility measured on groups of specimens. Studia Geophysica et geodetica 22, 50-62.

Kirschvink, J.L., 1980. The least-square line and plane and the analysis of palaeomagnetic data. Geophysical Journal of the Royal Astronomical Society **62**, 699–718.

Kollmeier, J.M., van der Pluijm, B.A. and Van der Voo, R., 2000. Analysis of Variscan dynamics; early bending of the Cantabria-Asturias Arc, northern Spain. Earth and Planetary Science Letters 181, 203-216.

Macedo, J. and Marshak, S., 1999. Controls on the geometry of fold-thrust belt salients. Geological Society of America Bulletin 111, 1808-1822.

Marshak, S., Salients, recesses, arcs, oroclines, and syntaxes; a review of ideas concerning the formation of map-view curves in fold-thrust belts. In: McClay, K.R., Editor, 2004. *Thrust tectonics and hydrocarbon systems*. American Association of Petroleum Geologists Memoir 82, 131-156.

Marshak, S. and Mitra, G., 1988. *Basic methods of structural geology*. New Jersey,

Prentice Hall, 446p.

McCaig, A.M. and McClelland, E., Paleaeomagnetic techniques applied to thrust belts. In: McClay, K. R., Editor, 1992. *Thrust Tectonics*. Chapman & Hall, London, United Kingdom, 209-216.

McElhinny, M. W., 1964. Statistical significance of the fold test in paleomagnetism. Geophysical Journal of the Royal Astronomical Society 8, 338-340.

Nickelsen, R.P., 1979. Sequence of structural stages of the Alleghany orogeny, Bear Valley strip mine, Shamokin, PA. American Journal of Science 279, 225-271.

O'Hara, K., Kanda, R. and Thomas, W. A., 2006. Thermal footprint of an eroded thrust sheet in the southern Appalachian Black Warrior basin, Alabama. Geological Society of America Abstracts with Programs 38, no. 3, 7.

Oliva-Urcia, B. and Pueyo, E.L., 2007. Gradient of shortening and vertical-axis rotations in the Southern Pyrenees (Spain), insights from a synthesis of paleomagnetic data. Revista de la Sociedad Geológica de España 20, 105-118.

Ong, P.F., van der Pluijm, B.A. and Van der Voo, R., 2007. Early rotation in the Pennsylvania Salient (US Appalachians): Evidence from calcite-twinning analysis of Paleozoic carbonates. Geological Society of America Bulletin 119, 796-804.

Pares, J.M. and van der Pluijm, B.A., 2002a. Evaluating magnetic lineations (AMS) in deformed rocks. Tectonophysics, 350, 283-298.

Pares, J.M. and van der Pluijm, B.A., 2002b. Phyllosilicate fabric characterization by Low-Temperature Magnetic Anisotropy (LT-AMS). Geophysical Research Letters 29, GRL2214.

Perroud, H. and Van der Voo, R., 1984. Secondary magnetizations from the Clinton-type iron ores of the Silurian Red Mountain Formation, Alabama., Earth and Planetary Science Letters 67, 391-399.

Pueyo, E.L., Millán, H. and Pocovi, A., 2002. Rotation velocity of a thrust; a paleomagnetic study in the External Sierras (southern Pyrenees). Sedimentary Geology 146, 191-208.

Pueyo, E.L., Pocovi, A., Millán, H., and Sussman, A.J., Map-view models for correcting and calculating shortening estimates in rotated thrust fronts using paleomagnetic data. In: Weil, A.B. and Sussman, A.J., Editors, 2004. *Orogenic curvature; Integrating paleomagnetic and structural analyses.* Geological Society of America Special Paper 383, 57-71.

Richter, C. and van der Pluijm, B.A., 1994. Separation of paramagnetic and ferrimagnetic susceptibilities using low temperature magnetic susceptibilities and comparison with high field methods. Physics of the Earth and Planetary Interiors 82, 113-123.

Rindsberg, A.K. and Osborne, W.E., 2001. Geology of the Bessemer 7.5 minute quadrangle, Jefferson County, Alabama. Alabama Geological Survey Quadrangle Series 20, 25p., 2 pl.

Rindsberg, A.K., Ward, W.E., Osborne, W.E. and Irvin, G.D., 2003. Geology of the Irondale 7.5 minute quadrangle, Jefferson County, Alabama. Alabama Geological Survey Quadrangle Series 26, 36p., 2 pl.

Rodgers, J., 1970. *The tectonics of the Appalachians*. New York, Wiley Interscience, 271p.

Saint-Bezar, B., Hebert, R.L., Aubourg, C., Robion, P., Swennen, R. and Frizon de Lamotte, D., 2002, Magnetic fabric and petrographic investigation of hematite-bearing sandstones within ramp-related folds; examples from the South Atlas Front (Morocco). Journal of Structural Geology 24, 1507-1520.

Satolli, S., Speranza, F. and Calamita, F., 2005. Paleomagnetism of the Gran Sasso range salient (central Apennines, Italy): Pattern of orogenic rotations due to translation of a massive carbonate indenter, Tectonics 24, TC4019.

Schwartz, S.Y. and van der Voo, R., 1984. Paleomagnetic study of thrust sheet rotation during foreland impingement in the Wyoming-Idaho overthrust belt. Journal of Geophysical Research 89, 10077-10086.

Somma, R., 2006. The south-western side of the Calabrian Arc (Peloritani Mountains): Geological, structural and AMS evidence for passive clockwise rotations. Journal of Geodynamics 41, 422-439.

Soto, R., Casas-Sainz, A.M. and Pueyo, E.L., 2006. Along-strike variation of orogenic wedges associated with vertical axis rotations. Journal of Geophysical Research 111, B10402.

Spang, J.H., 1972. Numerical method for dynamic analysis of calcite twin lamellae. Geological Society of America Bulletin 83, 467-472.

Spang, J.H. and Groshong, R.H., 1981. Deformation mechanisms and strain history of a minor fold from the Appalachian Valley and Ridge Province. Tectonophysics 72, 323-342.

Speranza, F., Adamoli, L., Maniscalco, R. and Florindo, F., 2003. Genesis and

evolution of a curved mountain front; paleomagnetic and geological evidence from the Gran Sasso Range (Central Apennines, Italy). Tectonophysics 362, 183-197.

Sussman, A.J., Butler, R.F., Dinares-Turell, J. and Verges, J., 2004. Vertical-axis rotation of a foreland fold and implications for orogenic curvature: an example from the Southern Pyrenees, Spain. Earth and Planetary Science Letters 218, 435-449.

Szabo, M.W., Osborne, E.W. and Copeland, C.W., 1988. Geologic map of Alabama, northewest sheet. Alabama Geological Survey Special Map 220, scale 1:250,000.

Tauxe, L., 1998. *Paleomagnetic Principles and Practice.* Boston, Kluwer Academic Publishers, 299pp.

Teufel, L.W., 1980. Strain analysis of experimental superposed deformation using calcite twin lamellae. Tectonophysics 65, 291-309.

Thomas, W.A., 1977. Evolution of Appalachian-Ouachita salients and recesses from reentrants and promontories in the continental margin. American Journal of Science 277, 1233-1278.

Thomas, W.A., 1991. The Appalachian-Ouachita rifted margin of southeastern North America. Geological Society of America Bulletin 103, 415-431.

Thomas, W.A., 2001. Mushwad: ductile duplex in the Appalachian thrust belt in Alabama. American Association of Petroleum Geologists Bulletin 85, 1847-1869.

Thomas, W.A. and Bayona, G., 2002. Palinspastic restoration of the Anniston Transverse Zone in the Appalachian thrust belt, Alabama. Journal of Structural Geology 24, 797-826.

Thomas, W.A. and Bayona, G., 2005. The Appalachian thrust belt in Alabama and Georgia: Thrust-belt structure, basement structure, and palinspastic reconstruction. Geological Survey of Alabama Monograph 16, 48pp.

Thomas, W.A. and Bearce, D.N., Birmingham Anticlinorium in the Appalachian fold-thrust belt, basement fault system, synsedimentary structure, and thrust ramp. In: Neathery, T.L., Editor, 1986. *Centennial Field Guide Volume 6, Southeastern section of the Geological Society of America*. Geological Society of America, Boulder, Colorado, 191-200.

Torsvik, T., Briden, J.C. and Smethurst, M.A., 1999. SuperIAPD1999 – Software Package, Geological Survey of Norway, Trondheim.

Tull, J.F., 1998. Analysis of a regional middle Paleozoic unconformity along the distal southeastern Laurentian margin, southernmost Appalachians: Implications for tectonic evolution. Geological Society of America Bulletin 110, 1149-1162.

Turner, F.J., 1953. Nature and dynamic interpretation of deformation lamellae in calcite of three marbles. American Journal of Science 251, 276-298.

Van der Voo, R., 1993. *Paleomagnetism of the Atlantic, Tethys and Iapetus Oceans*. Cambridge University Press, New York, NY, 411 pp.

Weil, A.B. and Sussman, A.J., Classification of curved orogens based on the timing relationships between structural development and vertical-axis rotations, In: Weil, A.B. and Sussman, A.J., Editors, 2004. *Orogenic curvature; Integrating paleomagnetic and structural analyses.* Geological Society of America Special Paper 383*, 1-17.*

Weil, A.B., Van der Voo, R., van der Pluijm, B.A. and Pares, J., 2000. The formation of an orocline by multiphase deformation; a paleomagnetic investigation of the Cantabria Asturias Arc (northern Spain). Journal of Structural Geology 22, 735-756.

Weil, A.B., Van der Voo, R. and van der Pluijm, B, 2001. New paleomagnetic data from the southern Cantabria-Asturias Arc, northern Spain : Implications for true oroclinal rotation and the final amalgamation of Pangea, Geology 29, 991-994.

Wilkerson, M.S., 1992. Differential transport and continuity of thrust sheets. Journal of Structural Geology 14, 749-751.

Winston, R. B., 1990. Vitrinite reflectance of Alabama's bituminous coal: Alabama Geological Survey Circular 139, 54 pp.

Zijderveld, J.D.A., 1967. AC demagnetization of rocks: analysis of results. In: D.W. Collinson and K.M. Creer, Editors, *Methods in Paleomagnetism*, Elsevier, Amsterdam, 254–286.

CHAPTER III

REMAGNETIZATION IN THE TENNESSEE SALIENT, SOUTHERN APPALACHIANS, USA: CONSTRAINTS ON THE TIMING OF DEFORMATION

ABSTRACT

The Appalachian fold-thrust belt is characterized by a sinuous trace in map-view, creating a series of salients and recesses. The kinematic evolution of these arcuate features remains a controversial topic in orogenesis. Primary magnetizations from clastic redbeds in the Pennsylvania salient show Carboniferous rotations that account for about half of the curvature, while Kiaman-aged (Permian) remagnetizations display no relative rotation between the limbs. The more southern Tennessee salient shows a maximum change in regional strike from ~65° in Virginia to ~10° in northern Georgia. Paleomagnetic results from thirty-two sites in the Middle to Upper Ordovician Chickamauga Group limestones and twenty sites from the Middle Cambrian Rome Formation redbeds were analyzed to constrain the relative age of magnetization as well as the nature of curvature in the Tennessee salient. Results from three sites of the Silurian Red Mountain Formation were added to an existing dataset in order to determine whether the southern limb had rotated.

After thermal demagnetization, all three sample suites display a down and southeasterly direction, albeit carried by different magnetic minerals. The syn-tilting direction of the Chickamauga limestones lies on the Late Carboniferous segment of the North American apparent polar wander path (APWP), indicating that deformation was about half completed by the Late Pennsylvanian. The Rome and Red Mountain Formations were also remagnetized during the Late Carboniferous. Both the Chickamauga limestones and Rome redbeds fail to show a correlation between strike and declination along the salient, suggesting either that the salient was a primary, non-rotational feature or that secondary curvature occurred prior to remagnetization, as it did in Pennsylvania. Moreover, remagnetized directions from the Red Mountain sites show no statistical difference between the southern limb of the salient and the more northeasterly trending portion of the fold-thrust belt in Alabama. Thus, all of the studied units in the Tennessee salient are remagnetized and show no evidence for rotation. This confirms that remagnetization was widespread in the southern Appalachians and that any potential orogenic rotation must have occurred prior to the latest Carboniferous.

INTRODUCTION

Most fold-thrust belts worldwide display some degree of curvature (Carey, 1955; Eldredge et al., 1985; Marshak, 1988; Marshak et al., 1992; Macedo and Marshak, 1999; Marshak, 2004; Weil and Sussman, 2004), with curvature varying from tens of degrees to as much as 180°. Since Carey's (1955) development of the orocline hypothesis, many studies have focused on the evolution of arcuate orogens.

While several classification schemes have been proposed for orogenic curvature, arcuate orogens can generally be thought of as primary, with the orogen forming in an initial curved state, secondary, with secondary rotations of limbs from straighter geometry, or some combination (Eldredge et al., 1985; Marshak, 1988; Hindle and Burkard, 1999). Differentiating between the two endmembers is important in resolving the kinematic and mechanical evolution of curved orogens. Moreover, out-of-plane deformation limits the reliability of balanced cross-sections in curved belts (Hatcher, 2004; Pueyo et al., 2004; Hnat et al., 2008), making it imperative to constrain rotations before attempting palinspastic restoration and section balancing.

Because secondary curvature is characterized by rotations about a vertical axis, paleomagnetism provides an ideal method for curvature assessment (Eldredge et al., 1985; Lowrie and Hirt, 1986; McCaig and McClelland, 1992; Weil and Sussman, 2004). A coincident change in magnetic declination and orogenic strike is representative of secondary curvature, whereas primary curvature will reveal no such correlation. However, the use of paleomagnetism requires that the magnetization of the units is acquired prior to curvature, in order to record the total amount of rotation. In orogenic settings, meeting this condition can be difficult, as remagnetizations are frequently present. Therefore, paleomagnetic field-tests (fold test, conglomerate test, baked contact test, reversal test) are essential when assessing orogenic curvature with paleomagnetism.

One of the most obvious and well-studied fold-thrust belts to display significant curvature is the Appalachians, which extends from New York to Alabama.

It displays a sinuous pattern that consists of the Pennsylvania salient, the Roanoke recess, the Tennessee salient and the Alabama recess (Figure 3.1). The general shape of the fold-thrust belt has been interpreted to have evolved from the irregular shape of Laurentia's rifted Iapetan margin, which subsequently influenced the position of the fold-thrust belt during Late Paleozoic Alleghanian deformation (Rankin, 1975; Thomas, 1977; 1991; 2004).

Some of the earliest investigations testing Carey's (1955) orocline hypothesis using paleomagnetism occurred in the Pennsylvania salient (Figure 3.1). Studies from multiple Paleozoic clastic redbed units displayed seemingly contradictory results (Irving and Opdyke, 1965; Roy et al., 1967; Knowles and Opdyke, 1968; Van der Voo et al., 1979; Schwartz and Van der Voo, 1983). Later studies recognized two magnetizations from many of these units, both carried by hematite. The lower-temperature component is typical of a Late Paleozoic Kiaman remagnetization, while the higher-temperature component proved to be a depositional remanent magnetization (DRM) for the Upper Ordovician Juniata (Miller and Kent, 1989), Silurian Bloomsburg (Kent, 1988; Stamatakos and Hirt, 1994), Upper Devonian Catskill (Miller and Kent, 1986) and Lower Carboniferous Mauch Chunk Formations (Kent and Opdyke, 1985; Kent, 1988). These results allowed Kent (1988) and Stamatakos and Hirt (1994) to conclude that about half (23° and 18°, respectively) of the curvature (~55°) is accounted for by relative rotation between the limbs. The absolute rotation has been argued by Van der Voo (1993) to have been clockwise rotation that occurred entirely on the northern limb, based on the comparison of directions from the Silurian Rose Hill Formation (French and Van der Voo, 1979)

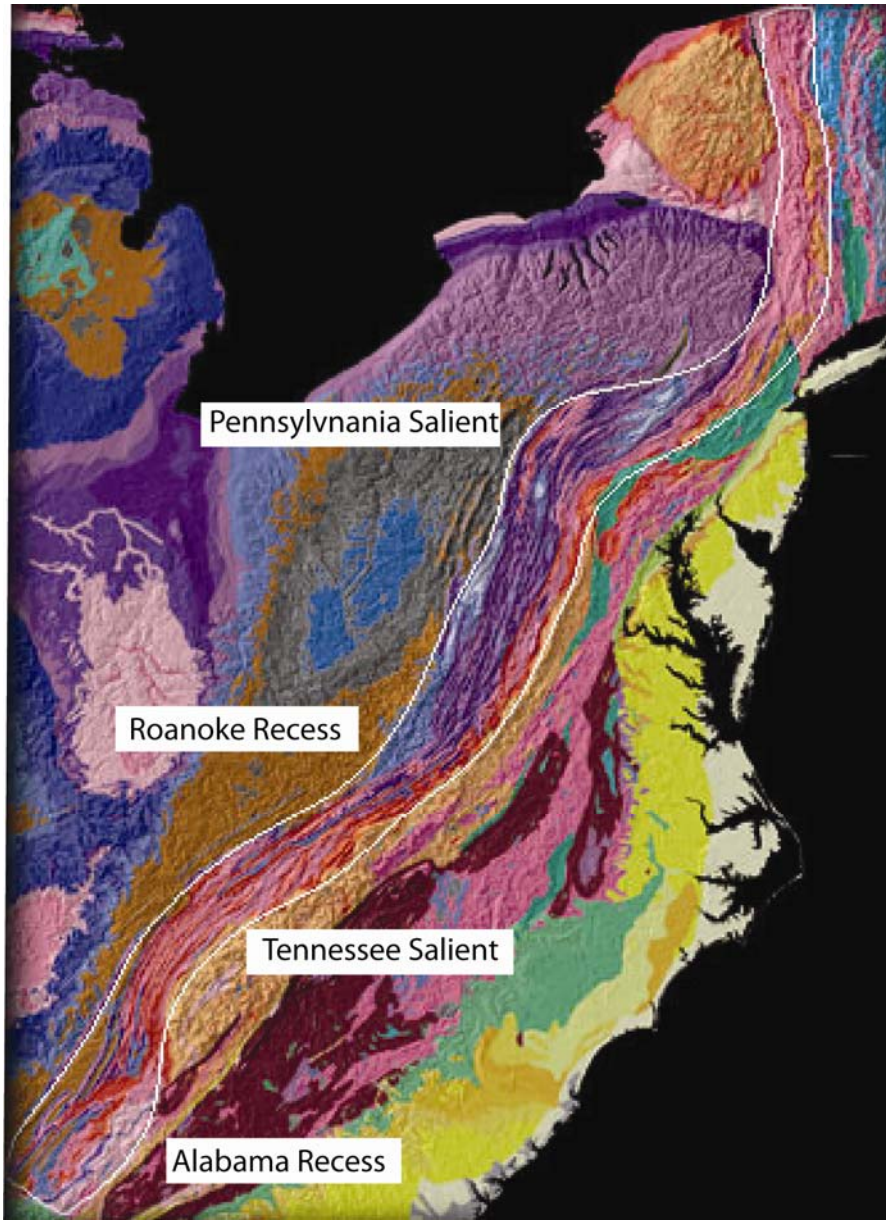

Figure 3.1: Map of Appalachian thrust belt, highlighting curvature (Vigil et al., 2000)

with those from the Silurian Wabash Reef in Indiana (McCabe et al., 1985), part of the stable Laurentian craton.

The remagnetized components, in contrast, show no relative difference between the limbs of the Pennsylvania salient. Kiaman-aged remagnetizations also dominate carbonate units in the region, though the magnetization is carried by magnetite (Kodama, 1988; Evans et al., 2000; Cederquist et al., 2006). Although the remagnetizations fail to record rotation in Pennsylvania, they do show a toward-the-foreland development of the fold-thrust belt, as remagnetizations carried by hematite and by magnetite are postfolding in the hinterland, synfolding in the middle and prefolding toward the foreland (Stamatakos et al., 1996; Cederquist et al., 2006).

The primary aim of this study is to provide a test of curvature in the Tennessee salient through paleomagnetic analysis of incompletely studied redbeds from the Rome Formation, which were thought to preserve a primary remanence (Watts et al., 1980), and newly sampled limestones (Chickamauga Group). We also add results to existing data from Silurian red beds (Red Mountain Formation) from the Alabama thrust belt. This large new dataset will allow us to test the timing of magnetization and origin of curvature in the Tennessee salient, as well as a comparison with the Pennsylvania salient in terms of age of magnetization and, if any, rotational history.

TENNESSEE SALIENT

Regional Structure

The Tennessee salient is defined by a change in regional strike from up to 65° in Virginia and northern Tennessee to approximately 10° in northern Georgia, before returning to a more northeasterly direction (~45°) into Alabama (Figures 3.1 and 3.2). Instead of being defined by fold traces like in Pennsylvania, the curved geometry of Tennessee is primarily delineated by southeast dipping thrust faults, with the overlying stratigraphy dipping in the same general direction (Hatcher et al., 1989; Hatcher et al., 2007). The curvature is not uniform throughout the belt, as evidenced by the southern limb of the salient, where the frontal portion of the fold-thrust belt diverges from the northern limb by only 35°-40° while the hinterland deviates up to 65°.

The southern Appalachian fold-thrust belt is a classic thin-skinned fold-thrust belt. The structural style of the belt significantly differs from that in the central Appalachians, which is primarily attributed to stratigraphic differences. The southern Appalachian fold-thrust belt consists of a west-verging stack of thin-skinned thrusts, with the basal decollément contained primarily within the shales of the Cambrian Rome and Conasauga Formations. The thrust stack in Tennessee is dominated by stiff Cambro-Ordovician carbonates, with the entire sedimentary package thickening toward the east (Rodgers, 1970; Harris and Milici, 1977; Hatcher et al., 1989). Most of the currently exposed stratigraphic units in this region consist of the Cambro-Ordovician carbonates, including those of the Conasauga, Knox and Chickamauga Groups. Unlike the central Appalachians, the southern Appalachian

Figure 3.2: Tennessee salient showing paleomagnetic sites sampled for this study. Stars show location of Chickamauga limestone sites. Saltville thrust is highlighted Filled circles represent Rome Formation sites and triangles from the inset show the three Red Mountain sites (Hardeman, 1966; Lawton et al., 1976; McDowell et al., 1981; Osbourne et al., 1988).

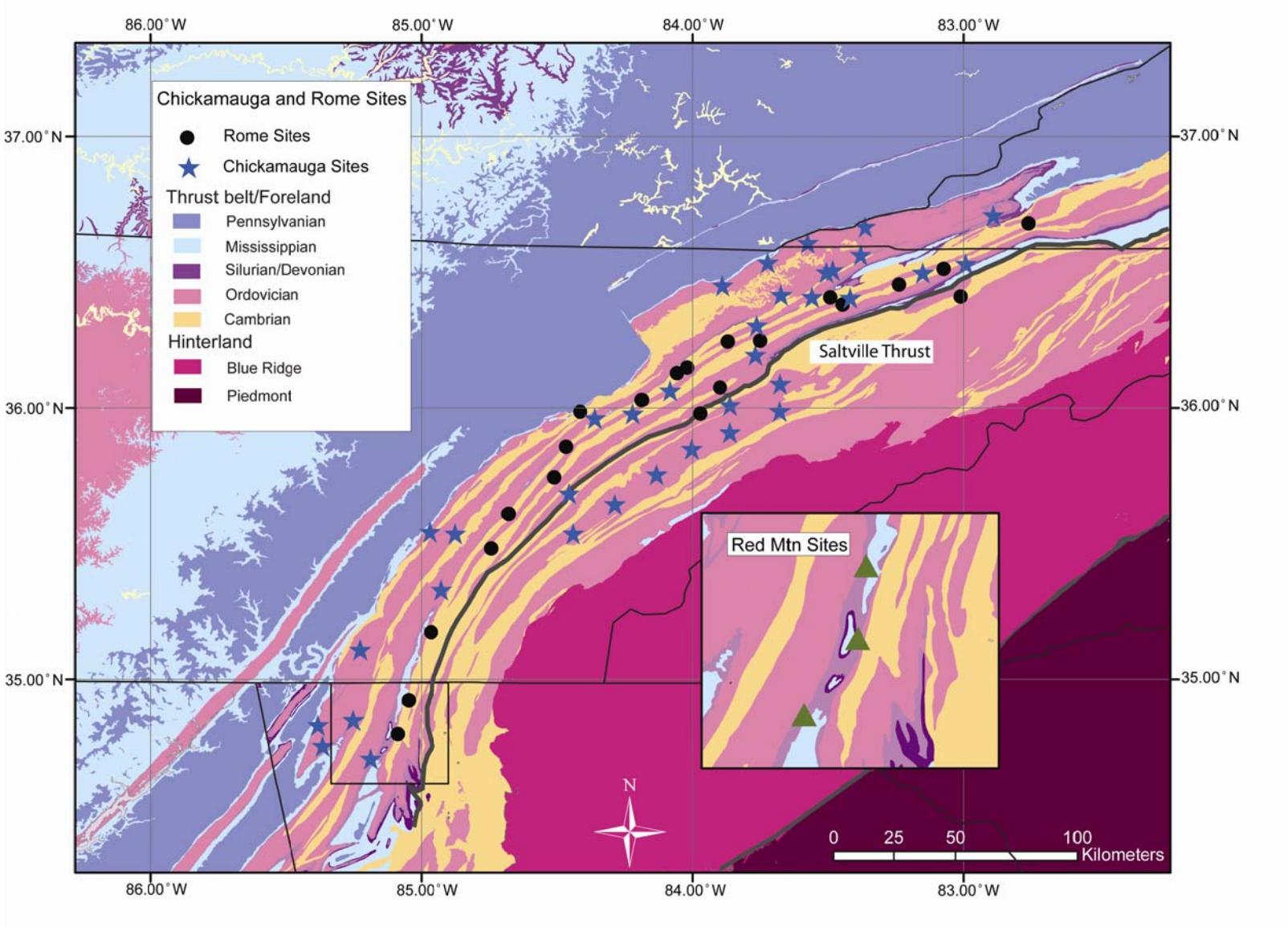
Chickamauga and Rome Sites
Rome Sites
Chickamauga Sites
Thrust belt/Foreland
Pennsylvanian
Mississippian
Silurian/Devonian
Ordovician
Cambrian
Hinterland
Blue Ridge
Piedmont
Saltville Thrust
Red Mtn Sites
86.00° W
85.00° W
84.00° W
83.00° W
37.00° N
36.00° N
35.00° N
N
0
25
50
100
Kilometers

belt lacks thick packages of Silurian through Mississippian units, therefore allowing the older carbonates to make up most of the surface area (Hatcher et al., 1989).

Previous Paleomagnetic Work

Compared to the Pennsylvania salient, the Tennessee salient has received much less attention. Paleomagnetic results from the thrust belt are few and were collected to determine either an apparent polar wander path (APWP) for Laurentia (Watts and Van der Voo, 1979; Watts et al., 1980) or the timing of remagnetizations associated with Mississippi Valley Type (MVT) deposits (Bachtadse et al., 1987; Symons and Stratakos, 2002; Pannalal et al., 2003). Watts et al. (1980) sampled the Cambrian Rome Formation and argued that the unit carries a Cambrian magnetization, although the reliability of these data is questionable (Van der Voo, 1993). The eight sites were distributed primarily along the northern limb of the salient, although one site was located on its southern limb. Results from this single site led the authors to conclude that the curvature in Tennessee is primary and that no significant rotation had occurred in the salient. However, since the timing of magnetization relative to deformation is suspect (Van der Voo, 1993), it is difficult to sustain this conclusion.

Other paleomagnetic efforts in the area were almost exclusively distributed in the northern limb. Watts and Van der Voo (1979) sampled Ordovician redbeds from the Bays Mountain, Chapman Ridge and Moccasin Formations. There, prefolding, primary magnetizations carried by hematite revealed an Ordovician pole for three units. A secondary magnetization also apparently carried by hematite was also identified in the Moccasin Formation and appears to be late Paleozoic.

Morrison and Ellwood (1986) also identified a direction from northwestern Georgia that was somewhat similar to an Ordovician direction, although this result only included data from a single geographic site, and therefore, like the Rome Formation, is not a reliable dataset for identifying the presence of rotations.

Results from carbonates of the Cambro-Ordovician Knox Group in the Tennessee salient have shown that this unit was remagnetized during the late Paleozoic, although the inferred age of magnetization has been interpreted to have ranged from Early Carboniferous (Symons and Stratakos, 2002; Pannalal et al., 2003) to Late Carboniferous (Bachtadse et al., 1987). Because the distribution of sites is exclusive to the northern limb, and given that these rocks are clearly remagnetized, it remains undetermined whether rotation occurred within the Tennessee salient.

The lack of suitable paleomagnetic data to test the nature of curvature in the Tennessee salienthas led us to sample a distribution of sites from multiple lithologies with the goal of determining whether regional rotations were involved in the development of the salient. Sampling focused primarily on limestones of the Chickamauga Group and redbeds of the Rome Formation, although three sites of Red Mountain Formation redbeds in northern Georgia were also collected. With this more expansive dataset, we hoped to elucidate whether oroclinal bending has occurred in the Tennessee salient.

PALEOMAGNETIC ANALYSIS OF THE TENNESSEE SALIENT

Methods

Samples were collected from both limestone and redbed sites in the Tennessee salient. Between five and thirteen 2.5 cm diameter cores were collected from each limestone site using a portable gasoline-powered drill. Six to ten oriented hand samples were collected from each redbed site and either cored or cut into standard 2.2 cm cubes, depending on the lithology. All cores were subsequently cut into standard length specimens. Core and hand sample orientations, as well as bedding attitude, were measured using a magnetic compass.

Prior to demagnetization, anisotropy of magnetic susceptibility (AMS) was measured on all specimens. AMS has previously been used to analyze curved mountain belts (Cifelli et al., 2004; Somma, 2006). Specimens were measured in fifteen positions, according to the method of Jelinek (1978), on a Geofyzika Brno Kappabridge KLY-2.03 at 920 Hz. Linear perturbation analysis was used to produce a statistical bootstrap using the 'bootams' program of Tauxe (1998). Site-mean eigenvectors were plotted and displayed as a scatter of points on an equal-area stereonet. Unfortunately, AMS fabrics were both weak and erratic for redbeds as well as limestones at the site and specimen levels. Therefore, AMS was disregarded for any analysis of curvature formation in the Tennessee salient.

Thermal demagnetization was carried out on all specimens in a magnetically shielded, low-field room using an Analytical Service Co. (ASC) thermal demagnetizer. Specimens were measured in a three-axis, cryogenic 2G Enterprises Model 755 Superconducting magnetometer after each heating step, with thermal

demagnetization steps ranging from 100°C to 690°C. Demagnetization was discontinued when the specimen intensity approached zero percent of the natural remanent magnetization (NRM) or became erratic because of spurious magnetizations acquired during cooling.

Principal component analysis (Kirschvink, 1980) of linear vectors selected from orthogonal projection demagnetization plots (Zijderveld, 1967) was used to calculate the characteristic remanent magnetization (ChRM) with the SuperIAPD software package (Torsvik et al., 1999). Individual specimen ChRM directions were used to determine site means using Fisher's (1953) method. Maximum angular deviation (MAD) up to 20° was accepted for each specimen, although most had MAD values less than 10°. The timing of magnetization acquisition relative to deformation was tested using a fold-test on the site mean directions (Graham, 1949; McElhinny, 1964; Mcfadden and Jones, 1981).

Chickamauga Limestone Results

A total of 323 samples were collected from thirty-five sites in limestones of the Chickamauga Group (Figure 3.2). These limestones were chosen because, unlike the underlying Cambro-Ordovician Knox Group, they are relatively undolomitized and are not typically affected by alteration due to Mississippi Valley Type (MVT) deposits, two phenomena that have been associated with remagnetizations (Bachtadse et al., 1987; Kesler and van der Pluijm, 1990; Leach et al., 2001; Pannalal et al., 2003). Therefore, these limestones were considered more likely to hold a primary remanence.

Figure 3.3: Representative thermal demagnetization plots of the Chickamauga Group limestones in geographic coordinates with associated intensity plots, showing normalized intensity versus temperature in degrees Celsius. In the demagnetization plots, closed (open) symbols represent vector endpoints plotted in the horizontal (vertical) plane. Temperature steps are in degrees Celsius. Ticks represent 0.5 mA/m.

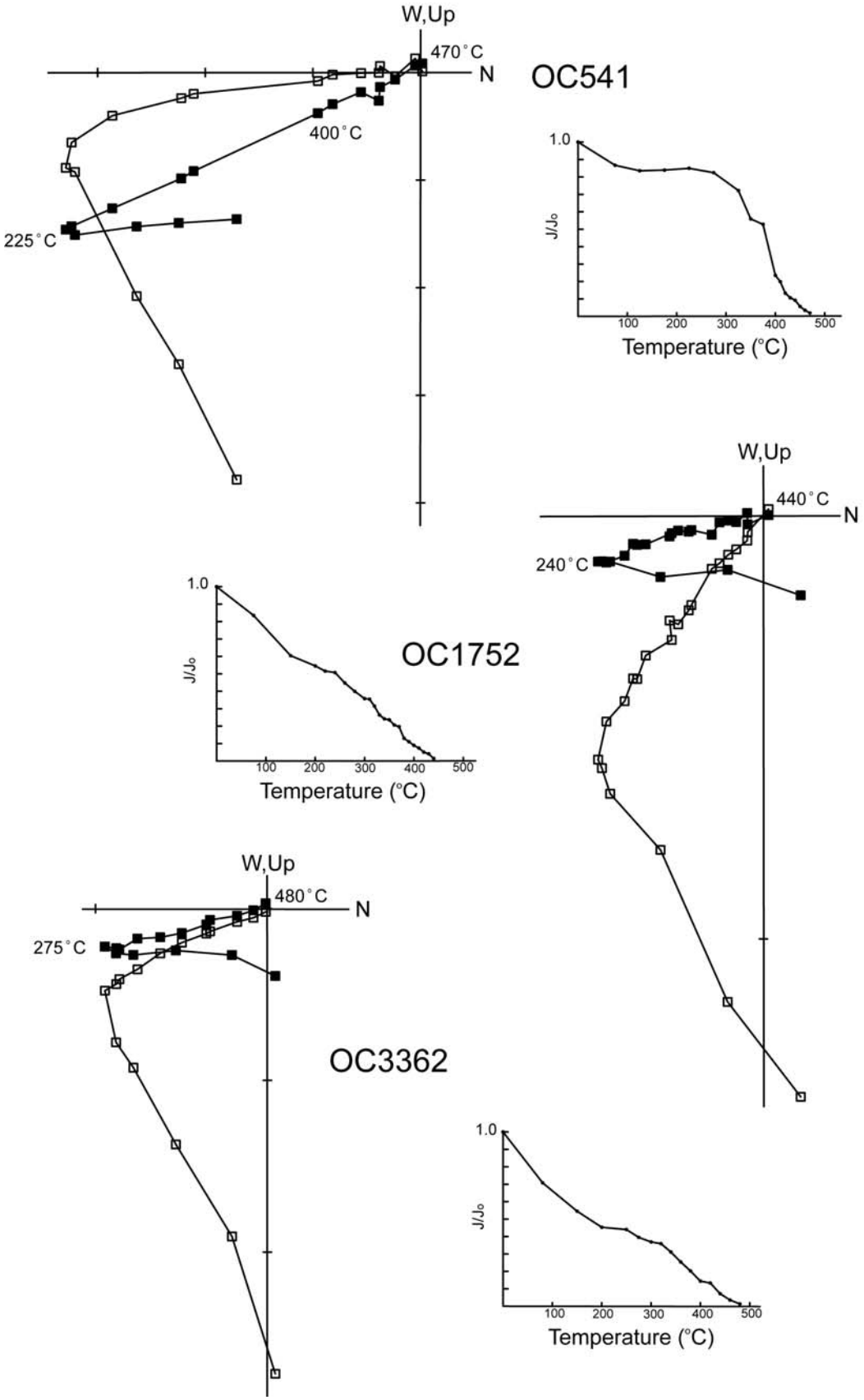
W,Up
470°C
N
400°C
225°C
OC541
1.0
J/Jo
100
200
300
400
500
Temperature (°C)
W,Up
440°C
N
240°C
1.0
J/Jo
OC1752
100
200
300
400
500
Temperature (°C)
W,Up
480°C
N
275°C
OC3362
1.0
J/Jo
100
200
300
400
500
Temperature (°C)

Table 3.1: Paleomagnetic results from the Chickamauga Group limestones. Mean directions are calculated from site means (Fisher, 1953); N/N_o, number of specimens (*sites*) accepted/studied; Geo Dec, In situ declination; Geo Inc, In situ inclination; TC Dec, Tilt-corrected declination; TC Inc, Tilt-corrected inclination; α95, radius of confidence circle in degrees; *k*, precision parameter (Fisher, 1953). Tilt-correction is 60% untilting. *OC08 excluded from calculation of mean.

Site	Latitude	Longitude	Strike	Dip	N/No	Geo Dec	Geo Inc	TC Dec	TC Inc	α95	k
OC01	36.566	-83.382	59°	17°	6/6	164.1°	33.0°	162.7°	23.1°	8.4°	65.02
OC02	36.510	-83.492	250°	31°	6/7	162.9°	28.8°	163.8°	47.4°	18.9°	13.48
OC03	36.502	-83.503	58°	26°	5/7	146.5°	54.1°	146.8°	38.5°	15.6°	24.99
OC04	36.408	-83.424	62°	36°	8/8	164.3°	45.9°	161.4°	24.7°	3.7°	227.36
OC05	34.851	-85.260	166°	3°	9/9	154.9°	8.3°	155.2°	8.6°	8.2°	40.1
OC06	35.112	-85.234	25°	15°	7/9	157.4°	32.4°	154.1°	25.6°	19.6°	10.46
OC07	35.331	-84.931	11°	10°	7/8	158.4°	19.1°	156.8°	15.8°	4.2°	209.8
OC08*	35.550	-84.973	37°	72°	8/9	201.0°	-35.3°	-	-	8.6°	42.37
OC09	35.543	-84.444	37°	44°	6/11	138.9°	55.3°	134.5°	29.2°	8.3°	65.52
OC10	35.754	-84.138	47°	11°	7/9	153.9°	27.7°	153.0°	21.4°	7.7°	62.27
OC11	35.644	-84.285	52°	15°	7/8	151.6°	36.5°	150.7°	27.6°	7.3°	70.23
OC12	35.981	-84.221	57°	34°	7/10	161.5°	53.9°	157.2°	34.0°	4.9°	150.9
OC13	35.539	-84.878	151°	3°	8/8	154.1°	23.6°	154.9°	23.5°	5.4°	107.4
OC14	35.852	-84.009	46°	23°	6/9	148.6°	38.8°	146.8°	25.3°	7.3°	84.81
OC15	36.309	-83.760	64°	33°	6/7	179.9°	60.8°	170.7°	42.3°	11.3°	35.97
OC16	36.022	-83.858	53°	59°	5/10	154.2°	50.3°	150.2°	15.4°	11.6°	44.16
OC17	36.200	-83.768	57°	39°	10/10	154.7°	53.6°	152.3°	30.3°	3.0°	257.89
OC18	36.498	-83.155	69°	31°	13/13	160.9°	38.6°	160.5°	20.0°	4.5°	87.63
OC19	36.536	-82.993	53°	57°	5/8	160.2°	73.8°	148.9°	40.2°	10.9°	50.4
OC20	36.714	-82.895	62°	33°	4/9	162.0°	48.3°	159.6°	28.7°	7.1°	168.11
OC21	36.612	-83.575	209°	12°	8/9	142.5°	11.7°	143.3°	18.3°	9.6°	33.93
OC22	36.479	-83.851	283°	21°	0/8	-	-	-	-	-	-
OC23	36.661	-83.390	248°	11°	6/10	156.3°	21.0°	156.2°	27.6°	9.8°	47.38
OC24	36.533	-83.722	238°	13°	11/11	160.0°	25.4°	160.9°	33.0°	10.2°	20.88
OC25	36.419	-83.677	53°	24°	9/12	159.7°	37.9°	157.4°	24.0°	7.5°	48.34
OC26	36.411	-83.563	49°	28°	12/12	169.8°	29.4°	166.5°	14.7°	6.9°	40.05
OC27	36.117	-83.658	246°	88°	0/12	-	-	-	-	-	-
OC28	35.913	-83.866	45°	21°	9/9	143.3°	35.8°	142.3°	23.3°	9.7°	29.07
OC29	35.992	-83.677	228°	15°	8/9	148.0°	31.5°	149.2°	40.3°	10.2°	30.23
OC30	36.068	-84.089	58°	28°	11/11	158.9°	43.4°	156.9°	26.8°	5.5°	70.5
OC31	35.969	-84.364	59°	33°	10/10	163.9°	40.2°	161.1°	20.9°	6.2°	62.1
OC32	35.690	-84.463	17°	36°	10/13	150.9°	56.0°	136.7°	38.5°	7.5°	42.81
OC33	34.708	-85.192	14°	14°	9/9	156.0°	21.5°	153.8°	16.2°	5.0°	107.06
OC34	34.756	-85.369	26°	13°	6/7	155.3°	13.1°	154.4°	7.0°	7.2°	86.85
OC35	34.832	-85.385	197°	35°	11/13	160.5°	-0.2°	162.3°	12.1°	4.7°	95.01
Chickamauga Mean					**32/35**	**-**	**-**	**154.5°**	**26°**	**3.9°**	**44.02**

* OC08 excluded from calculation of mean

The Chickamauga Group consists of all of the formations that lie between the pervasive Middle Ordovician unconformity above the Knox Group and the Upper Ordovician Juniata Formation (Rodgers, 1953; Milici, 1973). Toward the east, near the Blue Ridge, the Chickamauga Group consists primarily of clastic sediments (Sevier shale) while in the western thrust belt, limestones dominate the unit, although some terrigenous sediments are intercalated. Limestones vary from extremely fine-grained mudstones to coarsely crystalline, reefal grainstones.

NRM intensities for the Chickamauga limestone specimens range between 0.05 and 3.00 mA/m. Such low intensities are typical of limestone units in eastern North America (McCabe et al., 1984; McCabe and Elmore, 1989; Cederquist et al., 2007). Initially, thermal demagnetization was carried out in increments of 50°C and progressively decreased to 10°C heating steps, typically above 350°C depending on the specimen's behavior. Specimen demagnetization trajectories were usually well behaved and often revealed two components (Figure 3.3). The lower temperature (A) component show a moderately steep downward direction to the north. The A component is typically removed by 300°C and is parallel to the present-day field, thus interpreted as a recent viscous overprint. The higher temperature (B) component typically decays between ~300°C and 450°C, although it unblocks as high as 520°C in a few specimens. This temperature range has been observed in numerous paleomagnetic and rock magnetic studies of Paleozoic carbonates having a magnetization carried by magnetite. In general, the in situ site-mean directions for the B component lie in a southeast and down orientation, although inclination

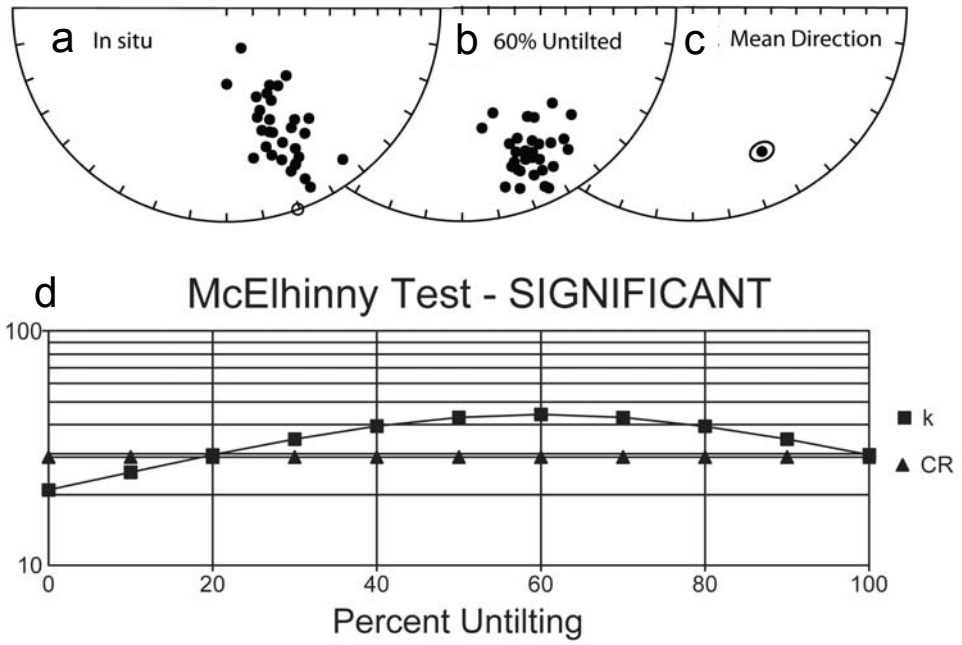

Figure 3.4: Tilt-test of the Chickamauga Group limestones. Equal area projections of site means in geographic (a) and partially tilt-corrected coordinates (b), as well as mean direction (c). Solid (open) circles represent down (up) directions. (d) Incremental tilt-test of site means plotting *k* on logarithmic scale versus percent unfolding. Squares represent *k* values and triangles represent the critical ratio (CR) at which *k* values become significant at the 95% confidence level for the number of data entries (McElhinny, 1964).

tends to vary considerably (Figure 3.4; Table 3.1). The B component is considered to represent the ChRM of the Chickamauga Group limestones and roughly corresponds to the Late Paleozoic segment of the Laurentian apparent polar wander path (APWP), indicating that the rocks have been remagnetized. Two sites (OC2 and OC27) carry magnetizations that are irresolvable due to weakly magnetized samples, while a third (OC8) has a magnetization that clusters in a southwest and up direction, which, when compared to other North American paleomagnetic data, yields a pole on the Jurassic portion of the path. These three sites were discarded from further analysis.

As evidenced in Pennsylvania and other orogens, resolving the age of remagnetization relative to deformation is quite important for curvature analysis. The fold-test performed on these rocks is better described as a tilt-test, since most of the sites were taken from limestones that are dipping gently to steeply to the southeast. Incremental untilting of the ChRM directions for the thirty-two sites reveals a statistically significant tilt-test, with the precision parameter (k) reaching a maximum at 60% untilting (Figure 3.4). This optimal untilting percentage indicates a syntilting magnetization of the Chickamauga Group limestones in the Tennessee fold-thrust belt, with a mean direction of D = 154.6°, I = 26.2°, $\alpha 95$ = 3.9°, k = 44 (Table 3.1).

Rome Formation Redbed Results

The Lower to Middle Cambrian Rome Formation is the oldest exposed unit in the Tennessee Salient (Milici, 1973; Harris and Milici, 1977; Watts et al., 1980;

Figure 3.5: Representative thermal demagnetization plots of the Rome Formation in geographic coordinates and associated intensity plots. Symbols as in Figure 3.3. Ticks represent 5.0 mA/m.

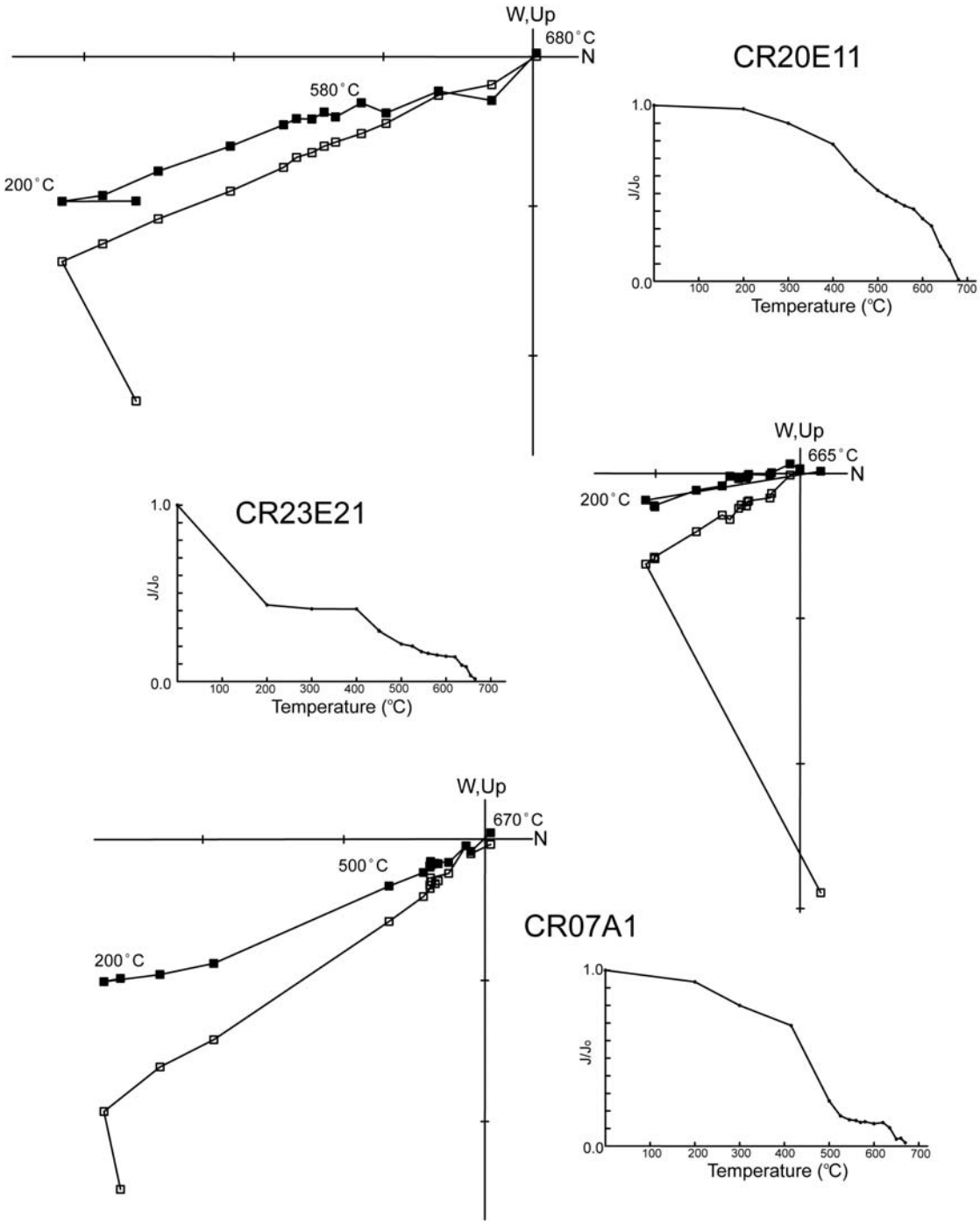
W,Up
680°C
N
580°C
200°C
CR20E11
1.0
J/J₀
0.0
100
200
300
400
500
600
700
Temperature (°C)
W,Up
665°C
N
200°C
CR23E21
1.0
J/J₀
0.0
100
200
300
400
500
600
700
Temperature (°C)
W,Up
670°C
N
500°C
200°C
CR07A1
1.0
J/J₀
0.0
100
200
300
400
500
600
700
Temperature (°C)

Site	Latitude	Longitude	Strike	Dip	N/No/H	Geo Dec	Geo Inc	TC Dec	TC Inc	α95	k
Cr01	36.249	-83.756	45°	70°	7/8/8	164.5°	44.8°	155.6°	6.3°	11.5°	28.37
Cr02	36.132	-84.062	35°	38°	8/8/8	155.2°	45.2°	148.0°	24.7°	19.2°	9.3
Cr03	36.514	-83.072	67°	60°	0/7/6	-	-	-	-	-	-
Cr04	36.449	-83.239	60°	50°	6/10/10	120.7°	57.8°	132.5°	30.0°	25.6°	7.8
Cr05	36.381	-83.450	63°	32°	7/7/7	160.9°	47.7°	159.0°	28.6°	16.5°	14.35
Cr06	36.408	-83.492	66°	37°	8/8/8	152.8°	45.8°	153.6°	23.6°	11.2°	19.42
Cr07	36.075	-83.900	65°	41°	6/7/7	165.7°	18.6°	165.2°	-5.6°	9.6°	50.1
Cr08	36.030	-84.187	57°	44°	8/8/6	171.2°	38.0°	166.4°	13.4°	16.8°	11.76
Cr09	35.984	-84.418	56°	33°	7/9/7	155.4°	39.5°	153.7°	19.9°	12°	26.22
Cr10	35.856	-84.466	41°	33°	6/10/6	179.0°	58.9°	163.0°	43.5°	13.6°	25.09
Cr11	35.981	-83.971	62°	66°	8/11/7	75.5°	66.6°	121.5°	40.4°	26.0°	5.51
Cr12	35.743	-84.512	35°	28°	6/7/6	158.4°	34.8°	153.8°	20.4°	14.5°	22.38
Cr13	35.611	-84.682	44°	47°	7/9/7	192.6°	48.5°	174.7°	29.8°	28.3°	5.49
Cr14	36.151	-84.024	53°	42°	11/13/7	192.4°	49.8°	177.8°	30.8°	13.5°	12.41
Cr15	35.172	-84.969	25°	69°	13/13/8	246.1°	60.0°	164.1°	60.1°	9.3°	20.86
Cr17	35.486	-84.746	60°	55°	7/11/6	147.8°	56.3°	148.7°	23.3°	22.0°	8.49
Cr18	34.802	-85.090	3°	75°	9/11/5	195.2°	64.8°	128.8°	44.7°	26.0°	4.87
Cr19	36.249	-83.873	50°	47°	10/14/7	153.0°	46.0°	149.5°	18.3°	15.4°	10.86
Cr20	36.411	-83.008	45°	38°	8/9/7	162.4°	30.5°	158.7°	9.9°	8.3°	46
Cr21	36.680	-82.759	66°	37°	7/7/7	158.5°	22.2°	158.3°	0.0°	11.3°	29.53
Cr23	34.927	-85.052	5°	45°	11/11/6	158.2°	29.2°	148.7°	14.8°	15.8°	9.34
Rome Mean					**20/21**	**-**	**-**	**154.4°**	**24.4°**	**8.2**	**16.83**

Table 3.2: Paleomagnetic results from the Rome Formation redbeds. $N/N_o/H$, number of specimens accepted/studied/number of hand samples collected. Other labels as in Table 3.1. Tilt-correction is 60% untilting.

Hatcher et al., 1989). As the major basal décollement unit of the fold-thrust belt, it is often exposed along the leading edges of the major thrust faults in the Valley and Ridge. Lithologically, the Rome Formation is quite heterogeneous, consisting of variegated shales and siltstones, as well as reddish to buff sandstones and in the lower portion, dolomitic beds (Milici, 1973; Watts et al., 1980).

Twenty-one sites were collected from the Rome Formation in the Tennessee Salient, with sampling focusing on reddish sandstones and siltstones. Site distribution was chosen in the thrust belt to maximize coverage of the curvature but was limited by outcrop distribution, especially on the southern limb of the salient (Figure 3.2). Since drilling of the Rome units in the field proved to be difficult, six to eight hand-samples were collected from each site, from which one or two cubes were cut to yield a total of 203 specimens.

Typical NRM intensities for the Rome Formation vary between 0.70 and 69.00 mA/m. Stepwise thermal demagnetization was carried out in intervals of 100°C starting at 200°C, with steps decreasing to 10°C above 600°C. Most specimens produce well behaved demagnetization trajectories, although some have MAD angles that approached the 20° maximum typically accepted for paleomagnetic data. As with the Chickamauga limestones, two components are observed. A present-day, viscous overprint is typically removed entirely by the first step at 200°C. Univectorial decay dominates between 200°C and endpoint temperatures ranging from 630°C to 690°C (Figure 3.5). The high unblocking temperature represents a hematite carrier of magnetization, although some specimens show a significant drop in intensity below 580°C (Figure 3.5), suggesting that some of the

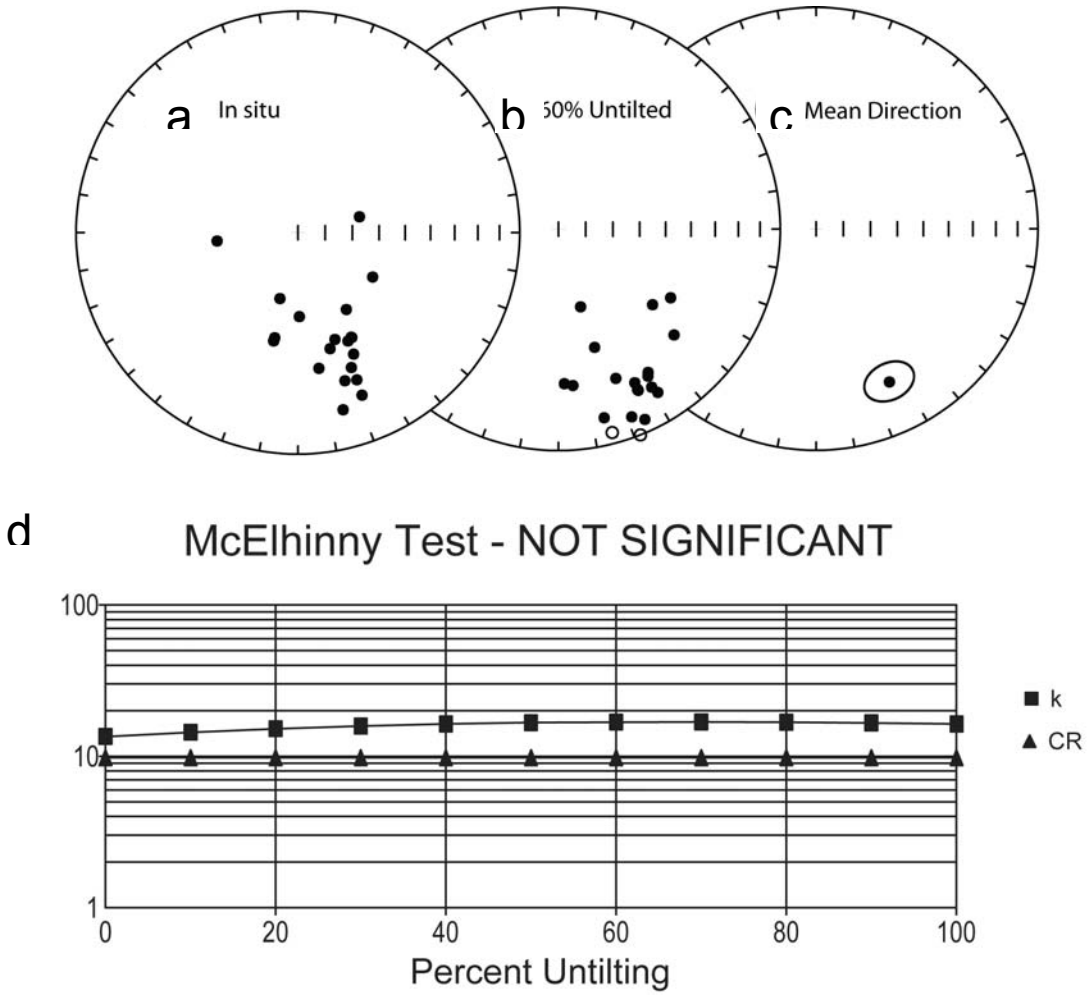

Figure 3.6: Equal area projections of site means for the Rome Formation in geographic (a) and 60% tilt-corrected coordinates (b), as well as the mean direction (c). Solid (open) circles represent down (up) directions. (d) Incremental fold test of site means plotting *k* on logarithmic scale versus percent unfolding. Symbols as in Figure 3.4.

magnetization may be carried by magnetite. Only one site (Cr03) is completely irresolvable and is therefore omitted from subsequent analysis.

Individual site mean directions typically have individual α95's that are larger than those of the Chickamauga limestones, ranging between 8.3° and 28.3° (Table 3.2). The site-mean directions from the twenty sites are generally in the southeast quadrant with intermediate down inclinations (Figure 3.6). As with the Chickamauga limestones, this roughly corresponds to the Middle to Late Paleozoic segment of the Laurentian APWP. The magnetization of the Rome Formation, therefore, can also be considered a remagnetization. Although this contradicts the claim of Watts et al. (1980) that the Rome holds a primary remanence, its reliability as a primary magnetization has long been suspect (see Van der Voo, 1993, table A1).

All Rome sites were collected from southeast dipping outcrops, with a limited range of dips. The incremental untilting of the ChRM directions reveals an insignificant tilt test, with only minor changes in the precision parameter *k* over the various untilting percentages (Figure 3.6). However, since the tilt-test of the younger Chickamauga Group limestones reveals 60% untilting, this amount can also be applied to the Rome data. At 60% untilting, the mean direction for the Rome Formation is $D = 154.4°$, $I = 24.4°$, $\alpha 95 = 8.2°$, $k = 16.8$ (Figure 3.6; Table 3.2), very similar to the Chickamauga direction.

Red Mountain Formation Redbed Results

The Red Mountain Formation consists of massive and laminated reddish hematitic sandstones, oolitic ironstones, interbedded shales and gray sandstones, lesser pebble conglomerates and limestone lenses. Sampling focused primarily on

Figure 3.7: Representative thermal demagnetization plots of the Red Mountain Formation in geographic coordinates and associated intensity plots. Symbols as in Figure 3.3. Ticks represent 10.0 mA/m.

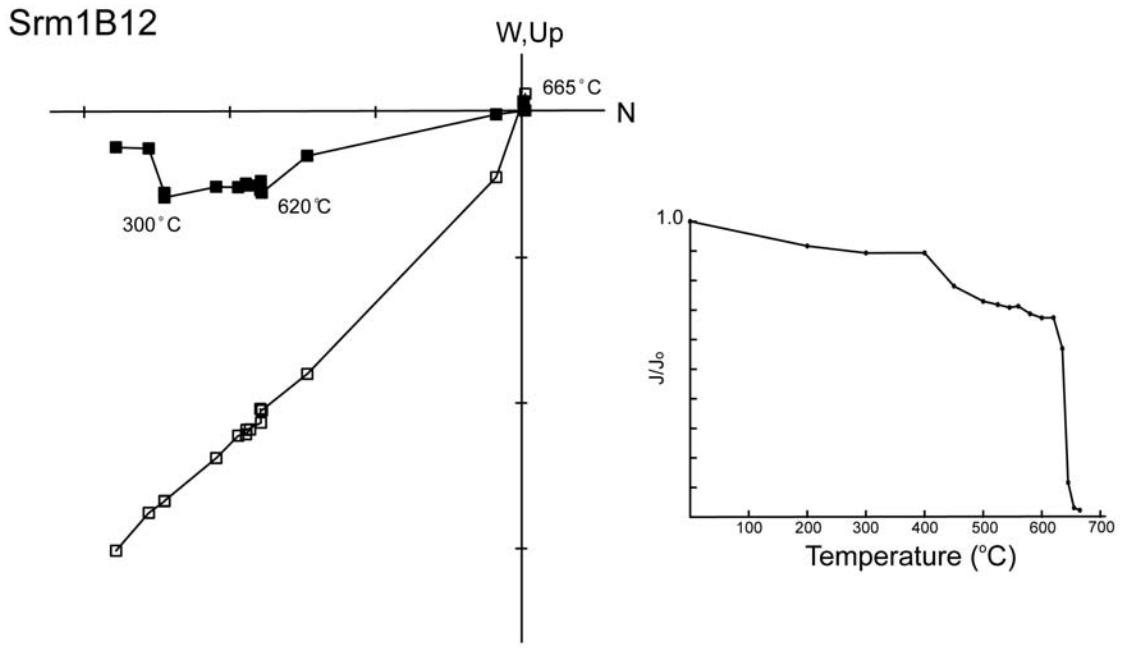
Srm1B12
W,Up
665°C
N
620°C
300°C
1.0
J/Jo
100
200
300
400
500
600
700
Temperature (°C)

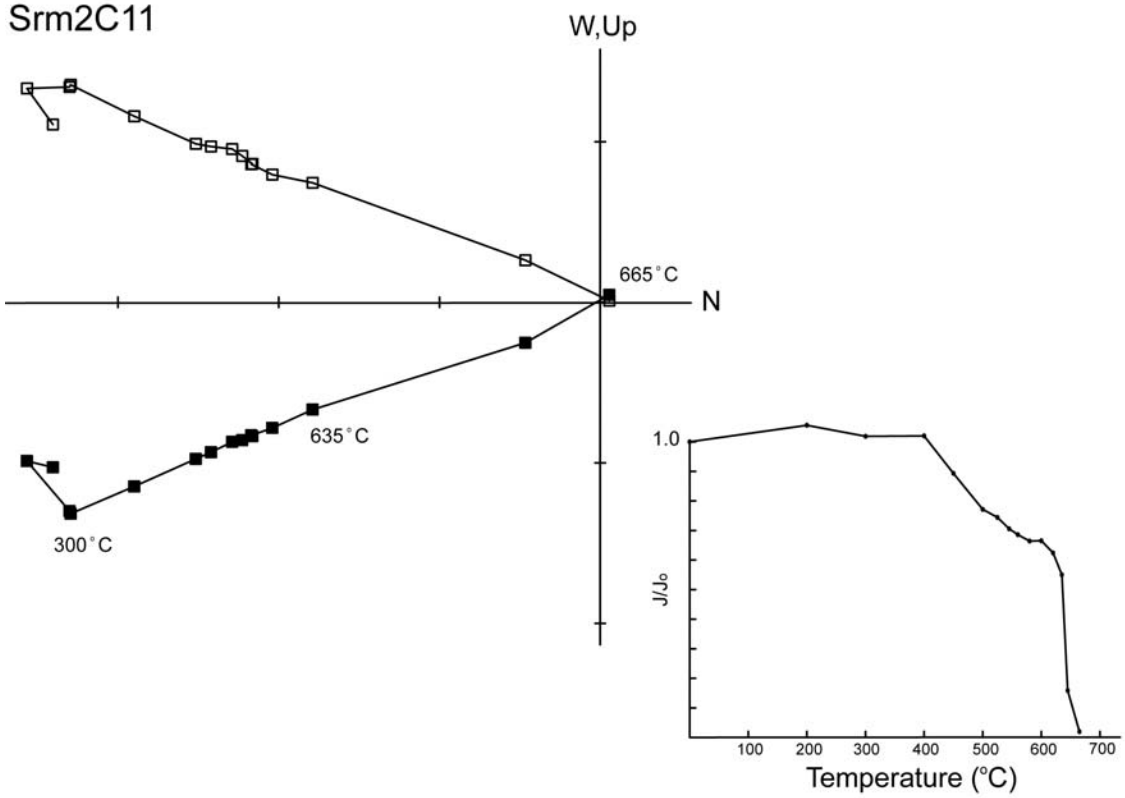
Srm2C11
W,Up
665°C
N
635°C
300°C
1.0
J/Jo
100
200
300
400
500
600
700
Temperature (°C)

Site	Latitude	Longitude	Strike	Dip	N/No/H	Geo Dec	Geo Inc	TC Dec	TC Inc	α95	k
Srm01	34.690	-85.189	27°	22°	10/12/7	153.7°	42.7°	145.8°	24.1°	7.5°	41.93
Srm02	34.801	-85.110	215°	60°	11/11/6	160.7°	-33.1°	156.0°	18.4°	5.2°	78.31
Srm03	34.907	-85.099	37°	15°	11/11/7	152.0°	36.2°	148.6°	22.4°	6.8°	45.60
SrmMean					**3/3**			**150.2°**	**21.7°**	**8.7°**	**200.53**
Perroud and Van der Voo, 1984					27/29			150.0°	20.0°	3.5°	64.00
Hnat et al., 2008					21/21			150.2°	19.0°	3.5°	107.74

Table 3.3: Paleomagnetic results from the Red Mountain Formation redbeds. Labels as in previous tables. Tilt-correction is 100% unfolding.

the hematitic sandstones, as best suited for a paleomagnetic study, and was restricted to the north-south striking thrust belt rocks in northwestern Georgia because of a lack of outcrop in Tennessee. In northwestern Georgia, the Red Mountain Formation's age ranges from Early Silurian (Llandoverian; Berry and Boucot, 1970) to Late Silurian (Pridolian; Berdan et al., 1986), with many internal disconformities as recognized by biostratigraphic work.

Six to seven hand-samples were collected from three sites of the Silurian Red Mountain Formation, with one to two specimens being cored from each sample totaling 32 specimens. Two sites from east-dipping strata and one from west-dipping strata were collected to obtain a fold-test. NRM intensities vary between 7.0 and 86.0 mA/m. Stepwise thermal demagnetization typically reveals univectorial decay to the origin, with intensity often dropping sharply between 630°C and 680°C (Figure 3.7), which is expected for the Red Moutain Formation based on previous results (Perroud and Van der Voo, 1985; Hodych et al., 1986; Hnat et al., 2008). The high unblocking temperature is indicative of a hematite carrier of magnetization.

In situ site mean directions are southeast and moderately down for the east-dipping sites and moderately up for the west-dipping site (Figure 3.8). A fold-test is carried out on all sites and after 100% tilt-correction, all sites are well clustered with k = 200.53, increased from k = 3.86 at 0% tilt-correction (Figure 3.8). The mean direction for the three Red Mountain Formation sites is a southeast and down direction of D = 150.2°, I = 21.7°, $\alpha 95$ = 8.7° (Table 3.3).

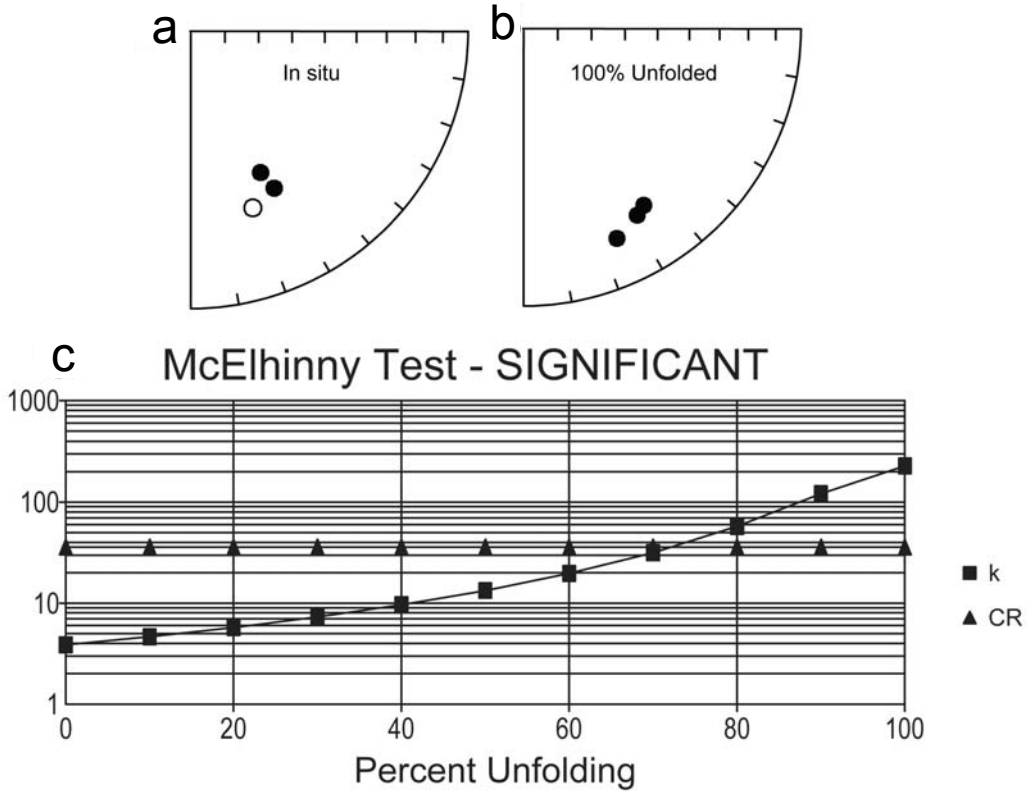

Figure 3.8: Equal area projections of site means for the Red Mountain Formation in geographic (a) and tilt-corrected coordinates (b). Solid (open) circles represent down (up) directions. (c) Incremental fold test of site means plotting *k* on logarithmic scale versus percent unfolding. Symbols as in Figure 3.4.

DISCUSSION

Age and Relative Timing of Magnetization in the Tennessee Salient

The paleomagnetic fold-test was applied to the results from all datasets to test the relative age of magnetization, producing significant results for the Chickamauga Group limestones (Figure 3.4) and the Red Mountain Formation redbeds (Figure 3.8). Since sampling of the limestones is widespread, the tilt-test for this unit is used to infer the relative age of deformation throughout our study area in the fold-thrust belt. At 60% untilting, *k* is at a maximum, suggesting more than half of the tilting had occurred on the dipping thrust sheets by the time remagnetization took place. Separating the data into two subsets from the foreland and hinterland sides of the Saltville thrust allows us to infer the progression of deformation. The Saltville thrust is a major displacement thrust (~100 km; Hatcher et al., 2007) in the southern Appalachian, separating a zone of major folding toward the hinterland and a zone dominated by imbricate thrusts toward the foreland (Woodward et al., 1988). While the difference is not statistically significant, the two tilt-tests suggest that the hinterland sites were more tilted (*k* maximum = 30% untilting) during remagnetization than sites located more toward the foreland (*k* maximum = 70% untilting) (Figure 3.9). This is a similar situation to that in the Pennsylvania-Maryland fold-thrust belt, which shows a post- to syn- to-prefolding magnetization from the hinterland to the foreland (Stamatakos et al., 1996). However, since the variation of untilting is not statistically significant, the bulk 60% untilting is used to calculate a paleomagnetic pole for the Chickamauga limestones.

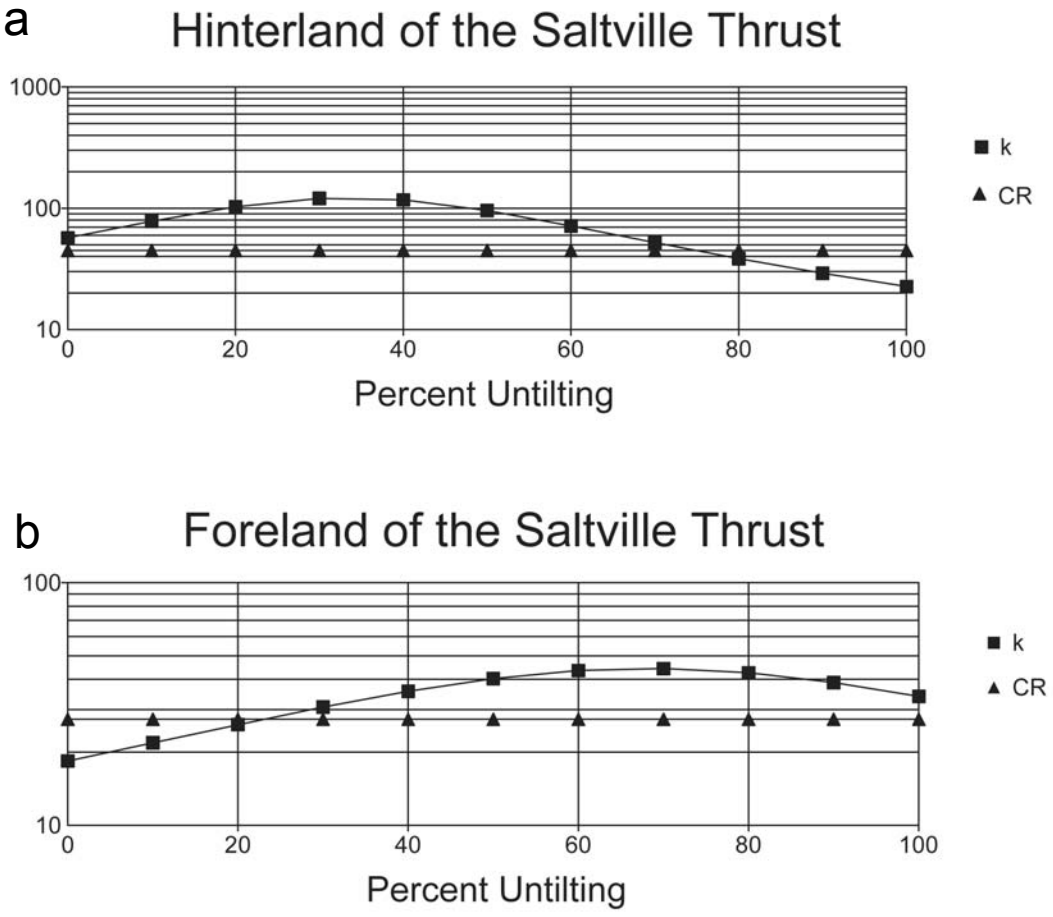

Figure 3.9: Incremental tilt-test results from Chickamauga sites located both in the hinterland (a) and foreland (b) of the Saltville thrust. Symbols as in Figure 3.4.

Moreover, the difference in paleomagnetic direction between the 60% tilt-correction and the two subsets is minimal (<1°).

To determine an approximate age for these remagnetizations, and thus, deformation, the mean directions for each dataset are compared to the APWP of Laurentia. The remagnetizations for all units occurred during a reversed polarity interval. The mean paleomagnetic pole for the tilt-corrected Ordovician Chickamauga limestones clearly lies on the Late Carboniferous segment of the path (Figure 3.10). The mean paleopole for the Rome Formation is calculated using a similar amount of untilting used for the Chickamauga limestones, despite the tilt-test being insignificant for the Rome. The resulting paleomagnetic pole also corresponds to the Late Carboniferous portion of the APWP and is statistically indistinguishable from the Chickamauga direction, further justifying our tilt correction procedure. Finally, the paleomagnetic pole calculated from the 100% unfolded Red Mountain Formation also lies on this segment of the path (Figure 3.10).

Based on our analysis of the data, we conclude that remagnetization in the southern Appalachians affected both carbonates and redbeds, and occurred during the Late Carboniferous. Previous studies of other units in the region show a similar remagnetization (Watts and Van der Voo, 1979; Bachtadse et al., 1987; McCabe and Elmore, 1989), implying that the bulk of the sedimentary package had experienced a major remagnetization event during the Late Carboniferous. Because the remagnetizations are carried by both hematite and magnetite, it is likely that the remagnetization is chemical in origin and due to orogenic brines that permeated the

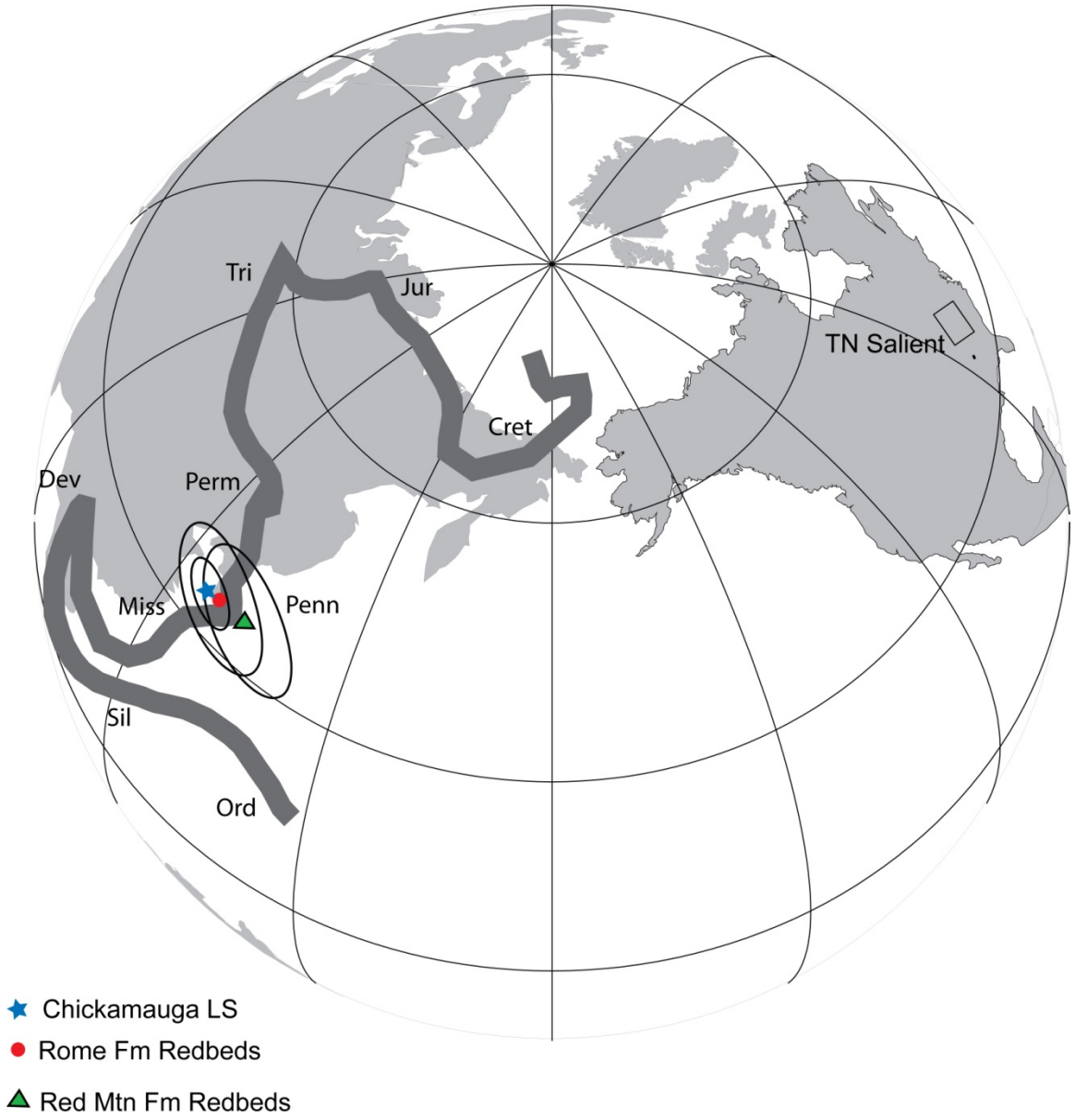

Figure 3.10: Calculated paleopoles and associated confidence ovals (dp, dm) for the Chickamauga Group limestones (star), Rome Formation redbeds (circle) and Red Mountain Formation redbeds (triangle). North American APWP derived from Van der Voo (1993) using a spline fit.

stratigraphy during deformation (Oliver, 1986; Bethke and Marshak, 1990), affecting various lithologies in different ways. The Late Carboniferous age of magnetization is slightly older than the Permian remagnetization that is pervasive in the central Appalachians and may be due to the diachronous nature of deformation along the trace of the Appalachians (Miller and Kent, 1988).

Assessment of the Nature of Curvature in the Tennessee Salient

Using the method of Eldredge et al. (1985) to determine whether units show any trace of secondary curvature, site-mean declinations of syn-tilting magnetizations for the Chickamauga and Rome sites are plotted against the regional strike. Regional orogenic strike is used to limit the effect of local strike variations. The slope of the best-fit line through the data indicates the approximate degree to which a curved belt experienced rotations. A slope of zero represents primary curvature and a slope of one reflects a pure orocline, while intermediate correlations indicate some amount of secondary curvature.

The thirty-two Chickamauga sites are plotted with the site-mean α95's as error bars in declination space (Figure 3.11a). Whereas the data are primarily clustered into two strike groups (with a large cluster from the northern limb), the lack of correlation is apparent, with the slope of the best-fit line being essentially zero (0.01). Also plotted are the twenty sites of the Rome Formation (Figure 3.11b). The Rome data show much more scatter and result in high residuals to the trendline, which requires a moving average analysis to properly evaluate. Using a window of n=3 significantly reduces the scatter and reinforces the lack of

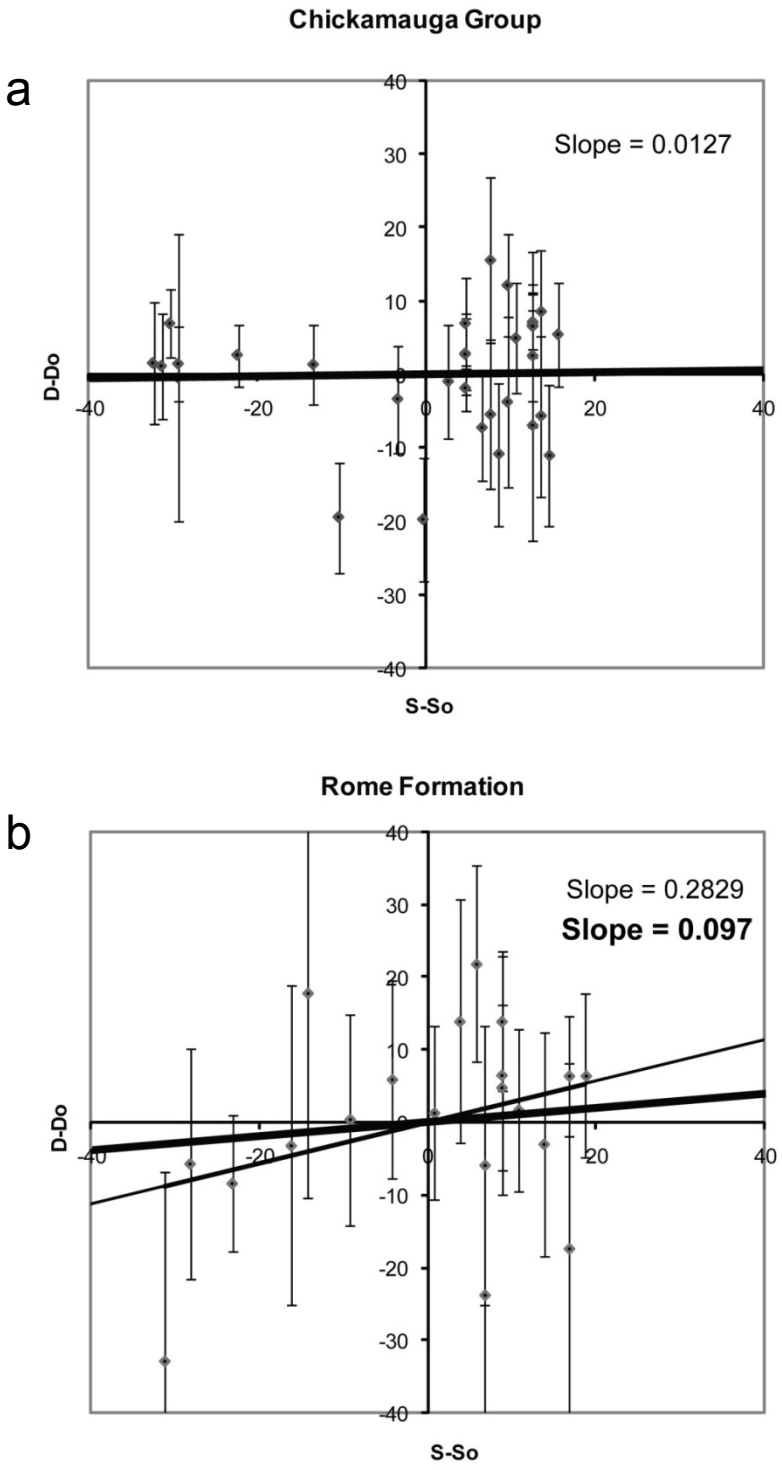

Figure 3.11: (a) Declination vs. strike plot for the Chickamauga limestones. Best-fit line through the raw data has a near-zero slope (0.0127). (b) Declination vs. strike plot for the Rome redbeds. Declinations are more scattered than in the limestones. Slope of best fit line through moving average of $n = 3$ data (heavier line) is also near-zero.

correlation between strike and declination. As with the limestone results, the slope of the best-fit line is near-zero (0.01).

Because Silurian redbeds are not exposed through much of the Tennessee fold-thrust belt, the Red Mountain Formation results cannot provide a test for the overall curvature of the Tennessee salient. However, we can compare our sites from the nearly north-south trending southern limb of the Tennessee salient with previously published results from the northeast-trending Alabama fold-thrust belt, thus allowing a test of the rotational history of the southern limb. Mean directions from Perroud and Van der Voo (1984) and Hnat et al. (2008) from the Red Mountain Formation in Alabama, with a regional strike of ~50°, are statistically indistinguishable from our mean direction, where the average strike is ~15° (Figure 3.12; Table 3.3). This indicates collectively that the southern limb of the Tennessee salient was not rotated relative to the Alabama trend.

Both redbeds of the Rome Formation and limestones of the Chickamauga Group show no correlation between regional strike and magnetic declination, indicating that the Tennessee salient possessed its curvature already in the Late Carboniferous when the magnetizations were acquired. The Red Mountain Formation also shows no difference in paleomagnetic direction from sites with different regional strikes, further supporting this finding.

CONCLUSION

Paleomagnetism of redbeds and limestones from the Tennessee salient displays late Paleozoic remagnetization, similar to rocks from other areas in the

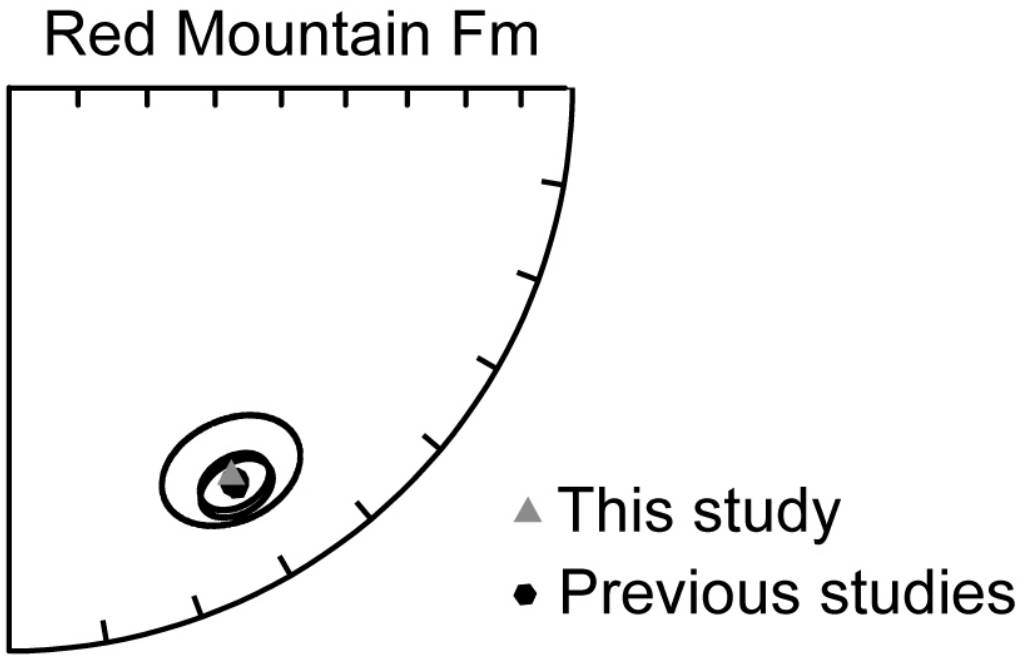

Figure 3.12: Comparison of the Red Mountain Formation results from the southern limb of the Tennessee salient (triangle) with results from previous studies (Perroud and Van der Voo, 1984; Hnat et al., 2008) in Alabama (circles).

Appalachians. Paleomagnetic analysis of the Ordovician Chickamauga Group limestones reveals a syn-tilting magnetization and Cambrian Rome Formation redbeds also display a remagnetization. Complementing these findings, the pre-folding paleomagnetic results from three sites in the Silurian Red Mountain Formation on the N-S striking southern limb of the Tennessee salient display an indistinguishable direction from previous results in Alabama. Comparison of these directions with the North American APWP shows that the regional remagnetization occurred during the Late Carboniferous, thus demonstrating that deformation (tilting) was partly completed by this time in the southern Appalachian fold-thrust belt. This timing is earlier than deformation in the central Appalachians, where syn-folding remagnetizations occurred during the Permian. The absence of correlation between orogenic strike and declination for both the Rome and Chickamauga results demonstrates that curvature in the Tennessee salient was either of primary origin or that secondary curvature was achieved before the Late Pennsylvanian. Although our results do not allow us to resolve the complete nature of curvature in the Tennessee salient, we can constrain the timing of any curvature development to Early Carboniferous or older. Other methods are currently being employed to examine this early history of the Tennessee salient, and particularly the presence of primary curvature.

ACKNOWLEDGEMENTS

Our Appalachian research at the University of Michigan has been supported by grants from the American Chemical Society-Petroleum Research Fund (most

recently 45893-AC8), a student grant from the Geological Society of America and by the Scott Turner Fund. Special thanks are given to Peter Lemiszki at the Tennessee Division of Geology – Knoxville Office for fieldwork assistance and insightful discussion.

REFERENCES

Bachtadse, V., Van der Voo, R., Hayes, F.M. and Kesler, S.A., 1987. Late Paleozoic remagnetization of mineralized and unmineralized Ordovician carbonates from east Tennessee: evidence for a post-ore chemical event. Journal of Geophysical Research B: Solid Earth 92, 14165-14176.

Berdan, J.M., Boucot, A.J. and Ferrill, B.A., 1986. The first fossiliferous Pridolian beds from the Southern Appalachians in northern Alabama, and the age of the uppermost Red Mountain Formation. Journal of Paleontology 60, 180-185.

Berry, W.B.N. and Boucot, A.J., Editors, 1970. *Correlation of the North American Silurian rocks.* Geological Society of America Special Paper 102, 289pp.

Bethke, C.M., and Marshak, S., 1990. Brine migrations across North America: the plate tectonics of groundwater. Annual Reviews of Earth and Planentary Science 18, 287-315.

Carey, S.W., 1955. The orocline concept in geotectonics. Proceedings of the Royal Society of Tasmania 89, 255-289.

Cederquist, D.P., Van der Voo, R., van der Pluijm, B.A., 2006. Syn-folding remagnetization of Cambro-Ordovician carbonates from the Pennsylvania Salient post-dates oroclinal rotation. Tectonophysics 422, 41-54.

Cifelli, F., Rossetti, F., Mattei, M., Hirt, A.M., Funiciello, R. and Tortorici, L. 2004. An AMS, structural and paleomagnetic study of Quaternary deformation in eastern Sicily. Journal of Structural Geology 26, 29-46.

Eldredge, S.V., Bachtadse, V. and Van der Voo, R., 1985. Paleomagnetism and the orocline hypothesis. Tectonophysics 119,153-179.

Evans, M.A., Elmore, R.D. and Lewchuk, M.T., 2000. Examining the relationship between remagnetization and orogenic fluids: central Appalachians. Journal of Geochemical Exploration 69-70, 139-142.

Fisher, R.A., 1953, Dispersion on a sphere. Proceedings of the Royal Society of London A 217, 295–305.

French, A.N. and Van der Voo, R., 1979. The magnetization of the Rose Hill Formation at the classical site of Graham's fold test. Journal of Geophysical Research B 84, 7688-7696.

Graham, J.W., 1949. The stability and significance of magnetism in sedimentary rocks. Journal of Geophysical Research 54, 131-167.

Hardeman, W.D., 1966. Geologic map of Tennessee. State of Tennessee Department of Conversation, Division of Geology, scale 1:250,000.

Harris, L.D. and Milici, R.C., 1977. Characteristics of a thin-skinned style of deformation in the southern Appalachians, and potential hydrocarbon traps. USGS Professional Paper 1018.

Hatcher Jr, R.D., Properties of thrusts and upper bounds for the size of thrust sheets. In: McClay, K.R., Editor, 2004. *Thrust tectonics and hydrocarbon systems*. American Association of Petroleum Geologists Memoir 82, 18-29.

Hatcher Jr, R.D., Lemiszki, P.J. and Whisner, J.B., Character of rigid boundaries and internal deformation of the Southern Appalachian foreland fold-thrust belt. In: Sears, J.W., Harms, T.A. and Evenchick, C.A., Editors, 2007. *Whence the mountains? Inquiries into the evolution of orogenic systems; a volume in honor of Raymond A. Price.* Geological Society of America Special Paper 433, 243-276.

Hatcher Jr, R.D., Thomas, W.A., Geiser, P.A., Snoke, A.W., Mosher, S. and Wiltschko, D.V., Alleghanian orogen. In: Hatcher Jr, R.D., Thomas, W.A. and Viele, G.E., Editors, 1989. *The Appalachian-Ouachita Orogen in the United States, The Geology of North America Volume F-2.* Geological Society of America, Boulder, Colorado, 233-318.

Hindle, D. and Burkhard, M., 1999. Strain, displacement and rotation associated with the formation of curvature in fold belts; the example of the Jura arc. Journal of Structural Geology 21, 1089-1101.

Hnat, J.S., van der Pluijm, B.A., Van der Voo, R. and Thomas, W.A., 2008, Differential displacement and rotation in thrust fronts: A magnetic, calcite twinning and palinspastic study of the Jones Valley thrust, Alabama, US Appalachians. Journal of Structural Geology 30, 725-738.

Hodych, J.P., Paetzold, R.R. and Buchan, K.L., 1985, Chemical remanent magnetization due to deep-burial diagenesis in oolitic hematite-bearing ironstones of Alabama. Physics of the Earth and Planetary Interiors 37, 261-284.

Irving, E. and Opdyke, N.D., 1965. The paleomagnetism of the Bloomsburg red beds and its possible application to the tectonic history of the Appalachians. Geophysical Journal of the Royal Astronomical Society 9, 153-167.

Jelinek, V., 1978, Statistical processing of anisotropy of magnetic susceptibility measured on groups of specimens. Studia Geophysica et geodetica 22, 50-62.

Kent, D.V., 1988. Further paleomagnetic evidence for oroclinal rotation in the

central folded Appalachians from the Bloomsburg and the Mauch Chunk Formations. Tectonics 7, 749-759.

Kent, D.V. and Opdyke, N.D., 1985. Multicomponent magnetization from the Mississippian Mauch Chunk Formation of the central Appalachians and their tectonic implications. Journal of Geophysical Research B 90, 5371-5383.

Kesler, S.E. and van der Pluijm, B.A., 1990. Timing of Mississippi Valley-type mineralization; relation to Appalachian orogenic events. Geology 18, 1115-1118.

Kirschvink, J.L., 1980. The least-square line and plane and the analysis of palaeomagnetic data. Geophysical Journal of the Royal Astronomical Society 62, 699–718.

Knowles, R.R. and Opdyke, N.D., 1968. Paleomagnetic results from the Mauch Chunk Formation: A test of the origin of curvature in the folded Appalachians of Pennsylvania. Journal of Geophysical Research 73, 6515-6526.

Kodama, K.P., 1988. Remanence rotation due to rock strain during folding and the stepwise application of the fold test. Journal of Geophysical Research B 93, 3357-3371.

Lawton, D.E. and others, 1976. Geologic map of Georgia. Georgia Department of Natural Resources and Georgia Geological Survey, scale 1:250,000.

Leach, D.L., Bradley, D., Lewchuk, M.T., Symons, D.T.A., de Marsily, G. and Brannon, J., 2001. Mississippi Valley-type lead-zinc deposits through geological time; implications from recent age-dating research. Mineralium Deposita 36, 711-740.

Lowrie, W. and Hirt, A.M. Paleomagnetism in arcuate mountain belts. In: Wezel, Forese-Carlo, Editor, 1986. *The Origin of Arcs*. Elsevier, Amsterdam, Netherlands, 141-157.

Macedo, J. and Marshak, S., 1999. Controls on the geometry of fold-thrust belt salients. Geological Society of America Bulletin 111, 1808-1822.

Marshak, S., 1988. Kinematics of orocline and arc formation in thin-skinned orogens. Tectonics 7, 73-86.

Marshak, S., Salients, recesses, arcs, oroclines, and syntaxes; a review of ideas concerning the formation of map-view curves in fold-thrust belts. In: McClay, K.R., Editor, 2004. *Thrust tectonics and hydrocarbon systems*. American Association of Petroleum Geologists Memoir 82, 131-156.

Marshak, S., Wilkerson, M.S. and Hsui, A.T., Generation of curved fold-thrust belts; insight from simple physical and analytical models. In: McClay, K.R., Editor, 1992. *Thrust tectonics.* Chapman & Hall, London, United Kingdom, 83-92.

McCabe, C., Van der Voo, R. and Ballard, M.M., 1984. Late Paleozoic remagnetization of the Trenton Limestone. Geophysical Research Letters 11, 979-982.

McCabe, C., Van der Voo, R., Wilkinson, B.H. and Devaney, K., 1985. A Middle/Late Silurian paleomagnetic pole from limestone reefs of the Wabash Formation, Indiana, USA. Journal of Geophysical Research B 90, 2959-2965.

McCabe, C. and Elmore, R.D., 1989. The occurrence and origin of late Paleozoic remagnetization in the sedimentary rocks of North America. Reviews of Geophysics 27, 471-494.

McCaig, A.M. and McClelland, E., 1992. Paleaeomagnetic techniques applied to thrust belts. In: McClay, K.R., Editor, *Thrust Tectonics*. Chapman and Hall, New York, New York, 209-216.

McDowell, R.C., Grabowski, G.J., Jr. and Moore, S.L., 1981. Geologic map of Kentucky. US Geological Survey, scale 1:250,000.

McElhinny, M. W., 1964. Statistical significance of the fold test in paleomagnetism. Geophysical Journal of the Royal Astronomical Society 8, 338-340.

McFadden, P.L. and Jones, D.L., 1981. The fold test in paleomagnetism. Geophysical Journal of the Royal Astronomical Society 67, 53-58.

Milici, R.C., 1973, The stratigraphy of Knox County, Tennessee. Bulletin – Tennessee, Division of Geology 70, 9-24.

Miller, J.D. and Kent, D.V., 1986. Paleomagnetism of the Upper Devonian Catskill Formation from the southern limb of the Pennsylvania Salient; possible evidence of oroclinal rotation. Geophysical Research Letters 13, 1173-1176.

Miller, J.D. and Kent, D.V., 1988. Regional trends in the timing of Alleghanian remagnetization in the Appalachians. Geology 16, 588-591.

Miller, J.D. and Kent, D.V., 1989. Paleomagnetism of the Upper Ordovician Juniata Formation of the Central Appalachians revisited again. Journal of Geophysical Research B 94, 1843-1849.

Morrison, J. and Ellwood, B.B., 1986. Paleomagnetism of Silurian-Ordovician sediments from the Valley and Ridge Province, Northwest Georgia. Geophysical Research Letters 13, 189-192.

Oliver, J., 1986. Fluids expelled tectonically from orogenic belts; their role in hydrocarbon migration and other geologic phenomena. Geology 14, 99-102.

Osbourne, W.E., Szabo, M.W., Neatherly, T.L. and Copeland, Jr., C.W., 1988. Geologic map of Alabama: Northeast sheet. Geological Survey of Alabama, Special Map 220, scale 1:250,000.

Pannalal, S.J., Symons, D.T.A. and Misra, K.C., 2003. Sweetwater Ba-F-Zn district, eastern Tennesseel a paleomagnetic age for dolomitisation from fluid flow. Journal of Geochemical Exploration 78-79, 235-241.

Perroud, H., Van der Voo, R., 1984. Secondary magnetizations from the Clinton-type iron ores of the Silurian Red Mountain Formation, Alabama. Earth and Planetary Science Letters 67, 391-399.

Pueyo, E.L., Pocovi, A., Millán, H., and Sussman, A.J. Map-view models for correctiong and calculating shortening estimates in rotated thrust fronts using paleomagnetic data. In: Weil, A.B. and Sussman, A.J., Editors, 2004. *Orogenic curvature; Integrating paleomagnetic and structural analyses.* Geological Society of America Special Paper 383, 57-71.

Rankin, D.W., 1975. The continental margin of eastern North America in the southern Appalachians; the opening and closing of the Proto-Atlantic Ocean. American Journal of Science 275-A, 298-336.

Rodgers, J., 1953. Geologic map of East Tennessee with explanatory text. Tennessee Department of Conservation, Division of Geology Bulletin 58.

Rodgers, J., 1970. *The tectonics of the Appalachians*. Wiley Interscience, New York, New York, 271p.

Roy, J.L., Opdyke, N.D. and Irving, E., 1967. Further paleomagnetic results from the Bloomsburg Formation. Journal of Geophysical Research 72, 5075-5086.

Schwartz, S.Y. and Van der Voo, R., 1983. Paleomagnetic evaluation of the orocline hypothesis in the Central and Southern Appalachians. Geophysical Research Letters 10, 505-508.

Somma, R., 2006. The south-western side of the Calabrian Arc (Peloritani Mountains): geological, structural and AMS evidence for passive clockwise rotations. Journal of Geodynamics 41, 422-439.

Stamatakos, J. and Hirt, A.M., 1994. Paleomagnetic considerations of the development of the Pennsylvania Salient in the Central Appalachians. Tectonophysics 231, 237-255.

Stamatakos, J., Hirt, A.M. and Lowrie, W., 1996. The age and timing of folding in the Central Appalachians from paleomagnetic results. Geological Society of America Bulletin 108, 815-829.

Symons, D.T.A. and Stratakos, K.K., 2002. Paleomagnetic dating of Alleghenian orogenesis and mineralization in the Mascot-Jefferson City zinc district of East Tennessee, USA. Tectonophysics 348, 51-72.

Tauxe, L., 1998. *Paleomagnetic Principles and Practice*. Kluwer Academic Publishers, Boston, Massachussetts, 299 pp.

Thomas, W.A., 1977. Evolution of Appalachian-Ouachita salients and recesses from reentrants and promontories in the continental margin. American Journal of Science 277, 1233-1278.

Thomas, W.A., 1991. The Appalachian-Ouachita rifted margin of southeastern North America. Geological Society of America Bulletin 103, 415-431.

Thomas, W.A., 2004. Genetic relationship of rift-stage crustal structure, terrane accretion, and foreland tectonics along the southern Appalachian-Ouachita orogen. Journal of Geodynamics 37, 549-563.

Torsvik, T., Briden, J.C. and Smethurst, M.A., 1999. SuperIAPD1999 – Software Package, Geological Survey of Norway, Trondheim.

Van der Voo, R., 1993, *Paleomagnetism of the Atlantic, Tethys and Iapetus Oceans*, Cambridge University Press, New York, New York, 411 pp.

Van der Voo, R., French, A.N. and French, R.B., 1977. A paleomagnetic pole position from the folded Upper Devonian Catskill red beds, and its tectonic implications. Geology 7, 345-348.

Vigil, J.F., Pike, R.J. and Howell, D.G., 2000. *A Tapestry of Time and Terrain*. USGS Geologic Investigations Series I 2720.

Watts, D.R. and Van der Voo, R., 1979. Paleomagnetic results from the Ordovician Moccasin, Bays, and Chapman Ridge formations of the Valley and Ridge Province, eastern Tennessee. Journal of Geophysical Research B 84, 645-655.

Watts, D.R., Van der Voo, R. and French, R.B., 1980. Paleomagnetic investigation of the Cambrian Waynesboro and Rome formations of the Valley and Ridge Province of the Appalachian Mountains. Journal of Geophysical Research B 85, 5331-5343.

Weil, A.B. and Sussman, A.J., Classification of curved orogens based on the timing

relationships between structural development and vertical-axis rotations, In: Weil, A.B. and Sussman, A.J., Editors, 2004. *Orogenic curvature; Integrating paleomagnetic and structural analyses.* Geological Society of America Special Paper 383, *1-17.*

Woodward, N.B., Walker, K.R. and Lutz, C.T., 1988. Relationships between early Paleozoic facies patterns and structural trends in the Saltville thrust family, Tennessee Valley and Ridge, Southern Appalachians. Geological Society of America Bulletin 100, 1758-1769.

Zijderveld, J.D.A. AC demagnetization of rocks: analysis of results. In: Collinson, D.W. and Creer, K.M., Editors, 1967. *Methods in Paleomagnetism*, Elsevier, Amsterdam, 254–286.

CHAPTER IV

SIGNATURE OF INDENTER TECTONICS: INSIGHTS FROM CALCITE TWINNING ANALYSIS IN THE TENNESSEE SALIENT OF THE SOUTHERN APPALACHIANS, USA

ABSTRACT

The Tennessee salient in the southern Appalachian fold-thrust belt is defined by a regional variation in strike of ~55° from southwestern Virginia to northern Georgia. The origin of the arcuate nature of this belt has yet to be established. Oriented limestone samples were collected from the thrust belt and the "undeformed" foreland for calcite twinning analysis to elucidate the nature of curvature in the Tennessee salient.

Layer-parallel paleostress orientations from 25 sites within the thrust belt reveal a radial pattern that varies systematically along the orogenic front. However, the amount of fanning (~75°) exceeds the belt's frontal curvature (~40°), indicating that passive rotation of originally parallel paleostress directions as proposed elsewhere is unlikely. In addition, results from 27 foreland sites display a similarly fanned pattern of paleostress directions, collectively showing that a radial stress regime was imparted on rocks along this part of the Appalachian margin. Differential stress values are comparable to previous results, with decreasing σ_d

values from >100 MPa within the thrust belt to ~50 MPa at 40 km from the orogenic front, regardless of orientation.

Fanning of paleostress directions in foreland limestones matches the predicted indenter geometry of the Blue Ridge to the east. We conclude, therefore, that radial paleostress directions were imparted in response to the advancing Blue Ridge, with differential thrust displacement creating (primary) curvature instead of secondary rotation during shortening. This produced the present-day geometry of the Tennessee Salient, and explains the previously noted increase in displacement and number of major thrusts near the indenter's apex, and as supported by simple analogue modeling in this paper. Paleomagnetic results reported previously do not contradict a primary origin for curvature in the Tennessee Salient, which contrasts with buttress-induced secondary rotation in the Pennsylvania Salient to the north in the Appalachian chain.

INTRODUCTION

The Appalachians have been one of the most studied orogens over the past two centuries, but several unresolved issues remain regarding the development of this belt. One such issue is the origin of orogenic curvature, manifested in the Appalachians as a series of salients and recesses along the trace of this foreland fold-thrust belt (Figure 4.1). In the US they consist of the Pennsylvania salient, the Roanoke recess, the Tennessee salient and the Alabama recess, from north to south. The general view of these curved segments is that they evolved from an irregular geometry of the rifted Iapetan margin of Laurentia, which became deformed during

the Late Paleozoic Alleghanian orogeny (Rankin, 1975; Thomas, 1977; 1991; 2004). However, it remains unclear whether the kinematic evolution of the arcuate segments, and in particular the salients, is similar or whether they have their own unique deformational histories.

A feature that is common to many fold-thrust belts, curvature can vary from tens of degrees to nearly 180° (e.g., Carey, 1955; Eldredge et al., 1985; Marshak, 1988, Marshak et al., 1992, Macedo and Marshak, 1999; Marshak, 2004; Weil and Sussman, 2004). Resolving the nature of curvature in a given orogen is key to understanding its kinematic and mechanical development. Whereas numerous classification schemes have been proposed, orogenic curvature can broadly be described as primary, with formation from an initially curved state, as secondary, with curvature forming from a straighter geometry that was subsequently rotated, or some combination (also called progressive curvature) (Weil and Sussman, 2004). Differentiating between these scenarios requires that the amount (if any) of relative rotation between the limbs is established. Once the origin is constrained, the nature of curvature, along with regional structural information, provides insight into the mechanism that forms curvature. The main mechanisms of curvature in fold-thrust belts include foreland buttressing, lateral variations in sediment thickness or mechanical strength, indentation and changes in the regional stress field (Marshak, 2004; Weil and Sussman, 2004).

Whereas paleomagnetism is a popular method for assessing orogenic curvature and rotations (Eldredge et al., 1985; McCaig and McClelland, 1992; Weil and Sussman, 2004) other methods complement paleomagnetic analysis or can

substitute in areas dominated by later remagnetization. Previous studies have recognized that pre-thrusting features, such as cleavage, fractures and paleocurrent orientations, can be used to determine relative rotations within thrust belts (Nickelsen, 1979; Gray and Mitra, 1993; Apotria, 1995). Layer-parallel paleostress orientations from the analysis of calcite twins, however, have been presented as being particularly useful in determining the nature of orogenic curvature (Ferrill and Groshong, 1993a; 1993b; Kollmeier et al., 2000; Ong et al., 2007), given the relative ubiquity of appropriate rock units within many foreland fold-thrust belts. The bulk orientation of stress derived from an aggregate of twinned calcite grains tracks the orientation of the remote stress field as it occurs at low critical resolved shear stress (~10MPa) in a strain-hardening process (Jamison and Spang, 1976; Teufel, 1980; Wenk et al., 1987). Previous work has shown that the collisional stress field is recorded in limestones far into the "undeformed" foreland (e.g., Craddock et al., 1993; van der Pluijm et al., 1997; Rocher et al., 2005). Early, bedding-parallel stress is preserved within a typical limestone, offering the potential to record subsequent rotation. Comparing paleostress orientations from limestones within the thrust belt and those from the foreland, furthermore, makes it possible to constrain the origin and quantify the amount of any rotation that may have occurred.

Calcite twinning analysis has been successfully implemented in a number of curved fold-thrust belts, including the Cantabrian-Asturias Arc in Spain (Kollmeier et al., 2000), the Subalpine Chain in France (Ferrill and Groshong, 1993), the Idaho-Wyoming overthrust belt (Craddock et al., 1988) and the Pennsylvania salient (Ong

et al., 2007). These studies all showed that curvature formed from an initially straighter geometry (secondary curvature), which is typically supported by paleomagnetic data. In the Pennsylvania salient, for example, changes in calcite twinning orientations correlate with changes in strike (~60°) of major fold-axes within the fold-thrust belt, while foreland data display no such variation (Ong et al., 2007). Likewise, primary paleomagnetic directions record rotation between the limbs of the Pennsylvania salient, whereas remagnetized directions do not (Kent, 1988; Stamatakos and Hirt, 1994; Cederquist et al., 2007).

Within the US Appalachians, the more southern Tennessee salient is also defined by a change in strike of structural trends, similar to Pennsylvania (Figure 4.1). To constrain the nature of curvature formation in the Tennessee salient, calcite twinning analysis of limestones from within the fold-thrust belt as well as the undeformed foreland was performed. Rock units are particularly suitable in this area, providing a new dataset with a means to evaluate the kinematics of the southern Appalachian fold-thrust belt that complements previous paleomagnetic and regional structural data acquired from the region.

GEOLOGIC SETTING

Curvature of the Tennessee Salient

The Tennessee salient is defined by a change in regional strike within the Valley and Ridge geomorphic province, from up to 65° in Virginia and northern Tennessee to roughly 10° in northern Georgia, before returning to a more

Figure 4.1: (a) Map of Appalachian thrust belt, highlighting curvature (Vigil et al., 2000). (b) Geologic map of the Tennessee salient displaying accepted calcite twinning sites.

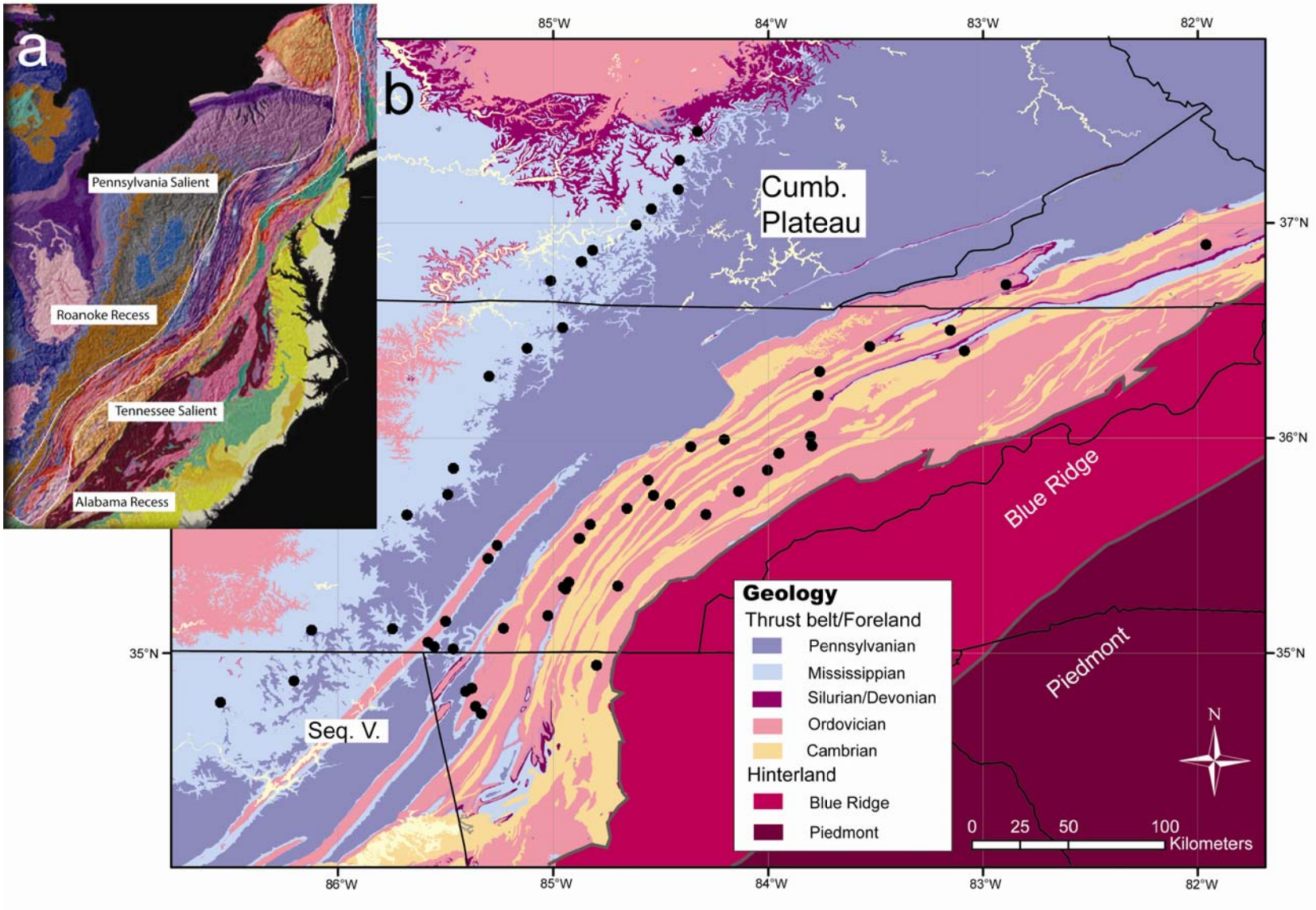
a
Pennsylvania Salient
Roanoke Recess
Tennessee Salient
Alabama Recess
b
Cumb.
Plateau
Blue Ridge
Piedmont
Seq. V.
Geology
Thrust belt/Foreland
Pennsylvanian
Mississippian
Silurian/Devonian
Ordovician
Cambrian
Hinterland
Blue Ridge
Piedmont
N
0 25 50 100
Kilometers
85°W
84°W
83°W
82°W
37°N
36°N
35°N
86°W

northeasterly direction (~45°) into Alabama (Figure 4.1). However, the curvature is not uniform across the belt. In the hinterland, the structural front of the Blue Ridge megathrust deviates up to 65° from Virginia into northern Georgia. The structural front of the fold-thrust belt (not including the thrusts of the Cumberland Plateau) is subparallel to the trend of the Blue Ridge front in the northeast. However, the structural front along the foreland edge of the fold-thrust belt only deviates by ~35° to the southwest, diverging from the Blue Ridge front.

Regional Structure

The southern Appalachian thrust belt is a classic thin-skinned fold-thrust belt, where many fundamental concepts of thrust belt architecture were first developed (e.g., the ramp-flat model of thrusting; Rich, 1934). Dominated by thick, mechanically strong Cambro-Ordovician carbonates, the southern Appalachian foreland fold-thrust belt consists of a west-verging stack of thin-skinned thrusts that sole out into a basal décollement within Cambrian shales (Milici, 1975; Woodward and Beets, 1988; Hatcher et al., 1989; Hatcher et al., 2007). Unlike the fold-dominated belt of the central Appalachians, the structural style of the exposed southern Appalachian fold-thrust belt is primarily defined by southeast dipping thrust faults, with overlying stratigraphy following the same general dip orientation (Hardeman, 1966; Harris and Milici, 1977; Hatcher et al., 1989).

The southern Appalachian fold-thrust belt intersects central Appalachian structures at the Roanoke recess (Figure 4.1), where the structural style changes from fault-dominated to fold-dominated. A regional strike change at a sharp intersection, with interfingered central and southern Appalachian structures, is

typically thought to be an intersection between two phases of deformation, oriented NNW for the southern Appalachian trend and WNW for the central Appalachian trend (Rodgers, 1970; Wiltschko *in* Hatcher et al., 1989). However, recent studies have shown shortening directions consistent with progressive migration of deformation around a pre-existing promontory (Spraggins and Dunne, 2002). Within the southern Appalachian trend in Virginia, three major thrust sheets exist that gradually increase in displacement to the southwest into Tennessee. The number of major thrust sheets increases to ten within the Tennessee salient at the latitude of Knoxville, where total displacement and depth of exposure also reach a maximum (Hardeman, 1966; Rodgers, 1970; Harris and Milici, 1977; Hatcher et al., 1989; Hatcher et al., 2007). South of this culmination into northern Georgia, the number of major thrust sheets again decreases, coincident with a decrease in displacement (Woodward, 1985; Hatcher et al., 2007). Here again, the regional strike abruptly changes from 10°-35° in the Tennessee salient to ~50° into the Alabama recess (Hardeman, 1966; Lawton et al., 1976).

The Blue Ridge-Piedmont megathrust sheet is a large-displacement (>300km), crystalline thrust sheet lying to the east of the foreland fold-thrust belt (Hatcher, 2004). This megathrust initially propagated from the east along the brittle-ductile transition before ramping onto the passive margin rocks of the foreland, as evidenced by the many windows in the thrust sheet, during the Alleghanian orogeny (Boyer and Elliott, 1982; Hatcher et al., 1989; Goldberg and Dallmeyer, 1997; Hatcher et al., 2007). The Blue Ridge is primarily comprised of basement rocks, metamorphosed during multiple events along the margin of

Laurentia, including the Grenville, Taconic, Neoacadian and earliest Alleghanian orogenies (Goldberg and Dallmeyer, 1997). By the Late Paleozoic, internal deformation of the Blue Ridge block was limited to a few minor brittle faults as the block propagated into the foreland (Hatcher et al., 2007).

Stratigraphy

The sedimentary package in the southern Appalachian fold-thrust belt is primarily comprised of Lower Paleozoic strata that thicken to the east, typical of passive margin sequences. The Lower to Middle Rome Formation is the oldest exposed unit within the fold-thrust belt and represents the mechanically weak unit that forms the basal décollement for much of the belt (Milici, 1973; Harris and Milici, 1977; Woodward and Beets, 1988; Hatcher et al., 1989). A lithologically heterogeneous unit, the Rome Formation is dominated by variegated shales and siltstones, with lesser amounts of reddish-to-buff sandstones, dolomitic beds and evaporites. Shales and limestones comprise the Cambrian Conasauga Group, grading from more carbonate rich in the east to more clastic in the west (Hardeman, 1966; Milici, 1973). Overlying the Conasauga is the Cambro-Ordovician Knox Group, which primarily consists of a thick (~1000m) package of massive dolomite beds. The Knox Group is the major mechanically strong unit in the southern Appalachians. Unconformably overlying the Knox Group is the Middle to Late Ordovician Chickamauga Group, which consists of all of the formations that lie between the pervasive Middle Ordovician unconformity above the Knox Group and the Upper Ordovician Juniata Formation (Rodgers, 1953; Milici, 1973). In the western portion of the thrust belt, limestones ranging from fine-grained mudstones to coarsely

crystalline reefal grainstones dominate the unit, while toward the east, the Chickamauga's facies grade into clastic sediments (Sevier shale).

Silurian and younger exposures are typically limited to outcrops in the footwall synclines within the Tennessee salient and Silurian clastics are better preserved to the northeast (Clinch Sandstone) and southwest (Red Mountain Formation) in large synclinoria. The Devonian Chattanooga shales are primarily relegated to the western edge of the fold-thrust belt, but represent an important detachment level in the Pine Mountain thrust sheet (Milici, 1970; Roeder and Witherspoon, 1978; Mitra, 1988). Mississippian rocks grade from more clastic within the Valley and Ridge province in the east and north to coarse grained fragmental and oolitic limestones on the western edge of the Cumberland Plateau and the Valley and Ridge in northern Georgia. Limited outcrops of the Mississippian clastic rocks (Grainger Formation) are exposed within the fold-thrust belt, being restricted to a few footwall synclines. Pennsylvanian clastic rocks, not presently exposed in most of the Valley and Ridge, dominate exposures in the Cumberland Plateau.

CALCITE TWINNING ANALYSIS

Calcite twinning analysis of limestones has yielded robust results on kinematics and mechanics in experimental (Groshong, 1974; Teufel, 1980; Groshong et al., 1984) and natural studies (e.g., Engelder, 1979; Ferrill and Groshong, 1993a, 1993b; van der Pluijm et al., 1997; Kollmeier et al., 2000). Calcite undergoes mechanical twinning under low differential stresses (<20 MPa) along one of three

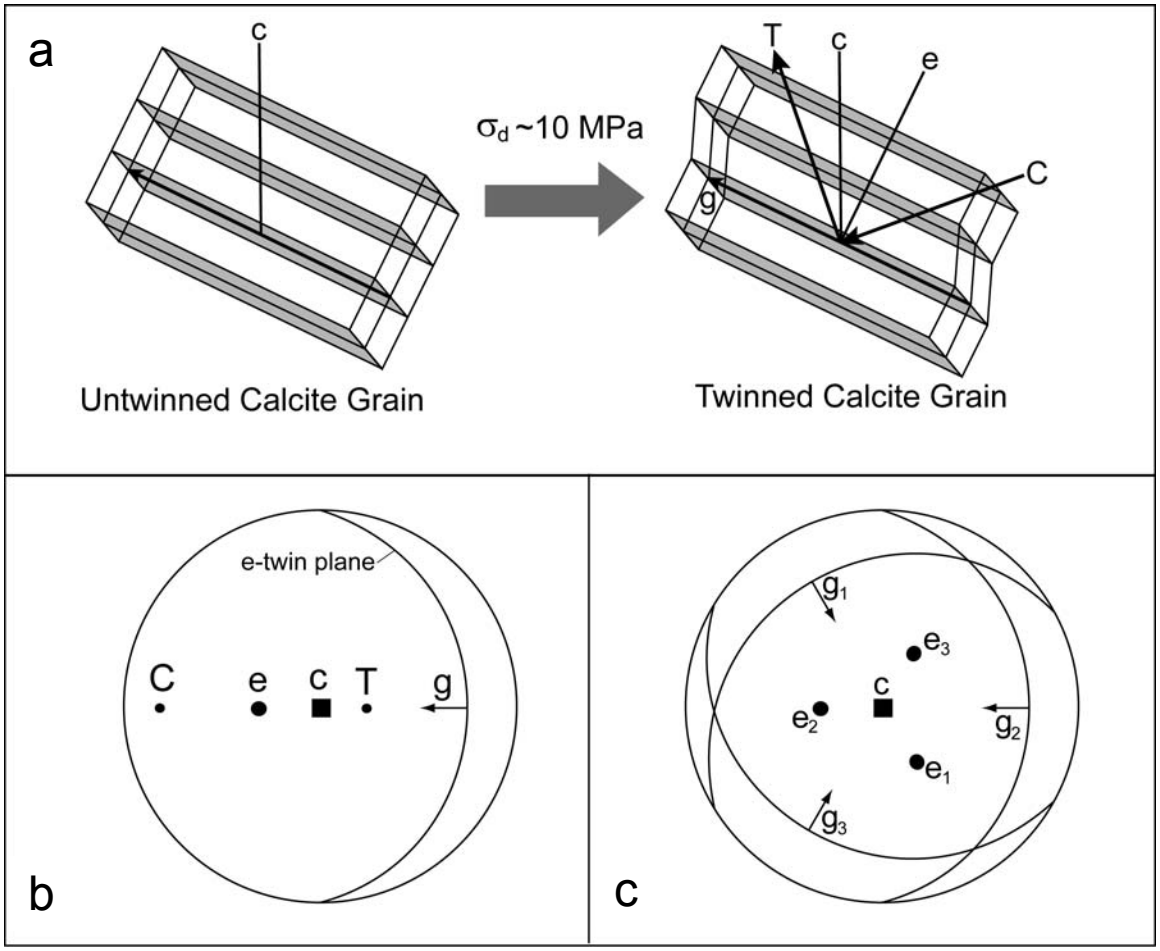

Figure 4.2: (a) Schematic of angular relationship between a single e-twin plane and the compressive (C) and tensile (T) stress axes (45° from the twin plane). The c-axis is fixed relative to the twin plane. (b) Equal area stereo projection showing the angular relationships of the geometry above. (c) All three potential twin planes relative to c-axis.

potential glide planes, where preferential twinning glide will occur along one plane depending on the orientation of the remote stress (Jamison and Spang, 1976; Wenk et al., 1987; Burkhard, 1993). Orientation of the paleostress is determined through optical determination of the *c*-axis of the host grain and the pole to the e-twin plane within the host grain (Figure 4.2; Turner, 1953). The orientation of these parameters and the fixed angular relationship between the *c*-axis and the e-twin plane are used to calculate orientations for the compression and tension axis within a grain (Figure 4.2). An average compression direction is subsequently determined for a given sample (or site) from the collective array in an aggregate of twinned grains (Spang, 1972).

Since the formation of calcite twins is a strain hardening process (Teufel, 1980), twinning patterns commonly preserve bedding-parallel shortening during the earliest deformation (e.g. Groshong, 1972; 1974; Engelder, 1979; Spang and Groshong, 1981). This creates the potential to act as a passive marker that records rotation (Craddock et al, 1988, Kollmeier et al., 2000, Ong et al., 2007). When present, multiple, discrete deformation events can be identified through superimposed populations of twins when the deformation orientations are at moderate to high angles to one another (Friedman and Stearns, 1971; Teufel, 1980). Separating the deformation events can be achieved by discriminating between twins that have a dominant compression direction (expected values) and those that have subordinate compression direction (residual values). This data "cleaning" method is fully described in Groshong (1972) and Evans and Groshong (1994).

Within the southern Appalachian fold-thrust belt, samples were primarily collected from the Middle to Upper Ordovician Chickamauga Group limestones, although some samples were collected from the Mississippian Newman limestones in northern Georgia. During sampling, areas of concentrated deformation (e.g., mesoscopic faults and fold hinges) were avoided to ensure that the results reflect regional patterns, following the recommendations of previous workers (Friedman and Stearns, 1971; Harris and van der Pluijm, 1998). In the minimally deformed foreland (including the Sequatchie Valley), sampling focused on Mississippian limestones, including the Bangor, Monteagle and Warsaw Formations. Samples were collected either as oriented hand samples or as standard paleomagnetic cores using a portable, gasoline-powered drill, and oriented using a compass. One to two oriented thin sections were cut from each sample and subsequently evaluated for appropriate grains. Thin sections were then optically analyzed on a Zeiss universal stage (U-stage) microscope to determine the crystallographic orientation of both twin sets and their host grains for fifty twin sets in most thin sections. To ensure the most accurate results, only straight, continuous twinsets were measured. Moreover, to ensure that crystallographic bias was not introduced during measurement, randomness of the crystallographic orientations of the host grains was confirmed for each thin section. Compression axes were calculated for each twinset using the method of Turner (1953) and mean paleostress orientations were determined using dynamic analysis of the compression axes (Spang, 1972). Strain tensor determinations using Groshong's (1972; 1974) method were calculated to separate positive and negative expected values in order to "clean" the data and identify

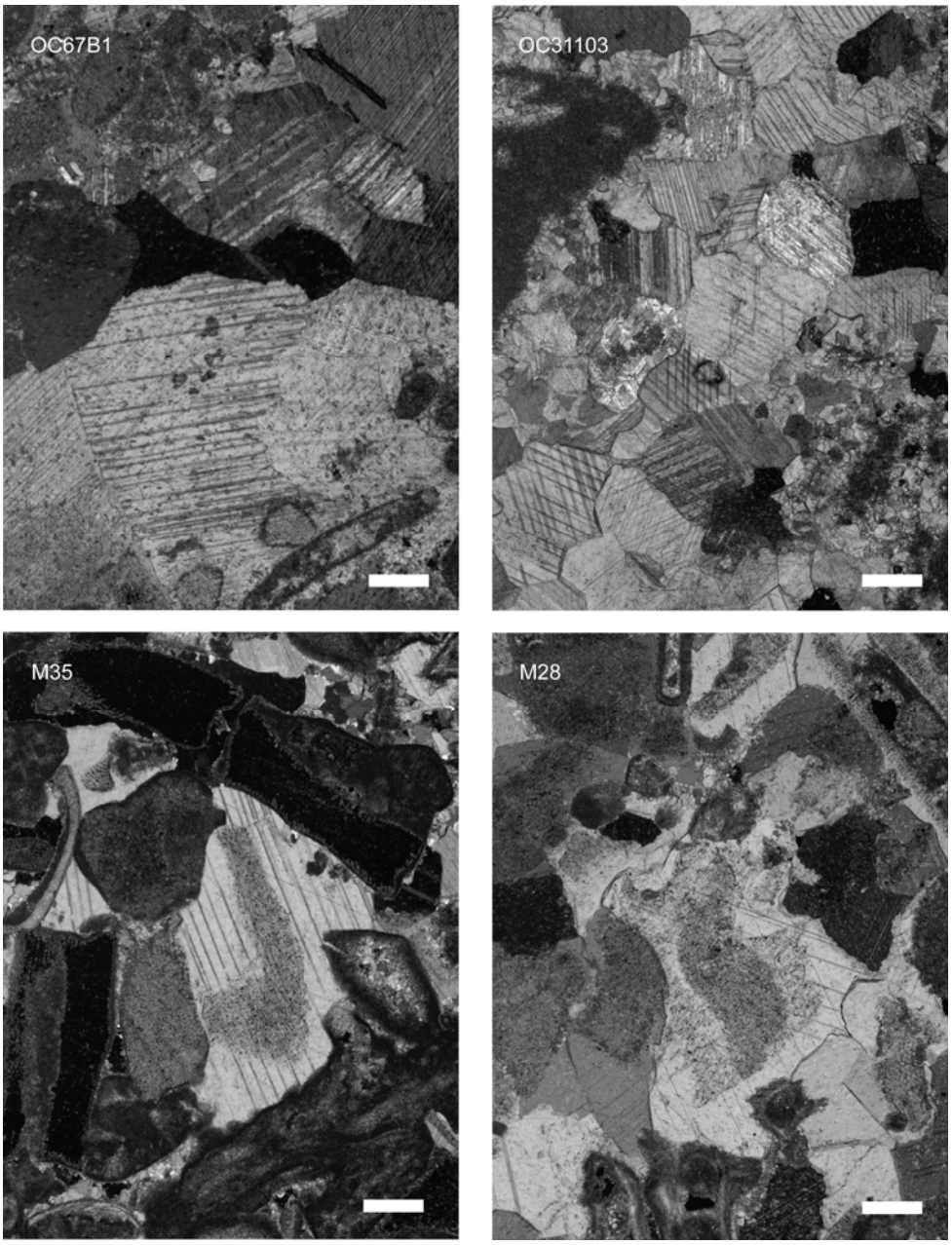

Figure 4.3: Photomicrographs of representative limestone samples analyzed in this study. Top two panels are samples from within the thrust belt whereas the bottom two panels show foreland samples. Scale bar is 200 μm

multiple deformations (Teufel, 1980; Groshong et al., 1984). Data were rotated into geographic coordinates and compared to bedding to verify layer-parallel paleostress orientations at each site, which occurred for 90% of the samples. All twinning calculations were performed using the GSG/Strain99 program of Evans and Groshong (1994).

Estimates of paleo-differential stress magnitudes can also be obtained for an aggregate of calcite grains. While several methods are available (Rowe and Rutter, 1990), the method of measuring the twin set density per grain (Jamison and Spang, 1976) has been shown to be the most reliable under low temperature (<200°C) conditions (Ferrill, 1998). Grains with one, two or three twinsets activated indicate progressively higher differential stresses that can be quantified, assuming a critical shear stress threshold for twinning of 10 MPa (Jamison and Spang, 1976; Lacombe and Laurent, 1996; Laurent et al., 2000; Ferrill, 1998). Point counts of at least 200 grains per section were measured on a standard petrographic microscope for a subset of thin sections from both the fold-thrust belt as well as the foreland.

RESULTS

Thrust Belt Paleostress Directions

A total of forty-five sites were collected within the fold-thrust belt for calcite twinning analysis. Samples with excess matrix and limited coarse fossil and cement grains were omitted from further analysis. Only straight, continuous twins were measured and grains typically contained relatively thin twins, indicating deformation at temperatures less than 200°C (Figure 4.3; Ferrill, 1991; Burkhard,

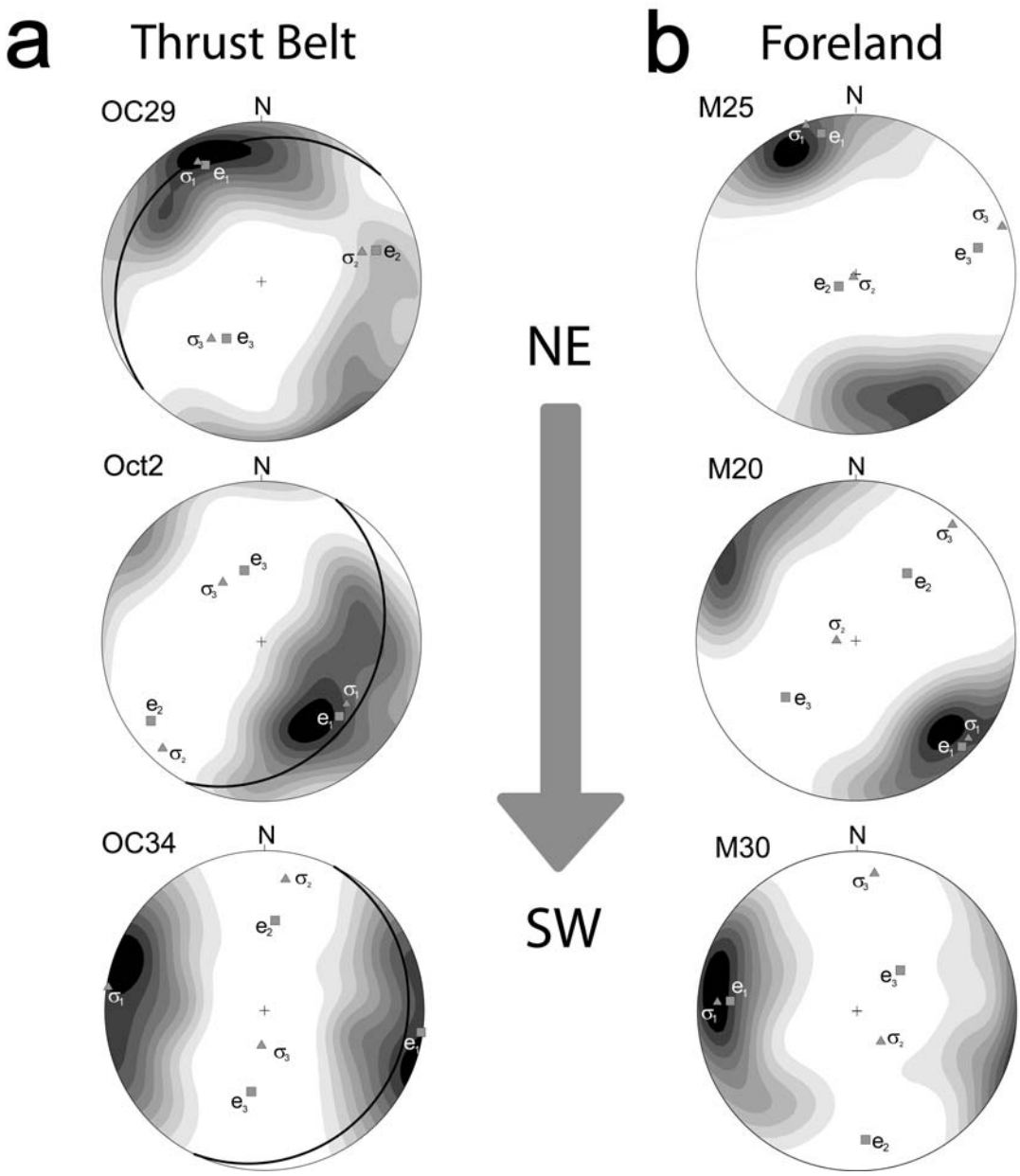

Figure 4.4: Equal-area stereo projections of results from the thrust belt (A) and the foreland (B), organized from northeast to southwest. Contoured data are Turner compression axes. Great circle represents bedding, triangles represent stress axes (σ_1, σ_2, σ_3) and squares represent strain (shortening) axes (e_1, e_2, e_3).

Figure 4.5: Geologic map of Tennessee salient with the geographic distribution and orientation of compression directions.

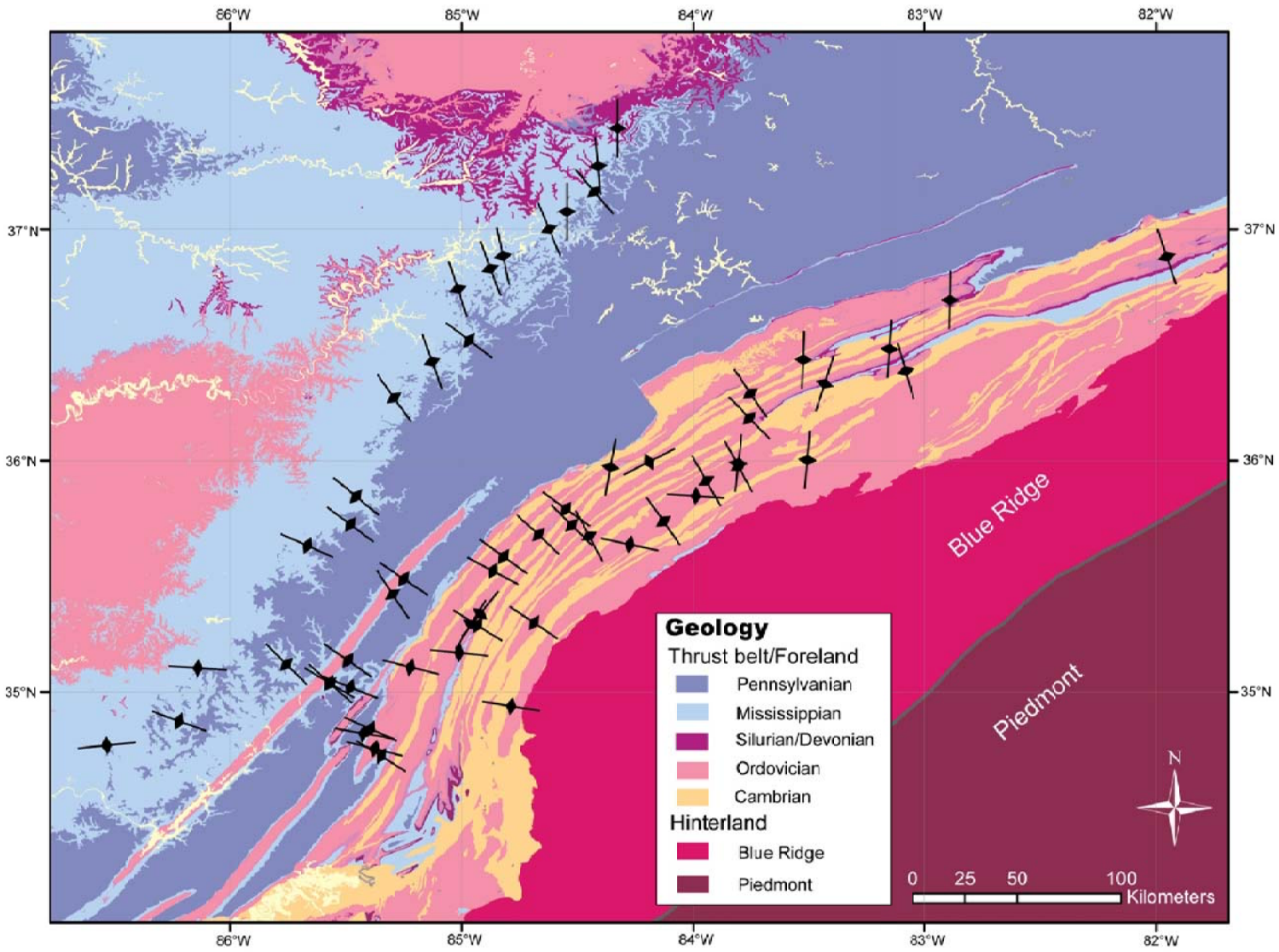
86°W
85°W
84°W
83°W
82°W
37°N
36°N
35°N
Blue Ridge
Piedmont
Geology
Thrust belt/Foreland
Pennsylvanian
Mississippian
Silurian/Devonian
Ordovician
Cambrian
Hinterland
Blue Ridge
Piedmont
N
0 25 50 100
Kilometers

Table 4.1: Calcite twinning data from the thrust belt. N, number of twinsets; % Strain, percent shortening strain; % NEV, percentage of negative expected values; N NEV, number of NEV's; e_x, strain axes in percent elongation (negative = shortening); e_x T/P, strain axes trend and plunge in geographic coordinates; σ_x T/P, stress axes trend and plunge in geographic coordinates.

Dominant Population

Site	Latitude	Longitude	Strike	Dip	N	Std Error	% Strain	% NEV	N NEV	e1	e1 T/P	e2	e2 T/P	e3	e3 T/P	σ1 T/P	σ2 T/P	σ3 T/P
CO12	36.90°N	81.96°W	008°	3°E	35	0.170	1.66%	0%	0	-1.764	157.1°/12.4°	0.222	2.0°/76.4°	1.542	248.3°/5.6°	342.3°/0.1°	72.4°/31.8°	252.1°/58.2°
CO19	35.86°N	83.80°W	051°	29°S	36	0.131	1.03%	0.00%	0	-1.137	21.7°/13.3°	0.257	116.1°/18.3°	0.88	257.6°/67.1°	13.6°/1.4°	104.0°/14.6°	278.1°/75.4°
CO24	35.76°N	84.14°W	058°	16°S	21	0.208	1.38%	4.75%	1	-1.195	137.4°/24.6°	-0.318	36.7°/22.0°	1.514	270.0°/55.9°	185.6°/12.3°	89.7°/25.4°	299.2°/61.4°
CO38	35.31°N	84.70°W	030°	15°E	30	0.256	1.60%	0.00%	0	-1.599	115.2°/2.2°	-0.005	225.5°/83.5°	1.603	25.3°/6.1°	129.2°/34.9°	305.2°/55.0°	37.9°/1.9°
CO42	34.95°N	84.80°W	037°	31°E	26	0.077	0.86%	0.00%	0	-0.643	77.7°/23.8°	-0.331	180.9°/27.4°	0.974	312.9°/52.2°	84.7°/24.8°	184.3°/19.8°	308.5°/57.4°
OC6	35.12°N	85.23°W	213°	81°W	34	0.117	0.89%	2.94%	1	-0.961	359.9°/67.6°	0.171	124.5°/13.9°	0.79	218.3°/17.9°	12.3°/69.8°	124.4°/7.9°	217.2°/18.2°
OC11	35.65°N	84.28°W	052°	15°S	29	0.147	1.65%	3.45%	1	-0.636	110.3°/24.6°	-0.018	17.6°/6.0°	0.654	274.9°/64.6°	101.8°/35.6°	327.5°/44.3°	210.9°/24.6°
OC13	35.54°N	84.88°W	350°	3°W	34	0.148	1.85%	0%	0	-1.978	121.5°/1.2°	0.288	31.1°/16.3°	1.69	215.7°/73.6°	118.1°/2.7°	28.0°/1.9°	263.1°/86.7°
OC14	35.86°N	84.00°W	046°	23°S	26	0.148	0.92%	7.69%	2	-0.993	108.8°/24.2°	0.16	212.7°/28.1°	0.832	344.6°/51.3°	94.2°/24.1°	208.9°/43.0°	344.3°/37.3°
OC16	36.01°N	83.80°W	053°	59°S	40	0.142	0.84%	0%	0	-0.756	173.4°/66.9°	-0.149	32.9°/18.3°	0.905	298.3°/13.7°	198.8°/34.3°	54.3°/50.1°	301.6°/18.0°
OC17	36.20°N	83.77°W	057°	39°S	33	0.130	0.58%	12.12%	4	-0.64	162.8°/34.5°	0.16	68.3°/6.6°	0.48	328.9°/54.7°	135.2°/21.1°	235.9°/25.8°	10.9°/55.7°
OC20	36.71°N	82.89°W	062°	33°S	48	0.129	1.24%	6.25%	3	-1.358	165.3°/46.8°	0.278	56.9°/16.5°	1.079	313.3°/38.5°	189.4°/38.6°	76.9°/25.6°	322.7°/40.6°
OC29	35.97°N	83.80°W	228°	15°N	38	0.099	0.99%	0%	0	-1.032	334.3°/20.2°	0.103	74.8°/26.4°	0.929	211.6°/55.7°	332.1°/16.0°	73.5°/34.6°	221.5°/50.9°
OC32	35.69°N	84.46°W	017°	36°E	24	0.163	1.15%	4.17%	1	-1.113	154.4°/18.2°	-0.077	328.0°/71.7°	1.191	63.8°/1.9°	151.9°/29.7°	18.7°/50.2°	256.6°/24.0°
OC34	34.82°N	85.41°W	026°	12°E	44	0.097	1.16%	0%	0	-1.283	97.9°/1.2°	0.306	6.8°/42.7°	0.976	189.2°/47.3°	278.7°/1.2°	9.1°/17.7°	184.9°/72.3°
OC35	34.76°N	85.36°W	197°	35°W	28	0.275	2.70%	0.00%	0	-2.862	288.4°/28.8°	0.363	190.8°/13.6°	2.499	78.4°/57.6°	284.1°/41.7°	179.9°/15.4°	74.3°/44.3°
Oct2	35.81°N	84.56°W	032°	28°S	37	0.097	0.76%	2.70%	1	-0.852	133.7°/32.9°	0.253	234.4°/16.0°	0.599	346.4°/52.5°	126.0°/34.4°	222.9°/10.0°	326.8°/53.7°
Oct3	35.73°N	84.53°W	039°	56°E	32	0.098	0.77%	0.00%	0	-0.853	136.7°/11.4°	0.227	41.1°/25.6°	0.625	248.6°/61.6°	134.4°/9.0°	39.2°/29.4°	239.6°/59.0°
Oct4	35.68°N	84.66°W	270°	1°N	20	0.260	1.18%	5%	1	-1.149	323.6°/17.8°	-0.067	61.2°/22.6°	1.217	198.9°/60.7°	313.3°/14.4°	51.3°/28.6°	199.6°/57.3°
Oct5	35.60°N	84.83°W	034°	22°S	25	0.135	0.69%	4.00%	1	-0.778	122.6°/5.6°	0.259	25.5°/51.6°	0.519	217.0°/37.8°	126.4°/6.8°	243.3°/75.3°	34.8°/13.0°
Oct11	35.18°N	85.02°W	013°	6°E	36	0.114	1.03%	5.56%	2	-1.164	101.2°/6.4°	0.355	193.3°/18.7°	0.809	353.2°/70.2°	96.5°/6.2°	286.0°/83.7°	186.6°/1.0°
Oct12	35.30°N	84.94°W	007°	8°E	39	0.061	0.59%	0.00%	0	-0.649	97.9°/16.3°	0.143	328.6°/65.2°	0.507	193.4°/18.1°	106.4°/15.8°	7.9°/27.6°	222.8°/57.4°
OH4	35.93°N	83.95°W	072°	29°S	35	0.123	1.67%	2.85%	1	-1.903	144.7°/34.7°	0.657	276.5°/43.9°	1.246	34.7°/26.2°	149.8°/37.5°	243.2°/4.5°	339.0°/52.1°
M6	34.72°N	85.34°W	010°	1°E	40	0.072	0.76%	0.00%	0	-0.753	301.4°/5.2°	-0.018	75.5°/82.5°	0.771	210.9°/5.3°	302.5°/36.8°	96.1°/50.1°	202.4°/13.2°
M7	34.84°N	85.38°W	189°	6°W	37	0.275	2.12%	10.80%	4	-2.316	302.6°/13.4°	0.475	32.8°/0.8°	1.841	126.0°/76.5°	293.6°/13.6°	24.6°/4.3°	131.8°/75.8°

Secondary Populations

CO17	36.40°N	83.08°W	063°	73°S	34	0.105	0.59%	0.00%	0	-0.415	3.2°/39.1°	-0.264	268.2°/6.1°	0.679	170.8°/50.3°	60.5°/12.8°	323.3°/28.9°	171.7°/57.9°
CO18	35.75°N	83.93°W	063°	46°S	29	0.129	0.56%	3.45%	1	-0.616	298.3°/31.5°	0.135	207.9°/0.7°	0.481	116.8°/58.5°	246.4°/22.5°	345.6°/21.2°	114.3°/58.3°
OC12	36.00°N	84.20°W	057°	33°S	33	0.128	1.08%	3.03%	1	-1.013	126.6°/25.3°	-0.119	227.1°/21.1°	1.133	352°/56.1°	63.4°/6.2°	157.6°/34.1°	324.5°/55.2°
Oct14	35.31°N	84.96°W	007°	7°E	46	0.077	0.75%	0.00%	0	-0.848	216.9°/6.3°	0.267	309.4°/21.0°	0.58	110.9°/68.0°	212.5°/5.1°	92.7°/79.7°	303.3°/8.9°
OC18 EV	36.50°N	83.15°W	069°	31°S	33	0.121	0.88%	3.03%	1	-0.91	321.6°/74.1°	0.06	197.8°/9.0°	0.85	105.7°/13.0°	311.3°/73.9°	184.4°/9.8°	92.1°/12.6°
Oct3 RV	35.73°N	84.53°W	039°	56°E	15	0.139	0.95%	0.00%	0	-0.833	244.8°/36.3°	-0.208	45.3°/52.1°	1.041	147.7°/9.5°	267.3°/46.0°	36.4°/31.2°	144.9°/27.6°

1993; Ferrill, 1998). Thirty-two samples that were identified to have the most favorable characteristics were measured and analyzed. Of these samples, twenty-five have a dominant population exhibiting paleostress orientations that are both layer-parallel and at a high angle to strike. Four samples of a subsidiary population are oriented sub-parallel to strike while the residual values of four other samples record a population that is roughly perpendicular to bedding. The location of bedding normal population can be attributed to loading due to either thrusting or sedimentation, which was also observed elsewhere along the belt (Ong et al., 2007). The few strike parallel compression directions are too few to be interpreted in a meaningful manner.

In the dominant population of paleostress directions, the compression axes are subparallel to the principal contraction axes (e_1), while the other principal strain axes (e_2 and e_3) tend to diverge from the principal stress axes (σ_2 and σ_3). Samples generally record less than 3% strain (Table 4.1), which is typical for this type of study. The dominant population's directions tend to be in or close to the bedding plane (Figure 4.4a), reflecting layer-parallel compression, with small deviations attributable to minor grain-scale rotations during progressive folding, as seen in limestones of the Hudson Valley (Harris and van der Pluijm, 1998). Most importantly, the compression directions display a systematic change in orientation along the trace of the Tennessee salient (Figures 4.4a and 4.5).

Foreland Paleostress Directions

Reliable paleostress directions were obtained for twenty-three samples from foreland limestones, including from the Sequatchie Valley. Twinsets were measured

Foreland Population

Site	Latitude	Longitude	Strike	Dip	N	Std Error	% Strain	% NEV	N NEV	e1	e1 T/P	e2	e2 T/P	e3	e3 T/P	σ1 T/P	σ2 T/P	σ3 T/P
Oct6	35.50°N	85.27°W	027°	21°E	39	0.08	0.74%	0.00%	0	-0.850	129.7°/26.6°	0.353	242.6°/37.8°	0.498	14.3°/40.5°	124.4°/17.9°	284.9°/71.1°	32.5°/5.9°
Oct7	35.44°N	85.30°W	025°	32°E	43	0.098	1.45%	0.00%	0	-1.466	138.5°/26.2°	0.028	46.5°/4.1°	1.439	308.3°/63.5°	146.2°/24.9°	52.3°/8.4°	305.0°/63.5°
Oct9	35.15°N	85.50°W	027°	19°E	42	0.095	0.83%	4.76%	2	-0.897	129.3°/13.2°	0.147	220.1°/3.4°	0.749	324.3°/76.3°	125.5°/1.3°	234.8°/86.1°	35.4°/3.7°
Oct10	35.05°N	85.58°W	034°	18°E	38	0.071	0.68%	2.63%	1	-0.782	121.9°/10.6°	0.369	16.8°/54.2°	0.414	219.0°/33.7°	121.2°/9.5°	257.7°/76.9°	29.8°/8.8°
M10	35.02°N	85.47°W	032°	5°E	34	0.522	2.31%	14.70%	5	-1.993	294.9°/5.3°	-0.537	25.4°/5.8°	2.530	162.9°/82.1°	292.2°/10.5°	27.5°/26.8°	182.8°/60.9°
M11	35.03°N	85.56°W	022°	7°E	37	0.106	0.90%	0.00%	0	-0.936	304.2°/3.1°	0.074	35.6°/23.8°	0.862	207.3°/65.9°	311.7°/15.3°	50.5°/29.2°	197.5°/56.3°
M13	35.12°N	85.75°W	000°	0°	37	0.074	0.54%	2.70%	1	-0.516	305.1°/14.6°	-0.042	204.5°/35.1°	0.558	54.0°/51.1°	315.1°/1.8°	224.6°/16.7°	51.2°/73.2°
M18	35.65°N	85.67°W	000°	0°	33	0.061	0.26%	6.06%	2	-0.237	107.5°/6.6°	-0.034	15.7°/15.5°	0.271	219.9°/73.1°	114.0°/1.9°	22.9°/30.2°	207.2°/59.7°
M19	35.74°N	85.49°W	000°	0°	42	0.057	0.37%	0.00%	0	-0.408	125.7°/7.6°	0.085	8.0°/74.0°	0.323	217.6°/14.0°	127.0°/2.4°	343.0°/87.0°	217.1°/1.8°
M20	35.86°N	85.47°W	000°	0°	39	0.064	0.48%	0.00%	0	-0.553	134.8°/6.9°	0.213	37.5°/46.1°	0.340	231.3°/43.1°	130.6°/7.8°	272.6°/80.2°	39.8°/6.0°
M23	36.29°N	85.30°W	000°	0°	43	0.03	0.33%	0.00%	0	-0.332	143.5°/7.3°	0.003	275.3°/79.1°	0.329	52.4°/8.0°	143.9°/4.0°	40.7°/73.2°	235.1°/16.4°
M25	36.74°N	85.01°W	000°	0°	29	0.03	0.28%	0.00%	0	-0.302	346.3°/5.5°	0.045	77.7°/13.8°	0.257	235.1°/75.2°	341.6°/0.8°	229.5°/87.9°	71.7°/2.0°
M26	36.88°N	84.82°W	000°	0°	36	0.095	0.55%	8.33%	3	-0.551	333.1°/11.9°	0.007	231.8°/42.9°	0.544	75.2°/44.7°	347.8°/4.3°	250.7°/59.0°	80.4°/30.7°
M28	34.77°N	86.55°W	000°	0°	47	0.055	0.75%	0.00%	0	-0.828	90.2°/14.6°	0.194	180.2°/0.0°	0.634	270.4°/75.4°	84.5°/12.5°	197.7°/60.6°	348.2°/26.2°
M29	34.87°N	86.21°W	000°	0°	49	0.118	1.40%	0.00%	0	-1.584	295.8°/23.7°	0.500	30.4°/10.3°	1.084	142.3°/63.9°	290.2°/14.9°	197.7°/9.5°	76.2°/72.2°
M30	35.11°N	86.13°W	000°	0°	46	0.099	0.71%	6.52%	3	-0.814	274.6°/21.6°	0.335	176.1°/20.5°	0.480	46.7°/59.4°	273.9°/13.4°	141.3°/70.5°	7.2°/13.8°
M31	37.16°N	84.42°W	000°	0°	44	0.061	0.62%	0.00%	0	-0.650	332.0°/4.8°	0.057	241.9°/1.9°	0.593	130.1°/84.8°	317.1°/7.7°	226.6°/4.0°	109.1°/81.3°
M32	36.99°N	84.62°W	000°	0°	44	0.052	0.43%	0.00%	0	-0.456	334.2°/8.3°	0.049	209.7°/75.6°	0.406	66.0°/11.7°	337.0°/0.6°	245.9°/62.7°	67.3°/27.2°
M33	36.82°N	84.87°W	000°	0°	40	0.083	0.69%	2.50%	1	-0.731	176.0°/7.9°	0.096	268.2°/16.1°	0.635	60.6°/72.0°	340.0°/6.1°	246.9°/26.6°	82.0°/62.6°
M35	36.52°N	84.96°W	000°	0°	44	0.073	0.62%	4.55%	2	-0.716	307.6°/1.2°	0.285	217.3°/15.8°	0.430	42.0°/74.1°	307.1°/2.6°	210.4°/61.7°	39.0°/28.0°
M37	36.42°N	85.12°W	000°	0°	46	0.066	0.72%	4.35%	2	-0.816	337.0°/5.7°	0.249	244.8°/21.0°	0.567	81.5°/68.1°	340.5°/5.8°	82.5°/63.7°	247.7°/25.6°
M39	37.07°N	84.55°W	000°	0°	36	0.095	0.55%	8.33%	3	-0.551	333.3°/10.2°	0.007	231.2°/40.1°	0.544	74.6°/42.8°	346.2°/3.1°	252.3°/58.2°	79.5°/31.5°
M40	37.29°N	84.41°W	000°	0°	47	0.102	1.11%	2.13%	1	-1.252	357.4°/1.3°	0.374	266.2°/42.5°	0.877	88.9°/47.4°	354.9°/3.1°	250.1°/77.8°	85.5°/11.8°

Table 4.2: Calcite twinning data from the foreland. Labels as in Table 4.1.

primarily in cement grains, although some fossil grains (mostly crinoids) were also measured; twins were typically thin and straight. Unlike samples from the fold-thrust belt, no residual stress directions are present. Paleostress orientations are generally layer parallel. Strains are typically less than 1% for these samples and the principal contraction axis (e_1) is subparallel to the compression direction (σ_1) (Table 4.2). Similar to the dominant population from the thrust belt, compression directions in the foreland show a systematic change in orientation from NNW in the north to E-W in the south (Figures 4.4b and 4.5).

Paleostress Magnitudes

Paleostress magnitudes were measured for fourteen samples within the thrust belt, and for twelve samples in the foreland. Within the thrust belt, limestones typically have high percentages of twinned grains, many with two or more twinsets, indicating higher differential stresses. Most samples in the thrust belt exceed 100 MPa (Table 4.3), with a wide range of values reflecting the diminished precision of the method at high stresses. Foreland results are variable, with higher values of σ_d near the orogenic front (taken here as the boundary between the Valley and Ridge and the Cumberland Plateau physiographic provinces) and lower values of ~30 MPa beyond 50 km into the foreland (Figure 4.6). This supports previous findings that differential stress values decrease systematically away from the orogenic front in the Appalachian foreland (Craddock and van der Pluijm, 1989; van der Pluijm, et al., 1997).

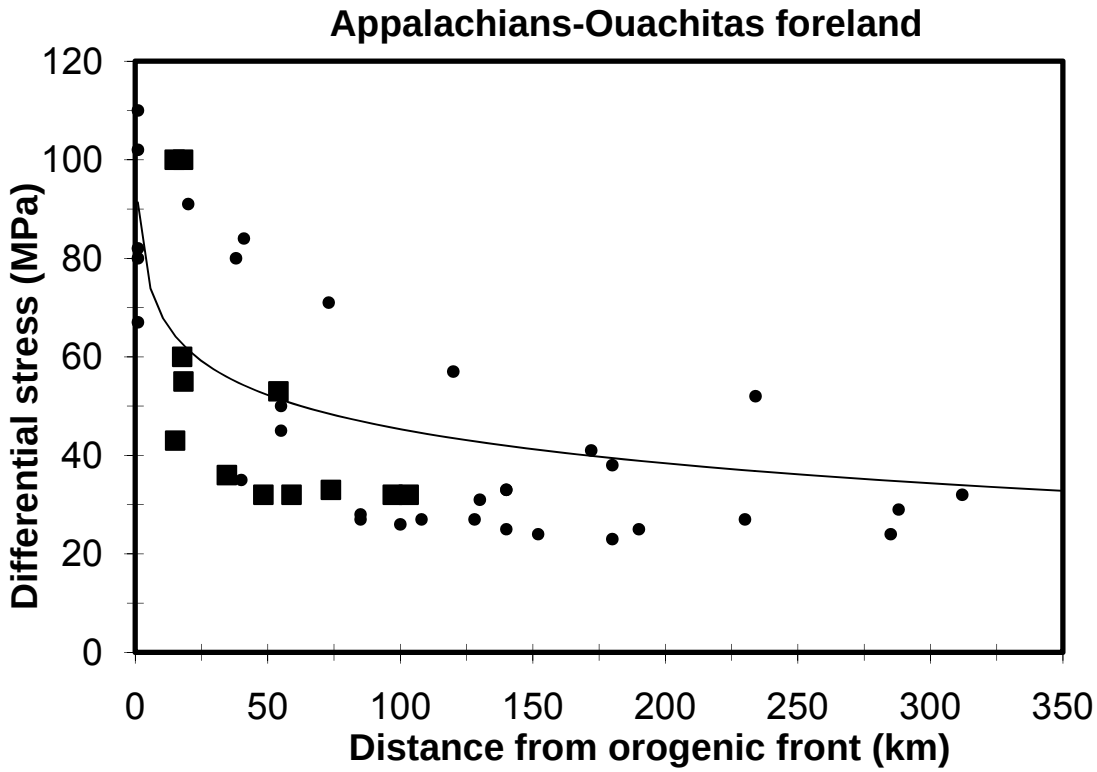

Figure 4.6: Plot of paleo-differential stress estimates versus distance from the orogenic front. Data from this study and those of van der Pluijm et al. (1997) represented by squares and circles, respectively.

Thrust belt		Foreland	
Site	Δσ	Site	Δσ
OC17	120	Oct6	60
OC20	150	Oct7	55
OC29	100	Oct9	100
OC32	133	Oct10	100
OC34	90	M11	43
OC35	111	M13	36
Oct2	83	M18	32
Oct3	100	M19	32
Oct4	166	M20	53
Oct11	63	M23	33
Oct12	87	M25	32
M6 EV	58	M26	32
M7	77		

Table 4.3: Differential stress data from the thrust belt and the foreland. Stress values are in MPa

DISCUSSION

Nature of curvature in the Tennessee salient

Paleostress directions in limestones of the southern Appalachians from both within the fold-thrust belt and from the "undeformed" foreland record a systematically fanning distribution of compression orientations along the Tennessee salient. Fanned compression patterns derived from calcite-twinning analysis in previous studies of curved fold-thrust belts have typically been used as an indication of secondary curvature (Craddock et al., 1988; Kollmeier et al., 2000; Ong et al., 2007). Secondary rotation of these belts has been supported by both paleomagnetic data and, in particular, an absence of similar fanning in foreland directions. In the Tennessee salient, on the other hand, a correlation between strike and compression directions exists both in thrust belt and in the foreland, confirming that the pattern is primary and that secondary rotation of the salient's limbs did not occur. Curvature in the Tennessee salient is therefore a primary feature, supported by syndeformational paleomagnetic data from the thrust belt (Chapter 3) and in contrast to the secondary origin of curvature in the Pennsylvania salient.

Mechanism of curvature

Comparing the compression directions with regional strike and orogenic features gives insight into the origin of curvature development. Plots of normalized, projected compression directions against strike, similar to declination versus strike plots used in paleomagnetic studies (Schwartz and Van der Voo, 1983), are shown for both the thrust front (Figure 4.7a; defined as the boundary between the Valley

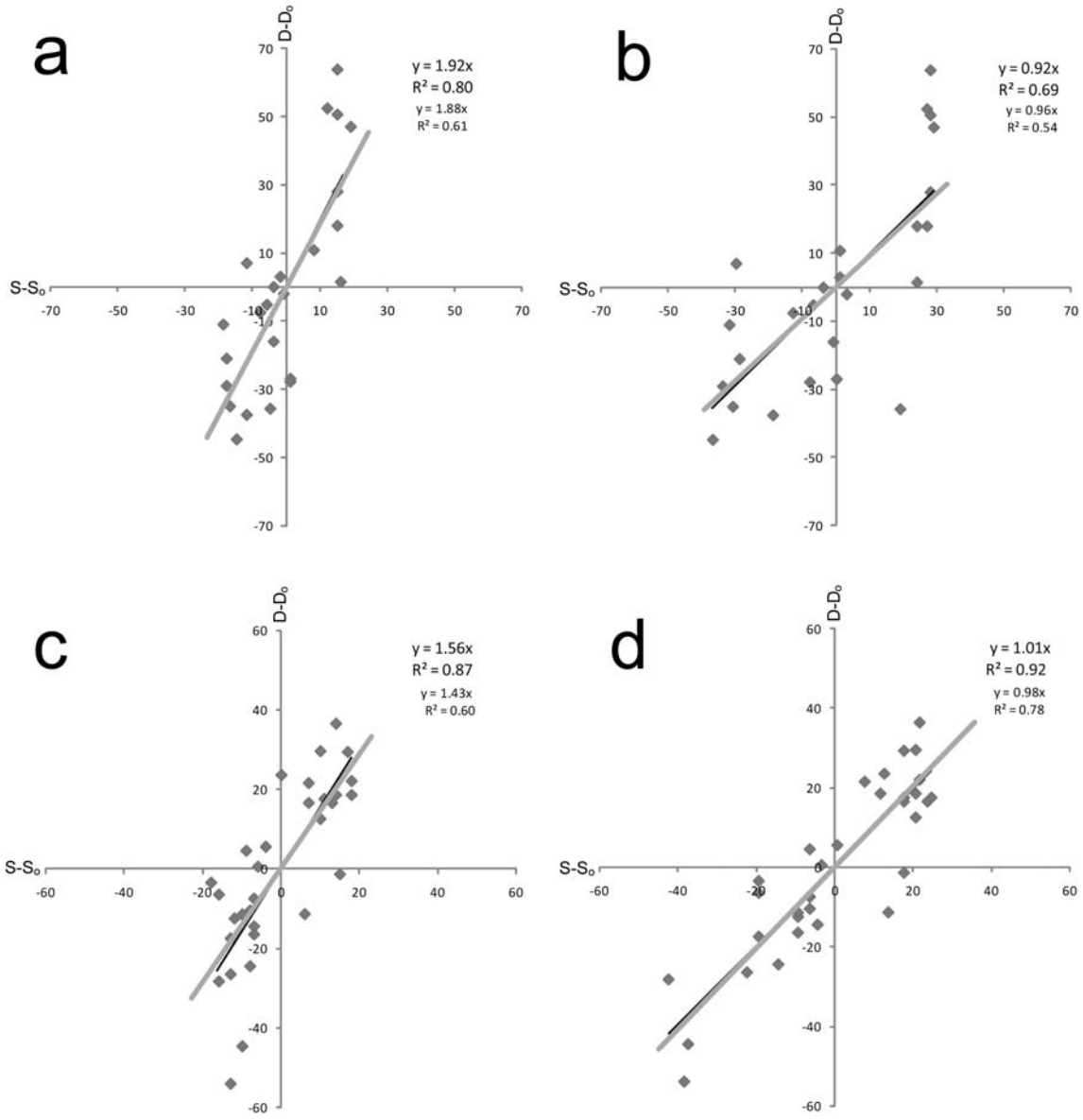

Figure 4.7: Plots of normalized compression direction (ordinate) versus regional strike (abscissa). The darker line represents the moving window analysis. (a) Thrust belt samples against orogenic front. (b) Thrust belt samples against Blue Ridge front. (c) Foreland samples against orogenic front. (d) Foreland samples against Blue Ridge front.

and Ridge and the Cumberland Plateau) and the more easterly Blue Ridge front (Figure 4.7b). Raw data projected to the orogenic front (Figure 4.7a) show a reasonable correlation (r^2=0.61), while a moving average window (n=3) of the data improves this correlation to r^2=0.80 (cf. Ong et al., 2007). Regardless, the slope of the best-fit line is ~1.9, indicating that these data record an "excess" fanning given the curvature of the front. Despite a lower correlation coefficient due to the presence of some data outliers, the data projected to the hinterland Blue Ridge front (Figure 4.7b) show a slope much closer to one (slope =0.96; r^2 = 0.54), which further improves with a moving window analysis (slope =0.92; r^2 = 0.69), suggesting a relationship between the shape of the Blue Ridge front and the distribution of paleostresses within the fold-thrust belt. For the foreland rocks, nine sites from previous work of Wiltschko (*in* Hatcher et al., 1989) are included with the twenty-three new sites of this study. Compression directions from the foreland, as with the thrust belt data, are projected to both boundaries of the fold-thrust belt (Figures 4.7c and 7d). As with limestones from within the thrust belt, the data projected to the orogenic front display excess fanning of compression directions (Figure 4.7c), but when projected onto the Blue Ridge front, display a nearly a 1:1 correlation (slope =0.98; r^2 = 0.78) that also improves with a moving window analysis (slope =1.01; r^2 = 0.92).

The similar radiating patterns of compression directions recorded in limestones from both the foreland and from within the thrust belt match the geometry of the hinterland Blue Ridge block, permitting a causal relationship between its history and the preserved paleostress field. Indentation of the fold-

thrust belt by the advancing Blue Ridge block is hypothesized to have imparted a radial stress field on foreland rocks, some of which were subsequently included in the thrust belt while others remained "undeformed" foreland. This pattern is therefore proposed as the origin for the fanned compression directions. While basement morphology and sediment thickness variation may have had minor influences, the primary mechanism driving curvature in the Tennessee salient is therefore the Blue Ridge indenter. Thrusting in the southern Appalachians developed via differential displacement along strike ahead of the Blue Ridge thrust. Maximum displacement and the number of thrusts in the fold-thrust belt at the apex of curvature of the Blue Ridge front (Figure 4.5; as noted by Hatcher et al., 2007), further support this indenter scenario for the southern Appalachians.

Indenter tectonics also explains the deviation in strike of the southern limb of the salient. Strikes of thrust sheets closest to the front of the Blue Ridge are more parallel, whereas those more distal tend to deviate and become closer to the trend of the northern limb. Basic analogue models of thrust belt geometries have previously shown that this deviation can be a kinematic response to an advancing indenter (Marshak et al., 1992; Lickorish et al., 2002). We repeated this approach in a simple sandbox model, modified from that in Marshak et al. (1992), which shows that the geometry can be readily achieved by indenting a rigid block with the shape of the Blue Ridge, into undeformed sand (Figure 4.8). As can be seen, thrusts forming toward the foreland tend to curve less than those closest to the indenter. Whereas the model is not mechanically scaled to natural conditions, this geometric model, along with the pattern of foreland compression directions, supports the

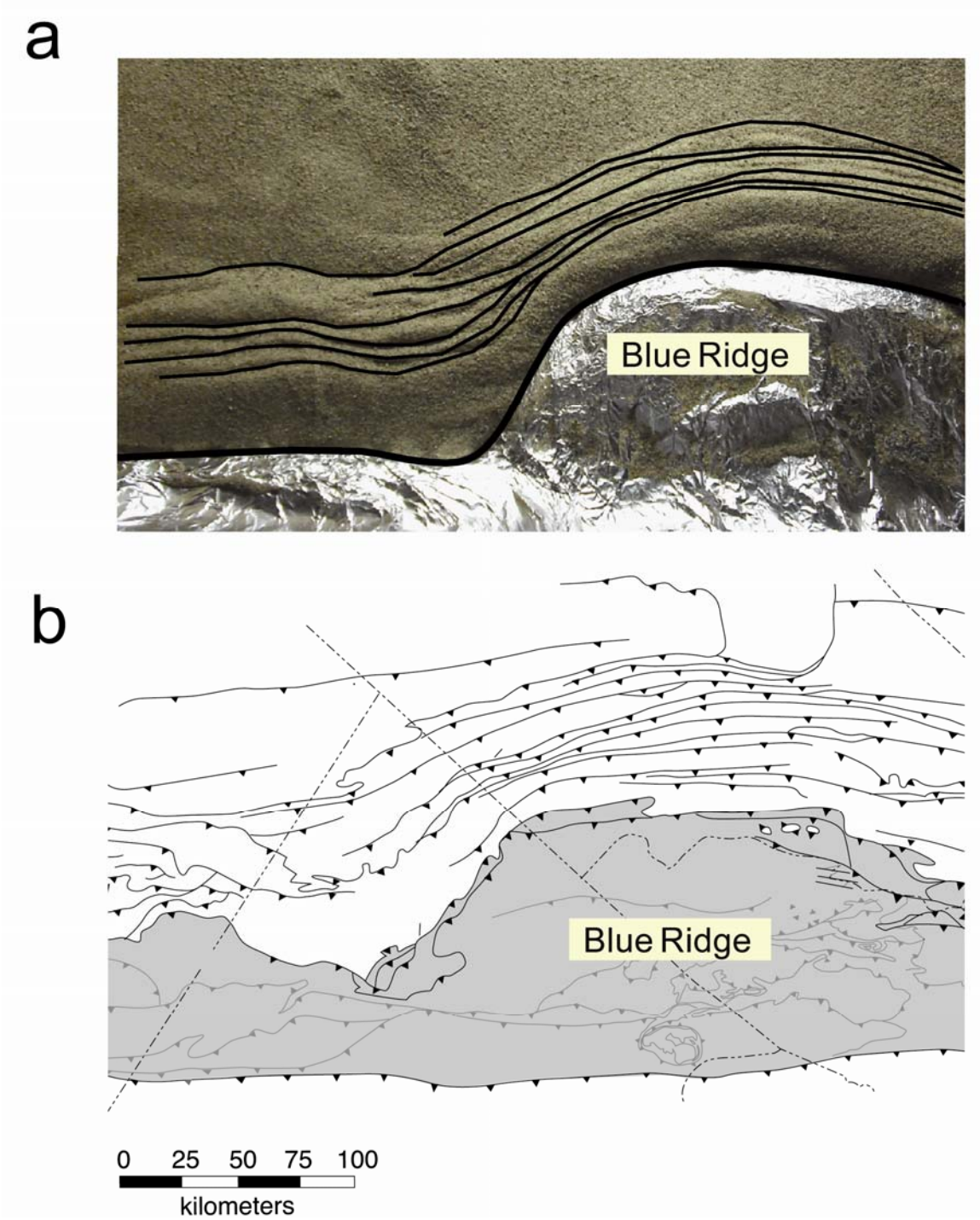

Figure 4.8: (a) Sandbox model showing deformation ahead of an indenter shaped after the Blue Ridge front. Lines trace the position of the faults in the sand (b) Thrust distribution in the Tennessee salient (modified from Hatcher, 2004). Note the excellent similarity between this basic geometric model and the natural thrust belt.

hypothesis that the rigid Blue Ridge block is the primary driver of curvature in the Tennessee salient.

Elsewhere, a radial pattern of compression directions has been documented in curved belts that have similarly been affected by an indenter. The Jura fold-thrust belt, analogous to the southern Appalachians, shows no paleomagnetic evidence for secondary curvature (Gehring et al., 1991) yet possesses a fanned distribution of paleostress orientations from calcite twinning analysis that extends into the foreland (Hindle and Burkhard, 1999; Rocher et al., 2005). A hinterland indenter has been identified as the primary driver of deformation in the Jura (Hindle and Burkhard, 1999; Homberg et al., 1999), indicating that a radial pattern of foreland compression directions may be used as an indicator of indenter tectonics in arcuate belts.

CONCLUSIONS

Calcite twinning analysis on limestones in the Tennessee salient of the southern Appalachians reveals a systematically fanned distribution of compression directions in both the fold-thrust belt as well as the undeformed foreland. This pattern implies that curvature of the Tennessee salient is primary, having initially formed in its present geometry. Since the Pennsylvania salient of the central Appalachian fold-thrust belt reflects secondary curvature, it is postulated that the origin of curvature in salients of the Appalachians is not identical.

Within the Tennessee salient, paleostress orientations projected onto the frontal fold-thrust belt show a variation nearly twice that of the regional strike.

When projected onto the more hinterland Blue Ridge block, the compression directions match the frontal shape of this block. The "undeformed" foreland limestones display a similarly matching pattern, leading to the conlcusion that the rigid Blue Ridge block imparted a radial stress pattern on rocks in this part of the Appalachian margin of the Laurentia. Differential displacement during thrusting instead of secondary rotation produced the present day geometry of the salient, which also explains the increase in displacement and number of thrusts near the indenter's apex. This signature of indenter tectonics would seem to be applicable to other curved belts with rigid crystalline thrust sheets in the hinterland.

ACKNOWLEDGEMENTS

Our Appalachian research at the University of Michigan has been supported by grants from the American Chemical Society-Petroleum Research Fund (most recently 45893-AC8) and the Scott Turner Fund at the University of Michigan. Special thanks are given to Peter Lemiszki at the Tennessee Division of Geology – Knoxville Office for discussions on regional structure and outcrop suggestions.

REFERENCES

Apotria, T.G., 1995. Thrust sheet rotation and out-of-plane strains associated with oblique ramps: An example from the Wyoming salient, U.S.A. Journal of Structural Geology 17, 647-662.

Boyer, S.E. and Elliott, D., 1982. Thrust systems. American Association of Petroleum Geologists Bulletin 66, 1196-1230.

Burkhard, M., 1993. Calcite twins, their geometry, appearance and significance as stress-strain markers and indicators of tectonic regime; a review. Journal of Structural Geology 15, 351-368.

Carey, S.W., 1955. The orocline concept in geotectonics. Proceedings of the Royal Society of Tasmania 89, 255-289.

Cederquist, D.P., Van der Voo, R., van der Pluijm, B.A., 2006. Syn-folding remagnetization of Cambro-Ordovician carbonates from the Pennsylvania Salient post-dates oroclinal rotation. Tectonophysics 422, 41-54.

Craddock, J.P. and van der Pluijm, B.A., 1989. Late Paleozoic deformation of the cratonic carbonate cover of eastern North America. Geology 17, 416-419.

Craddock, J.P., Jackson, M., van der Pluijm, B.A. and Versical, R.T., 1993. Regional shortening fabrics in eastern North America; far-field stress transmission from the Appalachian-Ouachita orogenic belt. Tectonics 12, 257-264.

Craddock, J.P., Kopania, A.A. and Wiltschko, D.V., 1988. Interaction between the northern Idaho-Wyoming thrust belt and bounding basement blocks, central western Wyoming. Geological Society of America Memoir 171, 333-351.

Eldredge, S.V., Bachtadse, V. and Van der Voo, R., 1985. Paleomagnetism and the orocline hypothesis. Tectonophysics 119,153-179.

Engelder, T., 1979. The nature of deformation within the outer limits of the central Appalachian foreland fold and thrust belt in New York State. Tectonophysics 55, 289-310.

Evans, M.A. and Groshong, R.H., 1994. A computer program for the calcite strain-gauge technique. Journal of Structural Geology 16, 277-282.

Ferrill, D.A., 1991. Calcite twin widths and intensities as metamorphic indicators in natural low-temperature deformation of limestone. Journal of Structural Geology 13, 667-675.

Ferrill, D.A., 1998. Critical re-evaluation of differential stress estimates from calcite

twins in coarse-grained limestone. Tectonophysics 285, 77-86.

Ferrill, D.A. and Groshong Jr., R.H., 1993a. Kinematic model for the curvature of the northern Subalpine Chain, France. Journal of Structural Geology 15, 523-541.

Ferrill, D.A. and Groshong Jr., R.H., 1993b. Deformation conditions in the northern Subalpine Chain, France, estimated from deformation modes in coarse-grained limestones. Journal of Structural Geology 15, 995-1006.

Friedman, M. and Stearns, D.W., 1971. Relations between stresses inferred from calcite twin lamellae and macrofractures, Teton Anticline, Montana. Geological Society of America Bulletin 82, 3151-3161.

Gehring, A.U., Keller, P. and Heller, F., 1991. Paleomagnetism and tectonics of the Jura arcuate mountain belt in France and Switzerland. Tectonophysics 186, 269-278.

Goldberg, S.A. and Dallmeyer, R.D., 1997. Chronology of Paleozoic metamorphism and deformation in the Blue Ridge thrust complex, North Carolina and Tennessee. American Journal of Science 297, 488-526.

Gray, M.B. and Mitra, G., 1993. Migration of deformation fronts during progressive deformation: evidence from detailed structural studies in the Pennsylvania Anthracite region, U.S.A. Journal of Structural Geology 15, 435-449.

Groshong, R.H., 1972. Strain calculated from twinning in calcite. Geological Society of America Bulletin 83, 2025-2038.

Groshong, R.H., 1974. Experimental test of least-squares strain gage calculation using twinned calcite. Geological Society of America 85, 1855-1864.

Groshong, R.H., Teufel, L.W. and Gasteiger, C., 1984. Precision and accuracy of the calcite strain-gauge technique. Geological Society of America 95, 357-363.

Hardeman, W.D., 1966. Geologic map of Tennessee. State of Tennessee Department of Conversation, Division of Geology, scale 1:250,000.

Harris, L.D. and Milici, R.C., 1977. Characteristics of a thin-skinned style of deformation in the southern Appalachians, and potential hydrocarbon traps. USGS Professional Paper 1018.

Harris, J.H. and van der Pluijm, B.A., 1998. Relative timing of calcite twinning strain and fold-thrust belt development; Hudson Valley fold-thrust belt, New York, U.S.A. Journal of Structural Geology 20, 21-31.

Hatcher Jr, R.D., Properties of thrusts and upper bounds for the size of thrust sheets.

In: McClay, K.R., Editor, 2004. *Thrust tectonics and hydrocarbon systems*. American Association of Petroleum Geologists Memoir 82, 18-29.

Hatcher Jr, R.D., Lemiszki, P.J. and Whisner, J.B., Character of rigid boundaries and internal deformation of the Southern Appalachian foreland fold-thrust belt. In: Sears, J.W., Harms, T.A. and Evenchick, C.A., Editors, 2007. *Whence the mountains? Inquiries into the evolution of orogenic systems; a volume in honor of Raymond A. Price.* Geological Society of America Special Paper 433, 243-276.

Hatcher Jr, R.D., Thomas, W.A., Geiser, P.A., Snoke, A.W., Mosher, S. and Wiltschko, D.V., Alleghanian orogen. In: Hatcher Jr, R.D., Thomas, W.A. and Viele, G.E., Editors, 1989. *The Appalachian-Ouachita Orogen in the United States, The Geology of North America Volume F-2.* Geological Society of America, Boulder, Colorado, 233-318.

Hindle, D. and Burkhard, M., 1999. Strain, displacement and rotation associated with the formation of curvature in fold belts; the example of the Jura arc. Journal of Structural Geology 21, 1089-1101.

Homberg, C., Lacombe, O., Angelier, J. and Bergerat, F., 1999. New constraints for indentation mechanisms in arcuate belts from the Jura Mountains, France. Geology 27, 827-830.

Jamison, W.R. and Spang, J.H., 1976. Use of calcite twin lamellae to infer differential stress. Geological Society of America Bulletin 87, 868-872.

Kent, D.V., 1988. Further paleomagnetic evidence for oroclinal rotation in the central folded Appalachians from the Bloomsburg and the Mauch Chunk Formations. Tectonics 7, 749-759.

Kollmeier, J.M., van der Pluijm, B.A. and Van der Voo, R., 2000. Analysis of Variscan dynamics; early bending of the Cantabria-Asturias Arc, northern Spain. Earth and Planetary Science Letters 181, 203-216.

Lacombe, O. and Laurent, P., 1996. Determination of deviatoric stress tensors based on inverstion of calcite twin data from experimentally deformed monophase samples; preliminary results. Tectonophysics 255, 189-202.

Laurent, P., Kern, H. and Lacombe, O., 2000. Determination of deviatoric stress tensors based on inversion of calcite twin data from experimentally deformed monophase samples; Part II, Axial and triaxial stress experiments. Tectonophysics 327, 131-148.

Lawton, D.E. and others, 1976. Geologic map of Georgia. Georgia Department of Natural Resources and Georgia Geological Survey, scale 1:250,000.

Lickorish, W.H., Ford, M., Buergisser, J. and Cobbold, P.R., 2002. Arcuate thrust systems in sandbox experiments; a comparison to the external arcs of the Western Alps. Geological Society of America Bulletin 114, 1089-1107.

Macedo, J. and Marshak, S., 1999. Controls on the geometry of fold-thrust belt salients. Geological Society of America Bulletin 111, 1808-1822.

Marshak, S., 1988. Kinematics of orocline and arc formation in thin-skinned orogens. Tectonics 7, 73-86.

Marshak, S., Salients, recesses, arcs, oroclines, and syntaxes; a review of ideas concerning the formation of map-view curves in fold-thrust belts. In: McClay, K.R., Editor, 2004. *Thrust tectonics and hydrocarbon systems*. American Association of Petroleum Geologists Memoir 82, 131-156.

Marshak, S., Wilkerson, M.S. and Hsui, A.T., Generation of curved fold-thrust belts; insight from simple physical and analytical models. In: McClay, K.R., Editor, 1992. *Thrust tectonics.* Chapman & Hall, London, United Kingdom, 83-92.

McCaig, A.M. and McClelland, E., 1992. Paleaeomagnetic techniques applied to thrust belts. In: McClay, K.R., Editor, *Thrust Tectonics*. Chapman and Hall, New York, New York, 209-216.

Milici, R.C., 1970. The Allegheny structural front in Tennessee and its regional tectonic implications. American Journal of Science 268, 127-141.

Milici, R.C., 1973, The stratigraphy of Knox County, Tennessee. Bulletin – Tennessee, Division of Geology 70, 9-24.

Milici, R.C., 1975. Structural patterns in the southern Appalachians; evidence for a gravity slide mechanism for Alleghanian deformation. Geological Society of America Bulletin 86, 1316-1320.

Mitra, S., 1988. Three-dimensional geometry and kinematic evolution of the Pine Mountain thrust system, Southern Appalachians. Geological Society of America Bulletin 100, 72-95.

Nickelsen, R.P., 1979. Sequence of structural stages of the Alleghany orogeny, Bear Valley strip mine, Shamokin, PA. American Journal of Science 279, 225-271.

Ong, P.F., van der Pluijm, B.A. and Van der Voo, R., 2007. Early rotation in the Pennsylvania Salient (US Appalachians): Evidence from calcite-twinning analysis of Paleozoic carbonates. Geological Society of America Bulletin 119, 796-804.

Rankin, D.W., 1975. The continental margin of eastern North America in the southern Appalachians; the opening and closing of the Proto-Atlantic Ocean. American Journal of Science 275-A, 298-336.

Rich, J.L., 1934. Mechanics of low-angle overthrust faulting as illustrated by Cumberland thrust bloc, Virginia, Kentucky and Tennessee. American Association of Petroleum Geologists Bulletin 18, 1584-1596.

Rocher, M., Cushing, M., Lemeille, F. and Baize, S., 2005. Stress induced by the Mio-Pliocene Alpine collision in northern France. Bulletin de la Societe Geologique de France 176, 319-328.

Rodgers, J., 1953. Geologic map of East Tennessee with explanatory text. Tennessee Department of Conservation, Division of Geology Bulletin 58.

Rodgers, J., 1970. *The tectonics of the Appalachians*. Wiley Interscience, New York, New York, 271p.

Roeder, D. and Witherspoon, W., 1978. Palinspastic map of East Tennessee. American Journal of Science 278, 543-550.

Rowe, K.J. and Rutter, E.H., 1990. Palaeostress estimation using calcite twinning; experimental calibration and application to nature. Journal of Structural Geology 12, 1-17.

Schwartz, S.Y. and Van der Voo, R., 1983. Paleomagnetic evaluation of the orocline hypothesis in the Central and Southern Appalachians. Geophysical Research Letters 10, 505-508.

Spang, J.H., 1972. Numerical method for dynamic analysis of calcite twin lamellae. Geological Society of America Bulletin 83, 467-472.

Spang, J.H. and Groshong, R.H., 1981. Deformation mechanisms and strain history of a minor fold from the Appalachian Valley and Ridge Province. Tectonophysics 72, 323-342.

Spraggins, S.A. and Dunne, W.M., 2002. Deformation history of the Roanoke Recess, Appalachian, USA. Journal of Structural Geology 24, 411-433.

Stamatakos, J. and Hirt, A.M., 1994. Paleomagnetic considerations of the development of the Pennsylvania Salient in the Central Appalachians. Tectonophysics 231, 237-255.

Teufel, L.W., 1980. Strain analysis of experimental superposed deformation using calcite twin lamellae. Tectonophysics 65, 291-309.

Thomas, W.A., 1977. Evolution of Appalachian-Ouachita salients and recesses from reentrants and promontories in the continental margin. American Journal of Science 277, 1233-1278.

Thomas, W.A., 1991. The Appalachian-Ouachita rifted margin of southeastern North America. Geological Society of America Bulletin 103, 415-431.

Thomas, W.A., 2004. Genetic relationship of rift-stage crustal structure, terrane accretion, and foreland tectonics along the southern Appalachian-Ouachita orogen. Journal of Geodynamics 37, 549-563.

Turner, F.J., 1953. Nature and dynamic interpretation of deformation lamellae in calcite of three marbles. American Journal of Science 251, 276-298.

van der Pluijm, B.A., Craddock, J.P, Graham, B.R. and Harris, J.H., 1997. Paleostress in cratonic North America; implications for deformation of continental interiors. Science 277, 794-796.

Weil, A.B. and Sussman, A.J., Classification of curved orogens based on the timing relationships between structural development and vertical-axis rotations, In: Weil, A.B. and Sussman, A.J., Editors, 2004. *Orogenic curvature; Integrating paleomagnetic and structural analyses.* Geological Society of America Special Paper 383, *1-17.*

Wenk, H.R., Takeshita, T., Bechler, E., Erskine, B.G. and Matthies, S., 1987. Pure shear and simple shear calcite textures; comparison of experimental, theoretical and natural data. Journal of Structural Geology 9, 731-745.

Woodward, N.B., ed., 1985. *Balanced Structure Cross Sections in the Appalachians (Pennsylvania to Alabama)*: Department of Geological Sciences, University of Tennessee, Knoxville, Studies in Geology 12, 63 p.

Woodward, N.B. and Beets, J.W., Critical evidence for Southern Appalachian Valley and Ridge thrust sequence, In: Mitra, G. and Wojtal, S.F., Editors, 1988. *Geometries and mechanism of thrusting, with special reference to the Appalachians.* Geological Society of America Special Paper 222, *165-178.*

CHAPTER V

INFLUENCE OF DIAGENETIC GRADE ON ILLITE AGE ANALYIS: A STUDY OF APPALACHIAN FAULT GOUGE AND FORELAND SHALES

ABSTRACT

Illite age analysis has increasingly been applied to many rock types, such as fault gouge, shale and limestones, by comparing radiometric ages of successive size fractions with varying percentages of detrital illite. Determining detrital versus authigenic illite is now an established procedure, utilizing X-ray analysis to quantify illite polytypism. Less clear, however, is how to interpret $^{40}Ar/^{39}Ar$ ages as a function of crystallization temperature. Both a total gas age, incorporating the recoiled argon fraction after irradiation, and a retention age (omitting the recoiled fraction) can be determined for a sample. Their use may be related to diagenetic grade, and more specifically, the crystallite thickness. Based on this study, it appears that crystallites greater than 10 nm require that retention ages be used because of loss from increased potassium bearing defects, while crystallites less than 10 nm have few, if any defects, thus retaining argon.

New illite age analysis results are presented from four fault rocks from the deeply exhumed Appalachian foreland fold-thrust belt as well as three shales from the neighboring midcontinent. Three of the faults have thick crystallites, requiring

the retention age model for dating, while one fault and all three shales have thin crystallites in their fine fractions, requiring the total gas age model. Shale ages reveal separate diagenetic events, with the two Ordovician shales showing Pennsylvanian authigenic ages. Illite ages from gouge in the thrust belt represent the first attempt to directly date Appalachian deformation in the thrust belt. They indicate that the last major period of fault activity occurred during the Early Permian (~275 -280 Ma) and that these foreland faults were part of an internally deforming thrust wedge.

INTRODUCTION

It has long been established that the potassium rich clay mineral illite can be directly dated in both shales and clay rich fault rocks (Hower et al., 1963; Aronson and Hower, 1976; Lyons and Snellenburg, 1971; Kralik et al., 1987). Early studies of clay minerals in shales have shown that decreasing grain-sizes of illite display an increased percentage of the low-temperature, authigenic $1M/1M_d$ polytype, coincident with decreasing K-Ar ages (Hower et al., 1963). Until recently, these ages were not easily interpreted, since the absolute age represents a mixture of younger, low-temperature authigenic $1M_d$ illite and older, high-temperature detrital $2M_1$ illite polytype. The development of Illite Age Analysis (IAA) has provided a means to extrapolate both authigenic and detrital ages by quantifying the amount of each polytype for multiple grain sizes of illite-rich material and their respective radiometric ages (Pevear, 1992; Grathoff et al., 2001; Solum and van der Pluijm,

2007). Recent studies have benefited from the development of this method, including studies of shale diagenesis (Pevear, 1992; Grathoff et al., 1998; 2001) and of clay-rich gouges from brittle faults (e.g., van der Pluijm et al., 2001; Haines and van der Pluijm, 2008).

Most studies involving radiometric dating of illite have employed conventional K-Ar dating (e.g., Aronson and Hower, 1976; Pevear, 1992; Grathoff et al., 2001). Neutron irradiation applied to clay-sized material during the $^{40}Ar/^{39}Ar$ method releases significant amounts of ^{39}Ar gas, recoiled during the transmutation from ^{39}K. Encapsulation of the sample prior to irradiation allows the recoiled gas to be collected for analysis, resulting in two different ages per sample (Foland et al., 1992; Dong et al., 1995). Including the recoiled ^{39}Ar gas during the calculation of an age gives a "total gas age", which is the equivalent to conventional K-Ar ages, while omitting the recoiled fraction results in an older "argon retention age", only using the argon retained in the crystal structure after irradiation (Dong et al., 1995; 1997).

Others have noted that interpretation of $^{40}Ar/^{39}Ar$ ages from illite is dependent on the diagenetic grade, as the presence of smectite appears to affect ^{40}Ar retention (Dong et al., 1995; 1997; 2000; Hall et al., 2000). Total gas ages have been found to be geologically reasonable in low grade diagenetic settings, typically with interlayered smectite (Dong et al., 2000), while retention ages have been shown to be more suitable to higher grade diagenetic, anchizonal and epizonal illite (Dong et al., 1995; 1997; Hall et al., 2000). However, these studies primarily focused on rocks with purely neomineralized illite, requiring no adjustment for a detrital

component that characterizes many rocks and is the foundation of the IAA approach. Prior work on fault gouge using this method has been on relatively young (<100 Ma) faults, where illite was formed in low grade settings with or without smectite interlayers (van der Pluijm et al., 2001; 2007; Solum et al., 2005; Haines and van der Pluijm, 2008). The diagenetic grade of these rocks indicates that they were exhumed from relatively shallow depths. Thus, the total gas age model was used for their interpretation, while the retention ages were not applicable.

To examine the effect of increased diagenetic grade on the application and interpretation of polytype-based illite ages, fault rocks from the more deeply exhumed Late Paleozoic southern Appalachian foreland fold-thrust belt were collected (Figure 5.1). The resulting ages also elucidate the timing of foreland thrusting within the fold-thrust belt, giving insight into wedge dynamics of the frontal Appalachians. Additionally, shales from the undeformed midcontinent were sampled (Figure 5.2) to examine the role of diagenetic grade as well as compare with foreland faulting results, as proposed in the Late Paleozoic regional brine migration hypothesis (i.e., "squeegee model" of Oliver, 1986)

Figure 5.1: Map showing location of sampled faults in the southern Appalachian fold-thrust belt (Hardeman, 1966). Large squares represent sites with radiometric ages.

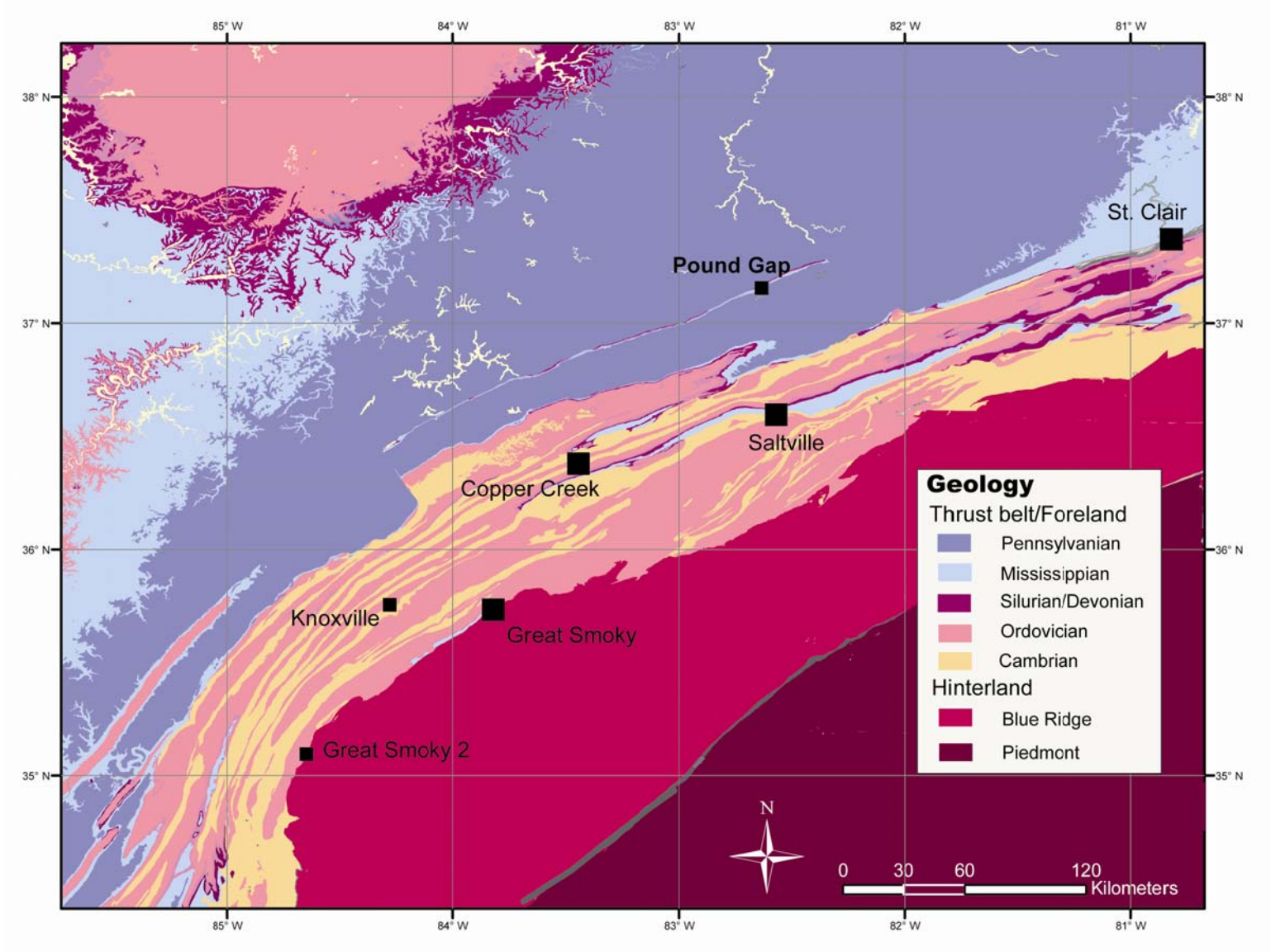
85° W
84° W
83° W
82° W
81° W
38° N
37° N
36° N
35° N
St. Clair
Pound Gap
Saltville
Copper Creek
Knoxville
Great Smoky
Great Smoky 2
Geology
Thrust belt/Foreland
Pennsylvanian
Mississippian
Silurian/Devonian
Ordovician
Cambrian
Hinterland
Blue Ridge
Piedmont
N
0 30 60 120
Kilometers

GEOLOGIC BACKGROUND

Appalachian Thrust Belt

The southern Appalachian thrust belt is a classic thin-skinned fold-thrust belt, which formed during the Late Paleozoic Alleghanian orogen. The fold-thrust belt consists of a west-verging stack of thin-skinned thrusts that sole out into a basal décollement within Cambrian shales, with the mechanically strong unit being thick Cambro-Ordovician carbonates, (Milici, 1975; Woodward and Beets, 1988; Hatcher et al., 1989; Hatcher et al., 2007). The structural style of the fold-thrust belt reflects the controlling nature of the thick carbonates, with southeast dipping thrust faults dominating instead of a fold-dominated belt like the central Appalachians to the north (Hardeman, 1966; Harris and Milici, 1977; Hatcher et al., 1989).

Timing of deformation in fold-thrust belts is mostly constrained by the age of synorogenic sedimentary units. However, given that the Appalachians have been tectonically quiet for more than 200 million years, much of this evidence has been eroded away, leaving only older, pre-orogenic sedimentary rocks in most places. Therefore, constraining the age of deformation is difficult and often crude. The currently best-constrained evidence for the age of thrusting comes from the central Appalachians, where timing of Alleghanian thrusting is based on deformation of the youngest unit, the Lower Permian Dunkard Group in the foreland-most portion of the belt in West Virginia. The Early Permian age (299-271 Ma) of the Dunkard can only constrain a lower limit for the timing of deformation (Hatcher et al., 1989; Becker et al., 2006). In the southern Appalachians, the youngest sedimentary units

involved in thrusting are Pennsylvanian clastic rocks, which are deformed along the Pine Mountain thrust as well as the Cumberland Plateau detachment.

Whereas radiometric ages in the southern Appalachians are numerous, they are limited to the metamorphic province in the hinterland, reflecting common radiometric dating approaches. Ages from the crystalline Blue Ridge province range from Precambrian to Permian, representing tectonic events during the Grenville, Taconic, Neoacadian and Alleghanian orogenies (Goldberg and Dallmeyer, 1997). Initial assembly of the crystalline thrust sheets during the Alleghanian within the Blue Ridge province has been dated at ~325 Ma, with progression into the foreland during later Pennsylvanian into Permian times (Goldberg and Dallmeyer, 1997). Results from the metamorphic Piedmont province have shown that Alleghanian deformation advanced during many stages, with the final stage occurring in the Permian, approximately 265-290 Ma (Dallmeyer et al., 1986; Secor et al., 1986; Hadizadeh et al., 1991; Steltenpohl et al., 1992; Steltenpohl and Kunk, 1993). In particular, the Brevard fault zone, representing the boundary between the Blue Ridge and the Piedmont provinces, records a whole rock Rb-Sr date of 273 Ma from an ultramylonite (Hatcher et al., 1988) that signifies the final stage of motion along this long-lived fault zone.

As with the absolute age of deformation in the foreland fold-thrust belt, the sequence of thrust imbrication has also remained a controversial topic in the southern Appalachians. Previous workers have shown evidence for both a forward propagating thrust belt (Woodward, 1985; Woodward and Beets, 1988), which is

typical of fold-thrust belt development, as well as backward breaking thrusting (Harris and Milici, 1977; Milici, 1986), with the frontal thrust being the first to break and gradually progressing toward the hinterland. Determining the absolute age of thrusting through radiometric dating of fault gouge would also resolve these conflicting scenarios.

Fluid Migration

Mineralization, petroleum occurrences and widespread remagnetization of various lithologies occurred throughout eastern North America during the Late Paleozoic, suggesting that fluids driven by the Alleghanian orogeny caused these phenomena (Oliver, 1986; Schedl et al., 1992; Bethke and Marshak, 1993). Remagnetized rocks occur throughout the Appalachian fold-thrust belt as well as the undisturbed foreland (McCabe and Elmore, 1989). The age of remagnetization ranges along the Appalachian chain, from Pennsylvanian-aged remagnetizations in the south to remagnetizatons that occurred during the Permian in the central and northern Appalachians (Miller and Kent, 1988; McCabe and Elmore, 1989; Chapter III of this thesis). As many of these rocks display no evidence for elevated temperatures, chemical processes associated with orogenic brines have been invoked as the most likely mechanism for remagnetization. These orogenic fluids have also been hypothesized to produce the widespread Mississippi Valley Type (MVT) ore deposits and petroleum migration from known source rocks in eastern North America. Timing of this fluid migration event has been indirectly determined

Figure 5.2: Map of eastern U.S., showing location of shale samples. Radiometric ages have been acquired for the sites with large squares. Fsh1 and Fsh7 are surface exposures, while the other sites are from cores.

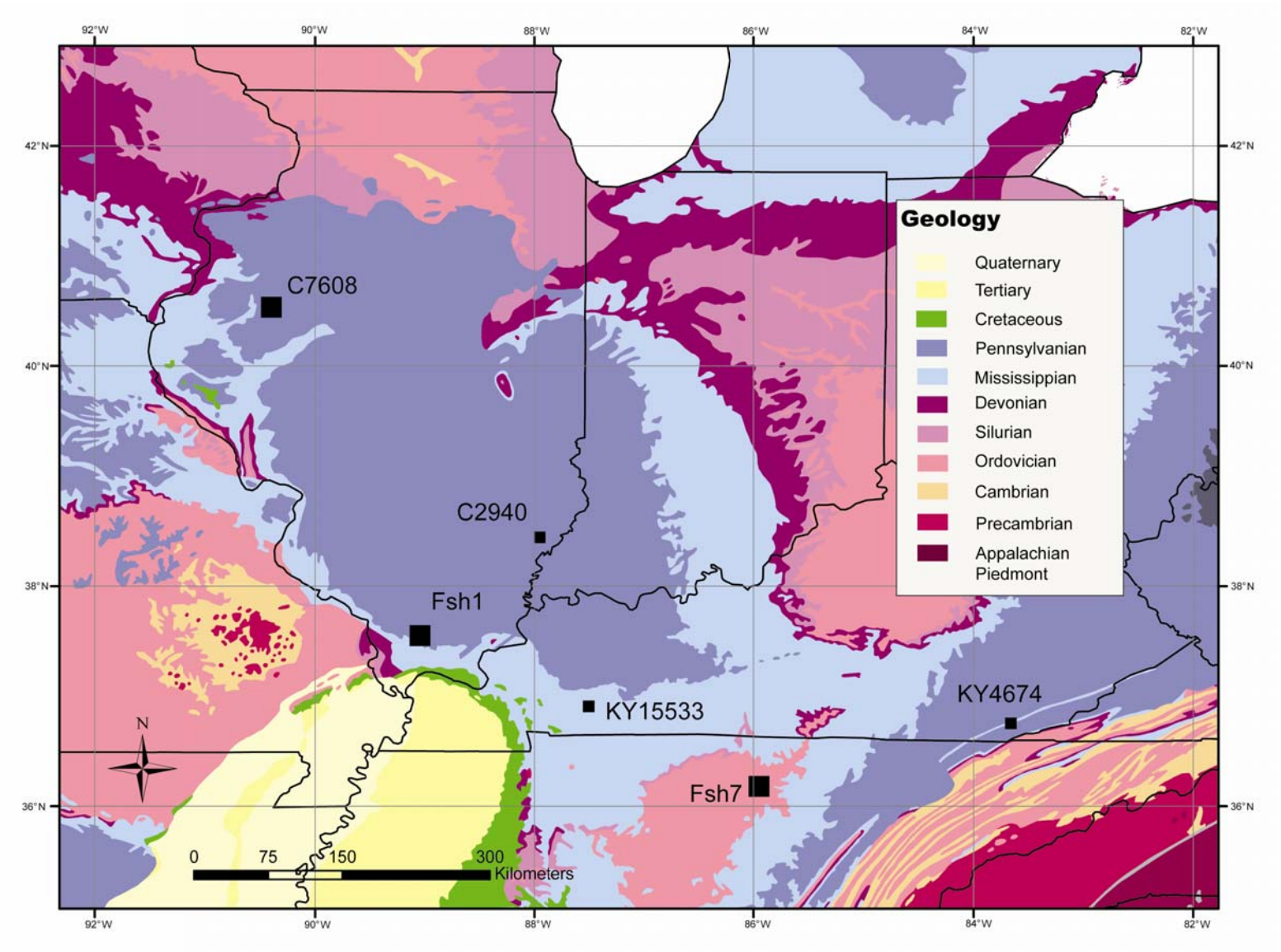
92°W
90°W
88°W
86°W
84°W
82°W
42°N
40°N
38°N
36°N
Geology
Quaternary
Tertiary
Cretaceous
Pennsylvanian
Mississippian
Devonian
Silurian
Ordovician
Cambrian
Precambrian
Appalachian Piedmont
C7608
C2940
Fsh1
KY15533
KY4674
Fsh7
N
0
75
150
300
Kilometers

using paleomagnetic data as well as radiometric techniques on K-bearing mineral phases, including K-feldspar associated with MVT deposits (Hearn et al., 1987) and illite from bentonites (Elliott and Aronson, 1987; 1993; Elliott and Haynes, 2002) and shales (Grathoff et al., 2001). These give a broad range of ages between 265-330 Ma.

SAMPLING AND METHODS

Sample Collection

Despite deep weathering of the southeastern U.S., several fault exposures for most major thrusts were identified. Samples were collected from fault exposures within the foreland fold-thrust belt of the southern Appalachians (Figure 5.1). Clayey gouge was collected at outcrops of the St. Clair, Copper Creek and Great Smoky thrusts (Figure 5.3), while the Saltville thrust exposure preserves a shale cataclasite with polished surfaces. Samples were taken after digging into the exposure to limit any effects of weathering (Figure 5.3). The Knoxville thrust, a second exposure of the Great Smoky thrust and a subsidiary fault of the Pine Mountain thrust (at Pound Gap) were also collected, but have not yet been analyzed. Wall rock samples from the Copper Creek and Great Smoky, as well as the clay residue from a remagnetized limestone (OC14; Chapter III), were prepared and submitted to ensure the ages reflect faulting and not a regional diagenetic event, but the results are not yet available. Data for these currently undated samples is in Table 5.3.

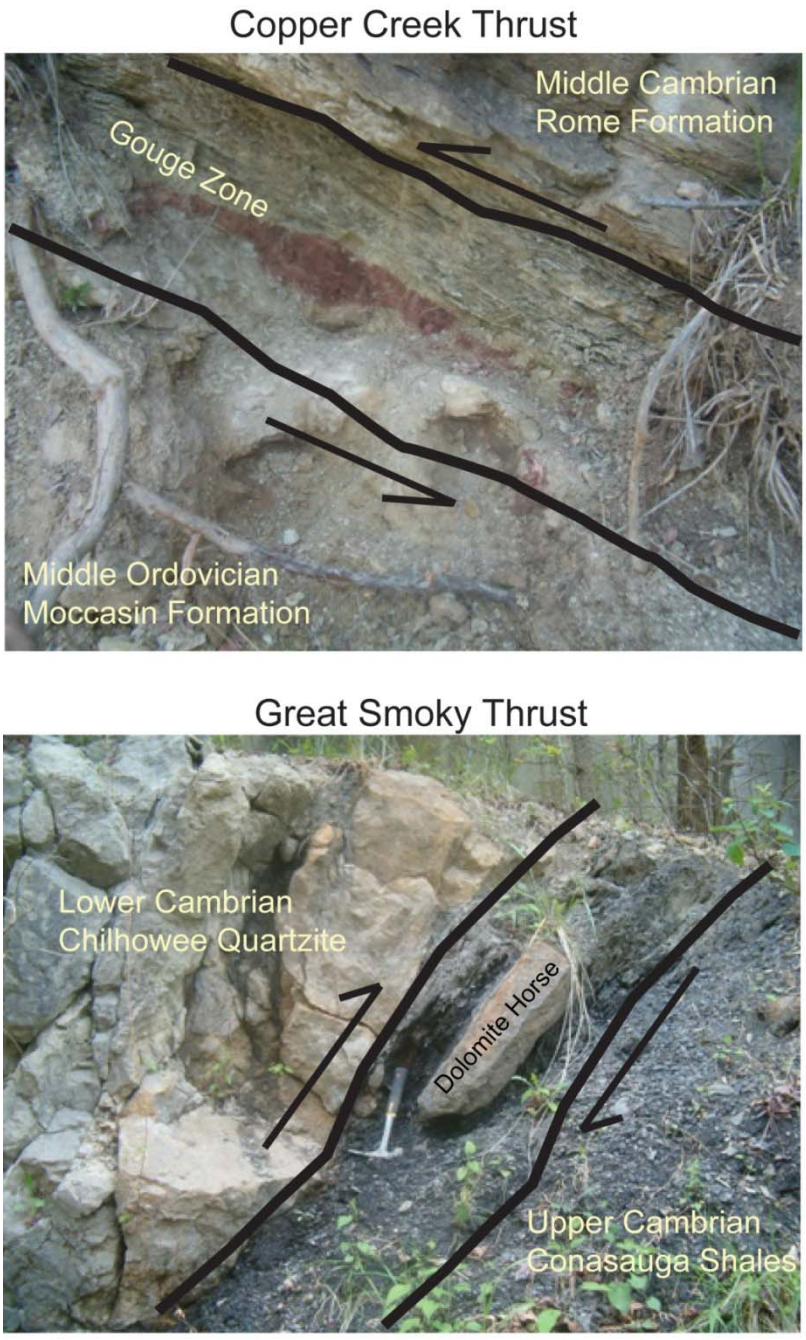

Figure 5.3: Photographs of fault exposures. Top: Copper Creek thrust placing Middle Cambrian Rome Formation on Middle Ordovician Moccasin shales. Bottom: Great Smoky thrust separating Blue Ridge rocks from foreland fold-thrust belt. Thrust places Lower Cambrian Chilhowee quartzite on Upper Cambrian Conasauga shales.

Shale samples were collected from both outcrop and core along a transect from the fold-thrust belt into the Illinois basin to examine any regional variation in ages (Figure 5.2). Most of the samples are Ordovician in age, although one from the Illinois basin is Pennsylvanian. Three samples have been dated thus far, while four others are awaiting analysis. The samples dated include an Ordovician shale (Fsh7) from an outcrop in the Nashville dome, a Pennsylvanian shale from the Illinois basin (Fsh1) and a sample of the Ordovician Maquoketa Formation from a core in the Illinois basin that was previously studied by Grathoff et al. (2001; Sample G 27) with K-Ar ages. This sample, from a depth of 775 ft (235m) represents a chance to test our results with other approaches to the IAA method, as the total gas age should match the K-Ar age (321 Ma). Other, currently undated samples are from cores across Kentucky and Illinois and are listed in Table 5.3.

Sample Preparation

Samples were disaggregated and allowed to settle in a large beaker in order to separate the clay-sized fraction. The suspension of deflocculated clays was decanted and allowed to dry. Oriented clay slurry mounts of the clay-sized fraction were created to characterize the mineralogy of each gouge by scanning from 2°-50° 2Θ (Cu Kα) at a rate of 1° per minute under both air-dried and glycolated conditions using a Scintag X-ray diffractometer. Samples with illite were separated into size fractions via centrifugation. The clay fraction was first placed in an ultrasonic bath for ~15 minutes to promote deflocculation and subsequently separated using centrifuge settling. Gouge samples were typically separated into coarse (2.0-0.5 μm), medium (0.5-0.05 μm) and fine (<0.05 μm) fractions. Samples from the St.

Clair thrust, the Pound Gap fault and the Ordovician shale from Bell County, KY were separated into medium (0.5-0.1 μm), medium-fine (0.1-0.05 μm) and fine (<0.05 μm) fractions in order to avoid contamination by K- feldspar in the coarse fraction. Since carbonate minerals often obscure peaks used for polytype quantification, size fractions of gouges containing carbonates were treated with a weak (~1N) acetic acid solution after separating material for $^{40}Ar/^{39}Ar$ dating, as the effects of acid treatment on Ar and K retention are not well documented.

Illite Characterization

To characterize the diagenetic grade, oriented slurry samples of the bulk clay-sized fraction as well as each size fraction were scanned from 2°-20° 2Θ with a step size of 0.05° under both air-dried and glycolated conditions, using a Scintag diffractometer. The percent illite in illite-smectite (I-S) was estimated based on the method of Środoń (1980) and verified for representative samples by comparing to modeled diffraction patterns from the program NEWMOD© (Reynolds and Reynolds, 1996). Illite crystallinity (IC) was estimated by measuring the full width at half maximum (FWHM) of the 001 illite peak in °2Θ, which is essentially a measure of sharpness. FWHM reflects the thickness distribution of the illite crystallites (Kübler, 1964; Kübler and Jaboyedoff, 2000), with each illite layer being 1 nm. Crystallite thickness was calculated using the Scherrer equation, which relates thickness to FWHM (Drits et al., 1997)

Illite age analysis requires quantifying the percentage of the two main polytypes of illite: the higher temperature, detrital $2M_1$ polytype and the lower

temperature $1M_d$ polytype, using X-ray diffraction methods. Oriented slurry mounts tend to obscure the $2M_1$ specific peaks, which all have non-(001) indices. Therefore, random orientation of the illitic material is necessary to quantify illite polytypes. Near random powder mounts were made using an end-packer device modeled after Moore and Reynolds (1997). Samples were step-scanned from 16°-44° 2Θ with a step size of 0.05° and count time of 30 sec/step. The relative intensity of the (002) and (020) peaks was used to determine whether randomness was achieved (Grathoff and Moore, 1996).

Illite polytype quantification was accomplished by modeling diffraction patterns using the program WILDFIRE©-generated XRD patterns (Reynolds, 1993). WILDFIRE© allows the user to apply different properties for $2M_1$ and $1M_d$ illite, varying such parameters as randomness of the sample ("Dollase" factor), hydration state, percentage cis- and trans-vacant interlayers as well as smectite interlayers. A spreadsheet program was used for matching the measured X-ray diffraction patterns to the synthetic three-dimensional X-ray diffraction patterns. In most cases, the lowest variance between the WILDFIRE© generated pattern and the powder pattern was used to constrain the best match except in instances where other minerals (e.g., quartz, plagioclase, carbonate) were present and obscured some of the illite peaks in the pattern. Typical precision for this method is on the order of 2-3% (Haines and van der Pluijm, 2008).

$^{40}Ar/^{39}Ar$ Dating

Samples were dated using the $^{40}Ar/^{39}Ar$ encapsulation method; details are described in Dong et al. (1995) and van der Pluijm et al. (2001). Along with the acquisition of both a total gas age and a retention age, the main advantages of $^{40}Ar/^{39}Ar$ dating over traditional K-Ar dating are the simultaneous measurement of both radiogenic ^{40}Ar and ^{39}Ar, resulting in higher precision for the analysis, as well as much smaller samples (<1mg) requiring less chemical treatment. Two batches were submitted, totaling seven faults, six shales and three fine fractions from wall rocks. Size fractions were first compacted into pellets using a high-speed centrifuge and placed into small quartz vials. They were subsequently evacuated to high vacuum and sealed prior to irradiation in order to retain any argon that is recoiled. After irradiation, the fused vial was broken so any recoiled gas could be analyzed first. The sample was then step-heated by a defocused laser (Coherent Innova 5 W Ar-ion laser) until fusion of the sample. Ages were calculated relative to the 520.4 Ma age for the Mmhb-1 hornblende standard, also irradiated in the same package as the illite size fractions. Both total gas ages (including the recoiled fraction) and retention ages (omitting the recoiled fraction) are plotted against percentage of $2M_1$ and subsequently extrapolated using a York regression (York, 1968) to determine authigenic and detrital ages for each sample along with 1σ errors.

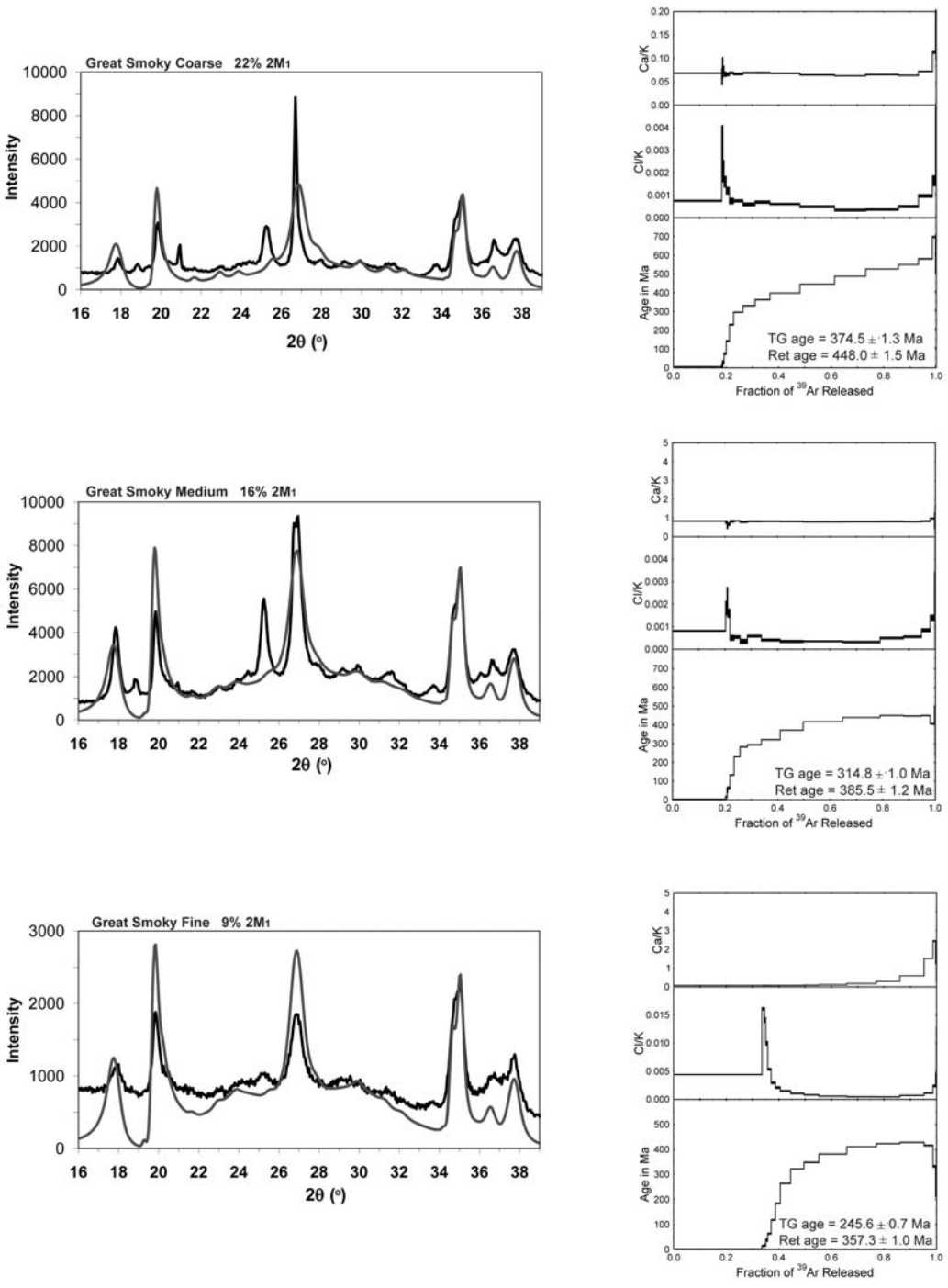

Figure 5.4: Modeled XRD patterns compared to actual XRD patterns on left for the Great Smoky thrust. Each size fraction and its corresponding argon release diagram are plotted from top to bottom according to decreasing grain size.

RESULTS

Radiometric ages have been acquired for four faults and three shale samples (Tables 5.1 and 5.2). These will be discussed seperately below, beginning with the Great Smoky thrust and proceeding westward to the midcontinent shales. Ar-release spectra display between 10-40% recoil, and do not have plateaus due to the mixture of authigenic and detrital phases. Modeling of illite polytypes for all samples shows a systematic decrease in the amount of the detrital ($2M_1$) illite with decreasing grain size. Of the samples, three faults (Great Smoky, Copper Creek and St. Clair) as well as Fsh7 contain more than 70% $1M_d$ illite (authigenic polytype) in any size fraction, while the other three samples contain more detrital illite.

Great Smoky Thrust

The Great Smoky thrust is the fault with largest displacement (>300 km) in the southern Appalachians (Hatcher et al., 2007), separating the mostly crystalline Blue Ridge province, which acted as the indenter (Chapter IV of this thesis), from foreland sediments in the thin-skinned fold-thrust belt. Two exposures of this thrust were sampled, with one dated for this study. An exposure of the fault along US Route 321 places Lower Cambrian Chilhowee Quartzite on Upper Cambrian Conasauga Group shales (Figure 5.3). The fault contact is a somewhat lithified gouge that gradually progresses into the footwall shales.

The percentage of smectite interlayers in the samples is negligible (<5%) and the crystallinity reveals a relatively high diagenetic grade (FWHM of fine fraction= 0.567 °2Θ). Polytype quantification gives a high percentage (>75%) authigenic $1M_d$

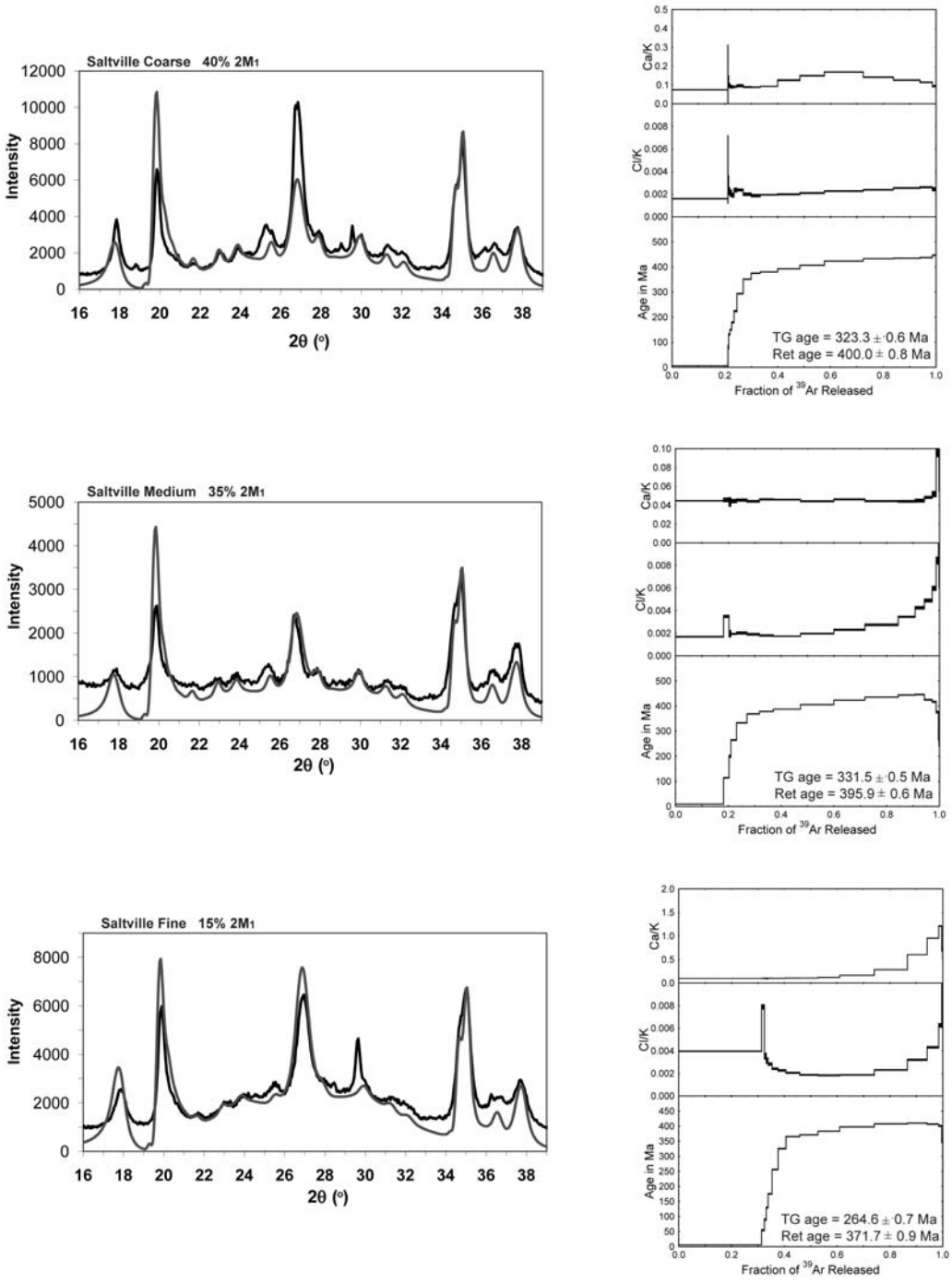

Figure 5.5: Modeled XRD patterns compared to actual XRD patterns on left for the Saltville thrust.

illite for the gouge (Figure 5.4; Table 5.1). The polytype derived authigenic age using total gas ages is 150.5 ± 41.0 Ma, whereas the retention age is 277.1 ± 34.0 Ma (Figure 5.8).

Saltville Thrust

The Saltville thrust represents the second largest displacement thrust in the southern Appalachian fold-thrust belt, separating a zone of major folding toward the hinterland and a zone of dominant faulting toward the foreland (Woodward et al., 1988). Displacement estimates based on facies changes in Mid-Ordovician sediments and strike length are ~100 km (Hatcher et al., 2007). The sampled exposure of the Saltville thrust is located along U.S. 23 at the Virginia-Tennessee border. The fault places Middle Cambrian Rome Formation onto a large dolomite horse of unknown age, which is in turn thrust onto Devonian black shales of the Chattanooga Formation. Clayey gouge was not identified; instead, shale cataclasite derived from the footwall with polished surfaces was collected and analyzed.

The FWHM value of the fine fraction (0.514 °2θ) and the lack of smectite interlayers (I in I-S is >98%) for the Saltville thrust suggests a relatively high diagenetic grade. While still dominated by $1M_d$ illite, polytypism in the Saltville contains more detrital $2M_1$ illite than the other fault rocks analyzed (Figure 5.5). The authigenic age derived using the total gas ages yields an age of 215.7 ± 25.1 Ma, while the retention age model yields an age of 354.2 ± 9.9 Ma (Figure 5.8).

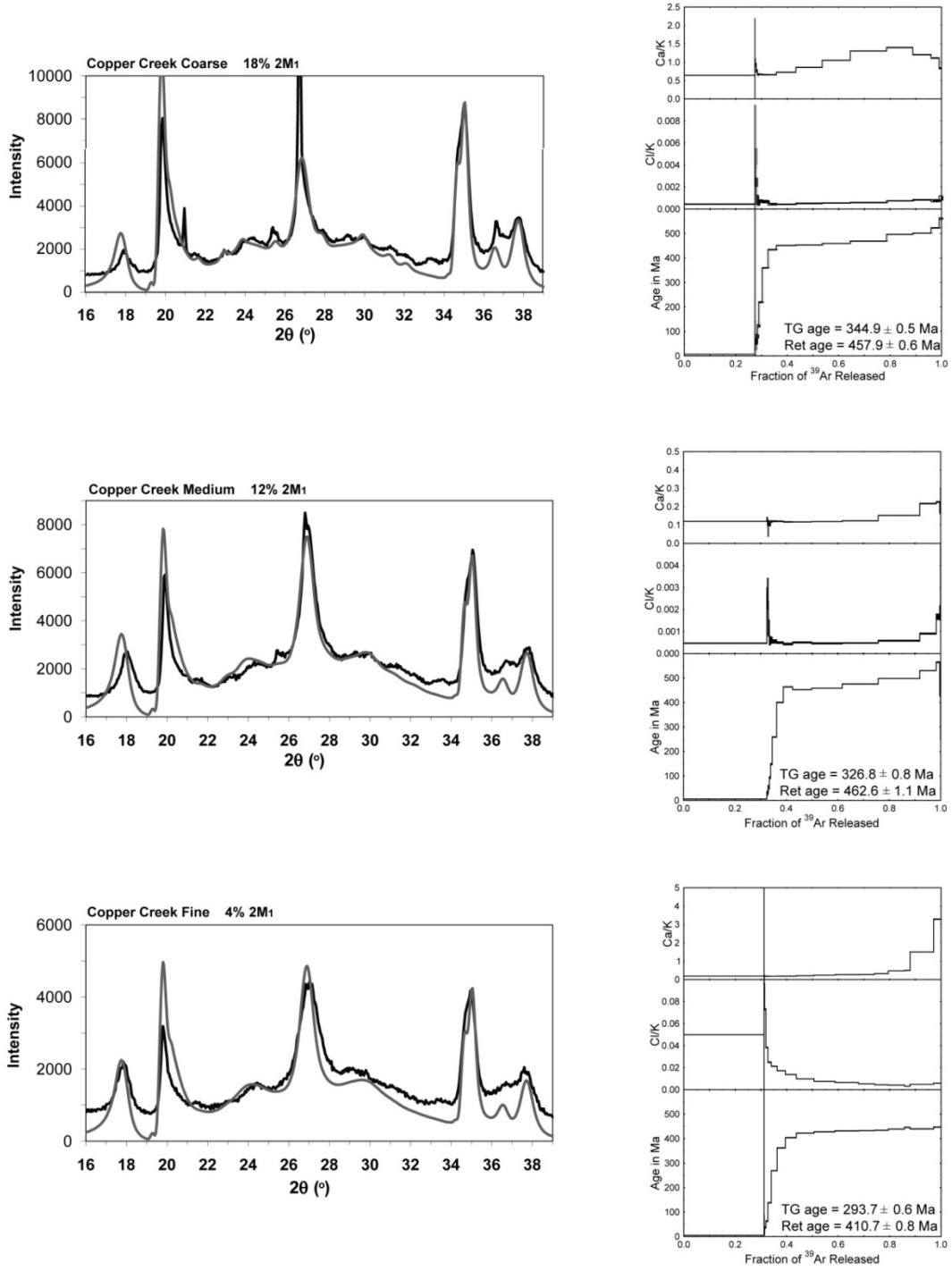

Figure 5.6: Modeled XRD patterns compared to actual XRD patterns on left for the Copper Creek thrust.

Copper Creek Thrust

The Copper Creek thrust is a major fault in the southern Appalachians, with a displacement of ~50 km (Hatcher et al., 2007). Although exposed at a number of locations, the one sampled is located along U.S. 25-E, at the "Thorn Hill Section", a popular locality of well exposed Paleozoic stratigraphy in the Appalachians. Here, dolomites of the Middle Cambrian Rome Formation are thrust onto red siltstones of the Middle Ordovician Moccasin Formation (Figure 5.3). The gouge zone is ~0.5 m thick and is mostly clay, with zones of reddish and gray gouge.

The percentage of illite in I-S is approximately 95%, given that no peak shift occurred after glycolation, but only some peak broadening. The crystallinity is low, with the FWHM value of the fine fraction being 1.149 °2Θ, suggesting low grade diagenetic conditions (Figure 5.14). The gouge has a very rich authigenic component, as even the coarse fraction displays <20% detrital $2M_1$ illite (Figure 5.6). The authigenic ages derived from the polytype analysis yield a total gas age of 279.5 ± 11.3 Ma and a retention age of 390.0 ± 17.2 Ma (Figure 5.8).

St. Clair Thrust

The St. Clair thrust is the northwestern-most major thrust in the Appalachian fold-thrust belt of southwestern Virginia (Figure 5.1). Displacement is on the order of ~29 km (Whisonant and Schultz, 1986; Perry et al., 1979). The sampled exposure lies along US 460 south of Rich Creek, Virginia, placing Cambro-Ordovician Knox Group (Beekmantown dolostones) onto Late Devonian-Early Mississippian shales.

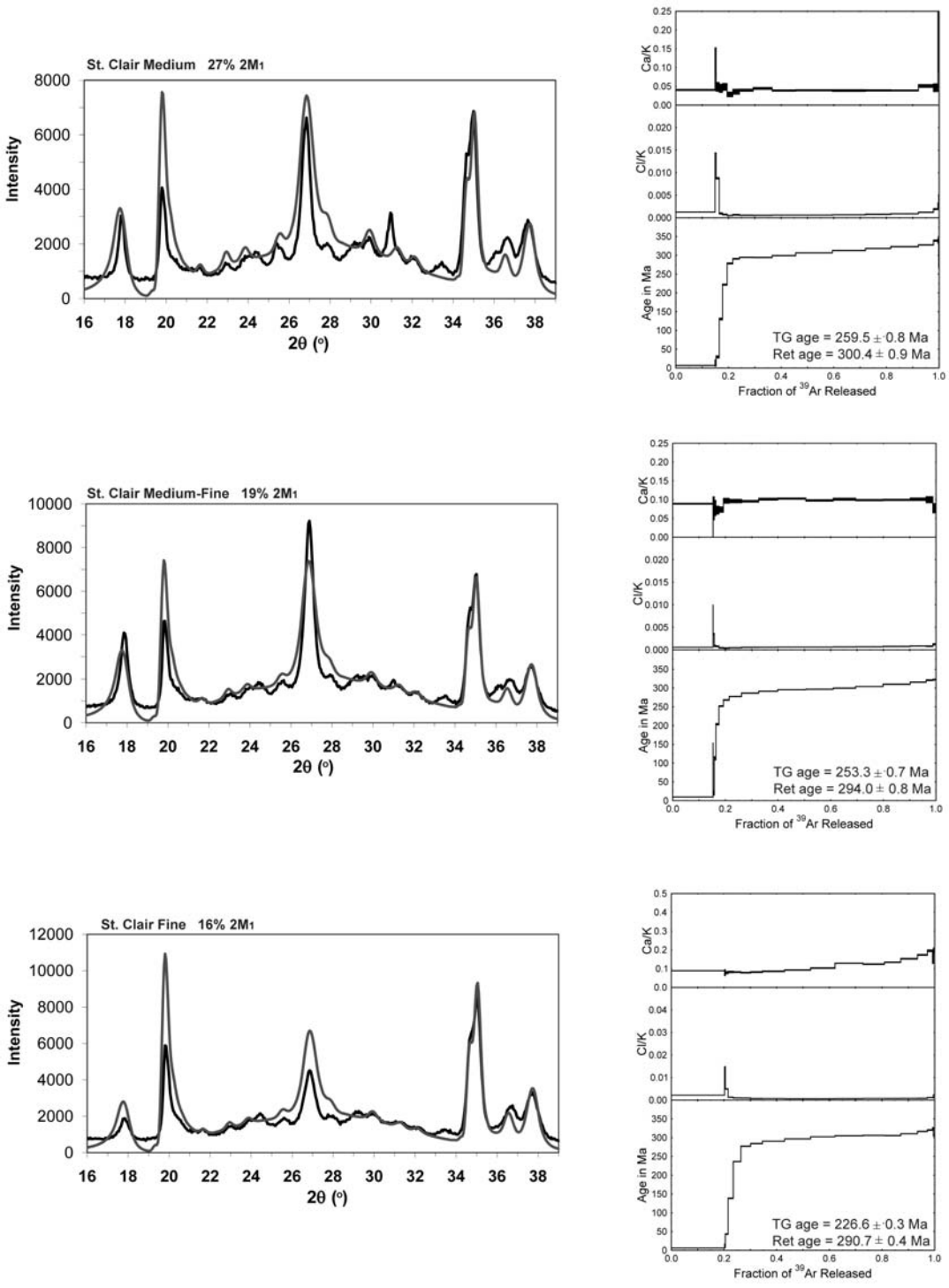

Figure 5.7: Modeled XRD patterns compared to actual XRD patterns on left for the St. Clair thrust.

Figure 5.8: Illite age analysis plots for Appalachian fault rocks. Plots display percent detrital ($2M_1$) illite versus the age (expressed as $e^{\lambda t}$-1). Gray symbols and lines represent retention ages while black symbols and lines represent total gas ages. Dashed lines represent errors. 100% $2M_1$ ages on the right side of the plots are interpreted as detrital ages, while 0% $2M_1$ illite represents authigenic ages.

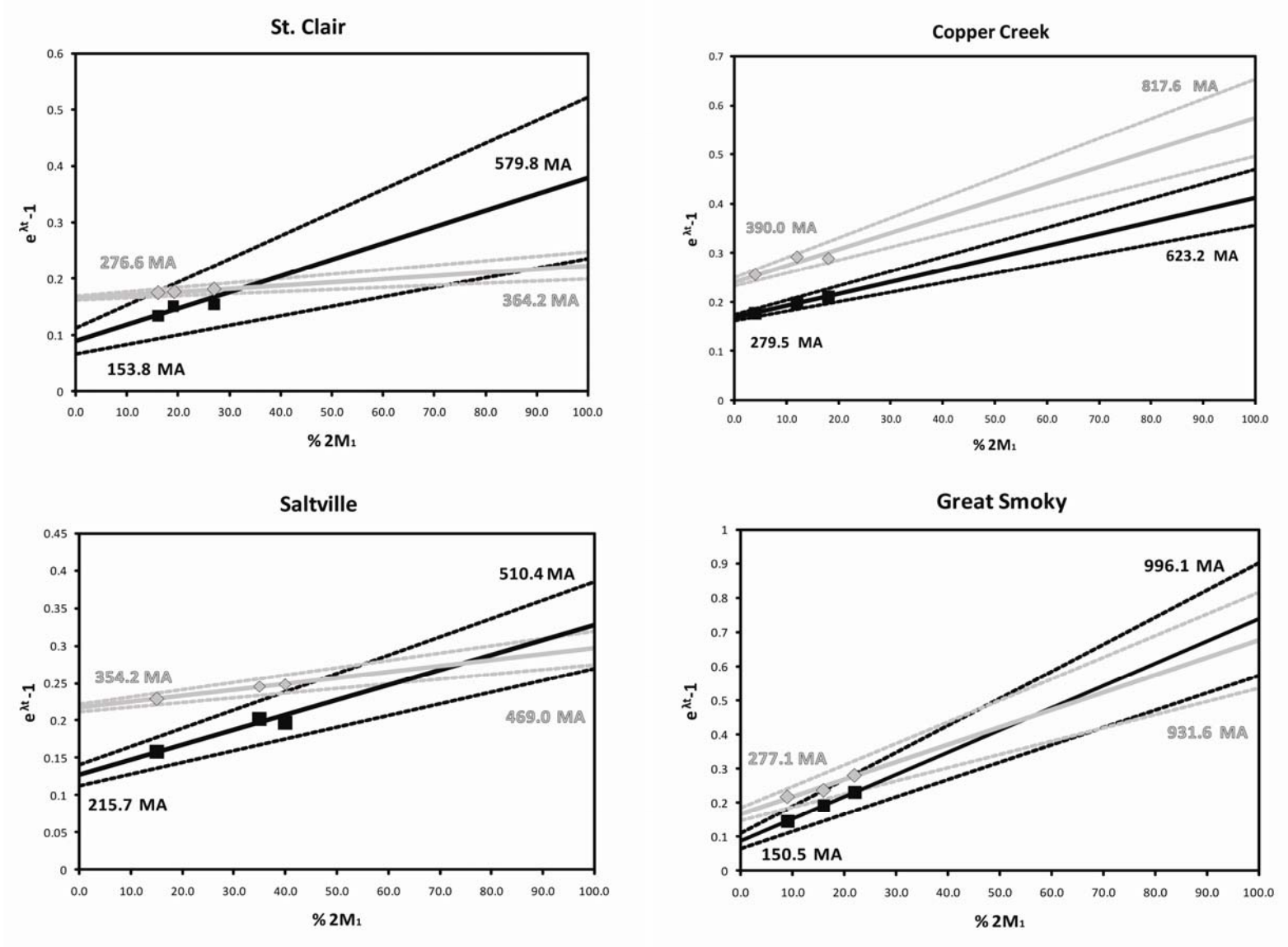
St. Clair
579.8 MA
276.6 MA
364.2 MA
153.8 MA
e^λt-1
% 2M1
Copper Creek
817.6 MA
390.0 MA
623.2 MA
279.5 MA
e^λt-1
% 2M1
Saltville
510.4 MA
354.2 MA
469.0 MA
215.7 MA
e^λt-1
% 2M1
Great Smoky
996.1 MA
931.6 MA
277.1 MA
150.5 MA
e^λt-1
% 2M1

Appalachian Faults

Great Smoky	%2M$_1$	FWHM	Scherrer Thickness	Total Gas Age	Retention Age
Coarse	22.0 ± 3.0 %	0.376 °2θ	21 nm	374.5 ± 1.3 Ma	448.0 ± 1.5 Ma
Medium	16.0 ± 3.0 %	0.419 °2θ	19 nm	314.8 ± 1.0 Ma	385.5 ± 1.2 Ma
Fine	9.0 ± 3.0 %	0.567 °2θ	14 nm	245.6 ± 0.7 Ma	357.3 ± 1.0 Ma
Authigenic Total Gas Age	150.5 ± 41.0 Ma			Detrital Total Gas Age	996.1 ± 161.8 Ma
Authigenic Retention Age	277.1 ± 34.0 Ma			Detrital Retention Age	931.6 ± 143.7 Ma
Saltville	%2M$_1$	FWHM	Scherrer Thickness	Total Gas Age	Retention Age
Coarse	40.0 ± 4.0 %	0.296 °2θ	27 nm	323.3 ± 0.6 Ma	400.0 ± 0.8 Ma
Medium	35.0 ± 3.0 %	0.373 °2θ	21 nm	331.5 ± 0.5 Ma	395.9 ± 0.6 Ma
Fine	15.0 ± 4.0 %	0.514 °2θ	16 nm	264.6 ± 0.7 Ma	371.7 ± 0.9 Ma
Authigenic Total Gas Age	215.7 ± 25.1 Ma			Detrital Total Gas Age	510.4 ± 77.2 Ma
Authigenic Retention Age	354.2 ± 9.9 Ma			Detrital Retention Age	469.0 ± 31.0 Ma
Copper Creek	%2M$_1$	FWHM	Scherrer Thickness	Total Gas Age	Retention Age
Coarse	18.0 ± 2.0 %	0.739 °2θ	11 nm	344.9 ± 0.5 Ma	457.9 ± 0.6 Ma
Medium	12.0 ± 2.0 %	0.837 °2θ	10 nm	326.8 ± 0.8 Ma	462.6 ± 1.1 Ma
Fine	4.0 ± 2.0 %	1.149 °2θ	7 nm	293.7 ± 0.6 Ma	410.7 ± 0.8 Ma
Authigenic Total Gas Age	279.5 ± 11.3 Ma			Detrital Total Gas Age	623.2 ± 70.5 Ma
Authigenic Retention Age	390.0 ± 17.2 Ma			Detrital Retention Age	817.6 ± 89.0 Ma
St. Clair	%2M$_1$	FWHM	Scherrer Thickness	Total Gas Age	Retention Age
Medium	27.0 ± 3.0 %	0.372 °2θ	21 nm	259.5 ± 0.8 Ma	300.4 ± 0.9 Ma
Medium-Fine	19.0 ± 2.0 %	0.453 °2θ	18 nm	253.3 ± 0.7 Ma	294.0 ± 0.8 Ma
Fine	16.0 ± 2.0 %	0.582 °2θ	14 nm	226.6 ± 0.3 Ma	290.7 ± 0.4 Ma
Authigenic Total Gas Age	153.8 ± 41.0 Ma			Detrital Total Gas Age	579.8 ± 178.0 Ma
Authigenic Retention Age	276.6 ± 6.8 Ma			Detrital Retention Age	364.2 ± 34.8 Ma

Table 5.1: Data from the fault rocks of the Appalachian fold-thrust belt. %2M$_1$ illite represents the percentage of detrital illite. Authigenic ages are calculated based on extrapolation to 0% of the 2M$_1$ polytype, whereas detrital ages are calculate based on extrapolation to 100% of the 2M$_1$ polytype.

The ~0.25 m fault zone contains a carbonate rich, clayey gouge with small horses of brecciated dolomite.

Smectite interlayers are virtually nonexistent in analysis of the bulk sample or of individual grain sizes. Crystallinity is high for all size fractions (Figure 5.14; fine fraction FWHM = 0.582 °2Θ), indicating a relatively high diagenetic grade. The percentage detrital illite is less than 30% in all size fractions (Figure 5.7). The authigenic age derived from polytype quantification using the argon total gas ages yields an age of 150.5 ± 41 Ma. Using the retention ages produces an authigenic age of 276.6 ± 6.8 Ma for this fault (Figure 5.8).

Midcontinent Shales

Sample Fsh7 is a Middle Ordovician shale collected from the Nashville dome and is ~60 km from the exposed front of the Appalachian foreland fold-thrust belt. Polytype analysis reveals that this shale is primarily comprised of authigenic $1M_d$ illite (<30% $2M_1$; Figure 5.9). Polytype quantification of the finest fraction (<0.05 μm) was done without removing carbonate minerals, as the sample was lost during acid treatment. The crystallinity is relatively low, with the fine fraction FWHM being 1.181 °2Θ, placing it in a low grade diagenetic regime similar to the Copper Creek thrust. The polytype-derived age using the total gas ages is 300.1 ± 28.6 Ma, whereas the retention ages result in an age of 487.3 ± 9.4 Ma. Note that the latter is older than deposition of the shale (Figure 5.12)

An Upper Pennsylvanian shale from an exposure within the Illinois Basin was collected to compare with the analyzed shales of Ordovician age. The crystallinity is

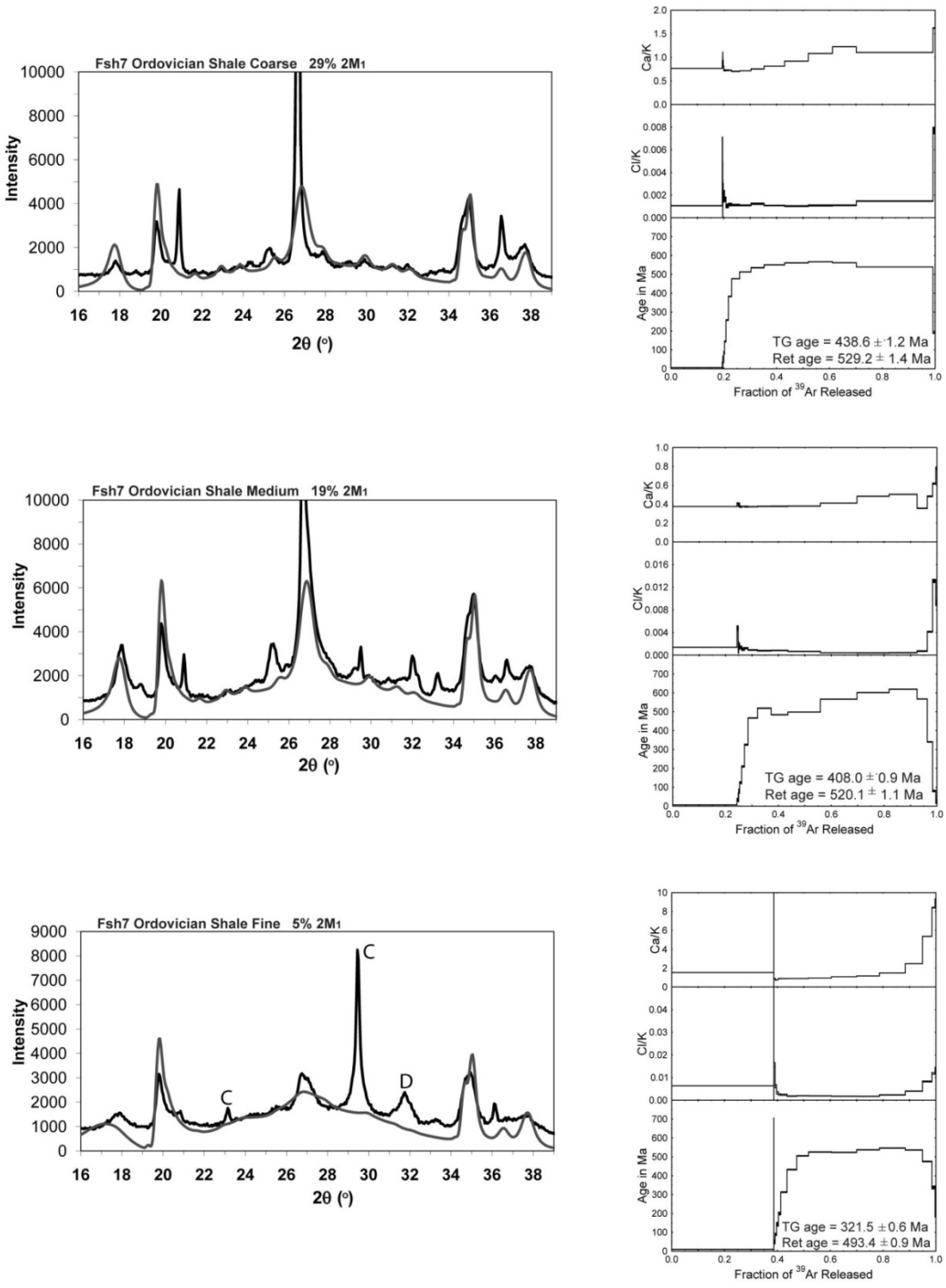

Figure 5.9: Modeled XRD patterns compared to actual XRD patterns on left for the Ordovician shale Fsh7. Fine fraction includes carbonate minerals calcite (C) and dolomite (D).

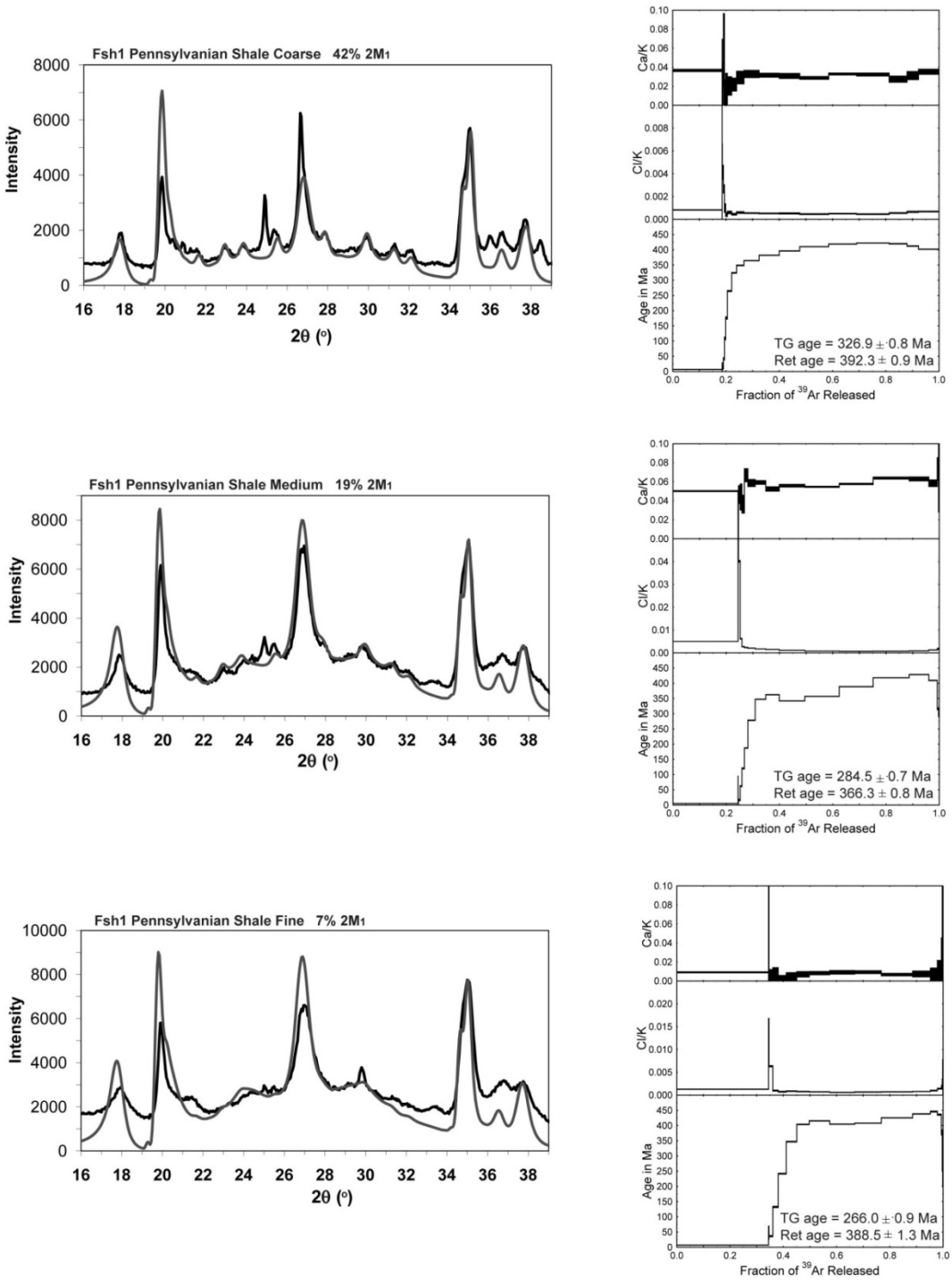

Figure 5.10: Modeled XRD patterns compared to actual XRD patterns on left for the Pennsylvanian shale Fsh1.

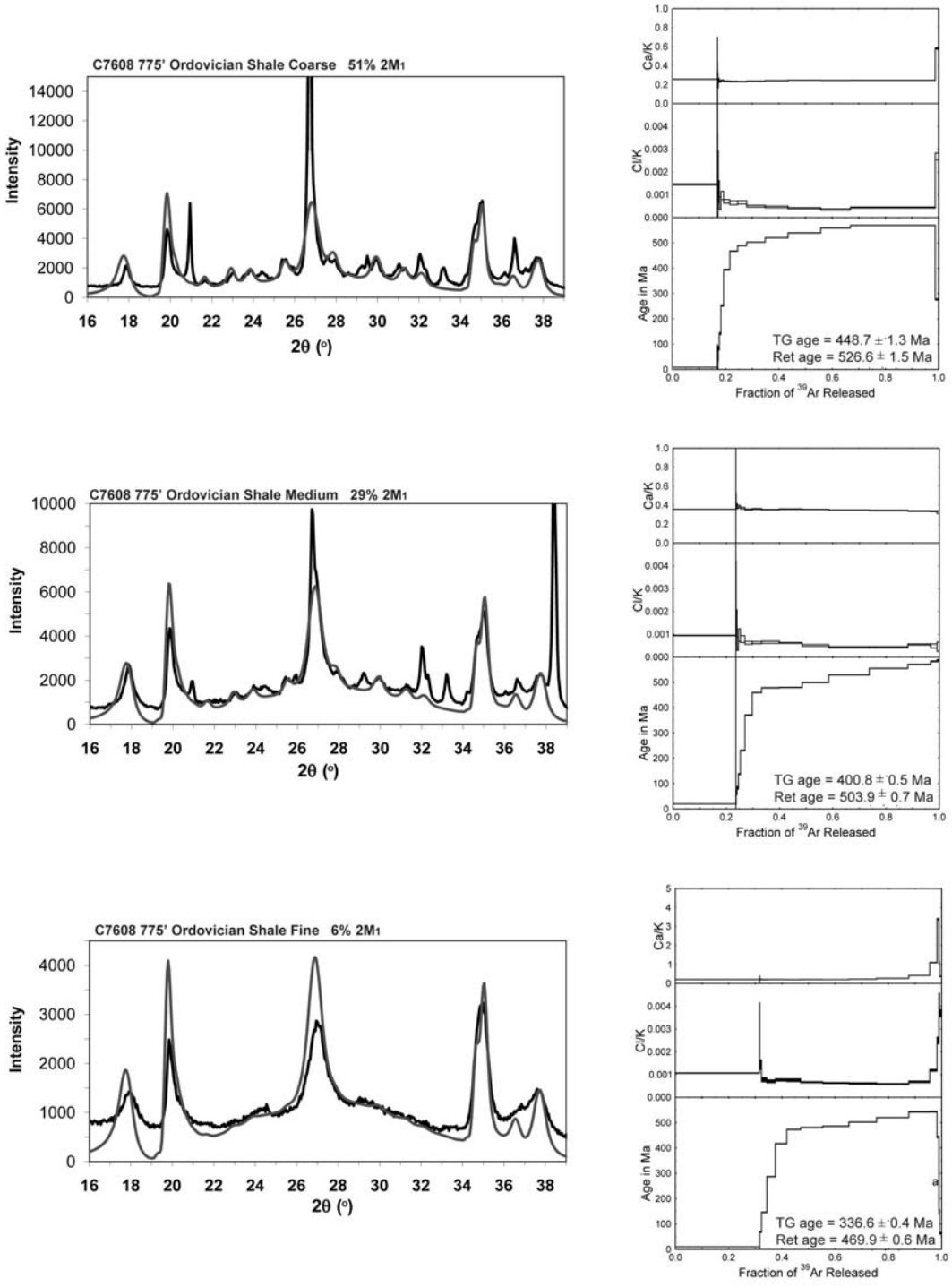

Figure 5.11: Modeled XRD patterns compared to actual XRD patterns on left for the Ordovician Maquoketa shale from a core (C7608) in Illinois.

low (fine fraction FWHM = 0.856 °2θ) and ~5% smectite exists as interlayers in I-S. Extrapolated authigenic ages are 251.5 ± 6.1 Ma and 373.5 ± 23.3 Ma using the total gas ages and retention ages, respectively (Figure 5.12). The retention ages, however, display a younger age for the medium fraction than for the fine fraction, suggesting that these ages are not meaningful. Moreover, the retention age is older than the depositional age of the shale.

Sample C7608 is from a shale in the Upper Ordovician Maquoketa Formation, which was taken from a core in northwestern Illinois. C7608 displays an average FWHM of 0.55 °2θ with virtually no I-S (<5% smectite interlayers), although the finest fraction has a FWHM of 0.91 °2θ, which places it in a lower diagenetic regime. Polytypism shows ~50% detrital illite in the coarse fraction, but only 6% in the finest fraction (Figure 5.11). Ages from both total gas ages and retention ages are 321.4 ± 8.1 Ma and 462.3 ± 4.1 Ma, respectively (Figure 5.12). The polytype derived age using the total gas ages is indistinguishable from the 321 Ma age determined by Grathoff et al. (2001) using the K-Ar method, while the retention ages are again older than deposition of the shale.

DISCUSSION

Total Gas vs. Retention Ages

Results from this study permit the examination of the application of total gas ages and retention ages to dating of faulting and diagenesis. In addition, preliminary interpretation based on these first results for regional tectonics is offered as well.

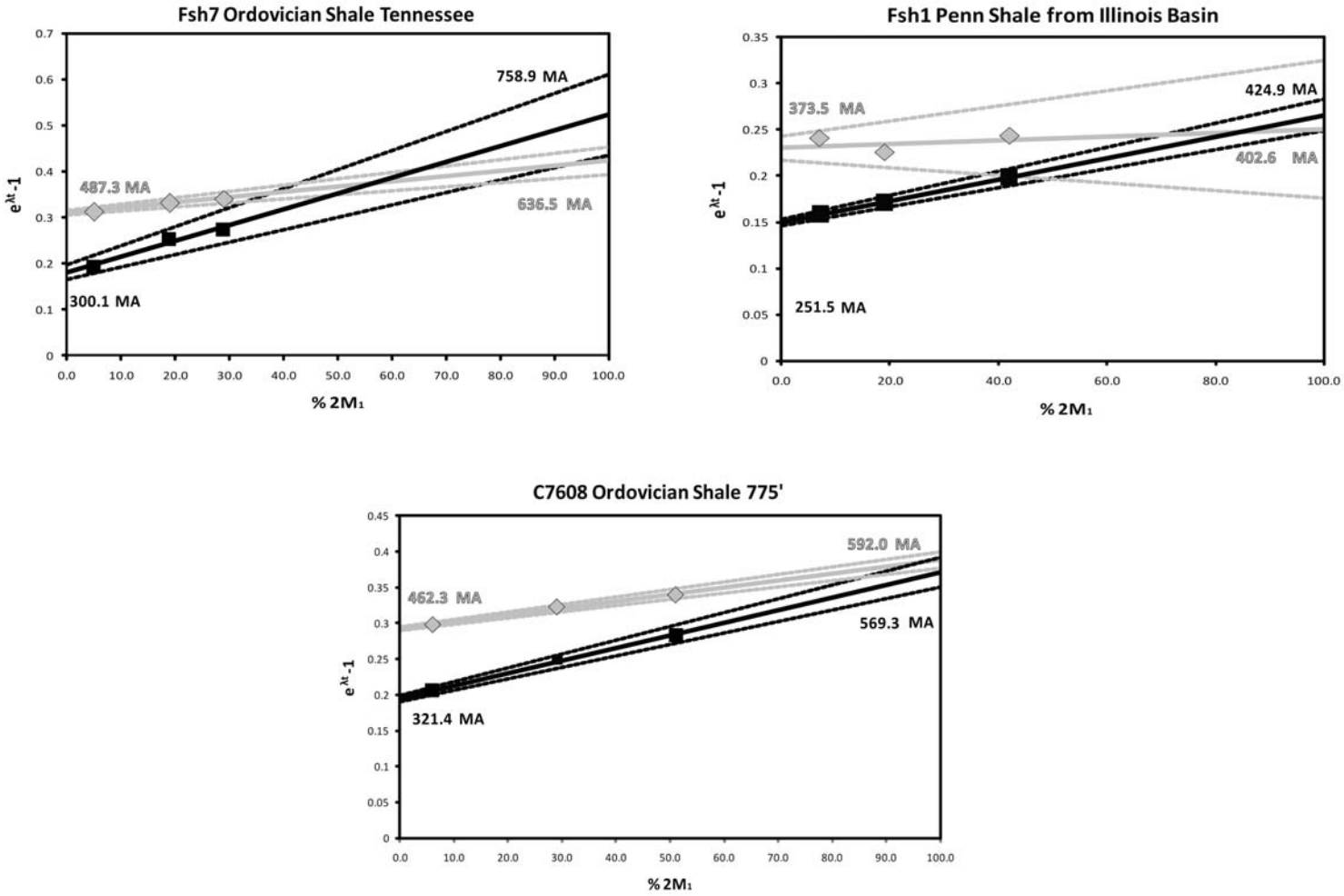

Figure 5.12: Illite age analysis plots for midcontinent shales. Symbols as in Figure 5.8.

Midcontinent Shales

Fsh7 Ord Tenn	%2M$_1$	FWHM	Scherrer Thickness	Total Gas Age	Retention Age
Coarse	29.0 ± 3.0 %	0.562 °2θ	14 nm	438.6 ± 1.2 Ma	529.2 ± 1.4 Ma
Medium	19.0 ± 3.0 %	0.617 °2θ	13 nm	408.0 ± 0.9 Ma	520.1 ± 1.1 Ma
Fine	5.0 ± 4.0 %	1.181 °2θ	7 nm	321.5 ± 0.6 Ma	493.4 ± 0.9 Ma
Authigenic Total Gas Age	300.1 ± 28.6 Ma			Detrital Total Gas Age	758.9 ± 101.3 Ma
Authigenic Retention Age	487.3 ± 9.4 Ma			Detrital Retention Age	592.0 ± 14.8 Ma
Fsh1 Penn III	%2M$_1$	FWHM	Scherrer Thickness	Total Gas Age	Retention Age
Coarse	42.0 ± 3.0 %	0.489 °2θ	17 nm	326.9 ± 0.8 Ma	392.3 ± 0.9 Ma
Medium	19.0 ± 2.0 %	0.620 °2θ	13 nm	284.5 ± 0.7 Ma	366.3 ± 0.8 Ma
Fine	7.0 ± 3.0 %	0.856 °2θ	9 nm	266.0 ± 0.9 Ma	388.5 ± 1.3 Ma
Authigenic Total Gas Age	251.5 ± 6.1 Ma			Detrital Total Gas Age	424.9 ± 24.6 Ma
Authigenic Retention Age	373.5 ± 23.3 Ma			Detrital Retention Age	402.6 ± 103.8 Ma
C7608 Ord Maq III	%2M$_1$	FWHM	Scherrer Thickness	Total Gas Age	Retention Age
Coarse	51.0 ± 5.0%	0.265 °2θ	30 nm	448.7 ± 1.3 Ma	526.6 ± 1.5 Ma
Medium	29.0 ± 3.0 %	0.469 °2θ	17 nm	400.8 ± 0.5 Ma	503.9 ± 0.7 Ma
Fine	6.0 ± 2.0 %	0.913 °2θ	9 nm	336.6 ± 0.4 Ma	469.9 ± 0.6 Ma
Authigenic Total Gas Age	321.4 ± 8.1 Ma			Detrital Total Gas Age	569.3 ± 26.8 Ma
Authigenic Retention Age	462.3 ± 4.1 Ma			Detrital Retention Age	592.0 ± 14.8 Ma

Table 5.2: Data from shales of the midcontinent. Labels as in Table 5.1.

Total gas ages, analogous to K-Ar ages, assume that radiogenic argon has been retained by the illite crystallites. This assumption requires that K does not reside in defect sites within the crystallite structure, where ^{40}Ar can be lost by diffusion. If, however, K^+ ions occupy defect sites, in the same proportion as K to the bulk composition of the structure, then radiogenic argon will be lost while the recoiled fraction of ^{39}Ar produced during neutron irradiation will represent the K from these defect sites (Dong et al., 1995; 1997; 2000; Hall et al., 2000). Therefore, the retention age model was introduced to correct for argon loss from defect sites. In cases where no K exists in defect sites, the total gas age is correct and the retention age will overcorrect for argon loss.

Previous studies of this phenomenon (Dong et al., 1995; 1997; 2000; Hall et al., 2000) have suggested that the presence of smectite interlayers appears to be the deciding factor between retention ages and total gas ages. They concluded that total gas ages are correct in the presence of smectite interlayers. Smectite, with a deficiency in K, would act as an ^{40}Ar sink while ^{39}Ar would be released from the crystal structure during irradiation, as a consequence of the force of the ^{39}K (n,p) ^{39}Ar reaction. A lack of smectite interlayers (a sign of higher diagenetic grade) would thus require the retention age be used. Comparing Rb-Sr ages with ages from illite of higher-grade diagenetic to epizonal regimes containing very few smectite interlayers supported this approach (Dong et al., 1995; 1997; Hall et al., 2000). A separate study of lower grade diagenetic illite in bentonites from the Gulf Coast showed that when smectite is present, the retention age overcorrects the age while the total gas age proved to be geologically significant (Dong et al., 2000).

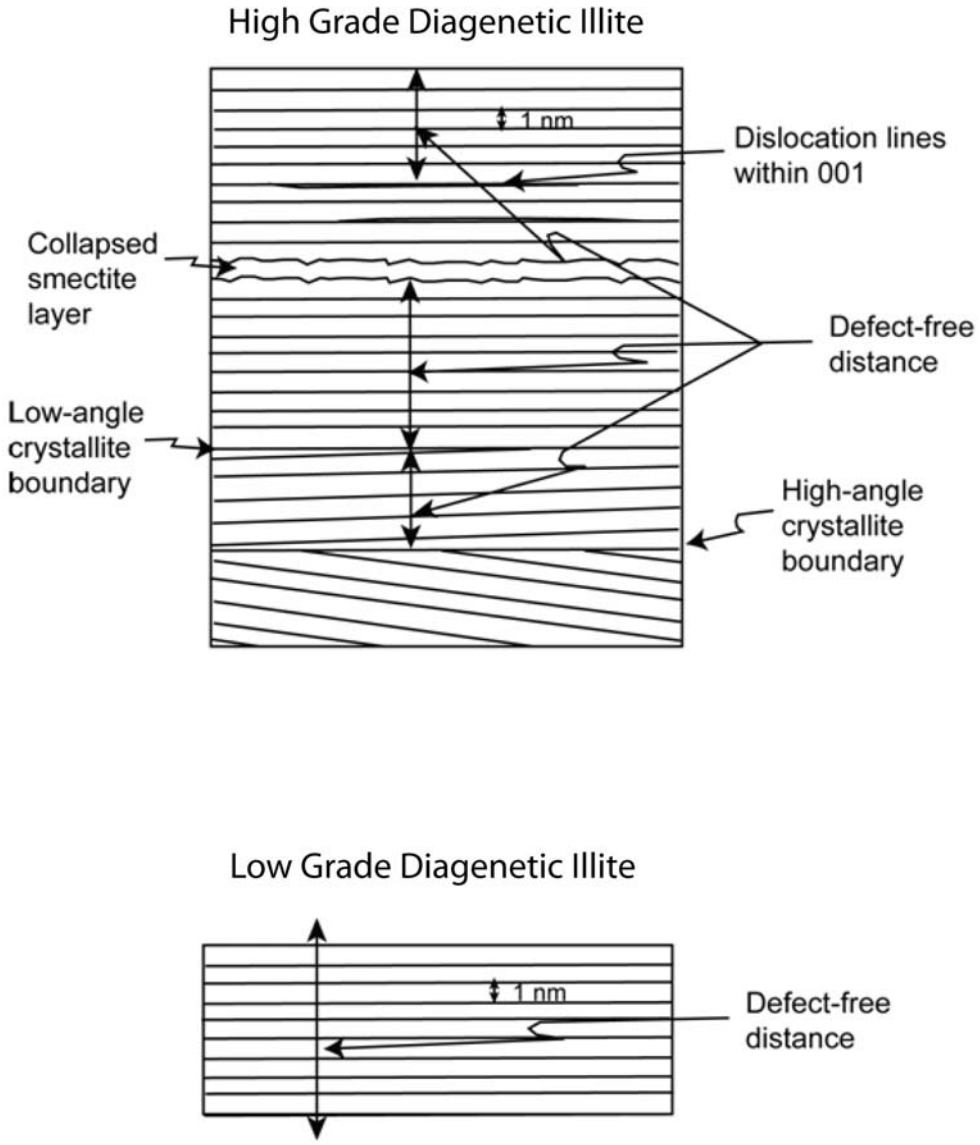

Figure 5.13: Schematic crystallites of higher grade diagenetic illite (top) and lower grade diagenetic illite (modified from Warr and Nieto, 1998). Defect-distance is contained within the crystallite for the high grade example, while the low grade diagenetic illite is smaller than the defect-free distance. Defect sites allow the crystallite to lose ^{40}Ar during radiogenic decay.

In the current study, smectite interlayers are present only in limited amounts (≤5%) for all samples. However, total gas ages for one fault and all shale samples have geologic meaning, suggesting that other mechanisms for argon retention are at work. The crystal lattice thickness for illite is 1 nm and natural illite is characterized by a stacking of these layers, with the sequence determining the polytype. Layer stacking increases with increased diagenetic grade, resulting in thicker illite crystallites as well as sharper basal 00l reflections on XRD patterns (Kübler, 1967; Eberl and Velde, 1989; Kübler and Jaboyedoff, 2000). Within a stacked illite crystallite, a certain defect free distance exists, which is the length of an interval of the illite crystallite that does not have any angular discontinuities (Warr and Nieto, 1998). Defects are typically collapsed smectite layers, low and high angle crystallite boundaries, layer terminations and layer-parallel features with incoherent rotations (Figure 5.13). Warr and Nieto (1998) suggested, based on TEM study, that diagenetic illite typically has an average defect-free distance of ~10 nm, corresponding to approximately 10 illite layers. Therefore, defects would be mostly non-existent in crystallites smaller than 10 nm, so would not be capable of releasing radiogenic argon, as argon diffusion through the crystal lattice is otherwise negligible at low temperatures (Hames and Bowring, 1994; Hall et al., 2000). Crystallites thicker than 10nm would have defect sites available to release radiogenic ^{40}Ar, and thus require the retention age model dating. Moreover, the higher diagenetic grade implies higher temperature (~200°C), which would further aid in radiogenic argon release from the defect sites.

Tables 5.1 and 5.2 show the average crystallite thickness for each size fraction, calculated using the Scherrer equation (Drits et al., 1997) applied to the FWHM. The Scherrer equation calculates crystallite thickness based on the peak breadth of the 001 peak by the function:

$$\beta_{001} = \frac{K\lambda}{T\ cos\theta_{001}}$$

where β_{001} is the FWHM of the 001 peak, K is a constant, λ is the wavelength of the incident X-rays, θ_{001} is the center angle of the 001 peak and T is the crystallite thickness. The difference in the broadness of the 001 illite peak is clearly illustrated by comparing the Copper Creek and St. Clair fine fractions (Figure 5.14). The fine fractions for each sample were used for this comparison, because the coarser grain sizes are more affected by detrital illite that gives large, muscovite-like thicknesses. The results show that samples with geologically meaningful ages using the total gas ages model always have a Scherrer thickness of less than 10 nm, while samples in which the retention age model works better consistently have a thickness of greater than 10 nm. Thus, while the presence of smectite interlayers may be important in some settings, our results suggest that the primary mechanism of radiogenic argon retention in illite is dependent on the average thickness of the crystallites. Our observations also provide a means to select the retention age or total gas age model for the interpretation of natural rocks.

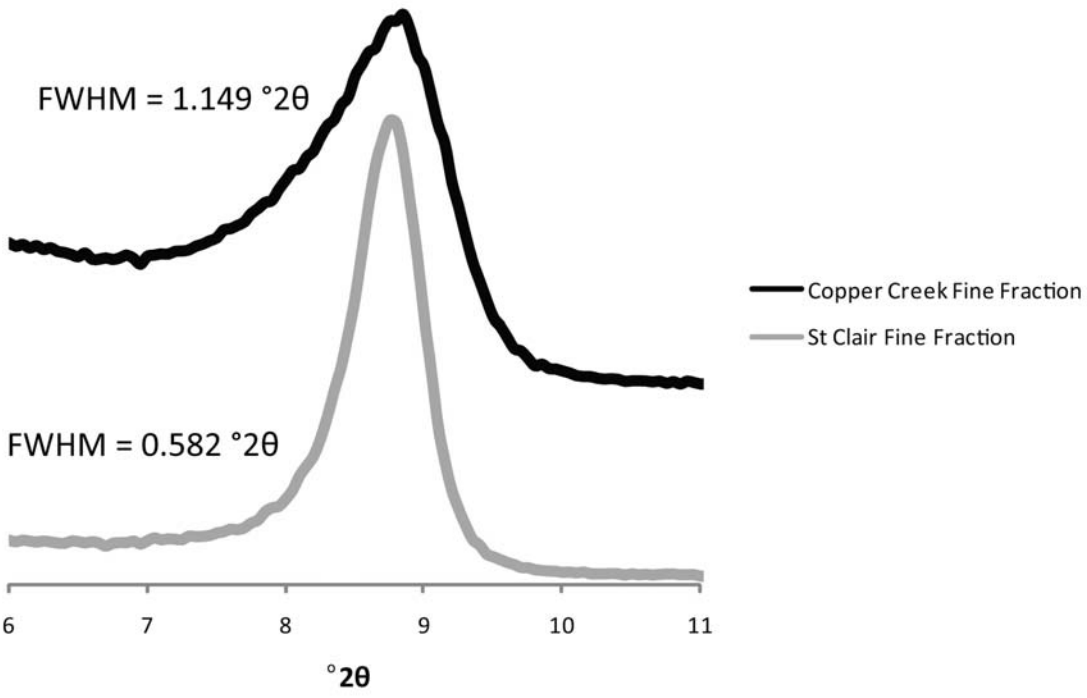

Figure 5.14: XRD patterns of the illite 001 peak, displaying the contrast between the broad peak of the fine fraction from the Copper Creek thrust and the sharper peak of the fine fraction of the St. Clair thrust.

Shale Diagenesis

The ages for three samples of shales from the eastern U.S. are dissimilar in age. Each shale seems to represent a separate history of diagenesis, with illite crystallization (or recrystallization) occurring at different times. Fsh7, the Ordovician shale closest to the thrust belt has a small crystallite thickness, giving an age of 300.1 ± 28.6 Ma from total gas ages. The Pennsylvanian authigenic age for this sample is roughly equivalent to the age of remagnetization in Ordovician limestones previously determined for the Appalachians and its foreland (McCabe and Elmore, 1989; Chapter III of this dissertation), supporting a link between the growth of authigenic illite and remagnetization as noted by previous workers (Katz et al., 1998; Gill et al., 2002; Tohver et al., 2008). Collectively these ages suggest that a widespread diagenetic event occurred around 300 Ma, perhaps involving orogenically driven fluids from the evolving Appalachian thrust wedge. The crystallite thickness of the Pennsylvanian shale (Fsh1) is also relatively low, again indicating that the total gas age model is the suitable choice. The poor fit of a mixing line along with an age of the fine fraction older than the medium fraction, further supports the rejection of the retention age model for this sample. The Permo-Triassic age (251.5 ± 6.1 Ma) is interpreted to represent the age of illitization for these sediments.

The Ordovician shale of the Maquoketa Formation taken from a core in the northwestern Illinois basin has a total gas age (321.4 ± 8.1 Ma) that is equivalent to the K-Ar age presented by Grathoff et al. (2001). The low crystallinity of the fine fraction, with a Scherrer thickness of 9 nm, suggests that the total gas age method is

the preferred approach, supported by the coincidence of these ages. The Pennsylvanian age was interpreted by Grathoff et al. as the result of K-rich fluids being introduced to the Illinois basin during illitization, which may be supported by similar analysis elsewhere in the basin.

Appalachian Thrusts

Authigenic illite dominates each of the sampled fault rocks. The Copper Creek fault is of a lower diagenetic grade than the Great Smoky, Saltville or St. Clair thrusts, based on the lower crystallinity (fine fraction = 7 nm). Therefore, the total gas age is used for the Copper Creek fault, while the retention age is used for the other three. The higher grade of these three faults is attributed to the greater depth at which they were active and subsequently exhumed. Studies using the conodont alteration index (CAI), apatite fission-track thermochronology and geodynamic modeling all show that the site where the Copper Creek fault was sampled has been exhumed from a shallower depth than those at from the Great Smoky, Saltville and St. Clair thrusts (Epstein et al., 1977; Beaumont et al., 1987; Roden, 1991). The increased diagenetic grade likewise supports greater depth of formation for these three faults compared to the Copper Creek thrust.

The Great Smoky, Copper Creek and St. Clair thrusts all have ages in the range of 275-280 Ma (Figure 5.7; Table 5.1), showing that, within error, they were all simultaneously active during Early Permian time. For the Saltville result, the sampled fault rock is polished shale cataclasite derived from the footwall, where the age (354 ± 9.9 Ma) represents the illitization age of the footwall Devonian shale.

Note that this old age cannot represent activity along the fault, since the Saltville thrust cuts younger (Mississippian) sediments in its footwall. Analysis of other wall rock samples is planned to confirm this interpretation.

As observed in the Rocky Mountains foreland of Alberta and Wyoming (van der Pluijm et al., 2006; Solum and van der Pluijm, 2007), fault ages from the southern Appalachians show that the entire frontal wedge was active during the Early Permian. This timing of activity for Appalachian faults can reconcile previous studies regarding the progression of thrusting where evidence for hinterland progression of the belt was based primarily on cross-cutting relationships of major faults. These relationships can be incorporated within an internally deforming wedge where many faults are active simultaneously.

CONCLUSIONS

$^{40}Ar/^{39}Ar$ dating of illite has been applied to both shales and fault rocks from the southern Appalachians and neighboring midcontinent. Prior studies of fault gouge dating relied on total gas ages when applying Illite Age Analysis (IAA). Results from this study highlight the implications of higher diagenetic grades, and particularly the retention age model,when applying IAA to clay-bearing rocks. Crystallites from low grade diagenetic regimes are smaller than the average, defect free distance for illites, thereby retaining radiogenic argon within the crystallite structure. Conversely, larger crystallites are more susceptible to argon loss during radiogenic decay because of increasing defect density. This distinction is crucial for

the application of $^{40}Ar/^{39}Ar$ dating to fault gouge and shales, as failure to recognize large crystallites and higher diagenetic grade can lead to misinterpreted ages. The present study constrains the use of total gas ages and retention ages from a sample based on crystallite size.

Shales that have been dated from the midcontinent each indicate distinct histories of diagenesis. All samples display evidence of low grade diagenetic setting, with authigenic illite crystallites of thicknesses less than 10 nm. Both Ordovician shales display authigenic growth of illite during the Pennsylvanian, and can be interpreted as an indication of large scale, staged fluid flow occurring across the eastern U.S. Further work is needed on shales from throughout the midcontinent to test this hypothesis. The age of thrusting in the Appalachian foreland fold-thrust belt has been constrained by our data from four fault rocks. These data are unlike prior applications of IAA, in that the higher diagenetic grade requires the use of the retention age instead of the total gas age. Illite ages from the Great Smoky, Copper Creek and St. Clair thrusts all preserve a period of motion at ~ 278 Ma in the Appalachian foreland , supporting the interpretation that faults were active simultaneously in this part of the orogen.

ACKNOWLEDGEMENTS

This work would not have been possible without the help of a number of people and agencies. Pete Lemiszki from the Tennessee Division of Geology – Knoxville Office and Bob Hatcher from the University of Tennessee are thanked for

pointing the way toward a number of excellent fault outcrops. I am grateful to the geological surveys of Illinois and Kentucky for allowing me to sample their core. Anja Schleicher is thanked for X-ray support and discussion; Sam Haines and John Solum provided generous assistance with modeling and initial application of IAA. Appalachian research at the University of Michigan has been supported by grants from the American Chemical Society-Petroleum Research Fund (most recently 45893-AC8) and by the Scott Turner Fund.

Faults yet to be dated

Great Smoky 2	$\%2M_1$	FWHM	Scherrer Thickness
Coarse	29.0 ± 3.0 %	0.353 °2θ	23 nm
Medium	16.0 ± 3.0 %	0.397 °2θ	20 nm
Fine	5.0 ± 3.0 %	0.519 °2θ	15 nm
Knoxville	$\%2M_1$	FWHM	Scherrer Thickness
Coarse	33.0 ± 2.0 %	0.371 °2θ	22 nm
Medium	17.0 ± 2.0 %	0.538 °2θ	15 nm
Fine	11.0 ± 3.0 %	0.875°2θ	9 nm
Pound Gap	$\%2M_1$	FWHM	Scherrer Thickness
Medium	55.0 ± 4.0 %	0.349 °2θ	23 nm
Medium-Fine	34.0 ± 3.0 %	0.539 °2θ	15 nm
Fine	15.0 ± 5.0 %	0.887 °2θ	9 nm
Limestone OC14	$\%2M_1$	FWHM	Scherrer Thickness
Coarse	40.0 ± 4.0 %	0.251 °2θ	32 nm
Medium	27.0 ± 3.0 %	0.462 °2θ	17 nm
Fine	16.0 ± 3.0 %	0.773 °2θ	10 nm
Wall Rock Fine Fractions	$\%2M_1$	FWHM	Scherrer Thickness
Cop Creek HW	12.0 ± 5.0 %	0.071 °2θ	89 nm
Cop Creek FW	10.0 ± 2.0 %	0.549 °2θ	15 nm
Great Smoky FW	5.0 ± 2.0 %	0.852 °2θ	10 nm

Ordovician Shales yet to be dated

KY 4674	$\%2M_1$	FWHM	Scherrer Thickness
Coarse	52.0 ± 5.0 %	0.231 °2θ	35 nm
Medium	32.0 ± 3.0 %	0.441 °2θ	18 nm
Fine	13.0 ± 3.0 %	0.738 °2θ	11 nm
KY 15533	$\%2M_1$	FWHM	Scherrer Thickness
Coarse	16.0 ± 3.0 %	0.528 °2θ	15 nm
Medium	11.0 ± 2.0 %	0.763 °2θ	10 nm
Fine	6.0 ± 3.0 %	1.247 °2θ	6 nm
C2940 Illinois	$\%2M_1$	FWHM	Scherrer Thickness
Medium	33.0 ± 3.0 %	0.383 °2θ	21 nm
Medium-Fine	13.0 ± 2.0 %	0.601 °2θ	13 nm
Fine	5.0 ± 4.0 %	0.942 °2θ	9 nm

Table 5.3: XRD measurements and polytype estimates of faults and shales that have yet to be radiometrically dated.

REFERENCES

Aronson, J.L. and Hower, J., 1976. Mechanism of burial metamorphism of argillaceous sediment; 2, Radiogenic argon evidence. Geological Society of America Bulletin 87, 738-744.

Beaumont, C., Quinlan, G. and Hamilton, J., The Alleghanian orogeny and its relationship to the evolution of the eastern interior of North America. In: Beaumont, C. and Tankard, A., Editors, 1987. *Sedimentary Basins and Basin-Forming Mechanisms, Canadian Geological Society of Petroleum Geologists Memoir 12*, 425-446.

Becker, T.P., Thomas, W.A. and Gehrels, G.E., 2006. Linking late Paleozoic sedimentary provenance in the Appalachian Basin to the history of Alleghanian deformation. American Journal of Science 306, 777-798.

Bethke, C.M., and Marshak, S., 1990. Brine migrations across North America: the plate tectonics of groundwater. Annual Reviews of Earth and Planentary Science 18, 287-315.

Dallmeyer, R.D., Wright, J.E., Secor Jr, D.T. and Snoke, A.W., 1986. Character of the Alleghanian Orogeny in the Southern Appalachians; Part II, Geochronological constraints on the tectonothermal evolution of the eastern Piedmont in South Carolina. Geological Society of America Bulletin 97, 1329-1344.

Dong, H., Hall, C.M., Peacor, D.R. and Halliday, A.N., 1995. Mechanisms of argon retention in clays revealed by laser ^{40}Ar-^{39}Ar dating. Science 267, 355-359.

Dong, H., Hall, C.M., Halliday, A.N., Peacor, D.R., Merriman, R.J. and Roberts, B., 1997. $^{40}Ar/^{39}Ar$ illite dating of late Caledonian (Acadian) metamorphism and cooling of K-bentonites and slates from the Welsh Basin, U.K. Earth and Planetary Science Letters 150, 337-351

Dong, H., Hall, C.M., Peacor, D.R., Halliday, A.N. and Pevear, D.R., 2000. Thermal $^{40}Ar/^{39}Ar$ separation of diagenetic from detrital illitic clays in Gulf Coast shales. Earth and Planetary Science Letters 175, 309-325.

Drits, V.A., Środoń , J. and Eberl, D.D., 1997. XRD measurement of mean crystallite thickness of illite and illite/smectite; reappraisal of the Kubler index and the Scherrer equation. Clays and Clay Minerals 45, 461-475.

Eberl, D.D. and Velde, B., 1989. Beyond the Kubler index. Clay Minerals 24, 571-577.

Elliott, W.C. and Aronson, J.L., 1987. Alleghanian episode of K-bentonite illitization in the southern Appalachian Basin. Geology 8, 735-739.

Elliott, W.C. and Aronson, J.L., 1993. The timing and extent of illite formation in Ordovician K-bentonites at the Cincinnati Arch, the Nashville Dome and north-eastern Illinois Basin. Basin Research 5, 125-135.

Elliott, W.C. and Haynes, J.T., 2002. The chemical character of fluids forming diagenetic illite in the southern Appalachian Basin. American Mineralogist 87, 1519-1527.

Epstein, A.G., Epstein, J.B. and Harris, J.D., 1977. Conodont color alteration; an index to organic metamorphism. U.S. Geological Survey Professional Paper, Report P 0995, 27pp.

Foland, K.A., Hubacher, F.A. and Arehart, G.B., 1992. $^{40}Ar/^{39}Ar$ dating of very fine-grained samples; an encapsulated-vial procedure to overcome the problem of ^{39}Ar recoil loss. Chemical Geology 102, 269-276.

Gill, J.D., Elmore, R.D. and Engel, M.H., 2002. Chemical remagnetization and clay diagenesis; testing the hypothesis in the Cretaceous sedimentary rocks of northwestern Montana. Physics and Chemistry of the Earth 27, 25-31.

Goldberg, S.A. and Dallmeyer, R.D., 1997. Chronology of Paleozoic metamorphism and deformation in the Blue Ridge thrust complex, North Carolina and Tennessee. American Journal of Science 297, 488-526.

Grathoff, G.H. and Moore, D.M., 1996. Illite polytype quantification using WILDFIRE calculated X-ray diffraction patterns. Clays and Clay Minerals 44, 835-842.

Grathoff, G.H., Moore, D.M., Hay, R.L. and Wemmer, K., Illite polytype quantification and K/Ar dating of Paleozoic shales; a technique to quantify diagenetic and detrital illite. In: Schieber, J., Zimmerle, W. and Sethi, P.S., Editors, 1998. *Shales and mudstones II; Petrography, petrophysics, geochemistry, and economic geology*. Schweizerbartsche Verlagsbuchhandlung, Stuttgart, Germany, 161-175.

Grathoff, G.H., Moore, D.M., Hay, R.L. and Wemmer, K., 2001. Origin of illite in the lower Paleozoic of the Illinois Basin; evidence for brine migrations. Geological Society of America Bulletin 113, 1092-1104.

Hadizadeh, J., Babaie, H.A. and Babaie, A., 1991. Development of interlaced mylonites, cataclasites and breccias; examples from the Towaliga Fault, south central Appalachians. Journal of Structural Geology 13, 63-70.

Haines, S.H. and van der Pluijm, B.A., 2008. Clay quantification and Ar-Ar dating of synthetic and natural gouge: Application to the Miocene Sierra Mazatán detachment fault, Sonora, Mexico. Journal of Structural Geology 30, 525-538.

Hall, C.M., Kesler, S.E., Simon, G. and Fortuna, J., 2000. Overlapping Cretaceous and Eocene alteration, Twin Creeks Carlin-type deposit, Nevada. Economic Geology 95, 1739-1752.

Hames, W.E. and Bowring, S.A., 1994. An empirical evaluation of the argon diffusion geometry in muscovite. Earth and Planetary Science Letters 124, 161-169.

Hardeman, W.D., 1966. Geologic map of Tennessee. State of Tennessee Department of Conversation, Division of Geology, scale 1:250,000.

Harris, L.D. and Milici, R.C., 1977. Characteristics of a thin-skinned style of deformation in the southern Appalachians, and potential hydrocarbon traps. USGS Professional Paper 1018.

Hatcher Jr, R.D., Hooper, R.J., McConnell, K.I., Hevin, T. and Costello, J.O., Geometric and time relationships between thrusts in the crystalline Southern Appalachians. In: Mitra, G. and Wojtal, S.F., Editors, 1988. *Geometries and mechanism of thrusting, with special reference to the Appalachians.* Geological Society of America Special Paper 222, 185-196.

Hatcher Jr, R.D., Lemiszki, P.J. and Whisner, J.B., Character of rigid boundaries and internal deformation of the Southern Appalachian foreland fold-thrust belt. In: Sears, J.W., Harms, T.A. and Evenchick, C.A., Editors, 2007. *Whence the mountains? Inquiries into the evolution of orogenic systems; a volume in honor of Raymond A. Price.* Geological Society of America Special Paper 433, 243-276.

Hatcher Jr, R.D., Thomas, W.A., Geiser, P.A., Snoke, A.W., Mosher, S. and Wiltschko, D.V., Alleghanian orogen. In: Hatcher Jr, R.D., Thomas, W.A. and Viele, G.E., Editors, 1989. *The Appalachian-Ouachita Orogen in the United States, The Geology of North America Volume F-2.* Geological Society of America, Boulder, Colorado, 233-318.

Hearn Jr, P.P., Sutter, J.F. and Belkin, H.E., 1987. Evidence for late-Paleozoic brine migration in Cambrian carbonate rocks of the Central and Southern Appalachians; implications for Mississippi valley-type sulfide mineralization. Geochemica et Cosmochimica Acta 51, 1323-1334.

Hower, J., Hurley, P.M., Pinson, W.H. and Fairbairn, H.W., 1963. The dependence of K-Ar age on the mineralogy of various particle size range in a shale. Geochemica et Cosmochimica Acta 27, 405-410.

Katz, B., Elmore, R.D., Cogoini, M. and Ferry, S., 1998. Widespread chemical remagnetization: orogenic fluids or burial diagenesis of clays? Geology 26, 603-606.

Kralik, M., Klima, K. and Riedmueller, G., 1987. Dating fault gouges. Nature 327, 316-317.

Kübler, B., Les argiles, indicateurs de metamorphisme. Revue de l'Institut Francais du Petrole 19, 1093-1112.1964;

Kübler, B. and Jaboyedoff, M., 2000. Illite crystallinity. Comptes Rendus de l'Academie des Sciences, Serie II. Sciences de la Terre et des Planetes 331, 75-89.

Lyons, J.B. and Snellenburg, J., 1971. Dating faults. Geological Society of America Bulletin 82, 1749-1751.

McCabe, C. and Elmore, R.D., 1989. The occurrence and origin of late Paleozoic remagnetization in the sedimentary rocks of North America. Reviews of Geophysics 27, 471-494.

Milici, R.C., 1975. Structural patterns in the southern Appalachians; evidence for a gravity slide mechanism for Alleghanian deformation. Geological Society of America Bulletin 86, 1316-1320.

Milici, R.C., 1986. West-to-east (break-back) imbrications of Alleghenian Allochthon in the southern Appalachian Plateau and Valley and Ridge. State of Tennessee Division of Geology Information Circular, 13pp.

Miller, J.D. and Kent, D.V., 1988. Regional trends in the timing of Alleghanian remagnetization in the Appalachians. Geology 16, 588-591.

Moore, D.M. and Reynolds Jr, R.C., 1997. *X-ray Diffraction and the Identification and Analysis of Clay Minerals*. Oxford University Press, New York, 400pp.

Oliver, J., 1986. Fluids expelled tectonically from orogenic belts; their role in hydrocarbon migration and other geologic phenomena. Geology 14, 99-102.

Perry, W.J., Harris, A.G. and Harris, L.D., 1979. Conodont-based reinterpretation of Bane Dome; structural reevaluation of Allegheny frontal zone. American Association of Petroleum Geologists Bulletin 63, 647-654.

Pevear, D.R., Illite age analysis, a new tool for basin thermal history analysis. In: Kharaka, Y.K. and Maest, A.S., Editors, 1992. *Proceedings of the 7th International Symposium on Water-Rock Interaction*. Balkema, Rotterdam, Netherlands, 1251-1254.

Reynolds Jr, R., 1993. WILDFIRE- A Computer Program fo the Calculation of Three-

dimensional Powder X-ray Diffraction Patterns for Mica Polytypes and their Disordered Variations. Hanover, N.H.

Reynolds Jr, R. and Reynolds III, R., 1996. NEWMOD-for-Windows. The Calculation of One-Dimensional X-ray Diffraction Patterns for Mixed-layered Clay Minerals. Hanover, N.H.

Roden, M.K., 1991. Apatite fission-track thermochronology of the southern Appalachian Basin; Maryland, West Virginia and Virginia. Journal of Geology 99, 41-53.

Schedl, A., McCabe, C., Montanez, I.P., Fullagar, P.D. and Valley, J.W., 1992. Alleghenian regional diagenesis; a response to the migration of modified metamorphic fluids derived from beneath the Blue Ridge-Piedmont thrust sheet. Journal of Geology 100, 339-352.

Secor Jr, D.T., Snoke, A.W. and Dallmeyer, R.D., 1986. Character of the Alleghanian Orogeny in the Southern Appalachians; Part III, Regional tectonic relations. Geological Society of America Bulletin 97, 1345-1353.

Solum, J.G., van der Pluijm, B.A. and Peacor, D.R., 2005. Neocrystallization, fabrics and age of clay minerals from an exposure of the Moab Fault, Utah. Journal of Structural Geology 27, 1563-1576.

Solum, J.G. and van der Pluijm, B.A., Reconstructing the Snake River-Hoback Canyon section of the Wyoming thrust belt through direct dating of clay-rich fault rocks. Sears, J.W., Harms, T.A. and Evenchick, C.A., Editors, 2007. *Whence the mountains? Inquiries into the evolution of orogenic systems; a volume in honor of Raymond A. Price.* Geological Society of America Special Paper 433, 183-196.

Środoń, J., 1980. Precise identification of illite/smectite interstratifications by X-ray powder diffraction. Clays and Clay Minerals 28, 401-411.

Steltenpohl, M.G. and Kunk, M.J., 1993. $^{40}Ar/^{39}Ar$ thermochronology and Alleghanian development of the southernmost Appalachian Piedmont, Alabama and southwest Georgia. Geological Society of America Bulletin 105, 819-833.

Steltenpohl, M.G., Goldberg, S.A., Hanley, T.B. and Kunk, M.J., 1992. Alleghanian development of the Goat Rock fault zone, southernmost Appalachians; temporal compatibility with the master decollement. Geology 20, 845-848.

Tohver, E., Weil, A.B., Solum, J.G. and Hall, C.M., 2008. Direct dating of carbonate remagnetization by $^{40}Ar/^{39}Ar$ analysis of the smecite-illite transformation. Earth and Planetary Science Letters 274, 524-530.

van der Pluijm, B.A., Hall, C.M., Vrolijk, P.J., Pevear, D.R. and Covey, M.C., 2001. The dating of shallow faults in the Earth's crust. Nature 412, 172-175.

van der Pluijm, B.A., Vrolijk, P.J., Pevear, D.R., Hall, C.M. and Solum, J., 2006. Fault dating in the Canadian Rocky Mountains; evidence for Late Cretaceous and early Eocene orogenic pulses. Geology 34, 837-840.

Warr, L.N. and Nieto, F., 1998. Crystallite thickness and defect density of phyllosilicates in low-temperature metamorphic pelites; a TEM and XRD study of clay-mineral crystallinity-index standards. The Canadian Mineralogist 36, 1453-1474.

Whisonant, R.C. and Schultz, A.P., Appalachian Valley and Ridge to Appalachian Plateau transition zone in southwestern Virginia and eastern West Virginia; structure and sedimentology. In: Neathery, T.L., Editor, 1986. *Centennial Field Guide Volume 6, Southeastern section of the Geological Society of America*. Geological Society of America, Boulder, Colorado, 113-118.

Woodward, N.B., ed., 1985. *Balanced Structure Cross Sections in the Appalachians (Pennsylvania to Alabama)*: Department of Geological Sciences, University of Tennessee, Knoxville, Studies in Geology 12, 63 p.

Woodward, N.B. and Beets, J.W., Critical evidence for Southern Appalachian Valley and Ridge thrust sequence, In: Mitra, G. and Wojtal, S.F., Editors, 1988. *Geometries and mechanism of thrusting, with special reference to the Appalachians.* Geological Society of America Special Paper 222, *165-178.*

Woodward, N.B., Walker, K.R. and Lutz, C.T., 1988. Relationships between early Paleozoic facies patterns and structural trends in the Saltville thrust family, Tennessee Valley and Ridge, Southern Appalachians. Geological Society of America Bulletin 100, 1758-1769.

York, D., 1968. Least squares fitting of a straight line with correlated errors. Earth and Planetary Science Letters 5, 320-324.

CHAPTER VI

CONCLUSION

The research presented in this dissertation provides an examination of the evolution of the southern Appalachian fold-thrust belt by integrating various kinematic and temporal approaches. Formed during the Alleghanian orogeny, the southern Appalachian fold-thrust belt displays a high degree of curvature (~55°) in the Tennessee salient. The previous absence of data constraining the nature and timing of deformation in this curved belt, as well as the kinematic development at the level of individual thrust sheets within the southern Appalachians, provided the motivation for this dissertation research. Combined paleomagnetic, anisotropy of magnetic susceptibility (AMS), radiometric and structural data produce a regional kinematic framework of the southern Appalachian foreland fold-thrust belt, primarily focusing on the Tennessee salient.

KINEMATIC EVOLUTION

The kinematic development of the southern Appalachian fold-thrust belt is examined in this dissertation at the scale of an individual structure (Chapter II) to the entire thrust wedge (Chapters III, IV and V). Both the Jones Valley thrust fault examined in Chapter II as well as the full frontal thrust wedge in the Tennessee

salient display significant gradients in displacement along strike. Such displacement gradients have been used to explain paleomagnetic rotations seen in other fold-thrust belts around the world (e.g., Allerton et al., 1993; 1998; Pueyo et al., 2004; Sussman et al., 2004).

In Chapter II, magnetic techniques were applied to the Jones Valley fault in the Alabama portion of the southern Appalachians in order to constrain the rotational history of this structure. Balanced cross-sections along the trace of the fault reveal a significant gradient in displacement (Thomas and Bayona, 2005), and predict a minimum rotation of ~15°. However, prefolding paleomagnetic directions from the hanging wall of the Jones Valley thrust do not differ from those in the footwall (Figure 2.8), indicating that rotation had not occurred on the fault. Moreover, AMS data reveal no difference in the orientation of the magnetic lineation, further supporting a lack of rotation (Figure 2.6). Instead, a self-similar model of thrusting is proposed, with differential displacement toward the foreland creating a classic bow-and-arrow fault geometry for the Jones Valley thrust. The lack of rotation found on the Jones Valley thrust fault, despite the presence of a significant displacement gradient, indicates that displacement gradients do not always involve vertical-axis rotations.

The kinematics of the entire thrust wedge of the Tennessee salient in the southern Appalachians is investigated in Chapters III, IV and V. Chapter III presents paleomagnetic data from three lithologic units to examine the origin of ~55° of curvature in the Tennessee salient. Paleomagnetic results from both redbeds of the Cambrian Rome Formation and limestones of the Ordovician Chickamauga Group

reveal a Late Paleozoic remagnetization that displays no correlation with strike (Figure 3.11). Furthermore, remagnetized directions from the Silurian Red Mountain Formation show no difference between sites from the southern limb of the salient and previous sites from the more northeasterly trending portion of the fold-thrust belt in Alabama (Figure 3.12; Perroud and Van der Voo, 1984; Chapter II). Therefore, remagnetized units preserve no evidence for rotation in the Tennessee salient, indicating that curvature in the Tennessee salient is either of primary origin or that secondary curvature occurred prior to remagnetization. Chapter IV provides a test among these options.

In Chapter IV, calcite twinning analysis was applied to limestones from both the fold-thrust belt and the undeformed foreland to further constrain the nature of curvature in the Tennessee salient. Layer-parallel paleostress orientations display a systematically-fanned distribution in both the fold-thrust belt and the "undeformed" foreland that correlates with the overall strike distribution of the belt, indicating that the curvature in the Tennessee salient is a primary feature (Figure 4.5). Furthermore, paleostress directions projected onto the frontal fold-thrust belt display a degree of fanning that exceeds the amount of curvature. When projected to the hinterland boundary, the more highly curved front of the Blue Ridge block, however, the paleostress orientations display a corresponding degree of fanning (Figure 4.7). Therefore, the curvature of the Tennessee salient, as well as the radial stress field are hypothesized to be the direct result of the shape of the rigid Blue Ridge indenter. Instead of secondary rotation, differential displacement during thrusting produced the present day geometry of the salient. This conclusion also

explains the increase in displacement and number of thrusts near the indenter's apex, and contrasts with the secondary origin of curvature in the Pennsylvania salient to the north (cf. Ong et al., 2007). Taken together, the results in Chapters III and IV reject the hypothesis that all curvature in the Appalachians is secondary.

In Chapter V, radiometric ages determined from illite-rich fault gouges in the southern Appalachian fold-thrust belt show that the entire thrust wedge was active simultaneously at approximately 278 Ma (Figure 5.7). Concurrent thrusting on faults in the hinterland (Great Smoky), the foreland (St. Clair) and in between (Copper Creek) implies that the southern Appalachian thrust wedge acted as a critically-stressed Coulomb wedge during Early Permian time. Simultaneous activity on these faults reconciles previously opposing views on the progression of thrusting in the southern Appalachians. Ages from shales in the foreland reflect local diagenetic conditions, rather than regional resetting during Alleghanian collision.

TEMPORAL EVOLUTION

Chapters III, IV and V permit a reexamination of the kinematics and timing of deformation in the southern Appalachian fold-thrust belt. Combined, the results presented in these chapters constrain the history of the southern Appalachian fold-thrust belt in Virginia, Tennessee and Georgia, from intiation to the waning stages of thrusting. Moreover, the data presented in these chapters reject the hypothesis that all deformation isPermian in age. In Chapter III, paleomagnetic data from the Chickamauga Group limestones were used to evaluate the age of magnetization

relative to deformation. A tilt-test indicates that at the time of magnetization, the beds had been tilted to about 60% of their current dip (Figure 3.4). By separating the data into subgroups, determined by site-position relative to a major structure (the Saltville thrust), the results of the tilt-test imply that more pre-magnetization folding occurred in sites toward the hinterland (70% untilting) than sites toward the foreland (30% untilting). While not statistically significant, these results suggest that the fold-thrust belt in Tennessee had developed in a forward-breaking mode, from the hinterland toward the foreland (Figure 3.9).

An approximate age for tilting was determined by comparing the mean direction of the syn-deformational magnetizations with the apparent polar wander path (APWP) of Laurentia. All directions occurred during a reversed polarity interval, and the mean paleomagnetic pole lies on the Pennsylvanian portion of the APWP (Figure 3.10), suggesting that deformation (tilting) was approximately half completed during Pennsylvanian time in the southern Appalachian fold-thrust belt.

Chapter IV presents layer-parallel paleostress orientations derived from calcite twinning analysis, complementing results of Chapter III indicating that tilting in the southern Appalachian fold-thrust belt was partially completed during the Pennsylvanian. Given that Middle to Upper Mississippian limestones recorded similar paleostress orientations as older units (Figure 4.5), it is concluded that twinning was induced during Early Pennsylvanian time. Since stress directions are thought to have been imparted by the Blue Ridge block, the Blue Ridge indenter was

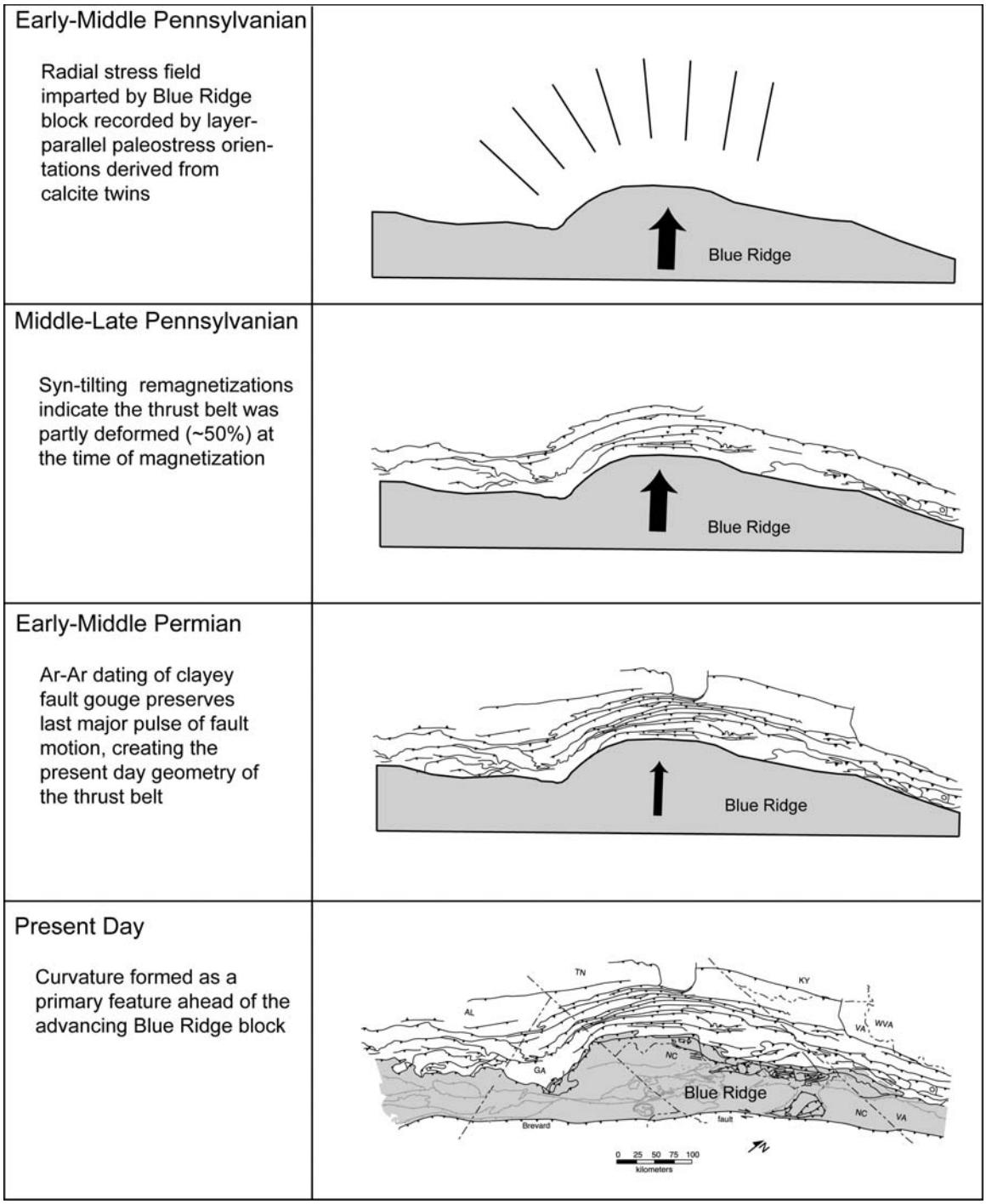

Figure 6.1: Temporal and kinematic evolution of the southern Appalachian fold-thrust belt. Map is modified from Hatcher, 2004.

advancing during the Early Pennsylvanian, a conclusion in agreement with previous radiometric estimates for the initiation of Alleghanian crystalline thrust sheets (Goldberg and Dallmeyer, 1997).

Chapter V provides radiometric ages for the final stages of deformation in the southern Appalachian fold-thrust belt. Illite $^{40}Ar/^{39}Ar$ ages were determined from gouge in three fault zones, as well as from a shale cataclasite. The age of the authigenic components from the fault rocks were derived by the Illite Age Analysis (IAA) approach, (Pevear, 1992; Grathoff, 2001; van der Pluijm et al., 2001). Clayey gouges all yield ages of ~278 Ma, while the shale cataclasite records illitization at around 354 Ma (Figure 5.7). These gouge ages indicate that the waning stages of Alleghanian deformation occurred in the southern Appalachian fold-thrust belt during Early Permian time.

SUMMARY AND BROADER IMPLICATIONS

The Appalachian fold-thrust belt was a long-lived orogen (~50 Myr) that can be viewed in terms of three general time-steps (Figure 6.1). An early, radial stress field was produced ahead of the advancing Blue Ridge indenter (the primary cause of the curvature in the Tennessee salient) during the Early to Middle Pennsylvanian. As the Blue Ridge continued to advance into the foreland, arcuate thrust faults formed ahead of the indenter, producing ~50% of the folding in the fold-thrust belt by the Middle to Late Pennsylvanian. The last stages of thrusting occurred in Early Permian time, as the entire thrust wedge of the southern Appalachians deformed into its current geometry.

Beyond the southern Appalachians, the research presented in this dissertation has a number of broader implications. The results of Chapter II suggest that, without passive markers such as paleomagnetic directions, interpreting rotations based purely on kinematic modeling is inconclusive. The data presented in Chapters III and IV offer a tectonic signature of indenter tectonics that can be applied to other fold-thrust belt settings. The results of Chapter V show that diagenetic grade, particularly crystallite thickness, is key to interpreting $^{40}Ar/^{39}Ar$ ages from encapsulated illite aliquots from higher grade diagenetic rocks, emphasizing the importance of careful clay characterization. This observation has significant consequences for future studies focusing on the timing of illitization in fault zones and sedimentary basins.

REFERENCES

Allerton, S., 1998. Geometry and kinematics of vertical axis rotations in fold and thrust belts. Tectonophysics 299, 15-30.

Allerton, S., 1998. Geometry and kinematics of vertical axis rotations in fold and thrust belts. Tectonophysics 299, 15-30.

Grathoff, G.H., Moore, D.M., Hay, R.L. and Wemmer, K., 2001. Origin of illite in the lower Paleozoic of the Illinois Basin; evidence for brine migrations. Geological Society of America Bulletin 113, 1092-1104.

Hatcher Jr, R.D., Properties of thrusts and upper bounds for the size of thrust sheets. In: McClay, K.R., Editor, 2004. *Thrust tectonics and hydrocarbon systems*. American Association of Petroleum Geologists Memoir 82, 18-29.

Ong, P.F., van der Pluijm, B.A. and Van der Voo, R., 2007. Early rotation in the Pennsylvania Salient (US Appalachians): Evidence from calcite-twinning analysis of Paleozoic carbonates. Geological Society of America Bulletin 119, 796-804.

Perroud, H. and Van der Voo, R., 1984. Secondary magnetizations from the Clinton-type iron ores of the Silurian Red Mountain Formation, Alabama., Earth and Planetary Science Letters 67, 391-399.

Pevear, D.R., Illite age analysis, a new tool for basin thermal history analysis. In: Kharaka, Y.K. and Maest, A.S., Editors, 1992. *Proceedings of the 7th International Symposium on Water-Rock Interaction*. Balkema, Rotterdam, Netherlands, 1251-1254.

Pueyo, E.L., Pocovi, A., Millán, H., and Sussman, A.J., Map-view models for correcting and calculating shortening estimates in rotated thrust fronts using paleomagnetic data. In: Weil, A.B. and Sussman, A.J., Editors, 2004. *Orogenic curvature; Integrating paleomagnetic and structural analyses.* Geological Society of America Special Paper 383, 57-71.

Sussman, A.J., Butler, R.F., Dinares-Turell, J. and Verges, J., 2004. Vertical-axis rotation of a foreland fold and implications for orogenic curvature: an example from the Southern Pyrenees, Spain. Earth and Planetary Science Letters 218, 435-449.

Thomas, W.A. and Bayona, G., 2005. The Appalachian thrust belt in Alabama and Georgia: Thrust-belt structure, basement structure, and palinspastic reconstruction. Geological Survey of Alabama Monograph 16, 48pp.

van der Pluijm, B.A., Hall, C.M., Vrolijk, P.J., Pevear, D.R. and Covey, M.C., 2001. The dating of shallow faults in the Earth's crust. Nature 412, 172-175.

APPENDICES

APPENDIX A

PRIMARY CURVATURE IN THE MID-CONTINENT RIFT: PALEOMAGNETISM OF THE PORTAGE LAKE VOLCANICS (NORTHERN MICHIGAN, USA)

ABSTRACT

Rocks of the North American Mid-Continent Rift (MCR) in the Keweenaw Peninsula of northern Michigan display a change in structural trend from east to west, varying in strike from 100° in the east to 35° farther west, before returning to a more east-west trend of 80° near Wisconsin. In general, curvature can be described either as of primary origin, meaning that the arc developed in its present curved state, or as of secondary origin, when the arc formed from an initially straighter geometry. A powerful tool in evaluating the origin and degree of curvature in any deformed belt is paleomagnetism, where coincident change in declination and strike is evidence for secondary curvature. Several paleomagnetic studies have been completed on rift-related sedimentary rocks, as well as lava flows, from the MCR in the Lake Superior region. Paleomagnetic directions for the sedimentary rocks vary much more in declination than in inclination, possibly reflecting a vertical axis rotation. If secondary rotation has affected the sedimentary rocks, then underlying volcanic rocks should also demonstrate a similar rotation.

Thirty-one sites were collected from the Portage Lake Volcanics in the most highly curved part of the Keweenaw Peninsula in the Upper Peninsula of Michigan. Sites were chosen to maximize the variation in structural trend. Thermal demagnetization results showed two components in samples from most sites, a lower temperature A component (<580°C) as well as a higher temperature B component (>580°C). Both components were tested for primary remanence using a conglomerate test. The A component, carried by magnetite, passes the conglomerate test at a 95% confidence level, and is therefore considered a primary remanence. The B component, carried by hematite, fails at the 95% level and is considered a secondary magnetization. Most importantly, declination of the primary (A) magnetization between sites shows no correlation with strike, demonstrating that vertical axis rotations cannot explain the curvature of the Mid-Continent Rift. We conclude that curvature in the Lake Superior Region is a primary feature, likely reflecting a pre-existing zone of weakness that was exploited during rifting.

INTRODUCTION

Curvature in mountain belts has been a topic of research for at least one hundred years (Hobbs, 1914) and became progressively more studied since Carey's (1955) introduction of the orocline concept. An orocline was originally defined as a belt with an initially straight geometry that subsequently was deformed into a curved feature (Marshak, 2004). However, the term orocline has also been used for "primary" curved features; that is, arcuate belts that initially formed with a curved

geometry. With the inception of plate tectonics, the process by which these arcuate belts form has become increasingly central to the understanding of the kinematic development of deformation belts.

A powerful tool for examining bending of an orogenic belt is paleomagnetism (e.g., Eldredge et al, 1985; Weil et al., 2001). By identifying vertical-axis rotations in a curved belt, it is possible to determine whether, and in some cases when, bending has occurred. A perfectly coincident variation in both paleomagnetic declination and strike of the belt indicates secondary curvature, whereas the absence of any correlation between the two datasets implies primary curvature. Past paleomagnetic investigations of oroclinal bending have primarily focused on thin-skinned fold-and-thrust belts, such as the Apennines (Gattacceca and Speranza, 2002), the Appalachians (Stamatakos and Hirt, 1994) and the Sevier fold-thrust belt (Grubbs and Van der Voo, 1976; Schwartz and Van der Voo, 1984), which all have demonstrated some degree of oroclinal bending. However, vertical axis rotations in thick-skinned belts, defined as regions where the entire crust may be involved, have remained less understood (e.g., Levashova et al, 2003; Johnston, 2004).

The Mid-Continent Rift (MCR) is a dominant feature in potential fields of central North America (Ocola and Meyer, 1973; Figure A.1a). The rift signature extends 2000 km from the Grenville front in southeast Michigan into Lake Superior and its features eventually terminate in Kansas (Hinze et al., 1997). Rocks of the rift are mostly obscured by Phanerozoic cover except in the Lake Superior region, where a thick (~30 km) sequence of mafic lava flows and associated rift rocks are found. The MCR is unique among continental rifts in that modern analogs, such as

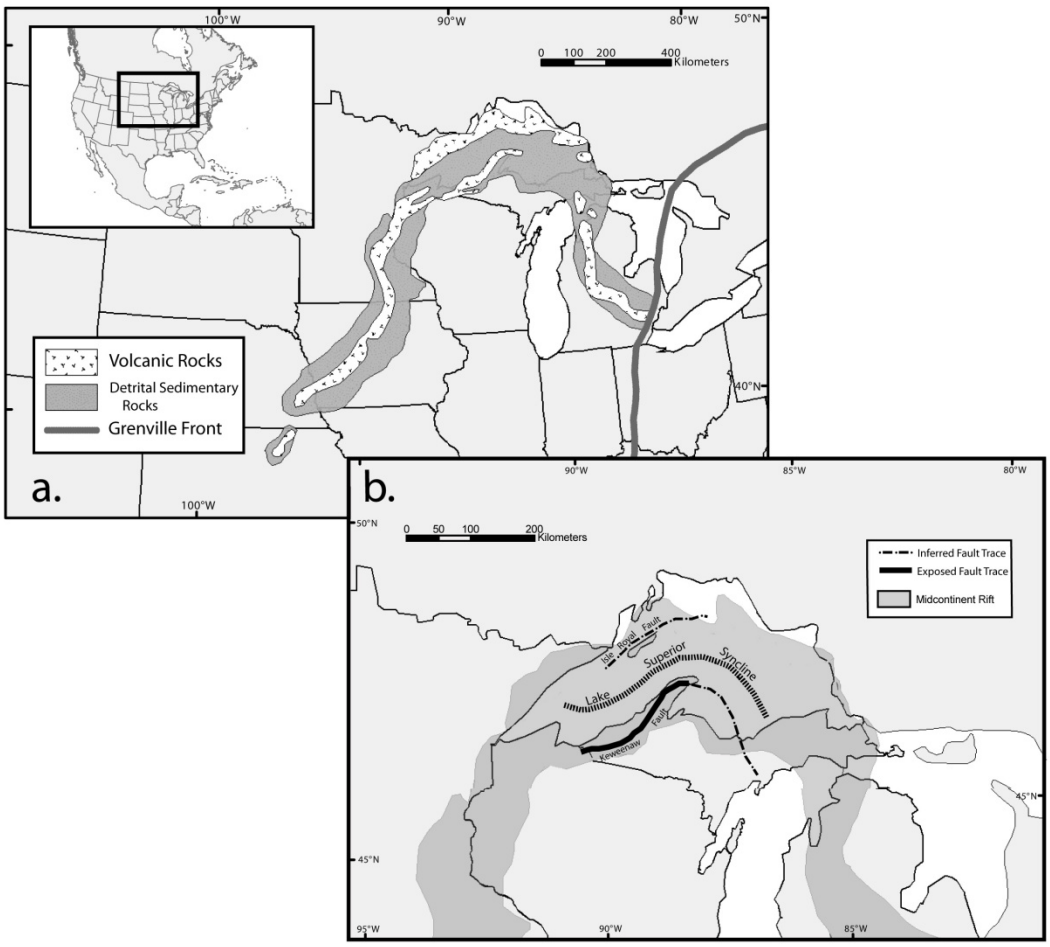

Figure A.1: (a) Outline of the North American Mid-Continent Rift as determined by geophysical methods. Redrawn from Ojakangas, 2001. (b) Curvature of rift related structures in the Lake Superior Region. Modified from Hinze et al, 1997.

the East African Rift or the European Rhine Graben, show no curved segments. The MCR has experienced rift inversion during the post-rifting compressional events of the Grenville orogeny (Cannon, 1994). This shortening of the rift involved thrusting along rift bounding faults and folding in the area. These rift structures show a large degree of curvature in the Lake Superior region (Figure A.1b). The rift related rocks cropping out on the Keweenaw Peninsula vary in structural trend from 100° on the eastern tip of the peninsula to 35° farther west, while returning to a more east-west strike of about 80° in westernmost Michigan and Wisconsin. The curvature in the rift was examined through paleomagnetic investigation of the Portage Lake Volcanics along this section of the Keweenaw Peninsula to evaluate whether all or some of the curvature can be explained through relative vertical axis rotation.

Fault inversion analysis of minor reverse faults of the MCR (Witthuhn-Rolf, 1997) and calcite-twinning analysis of calcite cemented amygdules in basalts and sedimentary rocks (Craddock et al., 1997) shows multiple paleostress directions that were attributed to rift closure. These varying stress directions may be associated with oroclinal bending of the structure, leading to rotation of at least parts of the MCR during rift closure. Previous work has documented that rift-bounding faults in northwestern Lake Superior region may have significant amounts of oblique-slip motion and possible associated counterclockwise rotation of the crust (Witthuhn-Rolf, 1997). This may offer a solution to rotating parts of the MCR if similar structures could be identified elsewhere along the rift margin beneath the Phanerozoic sedimentary cover. This could allow secondary development of at least

some of the curvature without disturbing much of the surrounding pre-MCR structures, which do not display any significant curvature.

Further incentive for studying curvature in the Lake Superior region comes from comparing various paleomagnetic studies of the rift-related sediments. The apparent polar wander path (APWP) for Laurentia for ~1110 Ma through ~1000 Ma is defined using rocks of the MCR. Paleomagnetic data from sedimentary rocks from the western part of the rift in Wisconsin and Minnesota vary much more in declination than in inclination compared to those in Michigan, perhaps indicating a relative rotation between the two areas (Weil et al., 1998). By investigating the volcanic rocks underlying the sedimentary sequences at sites with varying structural trend, it is possible to test whether oroclinal bending of the MCR has occurred in the Lake Superior Region during post-rift deformation. Whereas other curvilinear inverted rift structures are absent elsewhere in the world, intracratonic rotation has been previously observed. Recent paleomagnetic investigation of the Biscotasing dike swarm in Ontario, Canada has revealed that vertical axis rotation of "stable" cratonic elements has occurred in the Canadian shield, despite a lack of obvious structural features that support rotation (Halls and Davis, 2004).

This study thus intends to test whether secondary curvature can be documented in the Mid-Continent Rift. Secondary rotation of the rift sequence would have major implications for intracratonic tectonism, as it requires rotation within a "stable" continental block, presumably involving a large section of the lithosphere.

REGIONAL GEOLOGY

The Portage Lake Volcanics (PLV) represent a series of approximately 200 lava flows that were extruded during the main stage rifting (Li and Beske-Diehl, 1993). Along the Keweenaw Peninsula, the PLV are primarily comprised of tholeiitic flood basalts with minor interbedded conglomerates. The Copper City Flow, near the base of the exposed volcanic pile, has been dated at 1096.2 +/- 1.8 Ma, whereas the Greenstone Flow, located near the top, was dated at 1094 +/- 1.5 Ma using U-Pb analyses on zircons and baddeleyite (Davis and Paces, 1990). Livnat (1983) noted that the PLV experienced primarily prehnite – pumpellyite metamorphism and that maximum temperatures only reached 300^{o}C, which is well below the Curie temperature of most magnetization carriers.

Overlying the PLV is the Copper Harbor Conglomerate, a clast-dominated conglomerate with interbedded lava flows, known as the Lake Shore Traps, near the base of the unit, which represent the last stages of rifting (Ojakangas et al., 2001). The Copper Harbor Conglomerate is conformably overlain by the Nonesuch Shale, which has been assigned a minimum depositional age of 1047 +/- 35 Ma from Rb-Sr dating of petroleum inclusions (Ruiz et al., 1984). Conformably overlying the Nonesuch Shale is the Freda Sandstone. The Copper Harbor Conglomerate, the Nonesuch Shale and the Freda Sandstone are all part of the Oronto Group. The Jacobsville Sandstone, lying above the Freda, is a slightly arkosic sandstone that is included in the Bayfield Group. The Jacobsville is separated from the rest of the rift fill by the Keweenaw fault, a reverse fault that juxtaposes the PLV over the younger

Figure A.2: Geologic map of rift-related rocks in the Upper Peninsula of Michigan showing paleomagnetic sites. Units are shown in stratigraphic order.

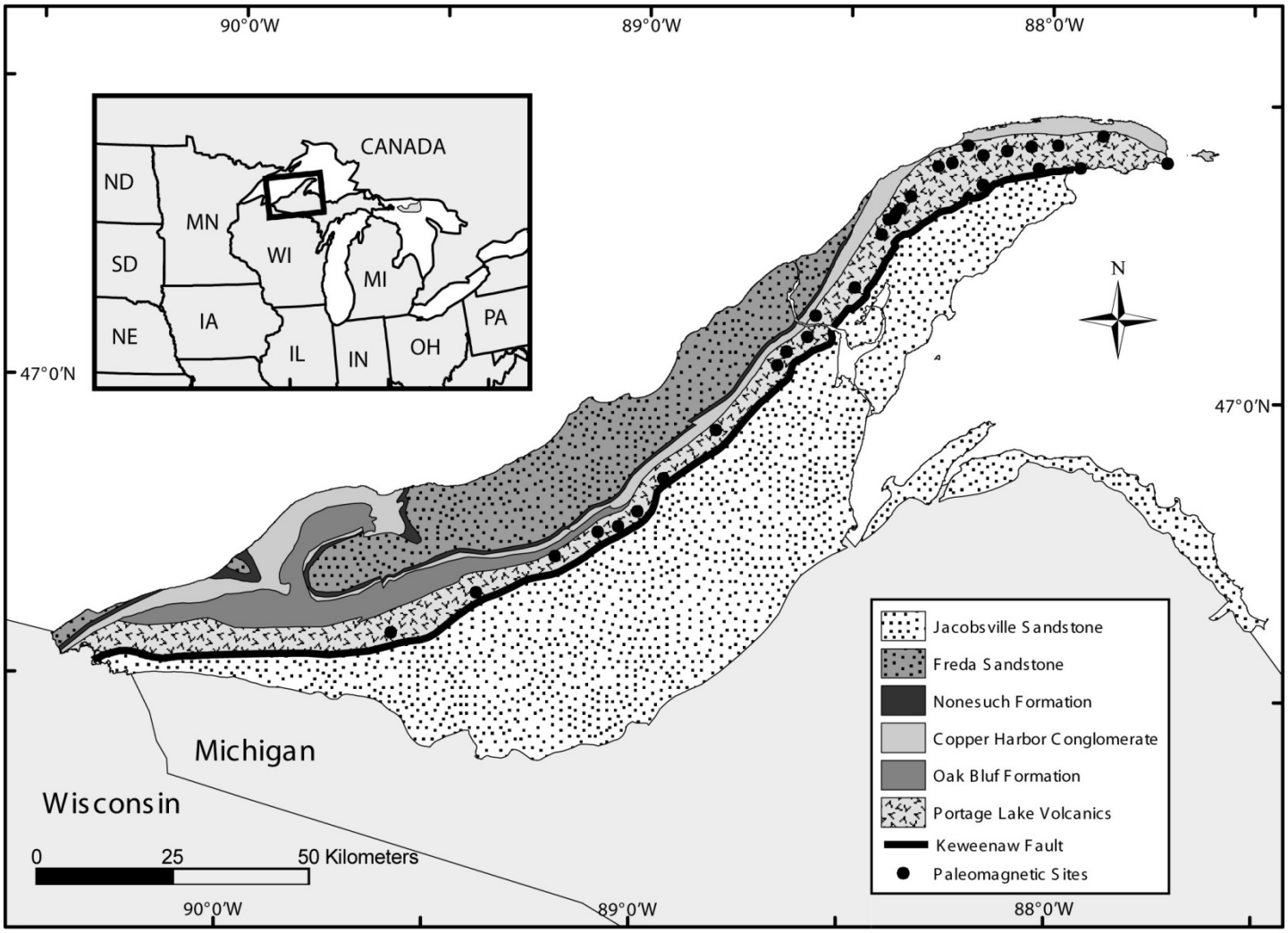
90°0′W
89°0′W
88°0′W
47°0′N
CANADA
ND
MN
SD
WI
MI
NE
IA
IL
IN
OH
PA
N
Michigan
Wisconsin
0
25
50 Kilometers
Jacobsville Sandstone
Freda Sandstone
Nonesuch Formation
Copper Harbor Conglomerate
Oak Bluf Formation
Portage Lake Volcanics
Keweenaw Fault
Paleomagnetic Sites

Jacobsville Sandstone. The Keweenaw fault originated as a rift-related normal fault that was subsequently inverted due to Grenvillian shortening (Cannon, 1994).

The Jacobsville sandstone has been correlated to several units in Wisconsin and eastern Minnesota, including the Fond du Lac Formation, as well as the Middle River and Eileen sections of the Orienta Sandstone. It is for these deposits that the discrepancy in paleomagnetic direction is found. Data obtained by Roy and Robertson (1978) for the Jacobsville Sandstone and by Watts (1981) for the Fond du Lac formation and Orienta sandstone vary much more in declination than in inclination, with some amount of vertical-axis rotation of the MCR perhaps being one hypothesis for the distribution of the declination data.

SAMPLING AND METHODS

Samples were taken from thirty-one sites in the Portage Lake Volcanics along the Keweenaw Peninsula to test for oroclinal bending using paleomagnetic declinations as a marker (Figure A.2). Two additional sites were sampled in intercalated volcanic conglomerate deposits. Sites were chosen to maximize variation in structural trend and each site is located within a single flow. Between six and ten, 2.5cm diameter cores were collected from each site using a portable gasoline-powered drill. Where drilling was complicated, oriented hand samples were collected for coring in the laboratory. Both cores and hand samples were oriented with a magnetic compass at all sites and, when possible, checked with a sun compass. Bedding attitude determinations of the flows were obtained using the orientation of flow tops. Prior to analysis, the samples were cut into 2.5 X 2.2cm

cylindrical specimens at the University of Michigan's Paleomagnetic Laboratory. The natural remanence magnetization (NRM) was measured and then subsequently stepwise thermally demagnetized in a magnetically shielded, low-field room using an Analytical Service Co. (ASC) thermal demagnetizer and measured using a three-axes cryogenic 2G Enterprises Model 755 Superconducting rock magnetometer. Stepwise demagnetization was used over a range of 100°C to 680°C until the specimen's intensity was less than 2% of the NRM.

Remanence directions were calculated using principal component analysis (Kirschvink, 1980) of linear vectors selected from orthogonal projection demagnetization plots (Zijderveld, 1967) with the SuperIAPD software package (Torsvik et al, 1999). Individual sample directions were used to determine site means using Fisher's (1953) method. Watson's (1956) test for randomness in the cobbles of intercalated conglomerate beds was performed to establish the relative age of magnetization.

RESULTS

Direction of Magnetization

NRM intensities of the PLV ranged from 20 to 9000 mA/m. Stepwise thermal demagnetization revealed two components in the PLV, a lower laboratory unblocking temperature (T_{lab}) "A" component and a higher T_{lab} "B" component. Specimen demagnetization trajectories are generally well behaved and tend to display either two components or the appearance of a single component during demagnetization, with the latter being either high or low laboratory unblocking

temperature (Figure A.3). The general direction of both magnetization components tend to be similar, being west-northwest and down after structural correction and varying by only a few degrees.

The lower T_{lab} "A" component was identified in twenty-eight of thirty-one sites. This component decayed progressively during demagnetization up to 580°C. Magnetite is considered the carrier of the magnetization component, based on its laboratory unblocking temperature. The higher T_{lab} "B" component was isolated in twenty-one of the thirty-one sites and tended to remain stable up to anywhere between 610°C and 660°C, where intensity would then rapidly decay towards the origin, indicating hematite as the carrier of magnetization.

Site 9 shows a magnetization that proved to be irresolvable. In situ sample directions were highly scattered, with orientations distributed throughout the southeast and northwest quadrants. This site is located near the base of the exposed section of the Portage Lake Volcanics, dated at ~1096.2 Ma. A paleomagnetic reversal has been previously recognized between 1096.2 Ma to 1097.6 Ma in the Osler Group in eastern Lake Superior (Davis and Paces, 1990). Specimens displayed directions that may be the result of this reversal; however, it is impossible to tell from one site.

Site means for the A component display a Fisherian distribution in situ (Figure A.4a), but structural correction enhances this distribution by decreasing the scatter and gives a corrected mean of D = 291.2°, I = 31.3°, $\alpha 95$ = 5.6° and k = 24.51 (Figure A.4b; Table A.1). This mean direction agrees with previous paleomagnetic

Figure A.3: Representative thermal demagnetization plots of the Portage Lake Volcanics in geographic coordinates and associated intensity plots. Intensity plots show normalized intensity versus temperature in degrees Celsius. In the demagnetization plots, closed (open) symbols represent vector endpoints plotted in the horizontal (vertical) plane. Temperature steps are in degrees Celsius. (a) Plot illustrating the B component carried by hematite. Ticks represent 10 mA/m. (b) Plot that was typical of most samples, showing two components. Note the similarity in the two components. Ticks represent 100 mA/m. (c) Plot of a specimen displaying only the A component carried by magnetite. Ticks represent 100 mA/m.

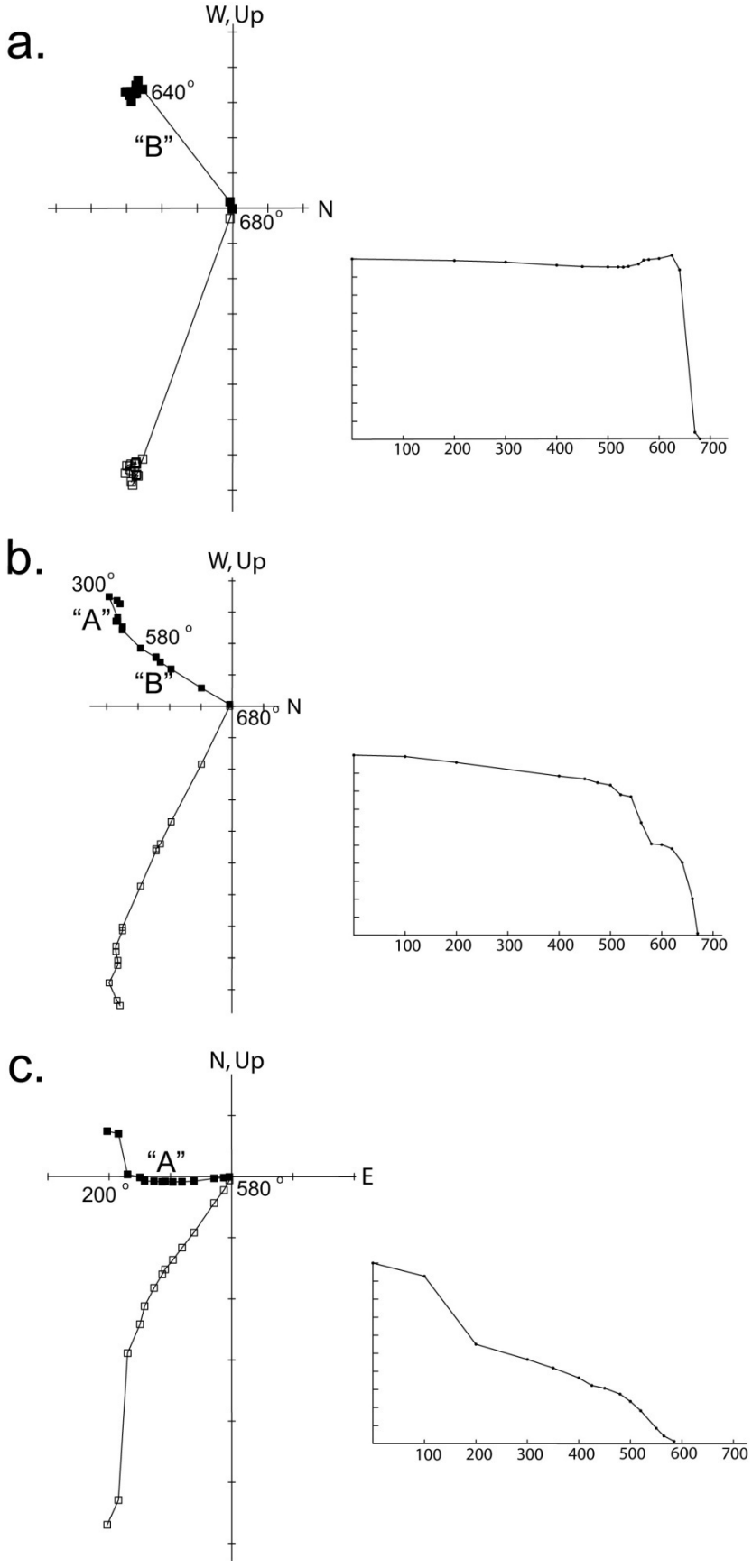
a.
W, Up
640°
"B"
680°
N
100 200 300 400 500 600 700
b.
W, Up
300°
"A"
580°
"B"
680°
N
100 200 300 400 500 600 700
c.
N, Up
"A"
200°
580°
E
100 200 300 400 500 600 700

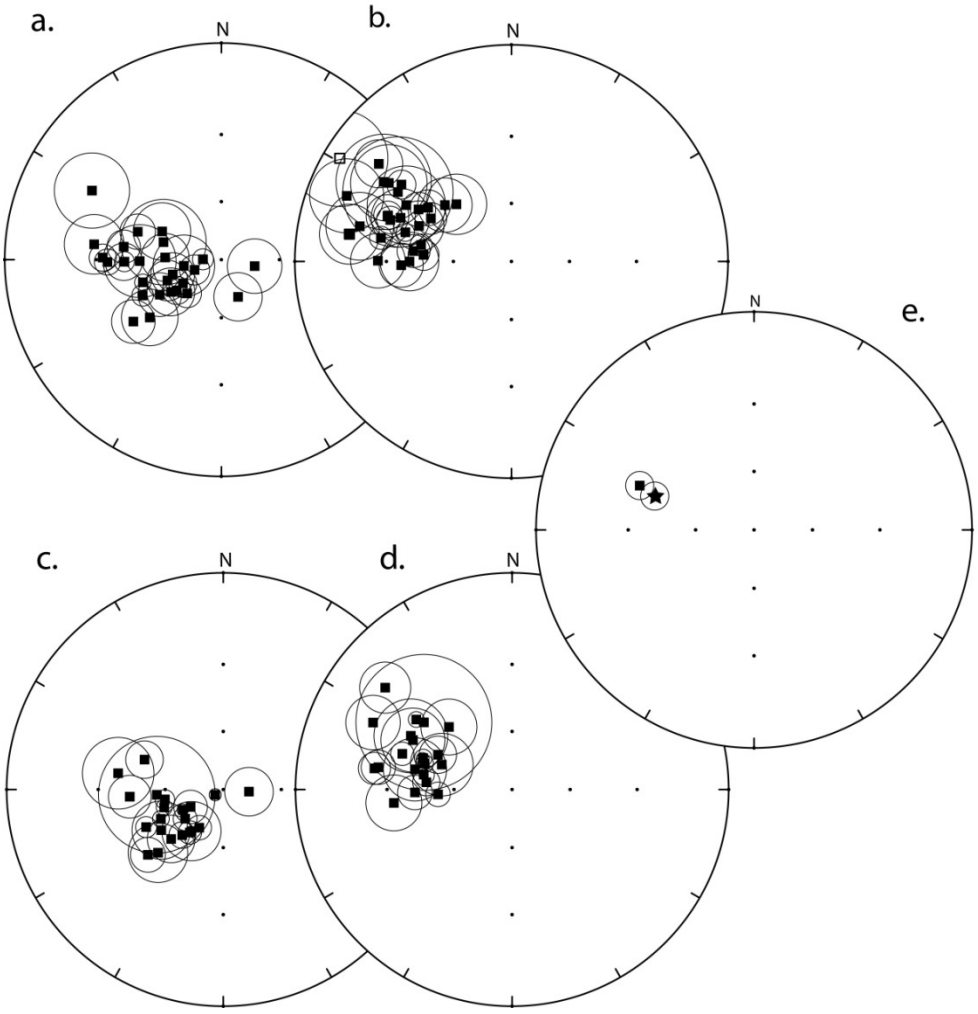

Figure A.4: (a,b) Lower hemisphere equal-angle projections showing distribution of site means and associated confidence circles for the A component both in situ (a) and tilt-corrected (b). This component, carried by magnetite, gives a mean direction of D = 291.2˚, I = 31.3˚, α95 = 5.2˚. (c,d) Lower hemisphere equal-angle projections showing distribution of site means and associated confidence circles for the B component both in situ (a) and tilt-corrected (b). This component, carried by hematite, gives a mean direction of D = 288.8˚, I = 38.6˚, α95 = 6.0˚. (e)Lower hemisphere equal-angle projection showing the orientations of the magnetization carried by magnetite and hematite. The square represents the magnetite component and the star represents the hematite component.

Table A.1: Paleomagnetic results from the Portage Lake Volcanics. A and B components are discussed in the text. Mean directions are calculated from site means (Fisher, 1953); N/N_o, number of samples (sites) accepted/studied; Dec, declination; Inc, inclination; α95, radius of confidence circle in degrees; R, the resultant vector; k, precision parameter (Fisher, 1953). α95 of the mean after (before) structural correction is 5.6° (7.9°) for the A component and 6.0° (7.5°) for the B component. The precision parameter, *k*, of the mean after (before) structural correction for the A component is 24.51 (12.29) and 29.22 (18.93) for the B component.

Site Number	Latitude	Longitude	Strike	Dip	Component	N/No	Dec In Situ/Corr	Inc In Situ/Corr
PL01	47.28	-88.41	232	43	A	8/10	249.2/302.8	74.9/40.8
PL02	47.30	-88.40	224	33	A	8/8	272.3/291.5	60.9/32.3
PL03	47.31	-88.38	226	31	A	8/9	235.5/274.3	61.9/45.7
					B	8/9	217.8/266.3	61.8/52.2
PL04	47.31	-88.38	218	42	A	7/8	240.4/270.3	53.8/26.7
					B	8/8	226.5/263.5	53.3/32.5
PL05	47.32	-88.38	228	45	A	6/8	260.7/298.2	70.1/32.3
PL06	47.32	-88.37	223	35	A	7/7	295.5/302.6	56.3/22.2
PL07	47.43	-88.21	252	41	A	6/7	288.5/306.4	45.7/15.5
					B	6/7	290.8/308.8	47.5/16.2
PL08	47.19	-88.48	220	41	A	7/8	225.4/276.0	65.0/41.1
					B	7/8	212.2/274.8	66.5/46.7
PL09	47.40	-87.93	274	71	Inconsistent	0/7	-	-
PL10	47.39	-88.03			B	5/7	225.9/296.5	44.5/35.8
PL11	47.34	-88.34	235	35	A	5/6	253.1/291.0	63.6/40.9
					B	5/6	241.9/295.1	71.6/48.6
PL12	47.14	-88.58	215	56	A	5/7	100.9/316.2	72.2/49.8
					B	5/7	94.8/314.7	76.4/45.4
PL13	47.39	-88.27	245	41	A	7/8	231.1/270.0	44.0/39.6
					B	8/8	236.8/281.7	52.2/40.8
PL14	47.43	-87.98	269	32	A	9/10	268.8/288.9	34.5/28.8
PL15	47.42	-88.10	259	33	A	8/8	245.6/280.3	46.5/44.0
					B	8/8	244.0/279.6	46.8/45.1
PL16	47.40	-88.28	233	22	A	8/8	268.8/280.2	41.8/27.0
PL17	47.37	-88.16	242	42	A	7/7	238.3/298.1	66.4/44.3
					B	5/7	217.4/289.5	62.8/52.0
PL18	47.08	-88.64	230	59	Conglomerate	-	-	-
PL19	47.08	-88.64	225	61	A	8/10	237.5/283.1	59.1/18.6
					B	9/10	222.0/279.4	58.4/25.9
PL20	47.43	-88.04	255	33	A	7/7	268.8/290.1	41.5/27.3
PL21	47.41	-88.18	250	35	A	7/7	253.9/285.4	48.7/36.1
					B	7/7	244.8/286.5	54.7/44.3
PL22	47.41	-87.71	281	26	A	5/6	277.6/299.2	41.1/37.6
					B	4/6	278.8/286.9	37.7/37.7
PL23	47.45	-87.87	272	33	A	9/9	271.0/290.5	32.6/27.4
PL24	47.11	-88.58	222	56	A	10/10	271.2/304.9	80.3/26.5
					B	9/10	236.9/306.2	84.9/32.5
PL25	47.06	-88.66	229	64	A	7/8	155.7/310.3	68.7/46.1
PL26	46.93	-88.83	215	55	A	7/8	248.9/279.6	60.1/15.6
					B	8/8	232.6/278.7	65.0/24.5
PL27	46.86	-88.94	231	69	Conglomerate	-	-	-
PL28	46.81	-89.00			B	9/9	243.4/288.8	66.4/42.9
PL29	46.78	-89.05	230	35	A	4/10	286.8/301.5	58.8/26.9
					B	10	260.3/288.0	59.4/33.9
PL30	46.77	-89.10	245	32	A	7/8	298.1/301.0	21.8/-4.5
					B	8/8	253.1/289.5	58.2/43.0
PL31	46.70	-89.23	250	42	A	7/8	234.9/268.0	37.2/36.0
					B	7/8	229.1/268.3	40.6/41.7
PL32	46.66	-89.39	255	51	A	4/8	269.0/301.9	48.7/20.4
					B	7/8	265.6/295.7	43.2/19.1
PL33	46.59	-89.59	261	42	A	7/10	276.9/291.7	28.8/11.4
					B	4/10	265.5/307.3	55.8/35.8
Mean	-	-	-	-	A	28/31	260.6/291.2	56.7/31.3
					B	21/31	243.6/288.8	60.4/38.6

studies of the PLV (Books, 1972; Halls and Pesonen, 1982; Browning and Beske-Diehl, 1987). Similarly, the B component also has a low dispersion both before (Figure A.4c) and after structural correction (Figure A.4d). The corrected mean for the hematite-carried component is D = 288.8°, I = 38.6 °, $\alpha 95$ = 6.0° and k = 29.22 (Figure A.4d; Table A.1).

The similarity between magnetite and hematite-carried components indicate that these magnetizations were acquired within a relatively short time span of each other (Figure A.4e). The higher T_{lab} B component direction agrees with a similar high temperature component found in the PLV by previous workers (Browning and Beske-Diehl, 1987; Li and Beske-Diehl, 1993).

Age of Magnetization

Samples from fourteen cobbles from two sites were collected from intraformational conglomerates to test the age of magnetization using Watson's (1956) test for randomness. As basaltic cobbles were sporadic and too small for sampling, rhyolitic cobbles were sampled. The source of these cobbles is inferred to be of Keweenawan affinity but has not yet been identified (Ojakangas, 2001). As with the Portage Lake samples, specimens from the cobbles were subjected to stepwise thermal demagnetization. The two components identified in the mafic flows were also defined in the rhyolite cobbles.

Thirteen cobbles displayed the lower temperature A component. The critical value of the resultant vector (R) for thirteen directions is 5.75 at the 95% confidence level (Table A.2). This A component has an R -value of 4.92, less than the critical value, indicating a random distribution of directions at the 95% confidence

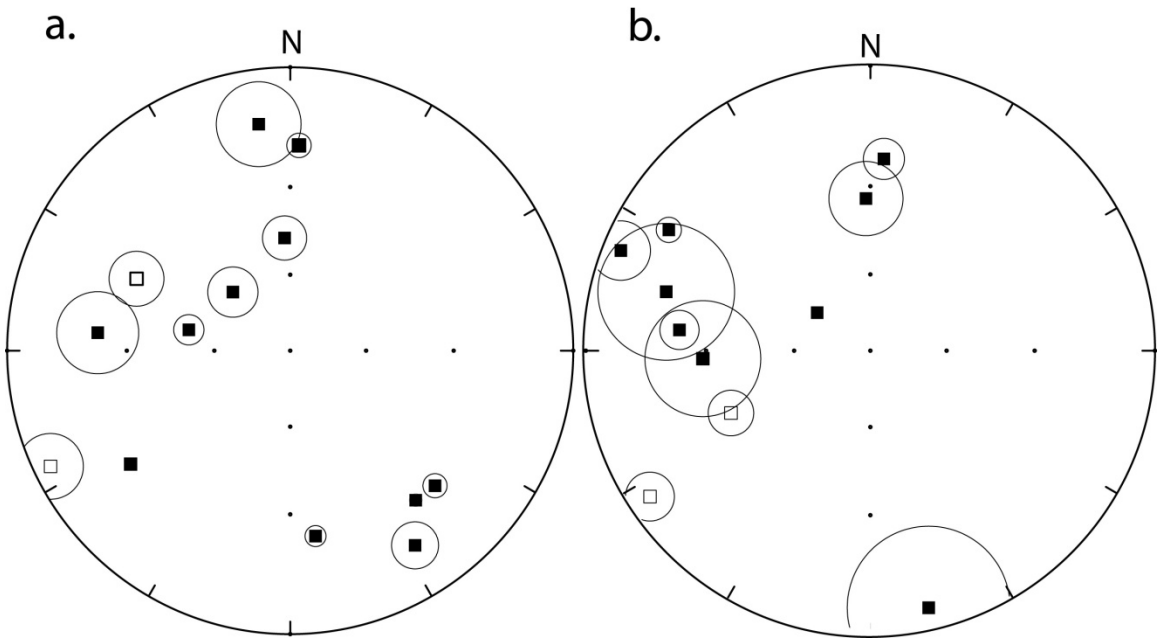

Figure A.5: Equal-angle projections of conglomerate samples for the A component (a) and the B component (b); full (open) symbols are projections onto the lower (upper) hemisphere. Confidence cones show specimens' maximum angular deviations (MAD's). Directions are in tilt-corrected coordinates and are also given in Table A.2.

Cobble	A component Declination	Inclination	α95	B component Declination	Inclination	α95
PL18-A	147.3	11.5	5.7	300.9	10.9	3.0
PL18-B	352.1	12.2	10.3	-	-	-
PL18-C	281.6	49.8	5.4	-	-	-
PL18-D	272.1	21.7	6.4	276.2	22.0	5.4
PL18-E	2.4	18.1	3.2	4.0	22.0	5.7
PL18-F	284.1	-40.3	4.1	291.8	3.2	6.3
PL27-A	133.0	20.1	3.3	286.1	16.5	17.3
PL27-B	172.2	23.1	3.0	167.2	4.5	17.2
PL27-C	315.6	57.7	9.4	358.3	33.8	11.5
PL27-D	-	-	-	305.5	64.1	1.8
PL27-E	234.7	20.7	1.0	267.3	29.0	17.0
PL27-F	244.3	-3.5	7.0	236.5	-4.3	5.3
PL27-G	357.1	46.6	7.7	245.9	-33.6	7.1
PL27-H	139.9	20.9	1.8	-	-	-
	R = 4.92			R = 6.86		

Table A.2: Paleomagnetic results from interbedded conglomerate samples. Notation as in Table A.1. Resultant vector given for the two components is a result of the mean direction from the 13 (11) samples for the A (B) component.

level (Watson, 1956) (Figure A.5a). Therefore, the A component passes the conglomerate test and indicates a primary magnetization for the component carried by magnetite. The B component was defined in eleven cobbles and, unlike the A component, has an R-value of 6.86 (Figure A.5b; Table A.2), higher than the required 5.29 at the 95% for eleven directions to be random (Watson, 1956). This component also has a dominant west-northwest and down orientation, which is similar in direction to the characteristic magnetization of the Portage Lake Volcanics. The B component, consequently, can be considered a secondary magnetization carried by hematite. The B component is different from secondary components identified in the overlying Copper Harbor Conglomerate, where the remagnetized component has an orientation similar to that of much younger rift-related sedimentary rocks (Palmer et al, 1981; Halls and Palmer, 1981).

DISCUSSION

The twenty-eight sites that displayed the A component, carried by magnetite, were used to test for the presence of oroclinal bending (or secondary rotation) in the Mid-Continent Rift. Because the B component is a secondary magnetization, it is omitted from further analysis for this study. Eldredge et al. (1985) proposed a method to test for oroclinal rotation by evaluating changes in declination as a function of observed deviations in strike for each site. This method was used in this study to assess the possibility of rotation in the Keweenawan rocks. Both strike and declination were normalized to a reference strike and declination (S_o and D_o, respectively), so that the best-fit line to the data passes through the origin. The

slope of the best-fit line is an indication of the magnitude of oroclinal bending a curved belt has experienced, with a slope of 0.0 representing no rotation and a slope of 1.0 indicating an originally straight belt that has been subsequently bent.

The resulting plot (Figure A.6a) shows a poor correlation between differential strike and differential declination. The best-fit line has a slope of essentially zero (0.004), although the data show high residuals to the trendline. Because the data are from volcanic rocks, which acquire their magnetization relatively quickly, and our sites each come from a singular basalt flow, the individual site-means do not represent a time-averaged direction of geomagnetic field. Therefore, the observed high degree of scatter in declination can be at least partly attributed to secular variation of the geomagnetic field during the eruption of the basalts. This has been demonstrated in recent basalts in areas with multiple flows (Herrero-Bervera and Valet, 1999). In order to diminish the effects of secular variation, we chose to bin the data into five-degree intervals of strike values. The declination values within each bin were then used to calculate a mean declination for that five-degree interval and thus average out Mesoproterozoic secular variation. Each mean was then weighted to minimize effects of varying numbers of data points contained within the bins. The resulting trendline is similar to the raw data pattern, showing a slope of essentially zero, and thus no correlation between strike and declination (Figure A.6b). Unlike the unbinned data, the declination data residuals are significantly less, resulting in a better fit to the trendline. The near zero slope and the lack of correlation lead to the clear conclusion that vertical-axis rotations have not affected the mafic flows of the MCR along the Keweenaw Peninsula and,

Figure A.6: (a) Declination deviations from a reference declination of $D_o = 292°$ for all site means plotted against strike variations from a reference strike of $S_o = 240°$. Data are presented so that the "best fit" line plotted for these data passes through the origin. Each site is contained within a single flow. (b) To minimize variations in declination, data are binned into 5-degree strike bins and a weighted best fit line is produced. As in (a), $D_o = 292°$ and $S_o = 240°$.

a.

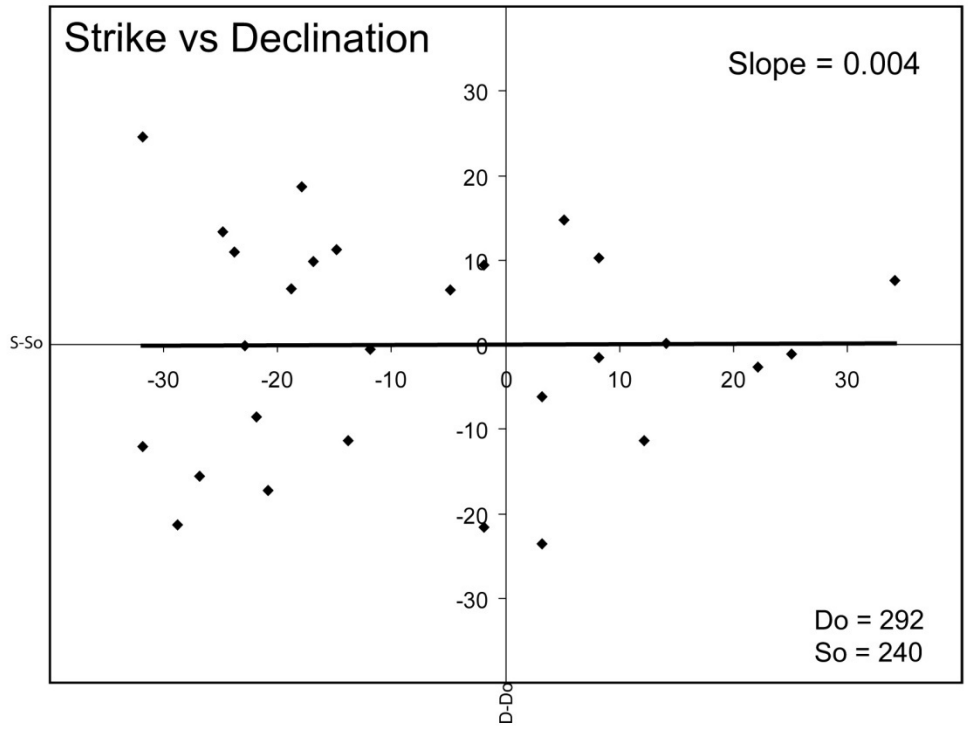
Strike vs Declination
Slope = 0.004
30
20
10
0
-10
-20
-30
S-So
-30
-20
-10
0
10
20
30
Do = 292
So = 240
D-Do

b.

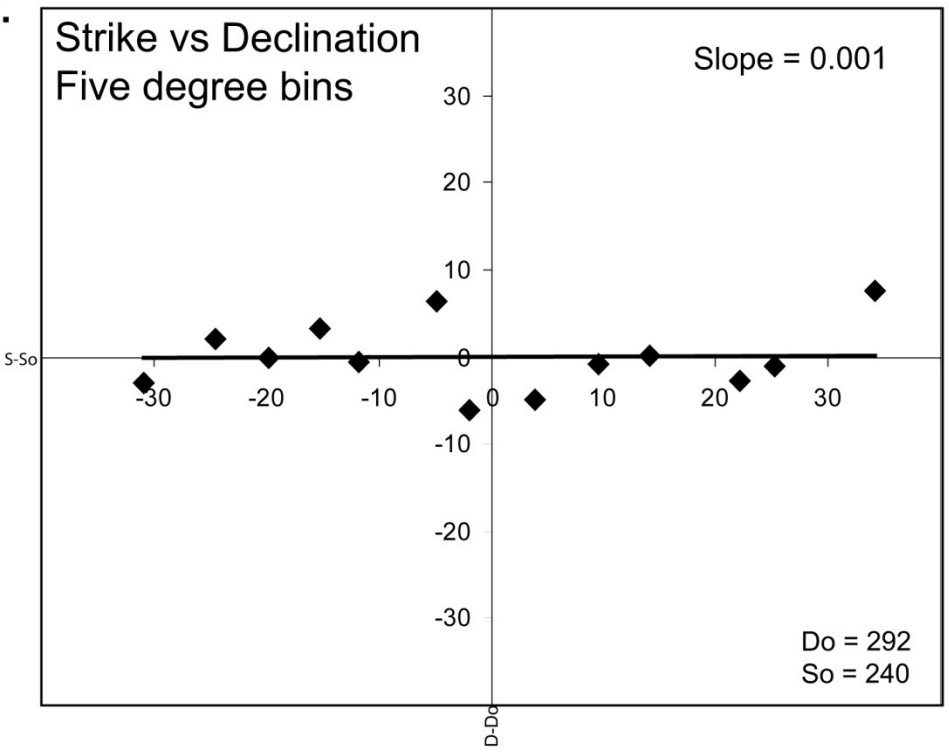
Strike vs Declination
Five degree bins
Slope = 0.001
30
20
10
0
-10
-20
-30
S-So
-30
-20
-10
0
10
20
30
Do = 292
So = 240
D-Do

thus, that the curvature of the belt is a primary feature.

Because secondary rotation does not explain the considerable strike variation of the MCR, other sources of curvature have to be considered. Most likely, a preexisting non-linear crustal feature may have been utilized by the MCR. For example, the MCR in the Lake Superior region has been proposed as being a failed triple junction initiated by a mantle plume (Hinze et al., 1972; Burke and Dewey, 1973; Green, 1983; Cannon and Hinze, 1992), with two of the limbs being the main rift segments and the third arm being an extensive suite of dike swarms extending northward from Lake Superior, known as the Nipigon arm (Cannon and Hinze, 1992). However, the triple-junction hypothesis does not sufficiently explain the gradual strike variation of the MCR. Klasner et al. (1982) suggested that the development of the rift in its present geometry is related to a large gravity low in central Wisconsin. This low has been recognized as the expression of the Wolf River Batholith, a large, late Mid-Proterozoic "anorogenic" granitic pluton that may have diverted rift development around its perimeter. Another possible origin for the curvature is the existence of Penokean (~1.85 Ga) crustal fault zones that are roughly parallel to the MCR. The Great Lakes Tectonic Zone (GLTZ) and the Murray fault strike approximately the same as the southwestern and southeastern arms of the rift, respectively (Riller et al., 1999) and zones of Penokean suturing directly adjacent to the rift have been identified in Minnesota (Wunderman, 1988). These planar zones of weakness could have facilitated arcuate development of the Mid-Continent Rift. It is more likely, however, that the arcuate zone of weakness directly responsible for the curvature in the MCR has not been identified or was destroyed

during the 25%+ crustal thinning that took place prior to basalt emplacement (Cannon et al., 1989). The most probable scenario is that both arcuate Penokean detachment zones and large, "anorogenic" plutons constrained the MCR to its current curved geometry. During rift inversion in the western Lake Superior region, rift bounding normal faults reversed their sense of motion to accommodate Grenville shortening; however, in eastern Lake Superior, east-west trending thrusts cut across the eastern limb of the MCR (Manson and Halls, 1997). Since inversion in western Lake Superior occurs without any rotation, we can speculate that during post-rift shortening, compression axes responsible for rift inversion must have been sub-parallel to the tension axes that initially formed the rift.

It follows that the variations in declination observed in earlier studies of the late Keweenawan sedimentary rocks (Watts, 1981) cannot be attributed to rotation of the crust. Instead, we speculate that this variation may be due to the poor age constraints of Precambrian sedimentary rocks and therefore apparent polar wander or to errors associated with structural corrections applied to these rocks.

Regardless of the origin, a pre-defined curved zone of crustal weakness is responsible for the arcuate nature of the MCR in the Lake Superior region, rather than secondary rotation. Thus, map-view curvature can form without significant rotations. In many of the world's other arcuate orogenic belts, at least part of the observed curvature can be explained by secondary rotation of the limbs. However, as shown in this study of Mid-Continent Rift volcanic rocks, secondary rotation is not characteristic of all curvature.

CONCLUSION

Paleomagnetism of mafic flows of the Portage Lake Volcanics of northern Michigan has revealed two remanence components during stepwise thermal demagnetization. The lower temperature component, carried by magnetite, passes the test of randomness on interbedded rhyolite conglomerate clasts and is interpreted to be a primary magnetization. The higher temperature component, carried by hematite, does not show a random distribution of directions, indicating a secondary magnetization. We used the primary component to assess the possibility of oroclinal bending of the Mid-Continent Rift in the Lake Superior Region. The ensemble of declination data shows considerable scatter along the trend of the Mid-Continent Rift. When analyzed using five-degree strike bins to account for secular variation of the paleomagnetic field during the eruption of the flows, the analysis shows no correlation between strike and declination, which leads to the conclusion that no oroclinal bending has occurred in the Mid-Continent Rift. Therefore, the rift's curvature is primary and must be explained by a pre-defined zone of weakness exploited by the rifting process. Post-rift shortening in the area involved rift inversion without resulting in significant rotation.

ACKNOWLEDGEMENTS

We would like to thank John Geissman and an anonymous reviewer for their helpful comments and suggestions. Our research of curved belts is supported by a grant from the American Chemical Society-Petroleum Research Fund (37505-AC2), a Grant In Aid of Research from Sigma Xi, The Scientific Research Society, the Scott

Turner Fund of the University of Michigan and partial support from the National Science Foundation (EAR 0207257).

REFERENCES

Books, K.G., 1972. Paleomagnetism of some Lake Superior Keweenawan rocks. USGS Professional Paper 760.

Browning, T.D. and Beske-Diehl, S.J., 1987. Paleomagnetism and the age of copper mineralization in the Portage Lake Volcanics, upper Peninsula, Michigan. Can. J. Earth Sci 24, 2396-2404.

Burke, K. and Dewey, J.F., 1973. Plume generated triple junctions: Key indicators in applying plate tectonics to old rocks. J. of Geol. 81, 406-433.

Cannon, W.F., 1994. Closing of the Mid-Continent rift – A far-field effect of Grenvillian compression. Geology 22, 155-158.

Cannon, W.F., Green, A.G., Hutchinson, D.R., Lee, M., Milkereit, B., Behrent, J.C., Halls, H.C., Green, J.C., Dickas, A.B., Morey, G.B., Sutcliffe, R. and Spencer, C., 1989. The North American Mid-Continent rift beneath Lake Superior from GLIMPCE seismic reflection profiling. Tectonics 8, 305-332.

Cannon, W.F., and Hinze, W.J., 1992. Speculations on the origin of the North American Mid-Continent Rift. Tectonophysics 213, 49-55.

Carey, S.W., 1955. The orocline concept in geotectonics. Proc. R. Soc. Tasmania 89, 255-289.

Craddock, J.P., Pearson, A., McGovern, M., Kropf, E., Moshoian, A., and Donnelly, K., 1997. Post-extension shortening strains preserved in calcites of the Mid-Continent Rift, In: Ojakangas, R.W., Dickas, A.B. and Green, J.C., Editors, 1997. Middle Proterozoic to Cambrian Rifting, Central North America. Geol. Soc. Am. Spec. Pap. 312, 115-126.

Davis, D.C. and Paces, J.B., 1990. Time resolution of geologic events on the Keweenaw Peninsula and implications for development of the Mid-Continent Rift System. Earth Plan. Sci. Lett. 97, 54–64.

Eldredge, S.V., Bachtadse, V., Van der Voo, R., 1985. Paleomagnetism and the orocline hypothesis. Tectonophysics, 119,153-179.

Fisher, R.A., 1953. Dispersion on a sphere. Proc. R. Soc. Lond., A **217,** 295–305.

Gattacceca, J. and Speranza, F., 2002. Paleomagnetism of Jurassic to Miocene sediments from the Apenninic carbonate platform (southern Apennines, Italy): evidence for a 60° counterclockwise Miocene rotation. Earth Plan. Sci. Lett. **201**, 19–34.

Green, J.C., 1983. Geologic and geochemical evidence for the nature and development of the Middle Proterozoic (Keweenawan) Mid-Continent Rift of North America. Tectonophysics 94, 413-437.

Grubbs, K.L. and Van der Voo, R., 1976. Structural deformation of the Idaho—Wyoming overthrust belt, as determined by Triassic paleomagnetism. Tectonophysics **33**, 321–336.

Halls, H.C. and Davis, D.W., 2004. Paleomagnetism and U-Pb geochronology of the 2.17 Ga Biscotasing dyke swarm, Ontario, Canada: evidence for vertical-axis crustal rotation across the Kapuskasing Zone. Can. J. of Earth Sci. 41, 255-269.

Halls, H.C. and Palmer, H.C., 1981. Remagnetization in Keweenawan rocks. Part II: lava flows within the Copper Harbor Conglomerate, Michigan. Can. J. of Earth Sci. 18, 1395-1408.

Halls, H.C. and Pesonen, L.J., 1982. Paleomagnetism of Keweenawan rocks. In: Wold, R.J. and Hinze, W.J., eds., Geology and Tectonics of the Lake Superior Basin. Geol. Soc. Am. Memoir 156, 173-201.

Herrero-Bervera, E. and Valet, J.P., 1999. Paleosecular variation during sequential geomagnetic reversals from Hawaii. Earth Planet. Sci. Lett. **171, 1**39–148.

Hinze, W.J., Roy, R.F., and Davidson, D.M., Jr., 1972. The origin of late Precambrian rifts (abs). Geol. Soc. of Am. Abstr. Prog. 4, 723.

Hinze, W.J., Allen, D.J., Braile, L.W., and Mariano, J, 1997. The Mid-Continent Rift System: a major Proterozoic continental rift. In: Ojakangas, R.W., Dickas, A.B. and Green, J.C., Editors, 1997. Middle Proterozoic to Cambrian Rifting, Central North America. Geol. Soc. Am. Spec. Pap. 312, 7–36.

Hobbs, W.H., 1914. Mechanics of formation of arcuate mountain belts. J. Geol., 22, 72-90.

Johnston, S.T., 2004. The New Caledonia-D'Entrecasteaux orocline and its role in clockwise rotation of the Vanuatu-New Hebrides Arc and formation of the North Fiji Basin. In: Sussman, A. and Weil, A.B., eds., Orogenic curvature; integrating paleomagnetic and structural analyses. Geol. Soc. Am. Spec. Pap. 383, 225-236.

Kirschvink, J.L., 1980. The least-square line and plane and the analysis of palaeomagnetic data. Geophys. J. R. Astron. Soc. **62**, 699–718

Klasner, J.S., Cannon, W.F. and Van Schmus, W.R., 1982. The pre-

Keweenawan tectonic history of southern Canadian Shield and its influence on formation of the Mid-Continent Rift. In: Wold, R.J. and Hinze, W.J., Editors, 1982. Geology and Tectonics of the Lake Superior Basin. Geol. Soc. Am. Mem. 156, 27–46.

Levashova, N.M., Degtyarev, K.E., Bazhenov, M.L., Collins, A.Q. and Van der Voo, R., 2003. Middle Paleozoic paleomagnetism of east Kazakhstan: post-Middle Devonian rotations in a large-scale orocline in the central Ural–Mongol belt. Tectonophysics 377, 249–268.

Li, H. and Beske-Diehl, S., 1993. Low-temperature metamorphism and secondary components in the Portage Lake Volcanics: a reassessment. Can. J. of Earth Sci. 30, 1404-1414.

Livnat, A., 1983. Metamorphism and copper mineralization of the Portage Lake Lava Series, northern Michigan. Ph.D. dissertation, University of Michigan, Ann Arbor.

Manson, M.L., and Halls, H.C., 1997. Proterozoic reactivation of the southern Superior Province and its role in the evolution of the Mid-Continent rift. Can. J. of Earth Sci. 34, 562-575.

Marshak, S., 2004. Salients, recesses, arcs, oroclines, and syntaxes – A review of ideas concerning the formation of map-view curves in fold-thrust belts. in K.R. McClay, ed, Thrust tectonics and hydrocarbon systems. AAPG Memoir 82, 131-156.

Ocola, L.C. and Meyer, R.P., 1973. Central North American rift system, 1. Structure of the axial zone from seismic and gravimetric data. J. of Geophys. Res. 78, 5173-5194.

Ojakangas, R.W., Morey, G.B. and Green, J.C., 2001. The Mesoproterozoic Mid-Continent Rift System, Lake Superior region, USA. Sediment. Geol. **141–142**, 421-442.

Palmer, H.C., Halls, H.C. and Pesonen, L.J., 1981. Remagnetization in Keweenawan rocks. Part I: conglomerates. Can. J. of Earth Sci., 18, 599-618.

Riller, U., Schwerdtner, W.M., Halls, H.C. and Card, K.D., 1999. Transpressive tectonism in the eastern Penokean orogen, Canada: consequences for Proterozoic crustal kinematics and continental fragmentation. Precambr. Res. 93, 51–70.

Roy, J.L. and Robertson, W.A., 1978. Paleomagnetism of the Jacobsville Formation and the apparent polar path for the interval 1100–670 m.y. for North America. J. Geophys. Res. **83**, 1289–1304.

Ruiz, J., Jones, L.M. and Kelly, W.C., 1984. Rubidium–strontium dating of ore deposits hosted by Rb-rich rocks, using calcite and other common Sr-bearing minerals. Geology **12**, 259–262

Schwartz, S.Y. and Van der Voo, R., 1984. Paleomagnetic study of thrust sheet rotation during foreland impingement in the Wyoming-Idaho overthrust belt. Geophys. Res. **89**, 10077–10086.

Stamatakos, J. and Hirt, A.M., 1994. Paleomagnetic considerations of the development of the Pennsylvania Salient in the central Appalachians. Tectonophysics 231, 237-255.

Torsvik, T., Briden, J.C., and Smethurst, M.A., 1999. SuperIAPD1999 – Software Package. Geol. Surv. of Norway, Trondheim.

Van Schmus, W.R., Green, J.C. and Halls, H.C., 1982. Geochronology of Keweenawan rocks of the Lake Superior region: A summary. In: Wold, R.J. and Hinze, W.J., eds., Geology and tectonics of the Lake Superior Basin. Geol. Soc. Am. Mem. 156, 165-171.

Watson, G.S., 1956. A test for randomness. Mon. Not. Roy. Astr. Soc., 7, 160-161.

Watts, D.R., 1981. Paleomagnetism of the Fond du Lac Formation and the Eileen and Middle River sections with implications for Keweenawan tectonics and the Grenville problem. Can. J. Earth Sci. **18**, pp. 829–841

Weil, A.B., Van der Voo, R., MacNiocaill, C. and Meert, J.G., 1998. The Proterozoic supercontinent Rodinia: paleomagnetically derived reconstructions for 1100 to 800 Ma. Earth Plan. Sci. Let.. 154, 13-24.

Weil, A.B., Van der Voo, R., van der Pluijm, B.A., 2001. Oroclinal bending and evidence against the Pangea megashear; the Cantabria-Asturias Arc (northern Spain). Geology 29, 991-994.

Witthuhn-Rolf, K.M., 1997. A structural analysis of the Mid-Continent Rift in Michigan and Minnesota. In: Ojakangas, R.W., Dickas, A.B. and Green, J.C., Editors, 997. Middle Proterozoic to Cambrian Rifting, Central North America. Geol. Soc. Am. Spec. Pap. 312, 97-114.

Wunderman, R.L., 1988. Crustal structure across the exposed axis of the Mid-Continent Rift and adjacent flanks, based on magnetotelluric data, central Minnesota-Wisconsin; a case for crustal inhomogeneity and possible reactivation tectonics. PhD Dissertation, Michigan Technological University, Houghton, MI.

Zijderveld, J.D.A., 1967. AC demagnetization of rocks: analysis of results. In: D.W. Collinson and K.M. Creer, Editors, Methods in Paleomagnetism. Elsevier, Amsterdam, 254–286.

APPENDIX B

PROCEDURE FOR CALCITE TWINNING ANALYSIS

INTRODUCTION

This manual is intended to help the reader through the process of measuring, analyzing and interpreting calcite twins. Along with my own contributions, it represents the combined effort of previous researchers John Harris, John Kollmeier and Philip Ong. Each researcher has previously commented on procedures for calcite twinning analysis (CTA) in their Master's theses. While much of their discussion on theory has been omitted, many of their comments regarding measurement have been directly incorporated and edited to produce a single coherent document.

SAMPLE COLLECTION AND PREPARATION

The small sample size required for calcite twinning strain analysis allows for collection of oriented samples using a gasoline powered corer equipped with a 2.5 cm diameter drill (Figure B.1). This method eliminates accuracy error that can be induced while cutting larger hand samples, although in some instances, hand samples are preferable. Furthermore, the drilling method is advantageous for field sampling because limestone is relatively soft and requires minimal water to be

carried when drilling. Before drilling the sample on a flat and non-weathered outcrop section, the area should be pre-marked so that if the sample breaks off in the core shaft the sample position relative to the outcrop can be determined. This can be done by drilling a small amount, and then continuing the core adjacent to the circle you just created. After the core has been oriented and removed, mark the long or z-axis.

Figure B.1: Left: Drilling a sample for calcite twinning analysis. Right: Oriented hand sample.

Groshong (1974) found that two mutually perpendicular thin sections allow an accurate and precise measurement (+/- 8°) of the principal strain (stress) axes. Optimal orientations for the thin sections to be cut are perpendicular to the transport direction in the vertical plane and parallel to the transport direction in the horizontal plane. If only one thin section is to be analyzed, try to make the cut as close to parallel to bedding as possible. Care should be taken to take into account all rotations of the data from collection in the field to microscope analysis. Namely, this involves: 1) taking the care to polish sample cores as near to orthogonal to the core

as possible, so as produce a thin section exactly perpendicular to the core; and 2) measuring any discrepancy between alignment of the core trend direction and the long axis of the slide in order to correct for it later through data rotation.

Thin sections should be cut and ground to a thickness of 30 μm or thinner. In thinner sections it is easier to 'see' the twin planes, especially when they are inclined at a high angle to the slide. However, if the section is too thin (<15 μm), increased birefringence makes the optical determination of the c-axis more difficult. Don't worry too much about polishing because the slide will be coated with oil during the analysis. Before performing the analysis, coat the thin-section with Alizarin Red S straining solution (1 g Alizarin Red S to 1000 ml distilled water and 2 ml concentrated HCl). After the stain is dry, the calcite will become red while any (renegade) dolomite will remain unstained.

Depending on the aim of the calcite twinning analysis, sample location within a structure is very important. To recover an original (primary) twinning event (commonly oriented layer parallel), or to recover an overprinting as recorded regionally within the limestone strata, some considerations should be made. First, highly deformed or sheared areas should be avoided, as should fold hinges due to potential anisotropy in stresses transmitted through a thrust-ramp hinge (Kilsdonk and Wiltschko, 1988). Also, whenever possible, sample limestone beds that are the thickest (most massive) grainstone or packstone when available. Calcite veins commonly record conditions of stress specific to the formation of that vein. It is important then, to distinguish between the vein and host rock before measuring any twin sets or even beginning sampling.

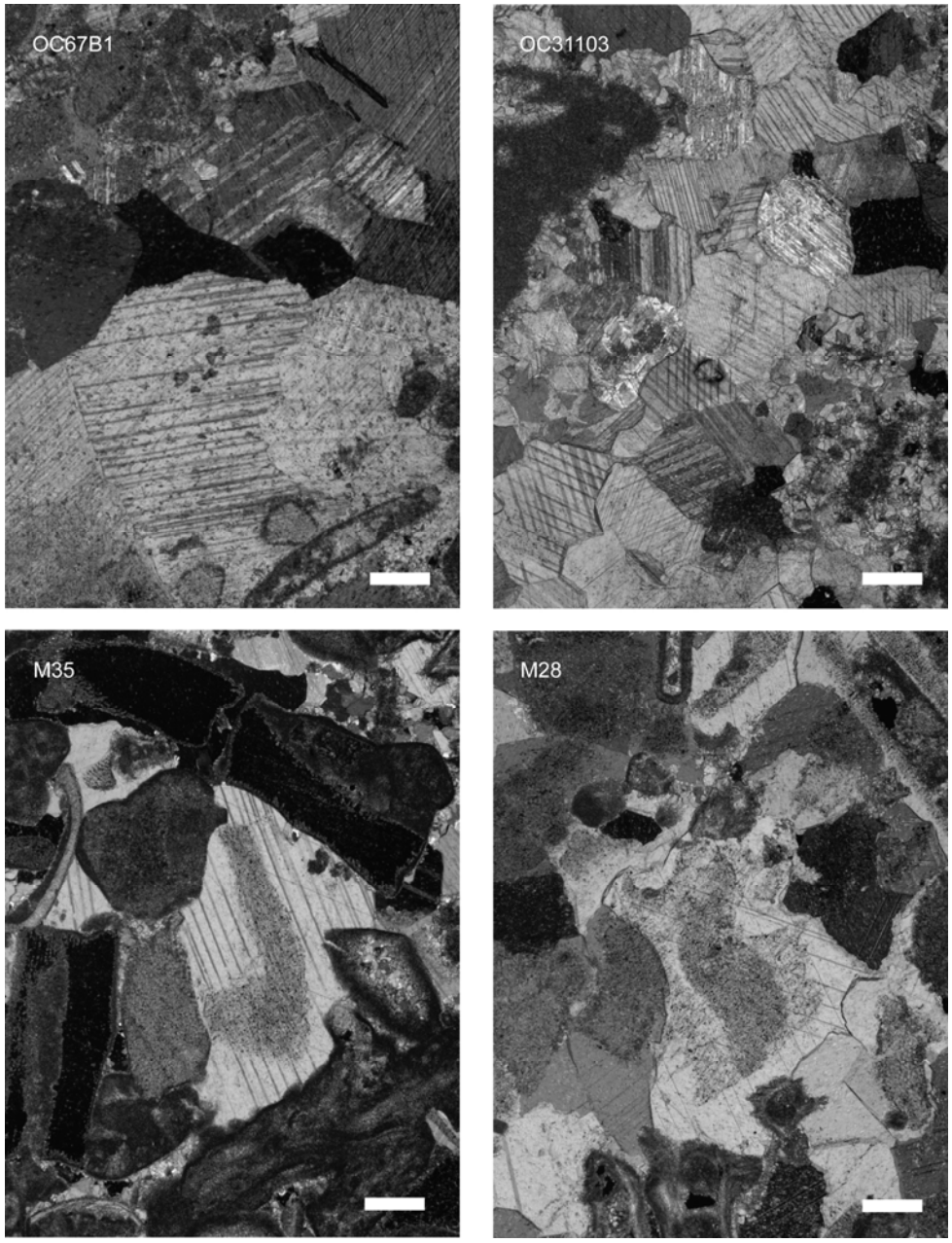

Figure B.2: Photomicrographs of calcite twins. Scale bar is 200 μm

OPTICAL DETERMINATION OF THE C-AXIS POLE TO THE E-PLANE OF CALCITE

Pole to *e*-twin Plane:

Before any measurement, the microscope should be cleaned and checked that all parts are in alignment, particularly the two polarizers and any of the many graduated mounts of the universal stage. Any misalignment will cause a systematic error in the data collection. Set up and adjust the universal stage. A thorough description of this lengthy procedure may be found in Turner and Weiss (1963; p.197). Use refraction oil *(n=1.536)* and orient the slide on the universal stage, so the long axis of the slide trends NS. Try not to use too much of the refraction oil, as it seemingly causes damage to the top-tray polarizer. The notch denoting the side of the sample you want to orient should be pointed toward you, facing the zero degree mark. Always use the guide sledge, which is set in the groove of the upper hemisphere mount, to maintain the NS orientation of the long axis. Using this, the thin-section will be free to move EW along the lower arm of the sledge, while the sledge and thin section may be moved NS in unison.

Locate a calcite grain large enough for analysis (>120 μm) that shows well defined twins and sharp extinction angles; do not attempt to analyze grains with undulatory extinction. If the twins appear bent, try to avoid measuring it and move on to another grain. If, however, it is necessary to include bent twins, make sure to analyze the innermost straightest segment of the twin (Figure B.2).

1. Align the universal stage so that all axes are at zero.
2. Rotate around the A_1 axis until the twins are parallel to *EW* (A_4 rotation axis).

3. Tilt on the A_4 axis until the twin-planes are rotated vertically and parallel to the *EW* axis. In this orientation the twins will appear to be thinnest, because the twins are vertical, and the viewer will be looking down the "true dip" of the twins. As this angle is changed the twins are rotated out of vertical, and the twins, oblique to the vertical axis, appear thicker because the viewer sees the "apparent dip."
4. Measure the strike of the twin planes on the A_1. Measure the dip of the twin planes on the A_4 axis.
5. Using the Excel sheet described further in this manual, record the directions for the twin planes.

Figure B.3: Universal-stage microscope.

Twin plane measurements contain three inputs into the Excel sheet; Strike (0°-359°), dip (0°-90°; although realistically only up to 55°) and direction (1 dipping away from you; 3 if dipping toward you; Figure B.4).

Determination of the c-axis

1. Rotate the grain about A_1 (innermost) vertical axis until maximum extinction is reached.
2. Tilt the slide on the A_2 (NS oriented) horizontal axis. If the grain remains at maximum extinction, the correct A_1 orientation was chosen. If the grain illuminates when tilted, set A_2 back to zero and rotate A_1 until it becomes extinct again. Remember there will be two positions at 180° that will show extinction on A1, but only one that will maintain the extinction upon tilt along A_2.
3. Tilt A_4 (EW oriented) horizontal axis about 30°. The grain will show some illumination.
4. Maintain the tilt performed in step 3 (about 30°). Achieve the maximum extinction by tilting A_2. The optic axis is not oriented either EW parallel to A_4, or parallel to the vertical axis of the scope. The extinction will be maintained as A_4 is tilted.
5. Return A_4 to zero and rotate the microscope stage. If the grain remains extinct, the c-axis is oriented vertically. If the grain illuminates, the c-axis is parallel to A_4.
6. Measure the angle from A_1, which is the bearing of the c-axis. Measure the angle from A_2, which is the plunge of the c-axis. If the slide is dipping to the left side of the U-stage, the corresponding plunge direction would be “4”, whereas if the

slide and stage are dipping to the right, the plunge direction is "2." Figure B.4 shows the relationship between universal-stage coordinates and the numeric directions required as input for the calcite twinning strain computer program.

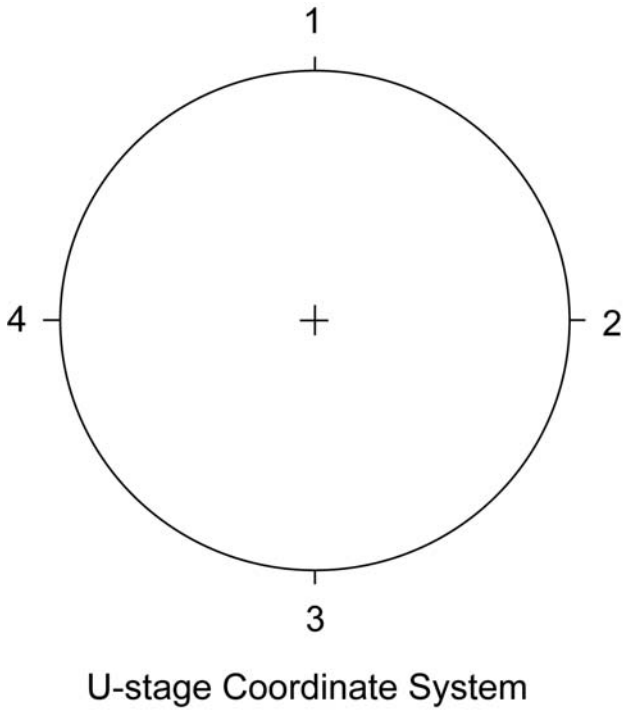

Figure B.4: Schematic detailing the relationship between U-stage coordinates and coordinates for Strain99 program.

When measuring the c-axis, the correct extinction angle for a calcite grain is almost always the one in which the twin lamellae make an acute (small) angle with the optical vertical. If more than one twin set exists in the grain, then the optical vertical will lie somewhere within the acute angle between the two twin sets at the proper extinction. Developing a consistent method utilizing this fact can save many hours of scope-work.

It is important to check the randomness of c-axis orientations within a sample. An intrinsic fabric in c-axes may impart any inhomogeneity that will affect

the validity of the data. Calcite veins with twins that are contemporaneous with crystal growth will have c-axis aligned with the direction of maximum extension.

Excel Program for Calcite Twinning

An Excel program has been created for data input to be used as the worker measures (Figure B.5) and replaces the outdated "C-Plunge" DOS program described in previous installments of this manual. The simplicity of it allows future workers to alter it to fit their needs. The program contains a worksheet titled "Input" where each measurement is recorded. To use this program, input the strike, dip and direction for each e-twin, as well as the trend for the c-axis. Two options for the plunge of the c-axis will be given. Check each on the microscope and choose the correct plunge. Input the number of twins, average twin thickness and grain thickness, as well as the number of twinsets, X-Y coordinates of the grain within the thin section and any notes that the user feels are relevant.

Many of the other sheets contained in the program are for calculation of the c-axes plunge and conversion from U-stage coordinates to sample coordinates. The "Evans" tab allows the user to convert the recorded data into the proper format for the Strain99 program.

Measurement #	Location X	Location Y	Epole Bearing	Epole plunge	Epole Direction (1 or 3)	C Bearing	plunge 1	plunge1 dir	plunge 2	plunge 2 dir	C plunge	C Direction (2 or 4)
1	68.6	7.8	300	8	3	42	15.4028	2	31.7555	4	15.4028	2
2							#DIV/0!	#DIV/0!	#DIV/0!	#DIV/0!		
3							#DIV/0!	#DIV/0!	#DIV/0!	#DIV/0!		
4							#DIV/0!	#DIV/0!	#DIV/0!	#DIV/0!		
5							#DIV/0!	#DIV/0!	#DIV/0!	#DIV/0!		
6							#DIV/0!	#DIV/0!	#DIV/0!	#DIV/0!		
7							#DIV/0!	#DIV/0!	#DIV/0!	#DIV/0!		
8							#DIV/0!	#DIV/0!	#DIV/0!	#DIV/0!		
9							#DIV/0!	#DIV/0!	#DIV/0!	#DIV/0!		
10							#DIV/0!	#DIV/0!	#DIV/0!	#DIV/0!		
11							#DIV/0!	#DIV/0!	#DIV/0!	#DIV/0!		
12							#DIV/0!	#DIV/0!	#DIV/0!	#DIV/0!		
13							#DIV/0!	#DIV/0!	#DIV/0!	#DIV/0!		
14							#DIV/0!	#DIV/0!	#DIV/0!	#DIV/0!		
15							#DIV/0!	#DIV/0!	#DIV/0!	#DIV/0!		
16							#DIV/0!	#DIV/0!	#DIV/0!	#DIV/0!		
17							#DIV/0!	#DIV/0!	#DIV/0!	#DIV/0!		
18							#DIV/0!	#DIV/0!	#DIV/0!	#DIV/0!		
19							#DIV/0!	#DIV/0!	#DIV/0!	#DIV/0!		
20							#DIV/0!	#DIV/0!	#DIV/0!	#DIV/0!		

Figure B.5: An example of the input table for the Excel sheet used during calcite twinning analysis.

THE CALCITE STRAIN GAUGE CSG99 PROGRAM

Input

The Strain99 computer program requires input in the following order:

1. grain number
2. c-axis bearing
3. c-axis plunge
4. direction of c-axis plunge in u-stage coordinates
5. u-stage direction of plunge
6. twin-pole bearing
7. twin-pole plunge
8. direction of twin pole plunge in the u-stage coordinates
9. number of twins within the grain
10. average thickness of the twins
11. 0,0,0
12. thickness of the grains.

These parameters must be compiled as a text file using one grain per line. The Excel sheet used for inputting the data has a tab labeled “Evans”, which transforms the data into the proper format (Figure B.6). However, the Excel sheet will need to be adjusted depending on the number of twinsets measured. The variables must be in

the same order as above separated by commas with the line ending in a zero. After the data for all grains are entered, the last line of the input file must be three nines followed by thirteen comma-separated zeros (999,0,0,0,0,0,0,0,0,0,0,0,0,0). The file must be compiled as a file with a ".dat" extension.

1	42	15	2	300	8	3	8	2.5	0	0	0	220	0
2	23	7	2	314	9	3	6	2.5	0	0	0	175	0
3	323	3	2	252	22	1	2	2.5	0	0	0	135	0
4	278	1	2	173	23	1	3	2.5	0	0	0	150	0
5	327	34	4	266	26	3	6	2.5	0	0	0	260	0
6	261	42	4	147	25	3	6	2.5	0	0	0	175	0
7	216	7	2	149	21	1	1	2.5	0	0	0	220	0
8	313	34	4	197	21	3	11	2.5	0	0	0	175	0
9	358	39	2	285	17	1	5	2.5	0	0	0	135	0
10	307	30	4	195	13	3	3	2.5	0	0	0	175	0
11	289	44	4	174	27	3	3	2.5	0	0	0	175	0
12	271	17	4	171	7	1	16	2.5	0	0	0	345	0
13	243	44	2	152	18	1	7	2.5	0	0	0	260	0
14	321	21	2	203	27	1	6	2.5	0	0	0	260	0
15	300	22	4	205	4	1	8	4	0	0	0	220	0
16	26	20	2	269	30	1	6	2.5	0	0	0	310	0
17	26	20	2	303	5	3	4	2.5	0	0	0	260	0
18	329	8	4	218	8	1	3	2.5	0	0	0	135	0
19	312	21	4	250	28	3	17	2.5	0	0	0	345	0
20	331	18	2	266	8	1	8	2.5	0	0	0	435	0
21	331	17	2	220	1	1	3	2.5	0	0	0	390	0
22	1	16	4	296	29	3	4	2.5	0	0	0	175	0
23	5	47	2	237	45	1	4	2.5	0	0	0	135	0
24	337	3	2	272	5	3	4	2.5	0	0	0	220	0
25	332	9	4	268	16	3	3	2.5	0	0	0	220	0
26	323	23	2	211	42	1	22	2.5	0	0	0	260	0
999	0	0	0	0	0	0	0	0	0	0	0	0	0

Figure B.6: Proper format from the "Evans" Excel sheet for input into the Strain99 program

Strain analysis

The Strain99 program may be run on a Windows personal computer. Operation of the program is briefly discussed here. For a more detailed description, see the program manual (Evans and Groshong, 1994; Evans, 2005). When started, the Strain99 program displays a menu consisting of:

*****Main Menu*****
S: Strain Analysis
R: Retrieve a Previously Saved Analysis
P: Plot Stereonets
E: Data Entry Routine
M: Modify Data Set
Q: Quit

To run the program, choose S: Strain Analysis and answer the questions that follow. The first question refers to print options. Choose the print options you desire and press enter. However, printing from a DOS program is not possible on network printers or to a PDF. Therefore, in order to see the printout, a program such as DOSPRN must be acquired. Answer "no" when asked whether to change the fudge factors. Input the proper sample name. If you answer "yes" to the question, Do you want a list of available files?, all the *.dat files in the same directory as the Strain99.exe application will be displayed. Enter the desired file name when asked what data file to use, but do not include the *.dat extension with the file name. Appropriately answer the question, Is this the correct file? With the first thin-section in the analyses, answer "no" to the question, Rotate slide coordinates? Following this, the program asks if the user wants to add another data file to the analysis. Answer "yes" if two or more thin sections are being analyzed. Enter the

data file containing the data from the second thin-section. This time answer "yes" to the question, Rotate slide coordinates?, and rotate the slide coordinates so the data in the second file will be analyzed in the same coordinates as the first file. These rotations should be determined using direction cosines. More on this procedure can be found in the Strain99 manual by Mark Evans included with the program (Evans, 2005).

After the rotations are entered, the program runs the analysis while the screen displays a message reading, "Thinking do not disturb." Generally this is an instantaneous message, given the speed of modern processors. The program to ask the user, save axis and pole data? It is a good idea to save this data because it contains, among other results, the orientation data for Turner (1953) compression and tension axes. If these data are saved, they will have the extension ".all" and will be saved in the same directory as the ".dat" files. Opening the *.all files with Excel allows the user to extract the compression, tension and c-axes, which can subsequently be opened using any number of stereonet programs.

INTERPRETATION

Residual Values (RV's)

The following is primarily the interpretation of Kollmeier, as his study dealt with multiple deformation events (See Kollmeier et al. 2000 for a more detailed account of this work). After the strain results have been obtained, check the percentage of Negative Expected Values (NEV's) within the sample, viewable on the printout. NEV's are grains having computed shear strains in an opposite sense of

shear, as expected given the orientation of the grain. Although the Strain99 program refers to them as NEV's, Kollmeier and Ong suggested replacing NEV's and PEV's (positive expected values) with RV's (residual values) and EV's (expected values). RV's represent grains that do not fit the strain calculated for most of the sample. These values may result from (1) local heterogeneous strain, (2) non-coaxial strain, or (3) superimposed strain. To determine which of the above situations is responsible for the NEV's, separate the positive and negative expected values. Run both sets and compare the orientation and dimensions of the two new stress ellipsoids. If the negative set has a definite cluster and a standard error of less than two, it probably represents a second or non-coaxial stress. On the other hand, if the negative set is less than 20-25% of the total population, has no definite cluster or girdle, and has a high standard error, then it may represent statistical noise or local heterogeneous strains.

As shown by Kollmeier, the calculated principal strain axes will not coincide exactly with the derived stress axes because the direction of maximum shortening is not expected to be collinear with the optimal orientation of compression to produce twinning. Specifically, the principal axis of shortening is inclined at 35° to the active twin plane, versus 45° for the assigned axis of compression (Turner, 1953). Thus, if a limestone bed does record pre-folding layer-parallel shortening, it is most accurate to refer to the stress as 'nearly' layer parallel. Calcite twinning is a strain hardening process where further twinning is resisted as beds tilt during progressive folding (Donath and Fruth, 1971; Teufel, 1980; Spang and Groshong, 1981; Kilsdonk and Wiltschko, 1988; Harris and van der Pluijm, 1998). However, deformed

limestone sometimes fails to record layer-parallel shortening, recording syn- or post-folding twinning instead. Also strain hardening does not preclude superimposed twinning, where overprinting deformations need only reach a sufficient magnitude and/or duration of applied differential stress (Friedman and Stearns, 1971; Teufel, 1980). If a given limestone does record superimposed deformation, early maximum compressive stresses will exhibit a characteristic orientation to the structure (i.e., nearly layer parallel and at a high angle to strike), whereas a later twinning event would be completely unrelated to earlier structures.

In regions where two, distinct twinning events have occurred, the stress axes are completely unrelated to calculated principal strain axes. This leads to erroneously assigned strain axes, where often intermediate strain axes are nearly coaxial with maximum compressive stress axes and vice versa. This discrepancy results because the strain gage computes deviatoric strain (recording only distortion, not dilation), where extension (+) and shortening (-) distributed among the three principle strain axes sum to zero. As plane strain is unlikely, two axes will share the same sign, and the third, most distinct, axis is referred to as the odd-signed axis. The odd-signed principal strain axis is often found to be the most accurate, while the two same-signed axes, if similar enough in magnitude, are assigned the remaining principle stress orientations with much less certainty (Groshong et al., 1984).. Therefore, strain results should always be checked against the stress directions.

Strain magnitudes calculated from multiply deformed samples in laboratory tests do not agree with experimentally applied strain magnitudes but yield

intermediate values (Teufel, 1980). However, the relative magnitudes of strain recorded in one population versus another can be determined where EVs represent greater deformation events than RVs (Friedman and Stearns, 1971; Teufel, 1980). Here it is important to mention that derived stress axes are less precisely defined than calculated strain axes, but perhaps more consistently accurate due to the potential for strain errors mentioned above.

The key is to make use of the sample(s) with the highest percent RVs to determine two coexisting populations within the same site, and then categorize the dominant (EV) populations of all other sites within that context. Additionally, bulk analyses on RV populations with a small number of measurement were used, with the knowledge that they carry a larger error, to confirm the presence of multiple populations within the data.

σ_1 Orientations

The printout from the Strain99 program provides an estimate of the stress tensor using the numeric dynamic analysis of Spang (1972). Generally, more than 30 twinsets, and preferably 50 twinsets, should be measured for this analysis. Given the Excel sheet that can be used for measurement, 50 twinsets per thin section can be achieved in a few hours of measurement. As Kollmeier et al. (2000) and Ong et al. (2007) have shown, paleostress and not strain orientations are important for studies regarding rotation. Contour the compression directions in a stereonet program to test whether the σ_1 direction from the numeric dynamic analysis corresponds to the contoured mean. In my experience, they are roughly equivalent.

A complete lack of pattern in compression directions indicates that the stress tensor is unreliable. In this case, the sample is inadequate and should be disregarded

PALEO-DIFFERENTIAL STRESS ESTIMATES USING CALCITE TWINNING DATA

Paleo-differential stress σ_D magnitudes responsible for twinning in calcite aggregates may be estimated using the technique developed by Jamison and Spang (1976). The technique is based on comparing the percentage of grains in a sample with one, two, and three twin sets with empirical data from laboratory deformation experiments done under known differential stress magnitudes. The technique is carried out by counting the number of grains having one, two, and three twin sets and comparing these values, as percentages, with empirically derived curves (Figure B.7) relating these percentages with S_1 (a value ranging from 0 to 0.5 for many to few twins respectively). To calculate σ_D the value S_1 is then used with the equation:

$$\sigma_D = t_c/S_1$$

Where t_c is the critical resolved shear stress for calcite assumed to be 10 Mpa. This twin density counting routine is most reliable in weakly deformed rocks where grains generally contain only one twin set. Rocks with multiple, non-coaxial stress histories allow for determination of the bulk differential stress, but the stress field magnitudes for each twinning deformation cannot be resolved using this method. An excellent review of paleostress estimation techniques for carbonates is given in Burkhard (1993).

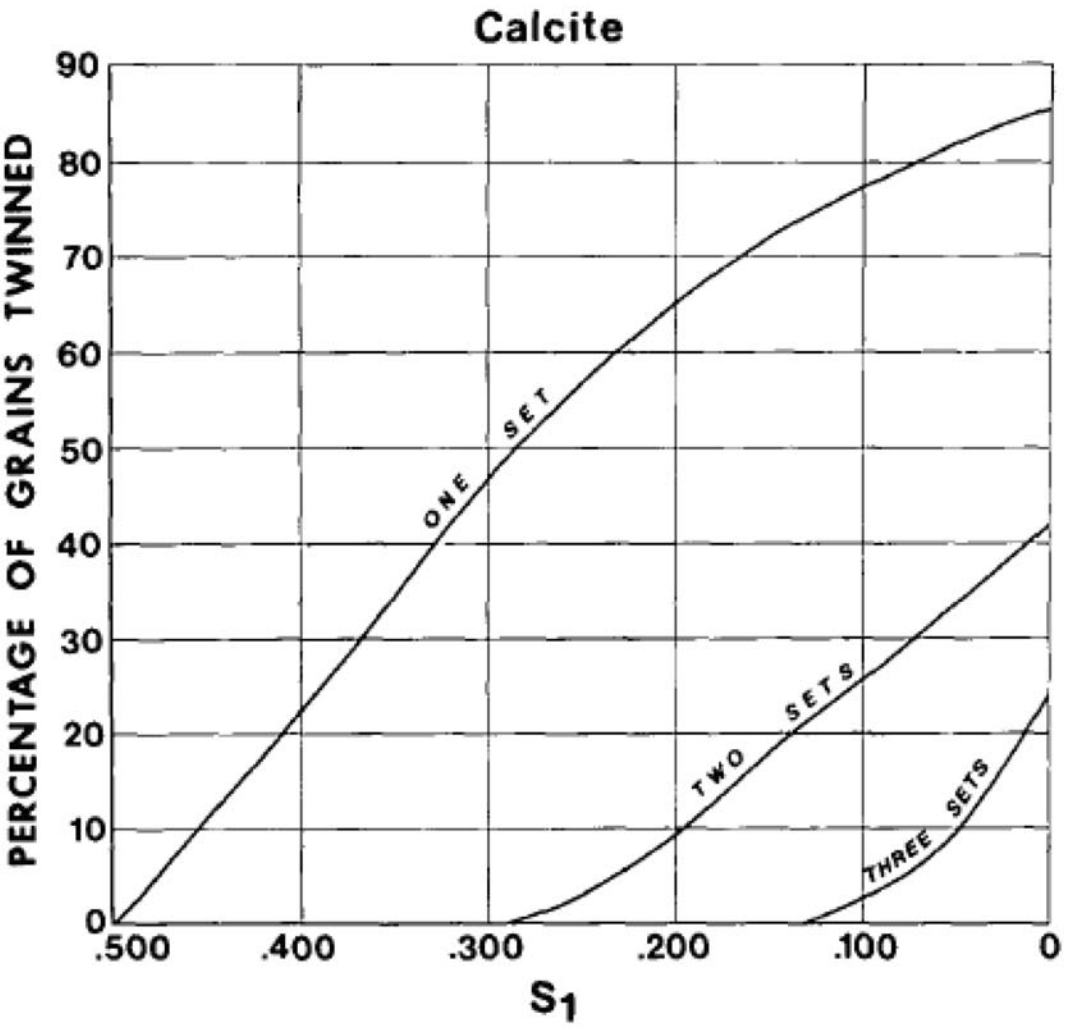

Figure B.7: Plot of twin set development versus S_1 for calcite. Curves are cumulative (i.e., one set curve includes all grains from two and three twin sets). From Jamison and Spang, 1976

REFERENCES

Burkhard, M., 1993. Calcite twins, their geometry, appearance and significance as stress-strain markers and indicators of tectonic regime; a review. Journal of Structural Geology 15, 351-368.

Donath, F.A. and Fruth, L.S., 1971. Dependence of strain rate effects on deformation mechanisms and rock type. Journal of Geology 79, 347-371.

Evans, M.A., 2005. The Calcite Strain Gauge Technique – A guide to sample preparation, data collection and data analysis using the CSG computer program, Version 1.2.

Evans, M.A. and Groshong, R.H., 1994. A computer program for the calcite strain-gauge technique. Journal of Structural Geology 16, 277-282.

Friedman, M. and Stearns, D.W., 1971. Relations between stresses inferred from calcite twin lamellae and macrofractures, Teton Anticline, Montana. Geological Society of America Bulletin 82, 3151-3161.

Groshong, R.H., 1974. Experimental test of least-squares strain gage calculation using twinned calcite. Geological Society of America 85, 1855-1864.

Groshong, R.H., Teufel, L.W. and Gasteiger, C., 1984. Precision and accuracy of the calcite strain-gauge technique. Geological Society of America 95, 357-363.

Harris, J.H. and van der Pluijm, B.A., 1998. Relative timing of calcite twinning strain and fold-thrust belt development; Hudson Valley fold-thrust belt, New York, U.S.A. Journal of Structural Geology 20, 21-31.

Jamison, W.R. and Spang, J.H., 1976. Use of calcite twin lamellae to infer differential stress. Geological Society of America Bulletin 87, 868-872.

Kilsdonk, B. and Wiltschko, D.V., 1988. Deformation mechanisms in the southeastern ramp region of the Pine Mountain block, Geological Society of America Bulletin 100, 653-664.

Kollmeier, J.M., van der Pluijm, B.A. and Van der Voo, R., 2000. Analysis of Variscan dynamics; early bending of the Cantabria-Asturias Arc, northern Spain. Earth and Planetary Science Letters 181, 203-216.

Ong, P.F., van der Pluijm, B.A. and Van der Voo, R., 2007. Early rotation in the Pennsylvania Salient (US Appalachians): Evidence from calcite-twinning analysis of Paleozoic carbonates. Geological Society of America Bulletin 119, 796-804.

Spang, J.H., 1972. Numerical method for dynamic analysis of calcite twin lamellae. Geological Society of America Bulletin 83, 467-472.

Spang, J.H. and Groshong, R.H., 1981. Deformation mechanisms and strain history of a minor fold from the Appalachian Valley and Ridge Province. Tectonophysics 72, 323-342.

Teufel, L.W., 1980. Strain analysis of experimental superposed deformation using calcite twin lamellae. Tectonophysics 65, 291-309.

Turner, F.J., 1953. Nature and dynamic interpretation of deformation lamellae in calcite of three marbles. American Journal of Science 251, 276-298.

Turner, F.J. and Weiss, L.E., 1963. *Structural Analysis of Metamorphic Tectonites*. McGraw-Hill, New York, 545pp.

APPENDIX C

SAMPLE PREPARATION FOR $^{40}AR/^{39}AR$ DATING OF ILLITE

INTRODUCTION

This guide is meant to aid the reader in preparing samples for Illite Age Analysis. It does not describe X-ray diffractometer use, mineral identification or polytype characterization. The procedures described below represent the combined effort of many former and present researchers at the University of Michigan, including John Solum, Sam Haines, Anja Schleicher, Chris Hall and myself, each of whom contributed some aspect to improve the process. Although the techniques described are mainly written for the Structural Geology and Argon Geochronology Labs at the University of Michigan, they can be applied anywhere with the proper equipment. Most of the early preparation work for X-ray diffraction (XRD) analysis generally follows the methods described in chapter 6 of Moore and Reynolds (1997).

SAMPLE COLLECTION

Perhaps the most difficult step in dating brittle faults is finding exposures that have suitable fault rocks to date. Often in the literature (maps, geologic field guides, etc.), detailed descriptions of fault rocks are absent. I have found that

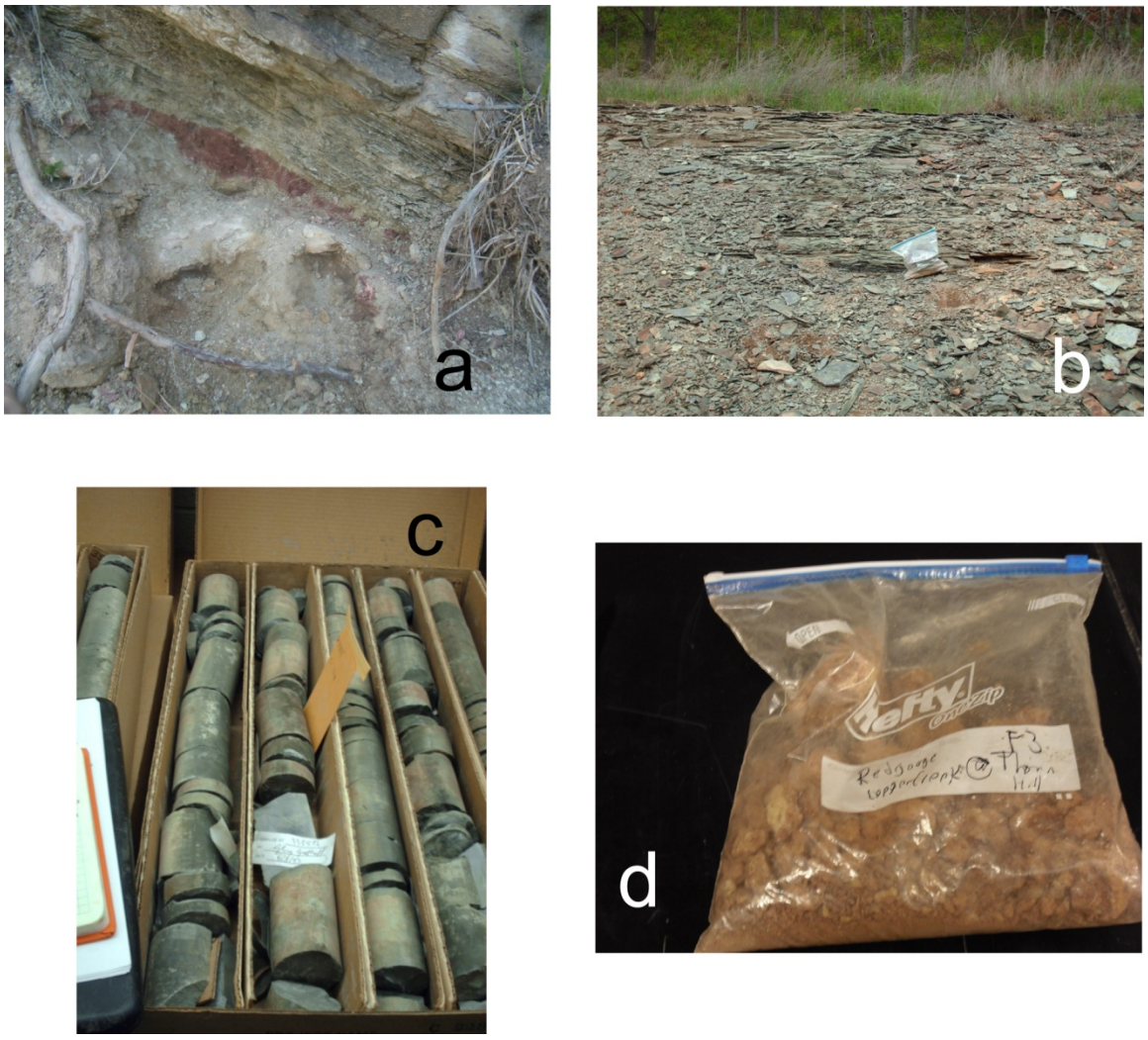

Figure C1: Various sources of rocks for illite age analysis a) Fault gouge b) Shale outcrop c) Shale in core d) Sample collected in a 1 gallon storage bag (example is fault gouge)

when descriptions are available, the varied terminology of fault rocks can cause confusion as to what is actually present. Gouge, cataclasite, mylonite, fault zone and breccias have all been used to describe fault rocks that would be classically defined as fault gouge. My experience has been that contacting local geological surveys is the best way to find fault gouge outcrops. While they generally are not interested in the nature of the fault rocks during their mapping expeditions, they have likely come across any potential fault rocks in the region.

When fault gouge is identified, sample collection is relatively simple, since orientation is not necessary, unless one is interested in doing fabric analysis (see Solum, 2004; appendix A). For fault gouge samples, it is best to fill a one gallon storage bag with as much material as possible (Figure C.1d). Be sure to dig as deep as possible into the exposure in order to minimize the effects of recent alteration.

Outcrop availability is almost never a problem with shale samples (Figure C.1b). Therefore, volume is generally not an issue. A one gallon storage bag full of shale will certainly suffice. However, sometimes it is necessary to take samples from core (Figure C.1c). Some core repositories are often reluctant to part with significant amounts of their core. If possible, it is best to obtain at least 50 grams of sample.

SIZE FRACTION SEPARATION

Sample Reconnaissance

One of the basic assumptions of the IAA is that the percentage of authigenic illite increases with decreasing grain size (Pevear, 1992; Grathoff et al., 2001). It is therefore necessary to separate any sample that we wish to date. The process described can be applied to any material containing illite, including fault gouges, shales and even digested limestones.

For clayey samples, such as fault gouge, first gently break the sample down using a mortar and pestle (Figure C.2a) and pour the powder sample into a 2 liter beaker (Figure C.2b). To deflocculate the clays in the sample, fill the beaker with deionized (DI) water (Figure C.2c) and stir the sample, trying to break up any

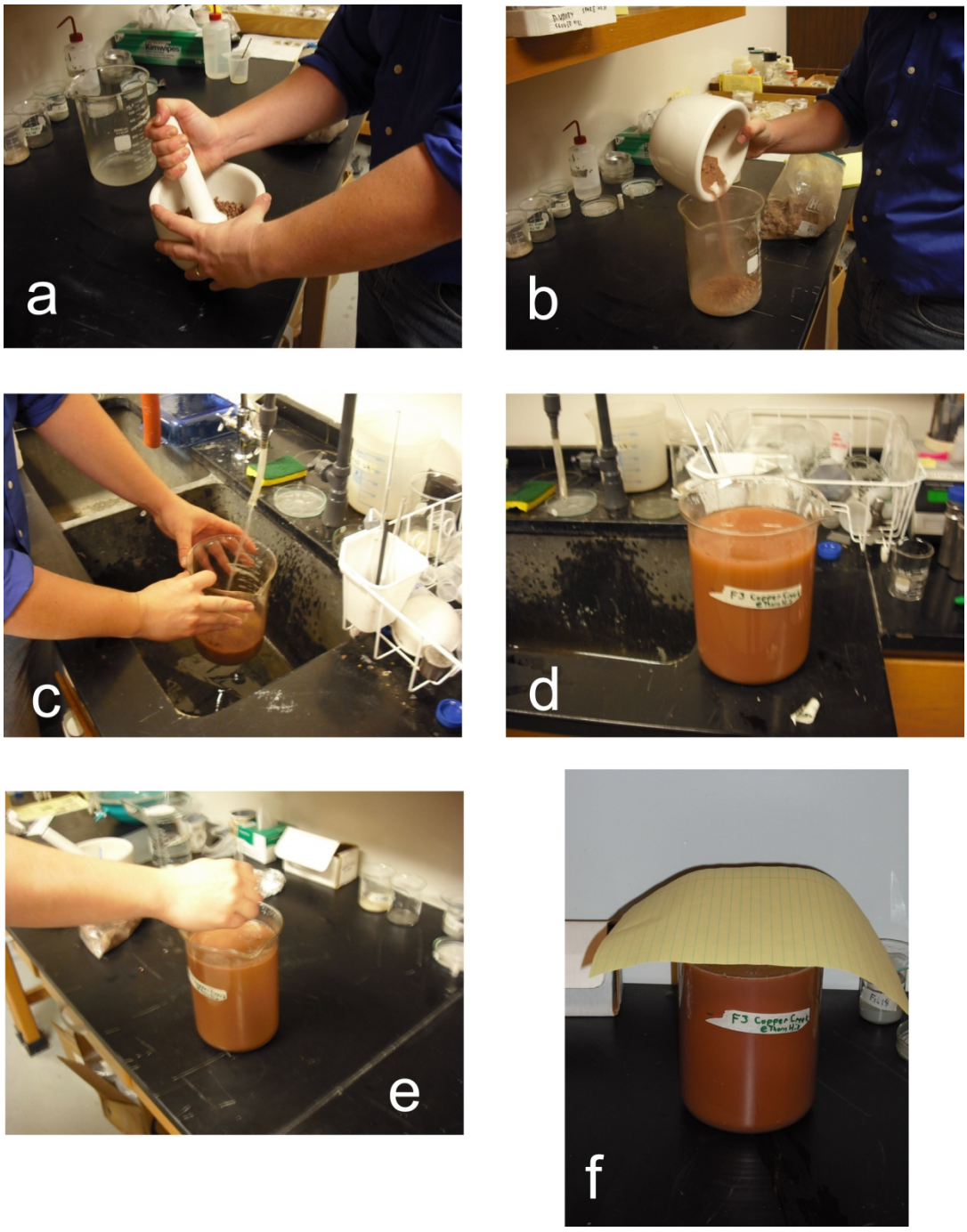

Figure C.2: Initial steps during sample preparation for IAA. (a) Gently crush the sample (b) pour into a beaker (c) fill with water (d) label the beaker (e) stir the sample (f) cover and allow to sit

chunks of clay that may be at the bottom of the beaker (Figure C.2e). Cover the beaker with a piece of paper and allow it to sit overnight (Figure C.2f). The following day, larger particles should have settled to the bottom, with a suspension of clay-sized grains (Figure C.3a). Sometimes, the clays will not to deflocculate, leaving nothing in suspension. This is likely due to the presence of salts. If nothing is in suspension, repeat the process by pouring off the water, rinsing the sample and allowing it to set overnight again. If nothing is left in suspension by the third attempt, add a small amount of deflocculant, such as sodium carbonate, to the sample. Small roots and other plant material may also be in the beaker with the sample. After the overnight soak, this organic material will float to the top and can be removed with a paper towel (Figure C.3b).

If the samples are indurated, they must first be broken down with a mortar and pestle. Indurated samples, such as shale, will obviously require a bit more force than the more friable samples. Since it is best to do as little as possible to the sample, I typically do not grind the sample too much. However, if there is only a limited amount of sample (such as a small piece of shale from a core), grinding may be required to ensure enough material is separated. I would suggest not using a shatterbox, since any detrital potassium bearing minerals (i.e., K-feldspar) can be ground into clay sized particles that will contaminate the sample. After crushing indurated samples, place the powdered sample into a 600 mL beaker and fill with DI water. Let the beaker sit in an ultrasonic bath for approximately 10 minutes, pour the supernatant liquid into a 2 liter beaker and repeat sonication until the 2 liter beaker is full. From here, follow the steps for deflocculation previously mentioned.

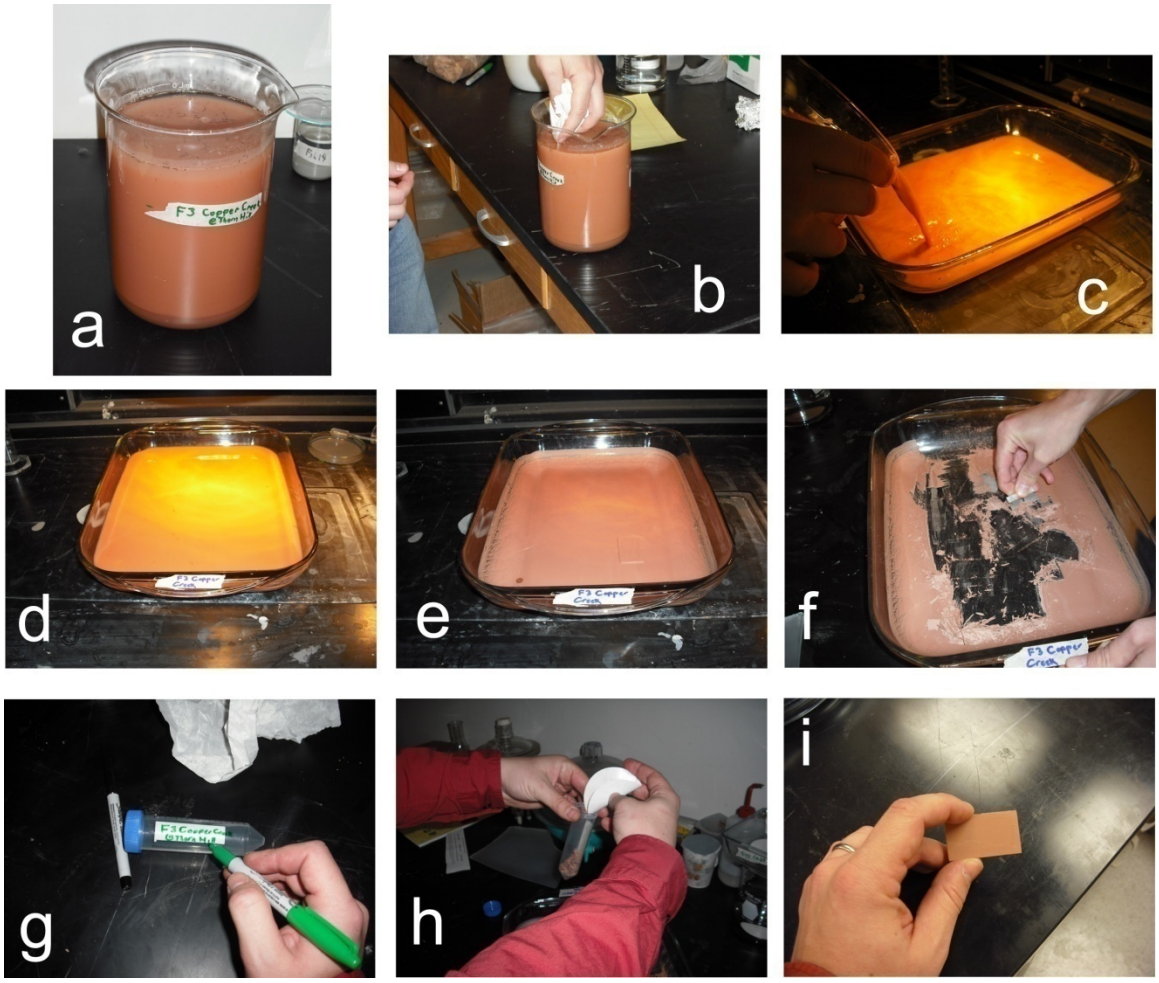

Figure C.3: Steps for obtaining a clay-sized fraction. (a) Suspension after settling at least 24 hours. (b) Removal of organic material using a paper towel. (c) Pouring suspension into a casserole dish under a heat lamp. (d) Allow to dry. (e) Sample after drying. (f) Scrape the dried sample from the casserole dish. (g) Label a container and (h) place the sample in the container. (i) Oriented texture slide for XRD

When a reasonable amount of clay is in suspension, pour the suspension into a large casserole dish under a ventilation hood (Figure C.3c). Our group has used standard heat lamps to facilitate evaporation. When the water has been evaporated from the dish (Figure C.3e), scrape the sample out of the dish using a razorblade (Figure C.3f). From the scraped material, Label a container (e.g., a 50 mL centrifuge tube) and put the scrapings in the container (Figure C.3h). Repeat the process until

at least three grams are collected. Make a suspension of a small amount (~0.1 g) of the sample in about 10 mL of DI water, then pour it onto a glass slide and allow it to dry (Figure C.3i). This oriented texture slide will be used to characterize the mineralogy of the sample.

Size Fractions

XRD analysis of the oriented texture slide will determine whether enough illite is present to continue separating grain size fractions. The standard size fractions used by our research group are 2.0 – 0.2 μm, 0.2 – 0.05 μm and <0.05 μm. Using Stoke's law, these fractions are separated via centrifugation. Although Stoke's law defines the grain size for spherical particles (phyllosilicates are not), the absolute grain size is not important, because we are only interested in obtaining aliquots with varying amounts of detrital illite. It is sometimes necessary to produce a different set of grain sizes for a variety of reasons (e.g., too much potassium feldspar in the coarse fraction, not enough fine fraction isolated, etc.). In these instances, use Stoke's law to calculate the desired grain size and centrifuge accordingly.

Start with approximately two to five grams of the sample, pour it into a 250 mL beaker and fill with slightly less than 200 mL (Figure C.4b). Stir the sample and set in the ultrasonic bath for about fifteen minutes (Figure C.4c). I recommend not using the ultrasonic probe as it has the potential to destroy clay mineral crystallites. After sonication, pour the suspension into four 50 mL centrifuge tubes, filling each to approximately the 50 mL line (Figure C.4d). Cap the tubes, place them in the centrifuge sleeves and weigh each tube (Figure C.4e). Each tube should weigh the

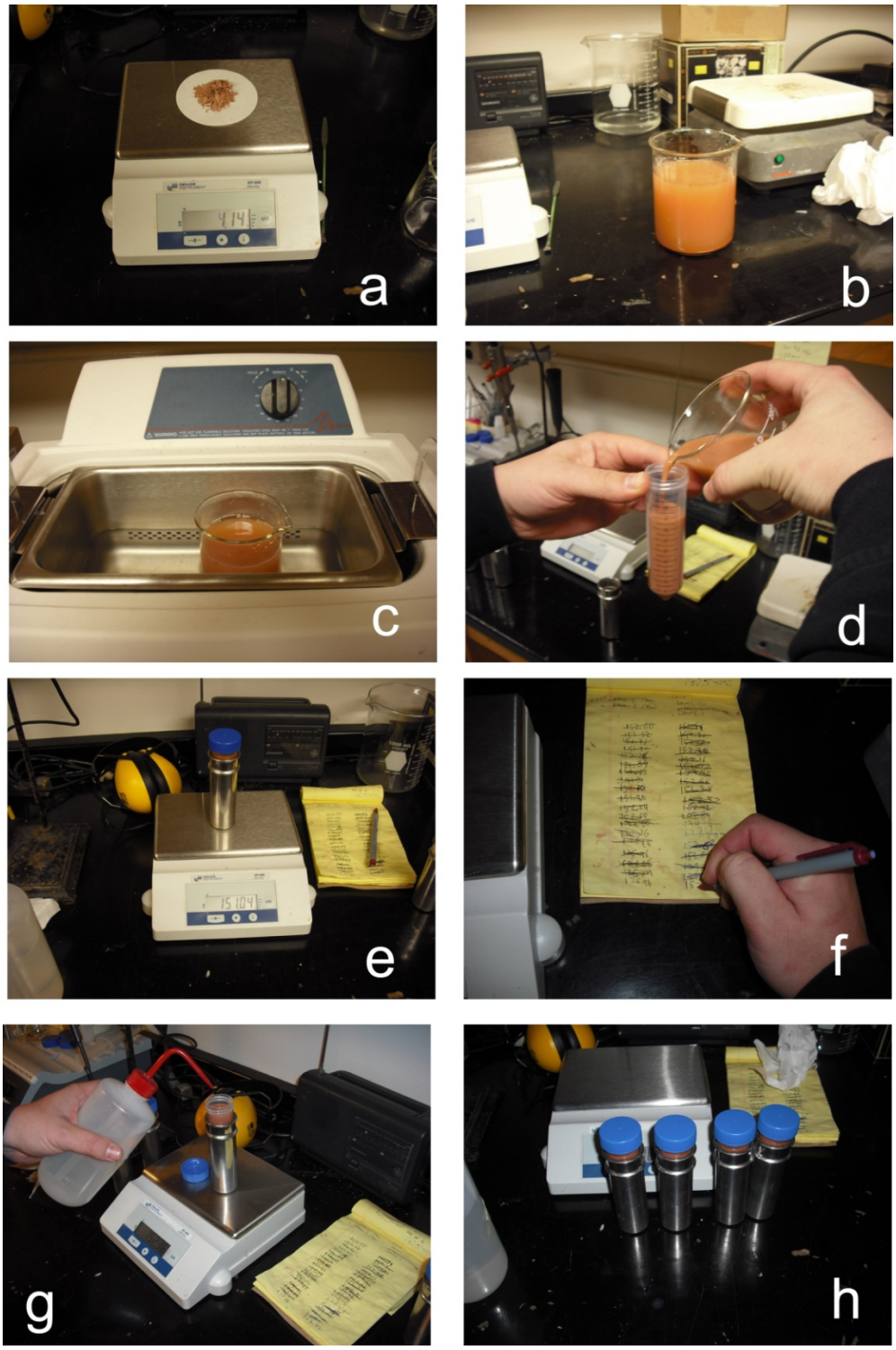

Figure C.4: Sample preparation for separating grain sizes. (a) Mix between 2-5 g with (b) ~200 mL of DI water. (c) Place into sonic bath for 15 minutes. (d) Pour suspension into centrifuge tubes. (e) Weigh all four tubes along with the tube sleeves and (f) note the tube with the maximum weight. (g) Add DI water to the remaining three tubes until (h) they all weigh the same.

same amount, to keep the centrifuge in balance. It is less important to be exact at lower RPM's, but it is worthwhile to get in the habit of matching the weight of each tube. Record the weight of the heaviest tube and add DI water to the other three to match (Figure C.4g).

The process of size fraction separation is detailed in Figure C.5. The first step is to separate the coarsest fraction. I typically begin with a 35 second run at 1000 RPM to separate out all the material that is greater than 2.0 μm. This is especially effective of removing any organic material that was missed in earlier steps and allows a chance to remove detrital potassium feldspar, if present. After centrifugation, remove each tube from their sleeves and carefully decant the supernatant suspension into a beaker. Using a squirt bottle, remove the residue from the bottom of the tube and set it aside to dry. It is wise to keep this "super coarse" fraction just in case. Sonicate the suspension in the beaker again for a few minutes, pour it into the centrifuge tubes and rebalance them. To separate the coarse fraction from the medium and fine fractions, run the centrifuge for 10 minutes at 2000 RPM. Decant the supernatant liquid into a small casserole dish and rinse out the residue. As the RPM's increase, it will be more difficult to remove the residue at the bottom of the centrifuge tubes. Pour the residue into a 250 mL beaker and refill with DI water. Sonicate for fifteen more minutes and repeat the centrifugation process two more times at 2000 RPM for 10 minutes. When approximately 600 mL of medium and fine suspension has been collected, pour the residue into a small dish to dry. Once dried, scrape it with a razorblade, put into a

Figure C.5: Separating size fractions. (a) Place tubes in the centrifuge. (b) The centrifuge. (c) Centrifuge tube showing the coarser material at the bottom and finer material in suspension. (d) Pour the supernatant suspension off, (e) label a small casserole dish and (f) allow the smaller size fraction to dry. (g) Remove the sediment at the bottom of the tube with a direct spray of water and (h) pour it into a 250 mL beaker. (i) Sometimes spraying with the water, placing the cap on the tube and shaking it helps to loosen the sediment. (j) After repeating the centrifugation process two times, remove the sediment from the bottom of the tube and (k) allow it to dry. (l) Scrape each size fraction from its dish, (m) pour onto a piece of weighing paper and (n) pour into a small labeled glass vial. (o) Final product

a
b
c
d
e
f
g
h
i
j
k
l
m
n
o

small vial and label accordingly. This is the coarse fraction that will be measured for polytypes of illite.

With the suspension of the medium and fine fractions, allow it to evaporate off ~400 mL of water, leaving about 200 mL. Repeat the centrifugation process, starting with the ultrasonic bath and centrifuging at 3000 RPM for 90 minutes. This will separate the fine (<0.05 μm) suspension and the medium (0.05-0.2 μm) residue. Given the high speed of the centrifuge, it is imperative that the weight of all tubes is exactly the same. The suspension of the fine fraction can range anywhere from murky to nearly colorless. Even if the supernatant liquid appears to be clear, continue to evaporate off the water as it is likely that some clay is still in suspension.

Tips for XRD analysis

The oriented texture slide can easily be measured, as most standard X-ray diffractometers are fitted with a slide holder. For polytype quantification, however, a randomly oriented powder diffraction pattern is necessary (Moore and Reynolds, page 222). To accomplish randomness, a specially milled aluminum holder is used. The procedure is shown in detail in Figure C.6. With the separate aluminum plate in the slot on the holder, place a small amount of the powder in the holder. The powder may require some disaggregation with a razorblade. Place a frosted glass slide on top of the holder with the rough side down. Be sure to have a tight hold on all three components and hold the aluminum holder a bit beyond vertical with the plate pointed down. Gently tap the side of the holder to create a randomly oriented surface at a microscopic level. Lay the holder back down and gently remove the frosted slide first without sliding (this will produce a preferred orientation),

followed by the aluminum plate. If randomness has been achieved, the 020 illite peak should be more intense than the 002 illite peak (i.e. higher "Dollase" factor).

There are some instances where not enough sample of a particular size fraction has been collected to use the aluminum holder (most commonly an issue

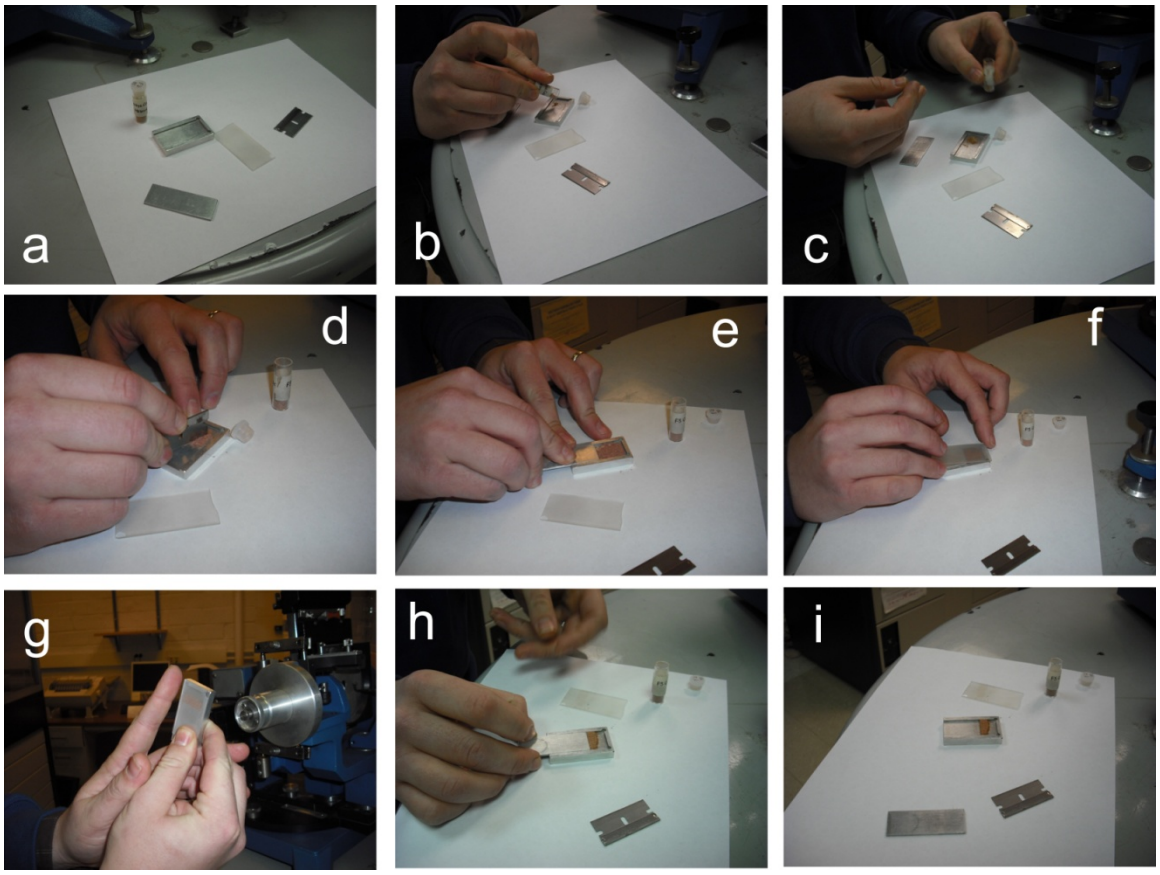

Figure C.6: Preparing a sample to produce a random powder diffraction pattern. (a) Materials. (b) Pour the sample in the aluminum holder and (c) replace the cap on the sample container. (d) Break up any chunks with a razorblade. (e) Using the aluminum packer, barely press on the powder. (f) Place the frosted slide (frosting down) on top of the powder. (g) Carefully keeping everything together, hold the aluminum holder vertical and gently tap on the side. (h) Remove the frosted slide first and then (i) the aluminum packer

with the fine fraction). In this case, place aluminum plate all the way in the holder and position the sample on top of the plate. Using a razorblade, scrape the sample into somewhat of a line and gently touch the frosted slide to the top of the sample,

not allowing the full weight of the slide to rest on it. This may require a few tries before randomness is achieved.

Carbonate minerals such as calcite and dolomite are often found within the clay-sized fractions of both shales and fault gouge and will dominate limestones. Calcite (2Θ) and dolomite (2Θ) both have XRD peaks that interfere with proper illite polytype quantification. However, they are easily removed with a weak (1N) acetic acid solution. With the size fractions, simply mix the sample with the acid and allow it to set for at least a few hours. Lower pH values tend to promote flocculation, so even fine fractions should settle to the bottom of the beaker. Rinse the sample a few times by decanting the supernatant acid and replacing with DI water. After at least two rinses, centrifuge the sample at 3000 rpm for thirty minutes and measure the XRD again. It is important to note that our understanding of the effects of acid treatment on argon retention is limited. As it is our goal to do as little as possible to the sample prior to irradiation, it would be wise to separate some of the sample for argon dating and treat the rest for carbonate minerals. Obviously, when dealing with illite dissolved from limestone, there are no alternatives to first treating the sample with acid.

IRRADIATION PREPARATION

After identifying samples that one wishes to date, they need to be carved down to be inserted in quartz tubes. Preparing samples for irradiation is a time-consuming, tedious process that requires a delicate touch. The step-by-step procedure is shown in Figure C.7. Dating samples rich in illite requires

encapsulation because of recoil effects that occur during irradiation (Halliday, 1978; Foland et al., 1984; Dong et al., 1995).

Start by labeling a 1 mL centrifuge tube with a marker. Using a small spatula, place two scoopfuls into the tube followed by 1 mL of DI water using a pipette. Repeat this process for all samples that are to be dated prior to moving to the next step. After all of the centrifuge tubes are filled, place them in the small desktop centrifuge and spin them at ~10000 RPM for one hour, ensuring the centrifuge is balanced. This will allow the sample, regardless of grain size, to form a tight pellet in the bottom of the tube. Once they have been spun down, remove each tube carefully from the centrifuge and remove as much of the supernatant water with the pipette as possible without disturbing the accumulated sample at the bottom. BE SURE TO RINSE THE OUTSIDE AND INSIDE OF THE PIPETTE BETWEEN EACH SAMPLE. Failure to do so risks contamination. When the supernatant water has been removed from all samples, place the tubes upright in a beaker and allow them to sit under a laminar flow hood for at least three days.

Carving

The quartz tubes used to encapsulate the sample need to be sealed at one end and are hereafter referred to as breakseals. It is preferable to have someone experienced in glass blowing to form the first sealed end because it must be strong enough to hold up during packaging, but also delicate so it will break once in the manifold attached to the mass spectrometer. Samples are treated differently depending on the approximate age. Samples that are relatively young (<5 Myr) need to be larger (~5 mg) to compensate for the limited amount of radiogenic

Figure C.7: Carving process for Ar dating. (a) Materials required for making a pellet. (b) Label the centrifuge tube and (c) place two spoonfuls of sample into it. (d) Using the pipette, place 1 mL of DI water into the tube and (e) centrifuge for one hour at 10000 rpm. (f) After centrifucation, remove supernatant water from each tube with the pipette and (g) allow to dry under a laminar flow hood for two days. Using the materials shown (h), begin by (i) removing the pellet from the centrifuge tube. (j) Carve the sample down to (k) 1mm X 2-3mm. (l) Measure the pellet's weight and record it. (m) Gently place the pellet into the breakseal and (n) pick the open breakseal up to allow the pellet to fall to the bottom. (o) Place the breakseal into an envelope in a way to guarantee the open end remains up and (p) label the envelope.

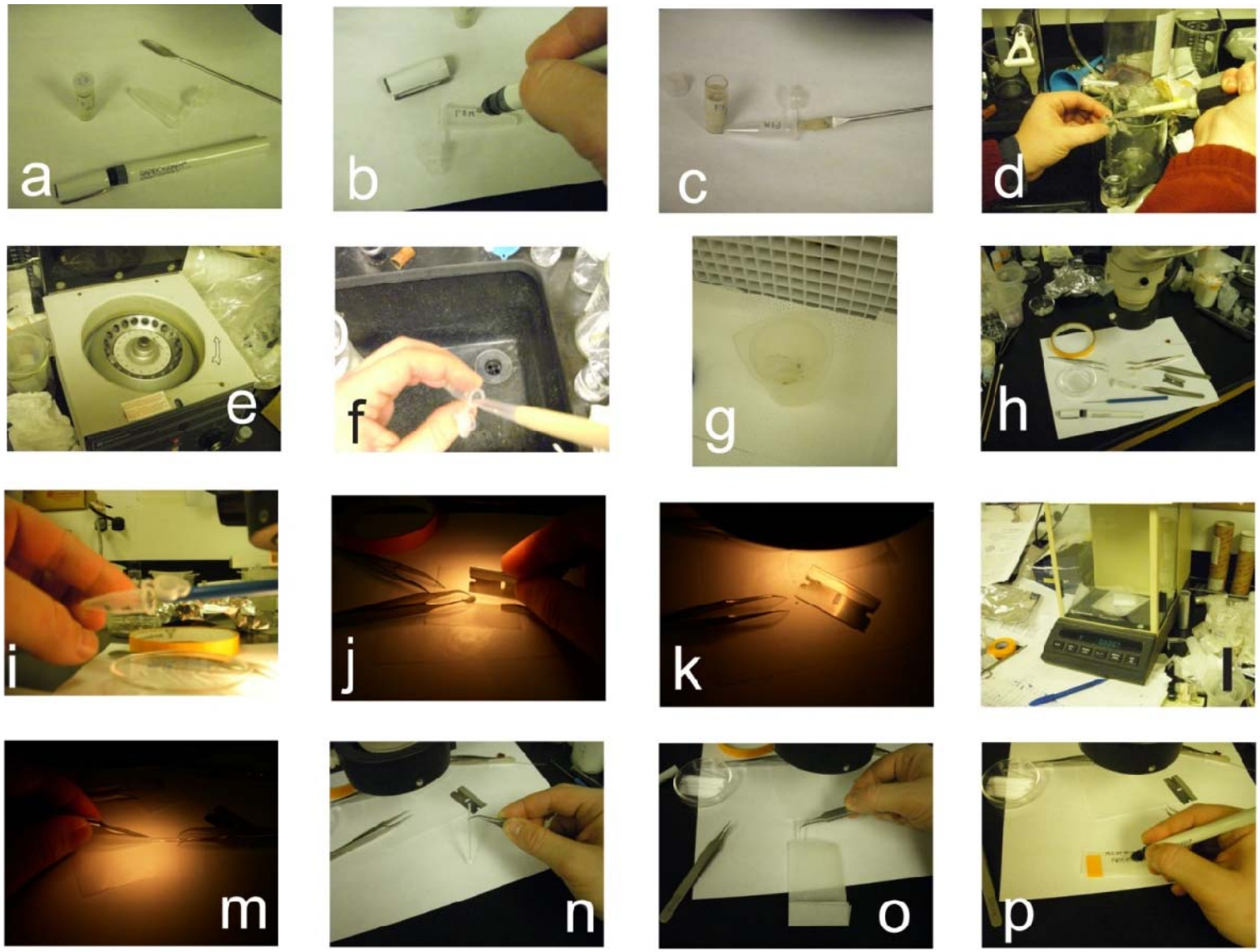
a
b
c
d
e
f
g
h
i
j
k
l
m
n
o
p

argon. Therefore, larger breakseals are needed (inner diameter = 3 mm). I have found that the tips of the large breakseals are extremely delicate and need to behandled with care. For older samples, pellets only need to be 0.5 to 1.0 mg. The smaller breakseals (ID = 1mm) are more robust and tend not to break as easily.

Once the pellets are dried, they must be carved down to fit into the quartz tubes for irradiation. First, if the sample is stuck to the bottom of the centrifuge tube, a dissection probe or paper clip can be used to remove it and maintain the integrity of the sample. Sometimes the sample will have separated from the centrifuge tube during drying. Carving the sample requires a binocular microscope and a razor blade. For larger, younger samples, the carved pellet needs to be larger and placed into the large breakseals. For these larger samples, carve down the sample to be between two to five milligrams. Once the sample has an appropriate mass and will fit into the breakseal (needs to be checked during the carving process), place the sample into the tube either by GENTLY picking it up with the curved tip tweezers or by putting it at the edge of the weighing paper and guiding it into the tube.

For most samples, the approximate age will be greater than 5 Ma, requiring a smaller sample for the irradiation. Since the inner diameter of the breakseals used for these samples is roughly one millimeter, carving the sample down to fit is difficult. Carefully carve the sample into a pellet that is roughly two to three millimeters long and one millimeter wide. I have found that during the carving process, the coarse fraction generally is the most susceptible to crumbling, primarily due to the larger quartz grains that are typically in this size fraction. Weigh the

sample, making certain the total mass lies between 0.5 and 1.0 mg. Placing the sample into the breaskseal is more difficult for the smaller samples and requires a patient, steady hand. As with the larger samples, place the pellet in the tube either by picking it up with the curved tip tweezers or by pushing it to the edge of the weighing paper and subsequently guiding into the tube. It is extremely important to maintain the integrity of the pellet, as the laser needs to focus on the sample during the step-heating process.

When the pellet has been placed in the breakseal, fold up another piece of weighing paper into an envelope and label it, ensuring that the breakseal doesn't fall out of the bottom of the envelope. It is important to label every sample in the same way to make certain that the open end of the breakseal is oriented upward, keeping the pellet from falling out. At this point, replace the unused sample back into the labeled centrifuge tube and repeat the carving process for each sample.

As I did not personally seal off the breakseals while they were evacuated with the vacuum pump, I can only give general guidance. Given that the breakseals need to be evacuated to approximately 10^{-5} Pa ($\sim 10^{-11}$ bar), a very powerful vacuum pump is required. In the Argon Geochronology Lab at the University of Michigan, the breakseals are attached to the vacuum system connected to the mass spectrometer, which can evacuate the breakseals to such low pressures. Seal the connection to the pump with appropriately sized rubber O-rings and squares of latex. Once the breakseals have been pumped down, seal them off using a torch appropriate for working with quartz. The end of the breakseal with the sample in it should be submerged in water, as to not overheat the sample and to immediately

quench the quartz after sealing the other end. The smaller breakseals should be ~ 1.6 cm long and the larger breakseals should be about 3.5 cm. Be sure to replace the breakseal back in its labeled envelope. Appropriate mineral standards for argon (typically MMhb hornblendes or FCT-3 biotites) should be packaged for irradiation by making pure aluminum foil envelopes with twenty grains per envelope.

REFERENCES

Dong, H., Hall, C.M., Peacor, D.R. and Halliday, A.N., 1995. Mechanisms of argon retention in clays revealed by laser ^{40}Ar-^{39}Ar dating. Science 267, 355-359.

Foland, K.A., Linder, J.S., Laskowski, T.E. and Grant, N.K., 1984. $^{40}Ar/^{39}Ar$ dating of glauconites; measured ^{39}Ar recoil loss from well-crystallized specimens. Isotope Geoscience 2, 241-264.

Grathoff, G.H., Moore, D.M., Hay, R.L. and Wemmer, K., 2001. Origin of illite in the lower Paleozoic of the Illinois Basin; evidence for brine migrations. Geological Society of America Bulletin 113, 1092-1104.

Halliday, A.N., 1978. ^{40}Ar-^{39}Ar stepheating studies of clay concentrates from Irish orebodies. Geochemica et Cosmochimica Acta 42, 1851-1858.

Moore, D.M. and Reynolds, Jr., R.C., 1997. *X-ray diffraction and the identification and analysis of clay minerals*. Oxford University Press, Oxford, United Kingdom, 278 pp.

Pevear, D.R., Illite age analysis, a new tool for basin thermal history analysis. In: Kharaka, Y.K. and Maest, A.S., Editors, 1992. *Proceedings of the 7th International Symposium on Water-rock Interaction.* Rotterdam, Netherlands, Balkema, 1251-1254.

Solum, J.G., 2004. Clay neomineralization in fault zones: Extracting information on fault properties and timing. Unpublished PhD Thesis, University of Michigan, 276pp.